



UNIVERSITÀ DEGLI STUDI DI SALERNO



UNIVERSITÀ DEGLI STUDI DI SALERNO

Dipartimento di Farmacia

PhD Program

in **Drug Discovery and Development**

XXXIV Cycle — Academic Year 2021/2022

**PhD Thesis in**

*Development of Innovative Agents  
for the Treatment of Metabolic Diseases*

Candidate

*Maria Luisa d'Aulisio Garigliota*

Supervisor

Prof. *Anna Ramunno*

PhD Program Coordinator: Prof. *Gianluca Sbardella*



*To my sister,  
the angel who guards my goals*



## Preface

*My PhD project in Drug Discovery and Development at the Department of Pharmacy, University of Salerno, under the supervision of Prof. Anna Ramunno, focused on the development of new lipid-lowering agents (Chapters 1-5).*

*During my PhD experience I also participated in a research study focused on the photo-responsive behavior of benzodiazopyrrole derivatives endowed with anticancer properties.*

## Publication

Imperatore, C.; Valadan, M.; Tartaglione, L.; Persico, M.; Ramunno, A.; Menna, M.; Casertano, M.; Dell'Aversano, C.; Singh, M.; **d'Aulizio Garigliota, M. L.**; Bajardi, F.; Morelli, E.; Fattorusso, C.; Altucci, C.; Varra, M. Exploring the photodynamic properties of two antiproliferative benzodiazopyrrole derivatives. *Int. J. Mol. Sci.* **2020**, *21*, 1246. doi: 10.3390/ijms21041246

## Attendance at courses, conferences and seminars

- Prof Rocco Romano; Advanced course in NMR spectroscopy, University of Salerno, April 5 - July 19, 2019;
- Prof. Maria Chiara Monti; Q-TOF mass spectrometry course; University of Salerno, January 10, 2019;
- Dr. S. Berardo; B2 level English language course; University Language Center, University of Salerno, April-July, 2020;
- Fontana, S.; Russ, T.; Micheli, F. Drug Discovery: from theory to practice, University of Salerno, July 14-16, 2020;
- ESMEC- European School of Medicinal Chemistry (40th Advanced Course of Medicinal Chemistry and "E. Duranti" National Seminar for PhD Students), virtual edition, abstract presentation, June 28 - July 1, 2021;
- Paul Ehrlich (PE) Euro-PhD Network, virtual meeting, July 26 - 28, 2021;
- Animal experimentation in biomedicine - A path of science, history, law, ethics and medicine, webinar, March 18, 2021;
- OPENS training "Campania towards Horizon Europe 2021-2027", Campania Training Path: Ethics in Horizon Europe, virtual meeting, May 14, 2021;
- OPENS training "Campania towards Horizon Europe 2021-2027", Campania Training Course: Dissemination, Communication and Exploitation in Horizon Europe how to maximize results, virtual meeting, May 21, 2021;
- OPENS training "Campania towards Horizon Europe 2021-2027", Campania Training Course: IPR in Horizon Europe, virtual meeting, May 25, 2021;
- OPENS training "Campania towards Horizon Europe 2021-2027", Campania Training Course: Open Access and Open Data in Horizon Europe, virtual meeting, May 28, 2021;
- 1st Edelris Symposium on Affinity Selection-Mass Spectrometry in Drug Discovery, virtual event, June 2 - 3, 2021;
- ACS Publications Symposium: Innovation in Measurement Science, virtual event, June 22-25, 2021.



## Abstract

Elevated LDL cholesterol (LDL-C) is an established risk factor in cardiovascular disease, the leading cause of death in the world. To date three main therapeutic strategies have been evaluated to reduce circulating LDL-C including: a) inhibition of critical steps of cholesterol synthesis, b) regulation of hepatic expression of the LDL-receptor (LDLR), and c) inhibition of Proprotein Convertase Subtilisin/Kexin type 9 (PCSK9)-mediated LDLR degradation.

Berberine (BBR) is a well known hypolipidemic agent able to upregulate LDLR expression. This alkaloid is also endowed with hypoglycemic, antitumor, antiviral, antioxidant and neuroprotective properties. However, BBR has poor oral bioavailability, is a substrate of P-glycoprotein (P-gp) and can affect the CYP450 system. Therefore, the development of new BBR analogues is encouraged in order to obtain new hypolipidemic compounds with improved pharmacokinetic/pharmacodynamic profile.

PCSK9 is a protein that binds LDLR and promotes its lysosomal degradation after internalization. Thus, LDLR cannot be recycled to the hepatic cell surface; on the contrary, the inhibition on PCSK9/LDLR increases hepatic cell-surface LDLR and improves the uptake of the LDL particles by the liver. To date, only two mAbs (alirocumab and evolocumab) directed against PCSK9 have been approved by FDA. However, these drugs need to be administered by injection, are expensive, and these aspects can greatly affect adherence to therapeutic regimen.

Therefore, an orally available small molecule inhibitor of PCSK9/LDLR interaction would be a desirable alternative in the management of hyperlipidemia, based on its ease of administration and lower cost.

This research project aimed to develop new lipid-lowering agents through two different approaches targeting: a) modulation of LDLR expression, and b) inhibition of PCSK9/LDLR interaction.

In this regard, for the first approach a small library of BBR analogues was designed and synthesized with the aim to improve the bioavailability compared to our lead compound, and shed light on the minimal structural requirements for its hypolipidemic action. The cytotoxicity of a small set of synthesized BBR analogues was evaluated by MTT assay on HepG2 and HaCaT cell lines, using BBR as reference compound. The results obtained were used to select three promising BBR analogues **18I**, **31** and **25a** which were tested to assess their ability to reduce total cholesterol (TCHO) and triglycerides (TG) levels in HepG2 cells after 48h of treatment at 5, 10 and 30 $\mu$ M. Compound **25a** proved to be the most active one showing at 30 $\mu$ M an inhibition rate of about 60% and 88% against TCHO and TG respectively. Finally, increased LDLR expression vs control was observed for **18I** and **31** by qRT-PCR analysis.

For the second approach, two sets of pyrrole derivatives were rationally designed through molecular docking studies, in order to mimic the critical residues of the LDLR implicated in the interaction with its protein partner PCSK9. Computational studies were performed using the crystallographic structure of the known PCSK9/LDLR inhibitor peptide Pep2-8 bound to PCSK9 (PDB code: 4NMX). For some synthesized putative PCSK9/LDLR inhibitors an *in vitro* binding assay (SPR) was performed, and two derivatives showed  $K_D$  lower than that of Pep2-8, used as reference compound.

# TABLE OF CONTENTS

## CHAPTER 1

<b>Introduction</b>	1
1.1 Cholesterol homeostasis	3
1.2 Dyslipidemias: classification	7
1.3 Cholesterol involvement in the pathogenesis of diseases	9
1.4 Lipid-lowering drug therapy	11
References	18

## CHAPTER 2

<b>Berberine and its therapeutic benefits</b>	25
2.1 Berberine	27
2.2 Lipid-lowering activity of BBR	28
2.3 Other pharmacological properties of BBR	32
2.3.1 <i>Anticancer activity</i>	32
2.3.2 <i>Antioxidant and anti-inflammatory activities</i>	33
2.3.3 <i>Hypoglycemic activity</i>	35
2.3.4 <i>Neuroprotective activity</i>	36
2.4 Limitations of BBR and strategies to improve its bioavailability	37
References	39

## CHAPTER 3

<b>Development of berberine analogues</b>	47
3.1 Background	49
3.2 Aim of the work	54
3.3 Synthesis of BBR and <b>1a</b>	55
3.4 Synthesis of structurally simplified BBR analogues	58
3.4.1 <i>Synthesis of 18a-l, 19a-c and 20a-e</i>	60
3.5 Biological evaluation	69
3.5.1 <i>Cell viability assay</i>	69
3.5.2 <i>Quantification of TCHO and TG</i>	74
3.5.3 <i>Real-time Quantitative Reverse Transcription PCR (qRT-PCR) analysis</i>	76

3.6 Experimental section	77
3.6.1 General	77
3.6.2 Synthesis of BBR and 17	77
3.6.3 Synthesis of 18a-f	84
3.6.4 Synthesis of 25a-d	89
3.6.5 Synthesis of 31	94
3.6.6 Synthesis of 18l	95
3.6.7 Synthesis of 19a-c	96
3.6.8 Synthesis of 20a-e	99
3.6.9 Cell viability assay	107
3.6.10 RNA isolation and reverse transcription-PCR (RT-PCR)	107
3.6.11 Quantitative Reverse Transcription PCR (qRT-PCR)	107
References	109

## CHAPTER 4

<b>PCSK9: a new target for fighting hypercholesterolemia</b>	113
4.1 PCSK9 and its role in cardiovascular diseases	115
4.2 PCSK9 gene and structure	116
4.3 PCSK9 polymorphisms	118
4.4 PCSK9–LDLR binding	119
4.5 PCSK9 inhibition strategies	122
References	125

## CHAPTER 5

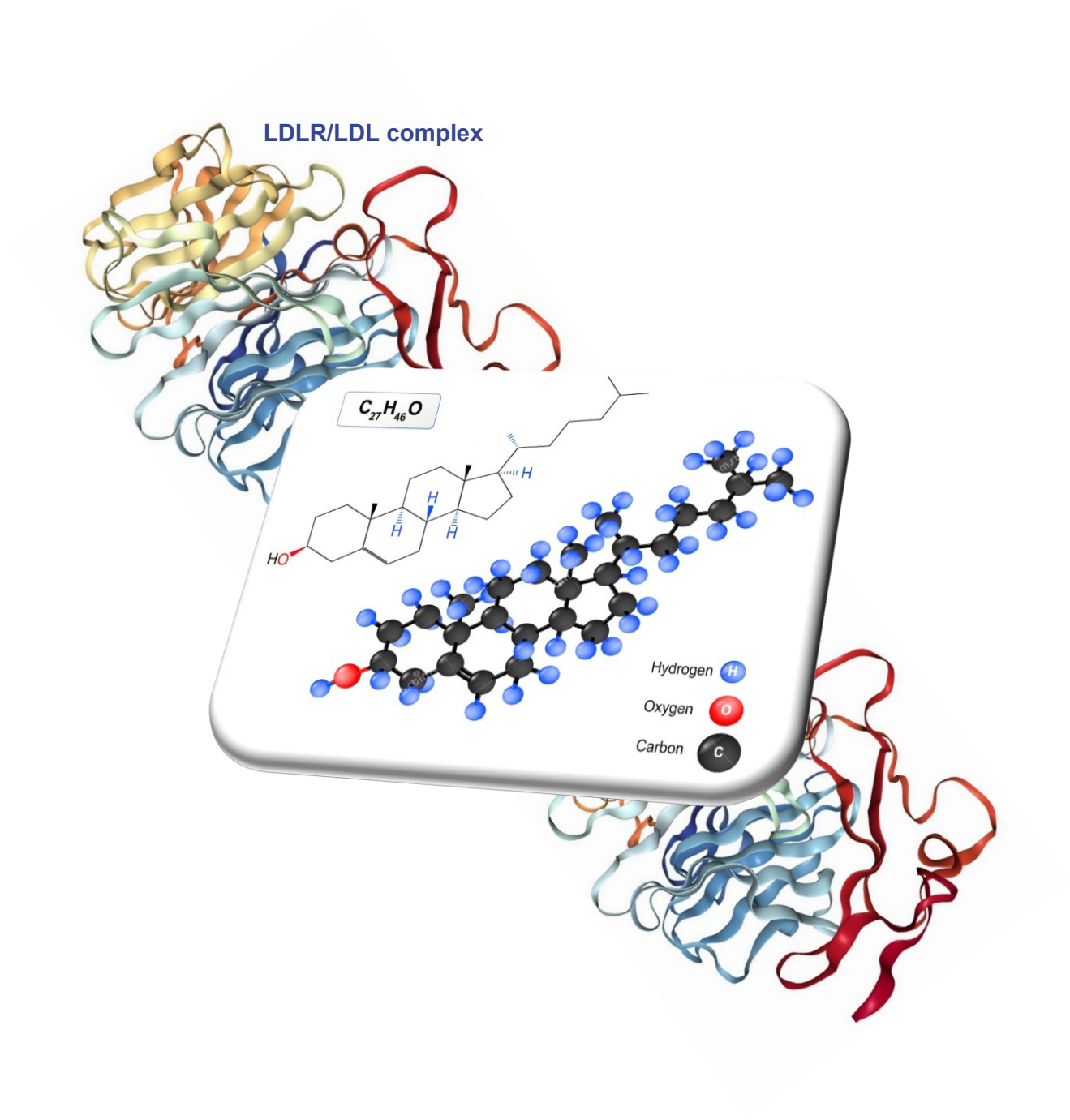
<b>Development of PCSK9/LDLR interaction inhibitors</b>	133
5.1 Background	135
5.2 Aim of the work	139
5.3 Synthesis	144
5.4 Biological evaluation	150
5.4.1 SPR binding assay	150
5.5 Molecular docking studies	153
5.6 Experimental section	156
5.6.1 General	156

5.6.2 <i>Synthesis of 49-53</i>	157
5.6.3 <i>Synthesis of 44a-g</i>	161
5.6.4 <i>General procedure for the synthesis of 44h-l</i>	164
5.6.5 <i>Synthesis of 55-60</i>	167
5.6.6 <i>General procedure for the synthesis of 45a-c</i>	170
5.6.7 <i>General procedure for the synthesis of 45d-f</i>	171
5.6.8 <i>Synthesis of 45g,h</i>	173
5.6.9 <i>Synthesis of 62-71</i>	174
5.6.10 <i>General procedure for the synthesis of 46a-c</i>	177
5.6.11 <i>Synthesis of 46d,e</i>	179
5.6.12 <i>SPR binding assay</i>	182
References	184
<b>CONCLUSIONS</b>	187
<b>APPENDIX</b>	191



# Chapter 1

## Introduction





## **1.1 Cholesterol homeostasis**

Cholesterol is a ubiquitous component of mammalian cell membranes and plays a critical role in regulating their fluidity, permeability and microstructures. It is also an important precursor for the synthesis of biomolecules essential for our body such as steroid hormones (androgens, estrogens, mineralocorticoids, etc.), bile acids and vitamin D.<sup>1</sup>

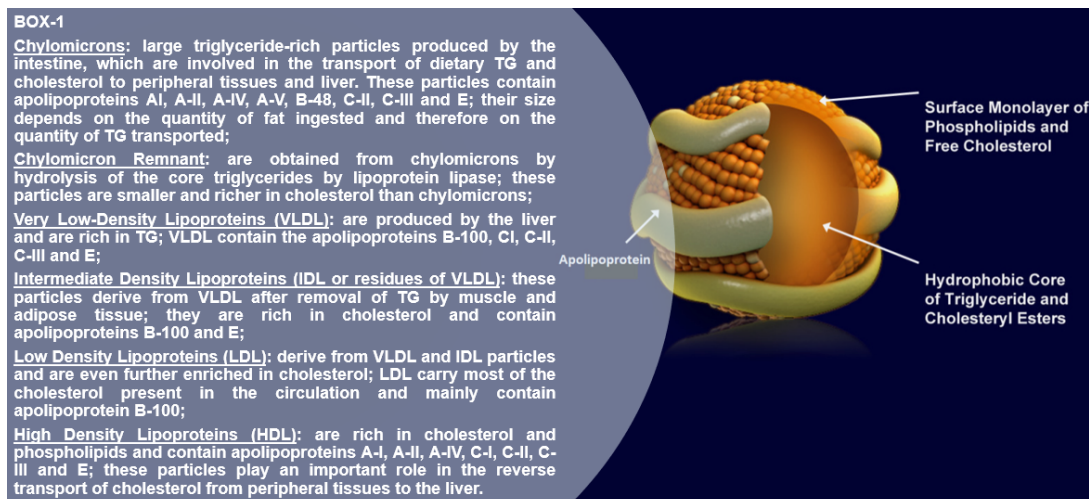
Cholesterol homeostasis includes de novo synthesis, transport, absorption and conversion into bile acids, or steroid hormones.<sup>2</sup>

One of the main organs responsible for its synthesis is the liver, but in part it is also produced in the intestine, skin and adrenal gland.<sup>1</sup>

Cholesterol is hydrophobic in nature and thus insoluble in the blood, and its transport in the bloodstream from the liver and intestine to peripheral tissues and vice versa, is carried within lipoproteins. The latter have a hydrophobic core (primarily consisting of cholesterol esters and triglycerides), surrounded by a monolayer of phospholipids and free cholesterol, all encased by apolipoproteins (Apo), which are cofactors and ligands for lipid processing enzymes.<sup>3</sup> Plasma lipoproteins are classified based on size, density (the higher the ratio of protein to lipid content the higher the density, and the smaller the size), lipid composition and apolipoprotein content (BOX-1).<sup>3</sup> For example, ApoB100 is present only in VLDL, IDL and LDL, while ApoA1 is the main apolipoprotein in HDL (70% of total protein content), followed by ApoA2. Other apolipoproteins (i.e ApoC, ApoE, ApoJ) are present in various combinations across the different lipoproteins.<sup>3</sup>

Cholesterol levels are kept constant through careful regulation of its synthesis and its absorption/elimination mechanisms, which means that when small amounts of cholesterol are ingested, absorption and synthesis are upregulated, while if the level of intake diet is high, its excretion is increased and its synthesis is decreased.<sup>4</sup>

## Chapter 1



Besides de novo biosynthesis (Figure 1.1), most mammalian cells take up cholesterol from the bloodstream via LDL receptor (LDLR).

The LDLR binds to circulating LDL, and the resulting LDLR/LDL complex is internalized by a clathrin-mediated endocytosis, and exposed to the acidic environment of endosomes. At low pH the LDLR/LDL complex dissociates, the receptor LDLR is recycled back to the cell surface (or, alternatively, it can be directed to lysosomes for degradation), while the ligand LDL is degraded and the free cholesterol is released. The latter is then exported by Niemann-Pick type C1 (NPC1) and NPC2 protein to the plasma membrane and other intracellular compartments.<sup>2</sup> Another mediator of cholesterol uptake is the NPC1-like1 (NPC1L1) on the apical surface of enterocytes, which is involved in the absorption of cholesterol from the diet.<sup>2</sup>

Although almost all mammalian cells are capable of synthesizing cholesterol, few of them are able to catabolize it, except hepatocytes and some steroid hormone-producing gland cells, in which cholesterol can be converted into bile acids and steroid hormones respectively.<sup>5</sup> In non-hepatic tissues, unable to catabolize the cholesterol, excess cholesterol is exported out by specific members of the ATP-binding cassette (ABC) transporter superfamily, i.e. ABCA1 and ABCG1. These transporters have a critical role in so-called reverse cholesterol transport (RCT), a complex process involving several stages, by which excess cholesterol in peripheral tissues is transported to the liver in form of HDL for subsequent catabolism and excretion.<sup>2</sup> RCT pathway

is particularly important in macrophages, where excess of cholesterol can promote their transformation in foam cells, the prototypical cells in the atherosclerotic plaques.<sup>2</sup> Other members of ATP-binding cassette (ABC) transporter superfamily are ABCG5 and ABCG8 (Figure 1.1). These transporters are expressed at the apical surface of enterocytes and hepatocytes, forming a heterodimer, which exports cholesterol to the intestinal lumen and bile ducts, where it is extracted by bile salts.<sup>2</sup>

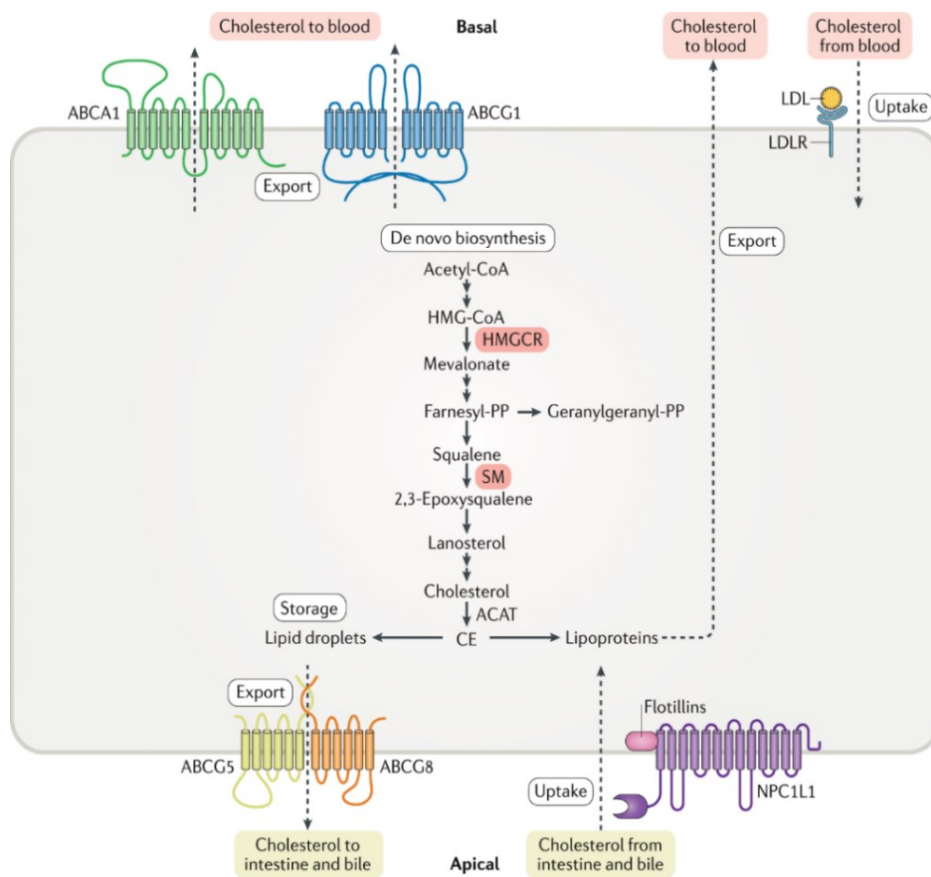


**Figure 1.1** Schematic representation of the regulation of the cholesterol homeostasis.<sup>2</sup>

Cholesterol homeostasis is also finely regulated by its abundance, and there are two main protective mechanisms adopted by cells to cope with the potential toxicity of excess free cholesterol:

- a) esterification of excess cholesterol by cholesterol acyltransferase (ACAT) and temporary storage in lipid droplets inside the cells<sup>2</sup> (Figure 1.1);

## Chapter 1

b) regulation of its biosynthesis, by the transcription factor SREBP2 (sterol regulatory element-binding protein 2). This protein, in the endoplasmic reticulum (ER), forms a complex with SCAP (SREBP-cleavage activating protein), that in turn serves a dual role as escort protein and sterol sensor. Low levels of cholesterol promote transport of SREBP2-SCAP complex from ER to the Golgi apparatus where two proteases (S1P and S2P) sequentially cleave SREBP2 to release the soluble amino-terminal transcription factor, allowing its entry into the nucleus. Here, active SREBP2 promotes the transcription of the two rate-limiting enzymes of de novo biosynthesis, HMG-CoA reductase and squalene monooxygenase, as well as LDLR expression. On the contrary, high cholesterol levels triggers a conformational change of SCAP protein, promoting its binding to an inhibitory protein known as INSIG (insulin-induced gene), and preventing the formation of SREBP2-SCAP complex. Thus SREBP2 is retained in the ER, and biosynthesis of cholesterol is inhibited.<sup>2</sup> Furthermore, ER retention of SREBP2 also modulates cholesterol uptake by decreasing the expression of NPC1L1 and LDLR and promoting the expression of the efflux transporter ABCA1 (Figure 1.1).<sup>2</sup>

Another important regulator of cholesterol homeostasis is the hepatic transcription factor X receptor (LXR), which is highly expressed in the liver, adipose tissue and macrophages. Activation of LXR by high concentrations of cholesterol leads to upregulation of the expression of ABCA1 and ABCG5/G8, which mediates cholesterol efflux into macrophages, hepatocytes and intestinal cells and downregulates NPC1L1 in intestinal cells<sup>6</sup> (Figure 1.1).

However, external risk factors (e.g. unbalanced diet, smoking, obesity, being overweight, physical inactivity, certain drugs) can affect all these protective mechanisms, and compromise their effectiveness in counteracting excess free cholesterol and progression of cholesterol-related diseases.

**1.2 Dyslipidemias: classification**

Dyslipidemias represent a group of pathologies characterized by a qualitative and quantitative alteration of blood lipids. They can occur either with an increase (hyperlipidemia), or a reduction (hypolipidemia) in the concentration of plasma lipoproteins.<sup>7</sup>

The World Health Organization (WHO), taking into account the phenotypic classification proposed by Donald Fredrickson, has classified dyslipidemias on the basis of the chemical-physical characteristics of the lipids and their content<sup>8</sup> (Table 1.1).

**Table 1.1** WHO/Frederickson classification of lipid disorders

Type	Average of overnight serum	Elevated particles	Associated clinical disorders	Serum TCHO	Serum TG
I	Creamy top layer	Chylomicrons	Lipoprotein lipase deficiency, apolipoprotein C-II deficiency	N	++
IIa	Clear	LDL	Familial hypercholesterolemia, polygenic hypercholesterolemia, nephrosis, hypothyroidism, familial combined hyperlipidemia	++	N
IIb	Clear	LDL, VLDL	Familial combined hyperlipidemia	++	+
III	Turbid	IDL	Dysbetalipoproteinemia	+	+
IV	Turbid	VLDL	Familial hypertriglyceridemia, familial combined hyperlipidemia, sporadic hypertriglyceridemia, diabetes	N+	++
V	Creamy top, turbid bottom	Chylomicrons, VLDL	Diabetes	+	++

\*IDL = intermediate-density lipoproteins; LDL = low-density lipoproteins; TC = total cholesterol; TG = triglycerides; VLDL = very low-density lipoproteins; + = increased; ++ = greatly increased; N= normal; N+ = normal or increased.

Alternatively, dyslipidemias can be classified into *primary type*, if caused by genetic mutations affecting one or more genes involved in lipoprotein metabolism, and *secondary type*, if they occur as a complication of other diseases (e.g. hypothyroidism, diabetes, obesity, hypertension, renal failure), or if associated with the intake of drugs (e.g. some types of  $\beta$ -blockers, cortisones, diuretics, contraceptives, anti-retrovirals), or with the absence of a healthy lifestyle and excessive consumption of saturated fats.<sup>7</sup>

## Chapter 1

Furthermore, dyslipidemias can be distinguished in: a) *hypercholesterolemia*, due to an increase in cholesterol only; b) *hypertriglyceridemia*, associated with an increase in triglycerides (TG) only, and c) *mixed hyperlipidemia*, due to an increase in both triglycerides and cholesterol.<sup>9</sup>

Hypercholesterolemia is the most common disorder and was reported in 39% of the world's adult population in 2008.<sup>10</sup>

Hypertriglyceridemia results from either increased TG production or decreased catabolism of TG-rich lipoproteins, and directly influences LDL and HDL composition and metabolism, which gives to TGs a critical role in the pathogenesis of atherosclerosis.

Several studies have proven the causal involvement of LDL-C in the development of atherosclerosis, and in the onset of atherothrombotic complications, such as coronary artery disease (CAD). Elevated levels of LDL-C can induce endothelial dysfunction, activate monocytes, change the vascular smooth muscle cell phenotype, and increase thrombogenicity.<sup>11</sup>

Physiological and pathological levels of circulating blood lipids are shown in Table 1.2.

**Table 1.2** *Physiopathological levels of lipids according to cardiovascular risk*

	Low	Optimum	High	Very High
TCHO (mg/dL)	–	≤200	201–240	>240
LDL-C (mg/dL)	–	≤100	101–129	>129
HDL-C (mg/dL)	<40	≥40 (men)	–	–
	<48	≥48 (women)	–	–
VLDL-C (mg/dL)	–	≤30	>30	–
ApoAI (mg/dL)	<120	≥120 (men)	–	–
	<140	≥140 (women)	–	–
ApoB (mg/dL)	20-60	≤89	90–115	>115
TG (mg/dL)	–	≤150	150–880	>880
Lp(a) (mg/dL)	–	≤50	>50	–

Like dyslipidemias, hypercholesterolemia is also divided into primary and secondary.

Among the primary hypercholesterolemia there is:

- *familial hypercholesterolemia (FH)*, in which abnormal levels of LDL cholesterol (LDL-C) are due either to mutations in the LDL receptor gene, or genetic alterations of apolipoprotein B (ApoB) or PCSK9;
- *polygenic hypercholesterolemia (PH)*, caused by the combination of genetic (e.g. mutation in several small LDL raising alleles) and environmental factors;
- *familial combined hyperlipidemia (FCHL)*, associated with an increase in the production of VLDL lipoproteins, reduced clearance of ApoB, impaired metabolism of lipoprotein particles, overall resulting in an increased amount of cholesterol and/or TG in the blood;
- *type B hypercholesterolemia*, involving a mutation of the ApoB-100 gene associated to a reduced absorption of LDL by the cell.

On the other hand, secondary hypercholesterolemia is characterized by an imbalance in the metabolism of lipoproteins caused by other pathologies and favored by many external risk factors, and usually occurs in adulthood.<sup>9,12</sup>

### **1.3 Cholesterol involvement in the pathogenesis of diseases**

It is now known that hyperlipidemia represents a serious risk factor for the development of cardiovascular disease (CVD), that is principally driven by atherosclerosis, an inflammatory process triggered by the presence of lipoprotein, essentially LDL, in the vascular wall.<sup>13,14</sup>

LDL is an atherogenic lipoprotein (the popular “bad” cholesterol) while HDL (the “good” one) is not. The atherogenicity of different lipoproteins is not related to cholesterol content, instead it is associated to the presence or absence of ApoB100. The latter is present in LDL (and also in other atherogenic lipoproteins as VLDL and IDL), but is absent in HDL. In

## Chapter 1

particular, ApoB100 promotes accumulation of LDL in the arterial intima, interacting with some constituents of extracellular matrix (e.g. chondroitin sulphate proteoglycans produced by smooth muscle cells in the arterial wall). However, it has been proposed that to initiate atherosclerosis process, LDL must undergo to oxidative modifications. Then, oxLDLs stimulate production of cytokines, promote recruitment of leukocytes (including blood monocytes, neutrophils, lymphocytes) to the arterial wall. The monocytes differentiate into macrophages, that take up modified LDL, given rise to so-call foam cells, a hallmark of early atherosclerotic lesions, also named fatty streaks. The latter evolve into plaques, some of which are “stable plaques”, endowed with a thin fibrous cap, while others are “vulnerable plaques” i.e. prone to rupture. These plaques are responsible for many vascular events including coronary lumen narrowing, and then obstruction of the blood supply, stroke, transient ischemic attack (TIA), thrombo-embolic episode(s), ischemic heart disease, and pulmonary embolism.<sup>15,16</sup>

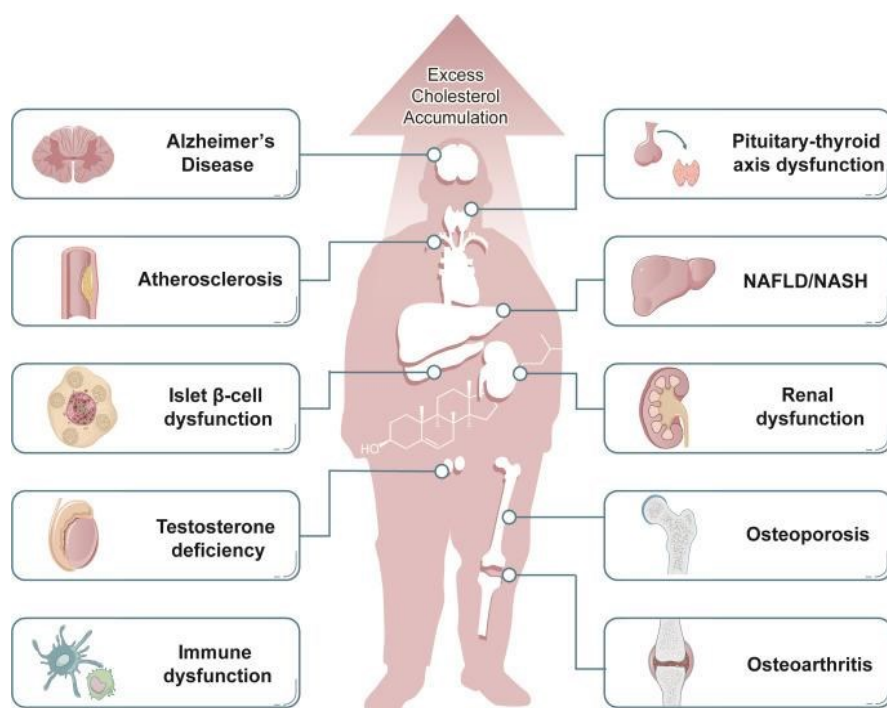


**Figure 1.2** Correlation between accumulation of excess cholesterol and pathogenesis of diseases.<sup>17</sup>

Furthermore, excess cholesterol accumulation, other than atherosclerosis, is involved in the pathogenesis of a number of diseases (Figure 1.2) including Alzheimer's disease, diabetes, immune dysfunction, hypothyroidism, renal dysfunction, osteoporosis, and osteoarthritis.<sup>18-22</sup>

It has also been evidenced that the accumulation of cholesterol in the liver plays a crucial role in the development of non-alcoholic fatty liver disease (NAFLD), and subsequent non-alcoholic steatohepatitis (NASH).<sup>23-25</sup> Finally, it has recently been observed that high cholesterol may also increase the incidence of severe COVID-19 progression.<sup>26,27</sup>

#### **1.4 Lipid-lowering drug therapy**

The main classes of lipid-lowering drugs currently in use include hydroxymethylglutaryl-CoA (HMG-CoA) reductase inhibitors (statins), cholesterol absorption inhibitors, fibric acid derivatives, bile acid sequestrants, nicotinic acid, PCSK9 inhibitors, and gene-based drugs (Figure 1.3). However, these compounds have many limitations, including drug resistance, intolerance due to their adverse side effects, and/or cost.

Statins (for example atorvastatin, simvastatin, and rosuvastatin, Figure 1.3, B) are the first line of lipid-lowering drugs, often used alone or administered in combination with other drugs in cases of statin intolerance or severe hypertriglyceridemia. Statins are competitive inhibitors of HMG-CoA reductase, a crucial rate-limiting enzyme in cholesterol biosynthesis.<sup>28</sup> This enzymatic inhibition leads to a reduction in serum LDL levels<sup>29,30</sup> (up to 63%) due to an upregulation of LDLR in the liver,<sup>31</sup> a reduction in triglycerides,<sup>32</sup> and an increase of HDL concentrations. Furthermore, statins may also reduce VLDL levels due to hepatic secretion of apolipoprotein B.<sup>33</sup> These effects depend on the statin and the dosage used. Additionally, statins, by reducing the intracellular synthesis of cholesterol, promote activation of SREBP2.<sup>34</sup> The latter upregulates hepatic expression of LDLR, leading to greater plasma clearance of LDL-C.<sup>35</sup> On the other hand, statins increase the PCSK9 protein, which binds to LDLR allowing its

## Chapter 1

lysosomal degradation. The statin-mediated increase in PCSK9 limits efficacy of statins in lowering LDL-C levels.<sup>36</sup> Although statins are among the safest lipid-lowering drugs, they have many side effects such as headache, muscle aches, tenderness or weakness (myalgia), nausea or vomiting, abdominal cramps or pain, rhabdomyolysis, new onset diabetes mellitus, and hepatotoxicity.<sup>37-39</sup>

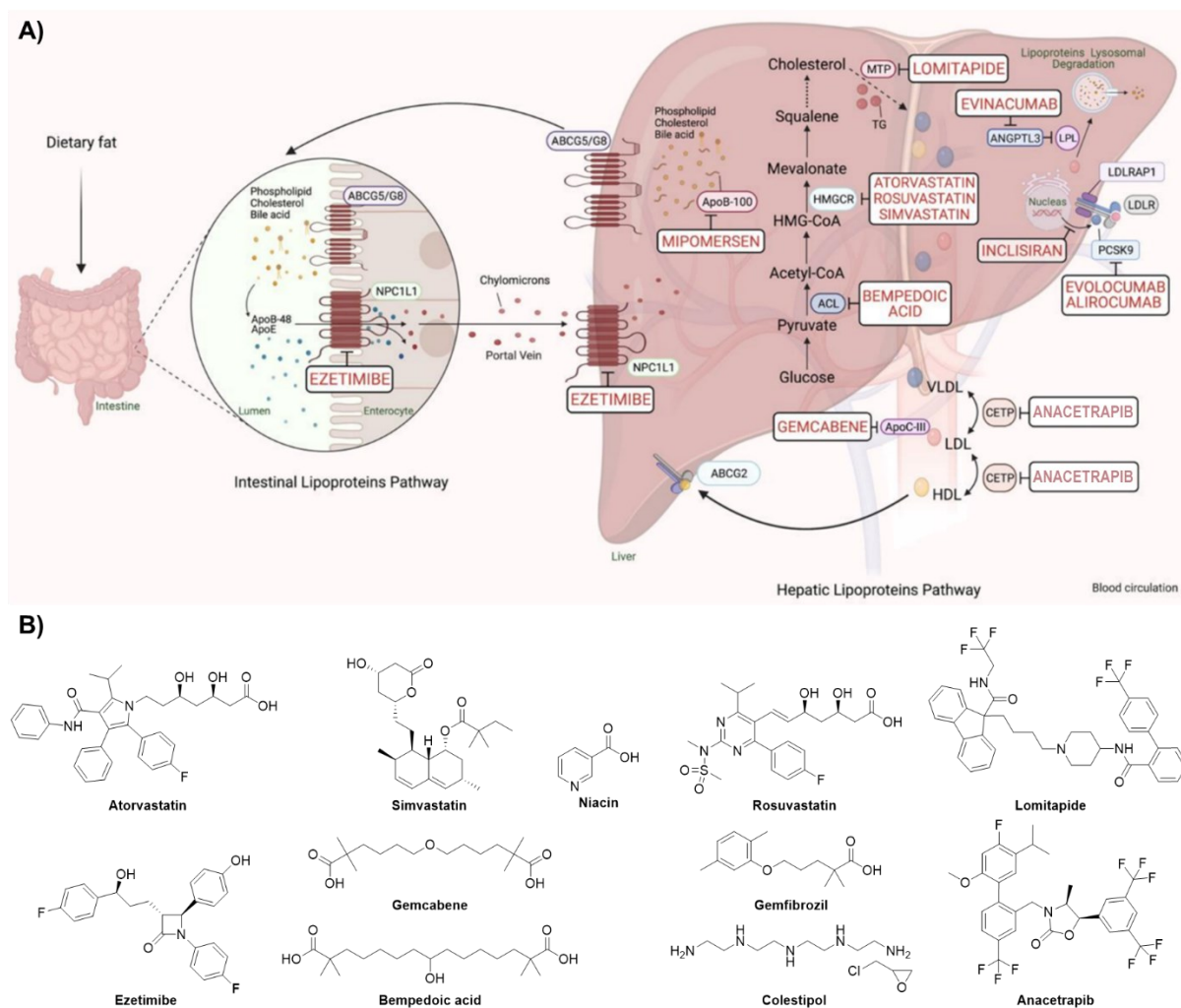


**Figure 1.3** (A) Mechanism of action and (B) chemical structures of representative lipid-lowering drugs.<sup>40</sup>

Ezetimibe (Figure 1.3, B) is used in patients with primary hyperlipidemia, mixed hyperlipidemia and familial hypercholesterolemia.<sup>41</sup> It inhibits the NPC1L1 protein present in both the gut and the liver.<sup>42,43</sup> This alters the absorption of dietary and bile cholesterol at the border of the gut brush without increasing the excretion of bile acids or inhibiting the synthesis

of cholesterol in the liver. Furthermore, ezetimibe reduces LDL cholesterol, ApoB and non-HDL cholesterol. Several studies have shown that it is reasonable to use ezetimibe as an add-on therapy to statin when statin alone fails to lower LDL-C. Moreover, ezetimibe has been co-administered with fenofibrate and bile acid sequestrants in patients with hyperlipidemia, mixed hyperlipidemia, homozygous familial hypercholesterolemia and homozygous sitosterolemia.<sup>44,45</sup> In particular, the combination with fenofibrate reduced LDL-C (22 versus 8.6%) non-HDL-C (31.6 versus 19.4%), ApoB (25.2 versus 16.2%) and TG (46.0 versus 41.8%), and increased HDL-C levels (20.9 vs 17.8%) compared to treatment with fenofibrate only.<sup>44</sup> However, ezetimibe can cause fatigue, diarrhea, headache, runny nose, muscle aches, back pain, chest pain, joint pain, sore throat, and increased serum transaminases. In addition, when used with statins, ezetimibe may increase the risk of muscle toxicity, kidney failure or hypothyroidism.<sup>46</sup>

Fibrates (e.g. gemfibrozil, Figure 1.3, B), are nuclear transcription factor peroxisome proliferator-activated receptor alpha (PPAR $\alpha$ ) agonists. This receptor downregulates apoprotein C-III (a lipoprotein lipase inhibitor) while upregulating the synthesis of apolipoprotein A-I, lipoprotein lipase and fatty acid transport protein, resulting in an increase in VLDL catabolism and elimination of triglyceride-rich particles.<sup>47</sup> Overall, its activity results in the reduction of total plasma triglycerides by up to 50% and the increase in HDL by 5 to 20%. Fibrates are primarily used to lower triglycerides preventing pancreatitis risk, while there are no outcome studies demonstrating the clinical benefit of using fibrates for LDL-C reduction or cardiovascular events. They commonly cause dyspepsia, fatigue, dizziness, pancytopenia and elevated serum transaminases.<sup>48</sup> Furthermore, gemfibrozil has never been used in combination with statins due to an increased risk of serious muscle complications.

## Chapter 1

Nicotinic acid, also known as niacin (Figure 1.3, B), significantly increases HDL-C levels, partially inhibits the release of free fatty acids from adipose tissue and increases the action of lipoprotein lipase, which in turn can increase removal rate of triglycerides from plasma.<sup>49</sup>

However, the mechanism by which nicotinic acid affects plasma lipoproteins is not fully understood. Niacin is no longer approved by the FDA for the treatment or prevention of atherosclerotic cardiovascular disease (ASCVD), since recent studies demonstrated lack of efficacy and potential harm.<sup>50,51</sup> In particular, nicotinic acid is often poorly tolerated, and can cause hot flashes, itching, paresthesia, nausea, hyperglycemia with an increased risk of diabetes mellitus, hyperuricemia, liver dysfunction, hypotension in patients taking vasodilators, increased chances of infection and bleeding as it reduces platelet function and increases prothrombin time.<sup>52-55</sup>

Bile acid sequestrants (BAS) include cholestyramine and colestipol (Figure 1.3, B), and are indicated for primary hypercholesterolemia, usually in combination with statins or nicotinic acid. They bind to bile acids in the intestine, thus hampering their reabsorption. This causes a reduction in the cholesterol pool, thus promoting the upregulation of LDL receptors and a further decrease in blood cholesterol. Furthermore, they also induce a minimal increase in HDL-C as well as triglyceride levels.<sup>56,57</sup> There are no studies yet demonstrating a clinical benefit of bile acid sequestrants (BAS) over statins for the treatment or prevention of ASCVD. However, BAS could be useful if ezetimibe and PCSK9 inhibitors are inadequate or unavailable. Bile acid sequestrants cause gastrointestinal side effects, including nausea, bloating, cramps and increased liver enzymes, and can inhibit the absorption of fat-soluble vitamins such as vitamin K and cause imbalances in clotting factors. In addition to gastrointestinal problems, BAS can interfere with the absorption of other drugs such as statins, ezetimibe, warfarin, NSAIDs and propranolol.<sup>58</sup>

PCSK9 inhibitors are a new group of drugs approved to lower LDL by up to 60% in patients taking statins. PCSK9 binds to LDLR on the surface of hepatocytes leading to its degradation by lysosomes and ultimately increasing plasma LDL-C levels. PCSK9 antibodies interfere with its binding to LDLR, allowing to higher hepatic expression of LDLR and lower plasma LDL-C levels.<sup>59</sup> The FDA has approved two mAbs alirocumab and evolocumab for adult patients with heterozygous/homozygous familial hypercholesterolemia, or ASCVD who need further lowering of LDL cholesterol in addition to diet modification and statin or ezetimibe therapy.

Common side effects of these PCSK9 inhibitors include local reactions at the injection site such as erythema, pain and bruising, and cold-like symptoms. Unlike statins, they rarely cause myalgia, while the link with early onset diabetes has still not been clearly demonstrated.<sup>60-62</sup>

However, PCSK9 monoclonal antibodies require subcutaneous injections once or twice a month and their manufacturing process is expensive, increasing the cost of therapy. For these reasons, PCSK9 mAbs are not currently recommended for primary prevention.

Based on the knowledge of the genetic mutations involved in the intrinsic or extrinsic pathways of cholesterol, new therapeutic approaches have been recently proposed that substantially improve the management of dyslipidemia including:<sup>63</sup>

- evinacumab, a monoclonal antibody that targets angiopoietin-like protein 3 (ANGPTL3). Loss of function mutations in this protein causes low levels of LDL-C, high-density lipoprotein cholesterol and triglycerides.<sup>64</sup> Evinacumab, by inhibiting ANGPTL3, leads to well-tolerated and potent triglyceride depletion of 50%, HDL-C by 30% and LDL-C by 47% by bypassing LDLR expression.<sup>65</sup> Extensive research has confirmed that this drug can be used to treat individuals with LDLR disabilities who are resistant to other hypolipidemic agents, such as PCSK9 and HMG-CoA reductase inhibitors.<sup>66,67</sup>

## Chapter 1

- bempedoic acid (Figure 1.3, B), an adenosine triphosphate citrate lyase (ACL) inhibitor and activator of AMP-activated protein kinase (AMPK) in the liver, recently approved for individuals with FH with CVD and statin intolerance;<sup>64</sup>
- gemcabene (Figure 1.3, B), that promotes the degradation of the apolipoprotein molecule by decreasing apolipoprotein C-III (ApoC-III) messenger RNA in the liver. It can significantly reduce ApoB, C-reactive protein and LDL-C by 30%, as well as increase HDL-C in patients with FH;<sup>68</sup>
- anacetrapib (Figure 1.3, B), an inhibitor of cholesterol ester transfer protein (CETP), which is a plasma protein responsible for moving triglycerides and cholesterol esters between atherogenic ApoB-lipoproteins (in particular VLDL) and HDL-C. Anacetrapib has been reported to cause a 9% reduction in major CVDs with a nearly 30% reduction in cholesterol in cases of heterozygous FH.<sup>69</sup> Compared to similar drugs that were early stopped due to their poor safety and/or efficacy over time, anacetrapib has reached Phase III clinical trial, and overall its side effects are tolerated. However, as it is stored in adipose tissues (with slow exit), long-term side effects might be evidenced.<sup>70</sup>

Finally, there are specific drugs for homozygous familial hypercholesterolemia (HoFH), a rare and severe form of FH, including two microsomal triglyceride transfer protein (MTP) inhibitors, lomitapide and mipomersen (Figure 1.3, B).

MTP is responsible for transferring TG onto ApoB in the assembly of VLDL and chylomicrons; this protein also catalyzes the transport of TG, cholesteryl esters, and phospholipids between membranes.<sup>71</sup> If transferred lipids are not enough, the emerging ApoB is destroyed, and lipoproteins secretion is inhibited.<sup>72</sup>

Lomitapide, by inhibition of MTP activity, prevents both hepatic VLDL and intestinal chylomicron secretion, and consequently lowers plasma lipids. Although lomitapide reduces LDL-C by 40-50% in HoFH<sup>72,73</sup> and is orally bioavailable, some safety concerns have been

evidenced. Indeed, it causes significant gastrointestinal side effects, including steatorrhea,<sup>74</sup> and fatty liver which can progress to cirrhosis. Instead, mipomersen is an injectable antisense oligonucleotide that inhibits the synthesis of apolipoprotein B-100. There are no data on cardiovascular outcome, but it has been shown to reduce LDL-C in homozygous FH by up to 25% when used in addition to the maximum tolerated statin dose.<sup>75</sup> However, like lomitapide, it has a significant risk of hepatic steatosis and potential for progression to cirrhosis.<sup>76</sup>

## Chapter 1

### References

1. Yang, S. T.; Kreutzberger, A. J. B.; Lee, J.; Kiessling, V.; Tamm, L. K. The role of cholesterol in membrane fusion. *Chem. Phys. Lipids*. **2016**, *199*, 136–143. doi: 10.1016/j.chemphyslip.2016.05.003
2. Luo, J.; Yang, H.; Song, B. L. Mechanisms and regulation of cholesterol homeostasis. *Nat. Rev. Mol. Cell Biol.* **2019**, *21*(4), 225–245. doi: 10.1038/s41580-019-0190-7
3. Feingold, K. R. Introduction to lipids and lipoproteins. Endotext [Internet]. **2021**, South Dartmouth (MA): MDText.com, Inc.; 2000–2001. PMID: 26247089
4. Cerqueira, N. M. F. S. A.; Oliveira, E. F.; Gesto, D. S.; Santos-Martins, D.; Moreira, C.; Moorthy, H. N.; Ramos, M. J.; Fernandes, P. A. Cholesterol biosynthesis: a mechanistic overview. *Biochemistry* **2016**, *55*(39), 5483–5506. doi: 10.1021/acs.biochem.6b00342
5. Russell, D. W. Fifty years of advances in bile acid synthesis and metabolism. *J. Lipid Res.* **2008**, *50* (Supplement), S120—S125. doi: 10.1194/jlr.r800026-jlr200
6. Mitro, N.; Mak, P. A.; Vargas, L.; Godio, C.; Hampton, E.; Molteni, V.; Kreuzsch, A.; Saez, E. The nuclear receptor LXR is a glucose sensor. *Nature* **2006**, *445*(7124), 219–223. doi: 10.1038/nature05449
7. Garg, A.; Simha, V. Update on dyslipidemia. *J. Clin. Endocrinol. Metab.* **2007**, *92*(5), 1581–1589. doi: 10.1210/jc.2007-0275
8. a) Fredrickson, D. S. An International classification of hyperlipidemias and hyperlipoproteinemias. *Ann. Intern. Med.* **1971**, *75*(3), 471. doi: 10.7326/0003-4819-75-3-471 b) <https://gpnotebook.com/simplepage.cfm?ID=-1294991318>
9. Nelson, R. H. Hyperlipidemia as a risk factor for cardiovascular disease. *Prim. Care Clin. Off. Pract.* **2013**, *40*(1), 195–211. doi: 10.1016/j.pop.2012.11.003
10. Paththinige, C.; Sirisena, N.; Dissanayake, V. Genetic determinants of inherited susceptibility to hypercholesterolemia – a comprehensive literature review. *Lipids Health Dis.* **2017**, *16*(1), 103. doi: 10.1186/s12944-017-0488-4
11. Badimon, L.; Vilahur, G. LDL-cholesterol versus HDL-cholesterol in the atherosclerotic plaque: inflammatory resolution versus thrombotic chaos. *Ann. N. Y. Acad. Sci.* **2012**, *1254*(1), 18–32. doi: 10.1111/j.1749-6632.2012.06480.x
12. Aboshahba, A. New trends approved in management of dyslipidaemia. *J. Clin. Cardiol. Card. Ther.* **2019**, *14*(4), 555894. doi: 10.19080/jocct.2019.14.555894
13. Badimon, L.; Martinez-Gonzalez, J.; Lorente-Cortes, V.; Rodriguez, C.; Padro, T. Cell biology and lipoproteins in atherosclerosis. *Curr. Mol. Med.* **2006**, *6*(5), 439–456. doi: 10.2174/156652406778018725
14. Storey, R.; Vilahur, G.; Badimon, L. Update on lipids, inflammation and atherothrombosis. *Thromb. Haemost.* **2011**, *105*(S 06), S34—S42. doi: 10.1160/th10-11-071

15. Goff, D. C.; Lloyd-Jones, D. M.; Bennett, G.; Coady, S.; D'Agostino, R. B. Sr; Gibbons, R.; Greenland, P.; Lackland, D. T.; Levy, D.; O'Donnell, C. J.; Robinson, J. G.; Sanford Schwartz, J.; Shero, S. T.; Smith, S. C. Jr; Sorlie, P.; Stone, N. J.; Wilson, P. W. F. 2013 ACC/AHA guideline on the assessment of cardiovascular risk. *J. Am. Coll. Cardiol.* **2014**, *63*(25), 2935–2959. doi: 10.1016/j.jacc.2013.11.005
16. National Cholesterol Education Program (NCEP) Expert Panel on Detection, Evaluation, and Treatment of High Blood Cholesterol in Adults (Adult Treatment Panel III). Third report of the national cholesterol education program (NCEP) expert panel on detection, evaluation, and treatment of high blood cholesterol in adults (adult treatment panel III) final report. *Circulation* **2002**, *106*(25), 3143–3421. PMID: 12485966
17. Song, Y.; Liu, J.; Zhao, K.; Gao, L.; Zhao, J. Cholesterol-induced toxicity: an integrated view of the role of cholesterol in multiple diseases. *Cell Metab.* **2021**, *33*(10), 1911–1925. doi: 10.1016/j.cmet.2021.09.001
18. Zambón, D.; Quintana, M.; Mata, P.; Alonso, R.; Benavent, J.; Cruz-Sánchez, F.; Gich, J.; Pocovi M.; Civeira, F.; Capurro, S.; Bachman, D.; Sambamurti, K.; Nicholas, J.; Pappolla, M. A. Higher incidence of mild cognitive impairment in familial hypercholesterolemia. *Am. J. Med.* **2010**, *123*(3), 267–274. doi: 10.1016/j.amjmed.2009.08.015
19. Fryirs, M.; Barter, P. J.; Rye, K.-A. Cholesterol metabolism and pancreatic  $\beta$ -cell function. *Curr. Opin. Lipidol.* **2009**, *20*(3), 159–164. doi: 10.1097/mol.0b013e32832ac180
20. Perego, C.; Da Dalt, L.; Pirillo, A.; Galli, A.; Catapano, A. L.; Norata, G. D. Cholesterol metabolism, pancreatic  $\beta$ -cell function and diabetes. *Biochim. Biophys. Acta. Mol. Basis. Dis.* **2019**, *1865*(9), 2149–2156. doi:10.1016/j.bbadis.2019.04.012
21. Li, X.; Zhen, D.; Zhao, M.; Liu, L.; Guan, Q.; Zhang, H.; Ge, S.; Tang, X.; Gao, L. Natural history of mild subclinical hypothyroidism in a middle-aged and elderly Chinese population: a prospective study. *Endocr. J.* **2017**, *64*(4), 437–447. doi: 10.1507/endocrj.ej16-0549
22. Yerges-Armstrong, L. M.; Shen, H.; Ryan, K. A.; Streeten, E. A.; Shuldiner, A. R.; Mitchell, B. D. Decreased bone mineral density in subjects carrying familial defective apolipoprotein B-100. *J. Clin. Endocrinol. Metab.* **2013**, *98*(12), E1999—E2005. doi: 10.1210/jc.2013-2471
23. Gan, L. T.; Van Rooyen, D. M.; Koina, M. E.; McCuskey, R. S.; Teoh, N. C.; Farrell, G. C. Hepatocyte free cholesterol lipotoxicity results from JNK1-mediated mitochondrial injury and is HMGB1 and TLR4-dependent. *J. Hepatol.* **2014**, *61*(6), 1376–1384. doi: 10.1016/j.jhep.2014.07.024
24. Marí, M.; Morales, A.; Colell, A.; García-Ruiz, C.; Fernández-Checa, J. C. Mitochondrial cholesterol accumulation in alcoholic liver disease: role of ASMase and endoplasmic reticulum stress. *Redox Biol.* **2014**, *3*, 100–108. doi: 10.1016/j.redox.2014.09.005
25. Tirosh, O. Hypoxic signaling and cholesterol lipotoxicity in fatty liver disease progression. *Oxid. Med. Cell. Longev.* **2018**, *2018*, 2548154. doi: 10.1155/2018/2548154

## Chapter 1

26. Radenkovic, D.; Chawla, S.; Pirro, M.; Sahebkar, A.; Banach, M. Cholesterol in relation to COVID-19: should we care about it? *J. Clin. Med.* **2020**, *9*(6), 1909. doi: 10.3390/jcm9061909
27. Cao, X.; Yin, R.; Albrecht, H.; Fan, D.; Tan, W. Cholesterol: a new game player accelerating vasculopathy caused by SARS-CoV-2? *Am. J. Physiol. Endoc. Metab.* **2020**, *319*(1), E197–E202. doi: 10.1152/ajpendo.00255.2020
28. Istvan, E. S.; Deisenhofer, J. Structural mechanism for statin inhibition of HMG-CoA reductase. *Science* **2001**, *292*(5519), 1160–1164. doi: 10.1126/science.1059344
29. Larsen, M. L.; Illingworth, D. R. Drug treatment of dyslipoproteinemia. *Med. Clin. North Am.* **1994**, *78*(1), 225–245. doi: 10.1016/s0025-7125(16)30184-5
30. Levy, R. I.; Troendle, A. J.; Fattu, J. M. A quarter century of drug treatment of dyslipoproteinemia, with a focus on the new HMG-CoA reductase inhibitor fluvastatin. *Circulation* **1993**, *87*(4 Suppl), III45–III53. PMID: 8462180
31. Ness, G. C.; Zhao, Z.; Lopez, D. Inhibitors of cholesterol biosynthesis increase hepatic low-density lipoprotein receptor protein degradation. *Arch. Biochem. Biophys.* **1996**, *325*(2), 242–248. doi: 10.1006/abbi.1996.0030
32. Bakker-Arkema, R. G.; Davidson, M. H.; Goldstein, R. J.; Davignon, J.; Isaacsohn, J. L.; Weiss, S. R.; Keilson, L. M.; Brown, W. V.; Miller, V. T.; Shurzinske, L. J.; Black, D. M. Efficacy and safety of a new HMG-CoA reductase inhibitor, atorvastatin, in patients with hypertriglyceridemia. *JAMA* **1996**, *275*(2), 128–133. PMID: 8531308.
33. Conde, K.; Vergara-Jimenez, M.; Krause, B. R.; Newton, R. S.; Fernandez, M. L. Hypocholesterolemic actions of atorvastatin are associated with alterations on hepatic cholesterol metabolism and lipoprotein composition in the guinea pig. *J. Lipid Res.* **1996**, *37*(11), 2372–2382. PMID: 8978489
34. Attie, A. D.; Seidah, N. G. Dual regulation of the LDL receptor--some clarity and new questions. *Cell Metab.* **2005**, *1*(5), 290–292. doi: 10.1016/j.cmet.2005.04.006
35. Horton, J. D.; Goldstein, J. L.; Brown, M. S. SREBPs: activators of the complete program of cholesterol and fatty acid synthesis in the liver. *J. Clin. Investig.* **2002**, *109*(9), 1125–1131. doi: 10.1172/JCI15593
36. Dubuc, G.; Chamberland, A.; Wassef, H.; Davignon, J.; Seidah, N. G.; Bernier, L.; Prat, A. Statins upregulate PCSK9, the gene encoding the proprotein convertase neural apoptosis-regulated convertase-1 implicated in familial hypercholesterolemia. *Arterioscler. Thromb. Vasc. Biol.* **2004**, *24*(8), 1454–1459. doi: 10.1161/01.ATV.0000134621.14315.43
37. Hu, M.; Cheung, B. M.; Tomlinson, B. Safety of statins: an update. *Ther. Adv. Drug Saf.* **2012**, *3*(3), 133–144. doi: 10.1177/2042098612439884

38. Rosenson, R. S.; Baker, S. K.; Jacobson, T. A.; Kopecky, S. L.; Parker, B. A. The national lipid association's muscle safety expert panel. An assessment by the statin muscle safety task force: 2014 update. *J. Clin. Lipidol.* **2014**, *8*(3 Suppl), S58–S71. doi: 10.1016/j.jacl.2014.03.004
39. Stroes, E. S.; Thompson, P. D.; Corsini, A.; Vladutiu, G. D.; Raal, F. J.; Ray, K. K.; Roden, M.; Stein, E.; Tokgözoğlu, L.; Nordestgaard, B. G.; Bruckert, E.; De Backer, G.; Krauss, R. M.; Laufs, U.; Santos, R. D.; Hegele, R. A.; Hovingh, G. K.; Leiter, L. A.; Mach, F.; März, W. European atherosclerosis society consensus panel. Statin-associated muscle symptoms: impact on statin therapy-european atherosclerosis society consensus panel statement on assessment, aetiology and management. *Eur. Heart J.* **2015**, *36*(17), 1012–1022. doi: 10.1093/eurheartj/ehv043
40. Hindi, N. N.; Alenbawi, J.; Nemer, G. Pharmacogenomics variability of lipid-lowering therapies in familial hypercholesterolemia. *J. Pers. Med.* **2021**, *11*(9), 877. doi: 10.3390/jpm11090877
41. Sizar, O.; Nassereddin, A.; Talati, R. Ezetimibe. StatPearls [Online] **2021**. PMID: 30422474.
42. Altmann, S. W.; Davis Jr, H. R.; Zhu, L. J.; Yao, X.; Hoos, L. M.; Tetzloff, G.; Iyer, S. P.; Maguire, M.; Golovko, A.; Zeng, M.; Wang, L.; Murgolo, N.; Graziano, M. P. Niemann-Pick C1 Like 1 protein is critical for intestinal cholesterol absorption. *Science* **2004**, *303*(5661), 1201–1204. doi: 10.1126/science.1093131
43. Temel, R. E.; Tang, W.; Ma, Y.; Rudel, L. L.; Willingham, M. C.; Ioannou, Y. A.; Davies, J. P.; Nilsson, L. M.; Yu, L. Hepatic Niemann-Pick C1-like 1 regulates biliary cholesterol concentration and is a target of ezetimibe. *J. Clin. Investig.* **2007**, *117*(7), 1968–1978. doi: 10.1172/JCI30060
44. Farnier, M. Update on the clinical utility of fenofibrate in mixed dyslipidemias: mechanisms of action and rational prescribing. *Vasc. Health Risk Manag.* **2008**, *4*(5), 991–1000. doi: 10.2147/vhrm.s3390
45. Bays, H.; Rhyne, J.; Abby, S.; Lai, Y. L.; Jones, M. Lipid-lowering effects of colesevelam HCl in combination with ezetimibe. *Curr. Med. Res. Opin.* **2006**, *22*(11), 2191–2200. doi: 10.1185/030079906X148436
46. Patel, J.; Sheehan, V.; Gurk-Turner, C. Ezetimibe (Zetia): a new type of lipid-lowering agent. *Proc. (Bayl. Univ. Med. Cent.)* **2003**, *16*(3), 354–358. doi: 10.1080/08998280.2003.11927928
47. Rubins, H. B.; Robins, S. J.; Collins, D.; Fye, C. L.; Anderson, J. W.; Elam, M. B.; Faas, F. H.; Linares, E.; Schaefer, E. J.; Schectman, G.; Wilt, T. J.; Wittes, J. Gemfibrozil for the secondary prevention of coronary heart disease in men with low levels of high-density lipoprotein cholesterol. Veterans affairs high-density lipoprotein cholesterol intervention trial study group. *N. Engl. J. Med.* **1999**, *341*(6), 410–418. doi: 10.1056/NEJM199908053410604
48. Keech, A.; Simes, R. J.; Barter, P.; Best, J.; Scott, R.; Taskinen, M. R.; Forder, P.; Pillai, A.; Davis, T.; Glasziou, P.; Drury, P.; Kesäniemi, Y. A.; Sullivan, D.; Hunt, D.; Colman, P.; d'Emden, M.; Whiting, M.; Ehnholm, C.; Laakso, M. Effects of long-term fenofibrate therapy on cardiovascular events in 9795 people with type 2 diabetes mellitus (the FIELD study): randomised controlled trial. *Lancet* **2005**, *366*(9500), 1849–1861. doi: 10.1016/S0140-6736(05)67667-2

## Chapter 1

49. Grundy, S. M.; Mok, H. Y.; Zech, L.; Berman, M. Influence of nicotinic acid on metabolism of cholesterol and triglycerides in man. *J. Lipid Res.* **1981**, *22*(1), 24–36. doi: 10.1016/S0022-2275(20)34737-4
50. Boden, W. E.; Probstfield, J. L.; Anderson, T.; Chaitman, B. R.; Desvignes-Nickens, P.; Koprowicz, K.; McBride, R.; Teo, K.; Weintraub, W. Niacin in patients with low HDL cholesterol levels receiving intensive statin therapy. *N. Engl. J. Med.* **2011**, *365*(24), 2255–2267. doi: 10.1056/NEJMoa1107579
51. Adhyaru, B. B.; Jacobson, T. A. Role of non-statins, LDL-C thresholds, and special population considerations: a look at the updated 2016 ACC Consensus Committee Recommendations. *Curr. Atheroscler. Rep.* **2017**, *19*(6), 29. doi: 10.1007/s11883-017-0666-x
52. Illingworth, D. R.; Stein, E. A.; Mitchel, Y. B.; Dujovne, C. A.; Frost, P. H.; Knopp, R. H.; Tun, P.; Zupkis, R. V.; Greguski, R. A. Comparative effects of lovastatin and niacin in primary hypercholesterolemia. A prospective trial. *Arch. Intern. Med.* **1994**, *154*(14), 1586–1595. doi: 10.1001/archinte.1994.00420140051007
53. Grundy, S. M.; Vega, G. L.; McGovern, M. E.; Tulloch, B. R.; Kendall, D. M.; Fitz-Patrick, D.; Ganda, O. P.; Rosenson, R. S.; Buse, J. B.; Robertson, D. D.; Sheehan, J. P. Diabetes multicenter research group efficacy, safety, and tolerability of once-daily niacin for the treatment of dyslipidemia associated with type 2 diabetes: results of the assessment of diabetes control and evaluation of the efficacy of Niaspan trial. *Arch. Intern. Med.* **2002**, *162*(14), 1568–1576. doi: 10.1001/archinte.162.14.1568
54. Pasternak, R. C.; Kolman, B. S. Unstable myocardial ischemia after the initiation of niacin therapy. *Am. J. Cardiol.* **1991**, *67*(9), 904–906. doi: 10.1016/0002-9149(91)90631-t
55. Garg, R.; Malinow, M.; Pettinger, M.; Upson, B.; Hunninghake, D. Niacin treatment increases plasma homocyst(e)ine levels. *Am. Heart J.* **1999**, *138*(6 Pt 1), 1082–1087. doi: 10.1016/s0002-8703(99)70073-6
56. Shepherd, J.; Packard, C. J.; Morgan, H. G.; Third, J. L.; Stewart, J. M.; Lawrie, T. D. The effects of cholestyramine on high density lipoprotein metabolism. *Atherosclerosis* **1979**, *33*(4), 433–444. doi: 10.1016/0021-9150(79)90036-4
57. Davidson, M. H.; Dillon, M. A.; Gordon, B.; Jones, P.; Samuels, J.; Weiss, S.; Isaacsohn, J.; Toth, P.; Burke, S. K. Colesevelam hydrochloride (cholestagel): a new, potent bile acid sequestrant associated with a low incidence of gastrointestinal side effects. *Arch. Intern. Med.* **1999**, *159*(16), 1893–1900. doi: 10.1001/archinte.159.16.1893
58. Jacobson, T. A.; Armani, A.; McKenney, J. M.; Guyton, J. R. Safety considerations with gastrointestinally active lipid-lowering drugs. *Am. J. Cardiol.* **2007**, *99*(6A), 47C–55C. doi: 10.1016/j.amjcard.2006.11.022
59. Mullard, A. Cholesterol-lowering blockbuster candidates speed into Phase III trials. *Nat. Rev. Drug Discov.* **2012**, *11*(11), 817–819. doi: 10.1038/nrd3879

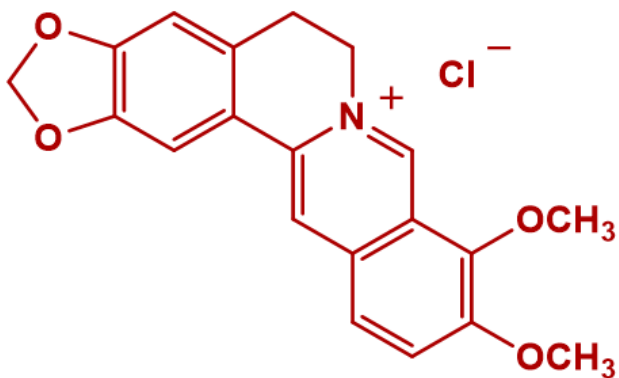
60. Robinson, J. G.; Farnier, M.; Krempf, M.; Bergeron, J.; Luc, G.; Averna, M.; Stroes, E. S.; Langslet, G.; Raal, F. J.; El Shahawy, M.; Koren, M. J.; Lepor, N. E.; Lorenzato, C.; Pordy, R.; Chaudhari, U.; Kastelein, J. J. P. Efficacy and safety of alirocumab in reducing lipids and cardiovascular events. *N. Engl. J. Med.* **2015**, *372*(16), 1489–1499. doi: 10.1056/NEJMoa1501031
61. Sabatine, M. S.; Giugliano, R. P.; Wiviott, S. D.; Raal, F. J.; Blom, D. J.; Robinson, J.; Ballantyne, C. M.; Somaratne, R.; Legg, J.; Wasserman, S. M.; Scott, R.; Koren, M. J.; Stein, E. A. Efficacy and safety of evolocumab in reducing lipids and cardiovascular events. *N. Engl. J. Med.* **2015**, *372*(16), 1500–1509. doi: 10.1056/NEJMoa1500858
62. Zhang, X. L.; Zhu, Q. Q.; Zhu, L.; Chen, J. Z.; Chen, Q. H.; Li, G. N.; Xie, J.; Kang, L. N.; Xu, B. Safety and efficacy of anti-PCSK9 antibodies: a meta-analysis of 25 randomized, controlled trials. *BMC Med.* **2015**, *13*, 123. doi: 10.1186/s12916-015-0358-8
63. Wang, L.; Muthuramu, I.; Somanathan, S.; Zhang, H.; Bell, P.; He, Z.; Yu, H.; Zhu, Y.; Tretiakova, A.P.; Wilson, J. M. Developing a second-generation clinical candidate AAV vector for gene therapy of familial hypercholesterolemia. *Mol. Ther. Methods Clin. Dev.* **2021**, *22*, 1–10. doi: 10.1016/j.omtm.2021.04.017
64. Corrigendum to: 2019 ESC/EAS Guidelines for the management of dyslipidaemias: lipid modification to reduce cardiovascular risk. *Eur. Heart J.* **2020**, *41*(44), 4255. doi: 10.1093/eurheartj/ehz826
65. Kuehn, B. M. Evinacumab approval adds a new option for homozygous familial hypercholesterolemia with a hefty price tag. *Circulation* **2021**, *143*(25), 2494–2496. doi: 10.1161/CIRCULATIONAHA.121.055463
66. Gaudet, D.; Gipe, D. A.; Pordy, R.; Ahmad, Z.; Cuchel, M.; Shah, P. K.; Chyu, K. Y.; Sasiela, W. J.; Chan, K. C.; Brisson, D.; Khoury, E.; Banerjee, P.; Gusarova, V.; Gromada, J.; Stahl, N.; Yancopoulos, G. D.; Hovingh, G. K. ANGPTL3 inhibition in homozygous familial hypercholesterolemia. *N. Engl. J. Med.* **2017**, *377*(3), 296–297. doi: 10.1056/NEJMc1705994
67. Banerjee, P.; Chan, K. C.; Tarabocchia, M.; Benito-Vicente, A.; Alves, A. C.; Uribe, K. B.; Bourbon, M.; Skiba, P. J.; Pordy, R.; Gipe, D. A.; Gaudet, D.; Martin, C. Functional analysis of LDLR (low-density lipoprotein receptor) variants in patient lymphocytes to assess the effect of Evinacumab in homozygous familial hypercholesterolemia patients with a spectrum of LDLR activity. *Arterioscler. Thromb. Vasc. Biol.* **2019**, *39*(11), 2248–2260. doi: 10.1161/ATVBAHA.119.313051
68. Gaudet, D.; Durst, R.; Lepor, N.; Bakker-Arkema, R.; Bisgaier, C.; Masson, L.; Golden, L.; Kastelein, J. J.; Hegele, R. A.; Stein, E. Usefulness of Gemcabene in homozygous familial hypercholesterolemia (from COBALT-1). *Am. J. Cardiol.* **2019**, *124*(12), 1876–1880. doi: 10.1016/j.amjcard.2019.09.010
69. Arai, H.; Teramoto, T.; Daida, H.; Ikewaki, K.; Maeda, Y.; Nakagomi, M.; Shirakawa, M.; Kakikawa, T.; Numaguchi, H.; Johnson-Levonas, A.O.; Vaidya, S.; Blaustein, R.O. Efficacy and safety of the cholesteryl ester transfer protein inhibitor anacetrapib in Japanese patients with heterozygous familial hypercholesterolemia. *Atherosclerosis* **2016**, *249*, 215–223. doi: 10.1016/j.atherosclerosis.2016.03.017

## **Chapter 1**

70. Bowman, L.; Hopewell, J. C.; Chen, F.; Wallendszus, K.; Stevens, W.; Collins, R.; Wiviott, S. D.; Cannon, C. P.; Braunwald, E.; Sammons, E. Effects of Anacetrapib in patients with atherosclerotic vascular disease. *N. Engl. J. Med.* **2017**, *377*(13), 1217–1227. doi: 10.1056/NEJMoa1706444
71. Hussain, M. M.; Rava, P.; Walsh, M.; Rana, M.; Iqbal, J. Multiple functions of microsomal triglyceride transfer protein. *Nutr. Metab.* **2012**, *9*, 14. doi: 10.1186/1743-7075-9-14
72. Hussain, M. M.; Bakillah, A. New approaches to target microsomal triglyceride transfer protein. *Curr. Opin. Lipidol.* **2008**, *19*(6), 572–578. doi: 10.1097/MOL.0b013e328312707c
73. Lilly, S. M.; Rader, D. J. New targets and emerging therapies for reducing LDL cholesterol. *Curr. Opin. Lipidol.* **2007**, *18*(6), 650–655. doi: 10.1097/MOL.0b013e3282f169c6
74. Cuchel, M.; Meagher, E. A.; du Toit Theron, H.; Blom, D. J.; Marais, A. D.; Hegele, R. A.; Averna, M. R.; Sirtori, C. R.; Shah, P. K.; Gaudet, D.; Stefanutti, C.; Vigna, G. B.; Du Plessis, A. M. E.; Probert, K. J.; Sasiela, W. J.; Bloedon, L. T.; Rader, D. J. Efficacy and safety of a microsomal triglyceride transfer protein inhibitor in patients with homozygous familial hypercholesterolaemia: a single-arm, open-label, phase 3 study. *Lancet* **2013**, *381*(9860), 40–46. doi: 10.1016/S0140-6736(12)61731-0
75. Blom, D. J.; Raal, F. J.; Santos, R. D.; Marais, A. D. Lomitapide and mipomersen-inhibiting microsomal triglyceride transfer protein (MTP) and ApoB100. *Curr. Atheroscler. Rep.* **2019**, *21*(12), 48. doi: 10.1007/s11883-019-0809-3
76. Cicero, A. F.; Tartagni, E.; Ertek, S. Safety and tolerability of injectable lipid-lowering drugs: a review of available clinical data. *Expert Opin. Drug Saf.* **2014**, *13*(8), 1023–1030. doi: 10.1517/14740338.2014.932348

# Chapter 2

## Berberine and Its Therapeutic Benefits





## 2.1 Berberine

Berberine (**1**, BBR, Figure 2.1) is a quaternary ammonium salt, (usually used as BBR chloride, hemisulfate or sulfate), derived from the protoberberine group of benzyloquinoline alkaloids.

In 1824, Hüttenschmid extracted from the bark of a plant that he believed to be *Geoffroya inermis*, a deep yellow substance and named it jamaicine. In 1826, Chevallier and Pelletan found a yellow alkaloid in the bark of *Xanthoxylum clava herculis*, and named it xanthopicrite. A few years later, these substances were found to be identical to berberine, isolated by Buchner and Herberger from *Berberis vulgaris* in 1830.<sup>1</sup>

BBR is usually found in the roots, rhizomes, stems, and bark of plants belonging to the Barberidaceae family such as *Berberis vulgaris* and *Berberis aquifolium*, as well as in other species used in traditional medicine including *Argemone mexicana*, *Thalictrum flavum*, *Hydrastis canadensis*, *Coptis japonica*, *Coptis chinensis*, *Phellodendron amurense*.<sup>2</sup>



**Figure 2.1** Chemical structure of BBR.

The classical extraction techniques used for isolation of berberine are based on maceration, percolation, Soxhlet extraction, using different solvent systems such as methanol, ethanol, chloroform, aqueous and/or acidified mixtures. Berberine's sensitivity to light and heat is the main challenge for its extraction. Hence, exposure to high temperature and light could lead to berberine degradation and thus affect its matrix recovery.<sup>3</sup>

## **Chapter 2**

Recently, alternative methods have been employed that improve the efficiency of the extraction process, including Microwave-Assisted Extraction (MAE), Ultrasound-Assisted Extraction (UAE), Ultrahigh-Pressure Extraction (UPE) and Supercritical Fluid Extraction (SFE). These techniques, aside from reducing both extraction times and volume of extraction solvent used, are simple, efficient, environmentally friendly and economical.<sup>3</sup>

BBR has multiple pharmacological effects, including antimicrobial, hypoglycemic, cholesterol-lowering, neuroprotective, anticancer and immunomodulatory properties.

The cholesterol-lowering effect of BBR was first noted in 1989 when it was observed that BBR lowered intracellular cholesterol in cultured human aortic intima cells.<sup>4</sup> However, its potential health benefits were overlooked until it was discovered (only in 2004) that BBR significantly lowered blood cholesterol levels in vivo in both humans and hamsters.<sup>5,6</sup> Since then, berberine has received a significant amount of attention, and a large number of studies have been made to understand the mechanisms involved in its hypolipidemic activity.<sup>6-11</sup>

### **2.2 Lipid-lowering activity of BBR**

Berberine shows a significant lipid-lowering activity through the regulation of different pathways (Figure 2.2-2.4).

In particular, it reduces triglycerides (TG) levels through the regulation of (Figure 2.2):

- a) *fatty acids oxidation (FAO)*: BBR promotes fatty acid oxidation, thus reducing the free fatty acids pool required for hepatic TG biosynthesis. BBR inhibits mitochondrial respiratory chain complex I, the first enzyme of the respiratory chain, leading to a change in the ATP/AMP ratio and AMPK activation.<sup>12-14</sup> The latter increases the expression of mitochondrial uncoupling proteins UCP1/UCP2 and other thermogenic proteins<sup>10,15,16</sup> in the adipose tissue, enhancing the breakdown of TG. Moreover, AMPK promotes FAO process also through inhibition of acetyl-CoA carboxylase (ACC),<sup>14,17</sup> that catalyzes the carboxylation of acetyl-CoA to malonyl-

CoA. Malonyl-CoA is a substrate for fatty acid synthase (FAS) and indirectly inhibits FAO since it is an allosteric inhibitor of carnitine palmitoyl-transferase 1 (CPT1), an enzyme involved in the translocation of fatty acids from the cytosol to mitochondrial matrix where FAO occurs. Furthermore, it has been reported that BBR is a potent PPAR $\alpha$  agonist, with an affinity similar to that of fenofibrate, and through PPAR $\alpha$  activation it can upregulate the expression of several lipid-lowering genes, accelerating fatty acids degradation.<sup>18,19</sup> Moreover, BBR also upregulates the expression of PPAR $\alpha$  at both mRNA and protein level;<sup>10</sup>

- b) *fatty acids hydrolysis*: BBR, through activation of AMPK kinase, increases the expression of two rate-limiting enzymes catalyzing the hydrolysis of triglycerides in adipocytes, i.e. adipose triglyceride lipase (ATGL) and hormone sensitive lipase (HSL);<sup>20,21</sup>
- c) *fatty acids synthesis (lipogenesis)*: BBR-induced AMPK activation also downregulates the expression of important transcriptional factors, which regulate triglycerides synthesis and fatty acid oxidation in the liver, such as C/EBP $\alpha$ , SREBP1c, and ChREBP.<sup>22,23</sup>

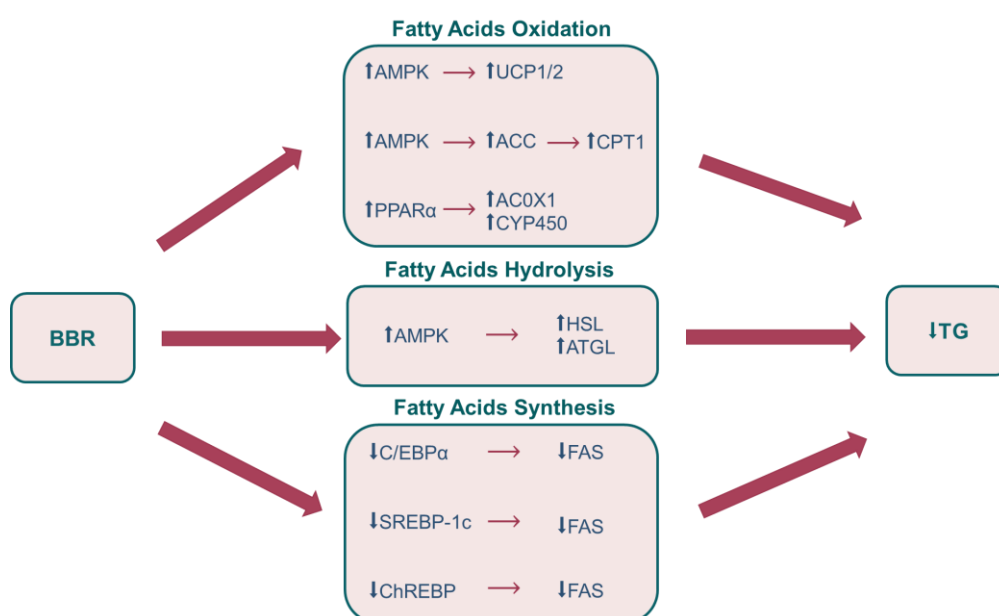


**Figure 2.2** TG-lowering activity of BBR.

## Chapter 2

BBR lowers total cholesterol (TCHO) levels mainly through two mechanisms: 1) stabilization of LDLR mRNA, and 2) upregulation of LDLR mRNA expression (Figure 2.3).

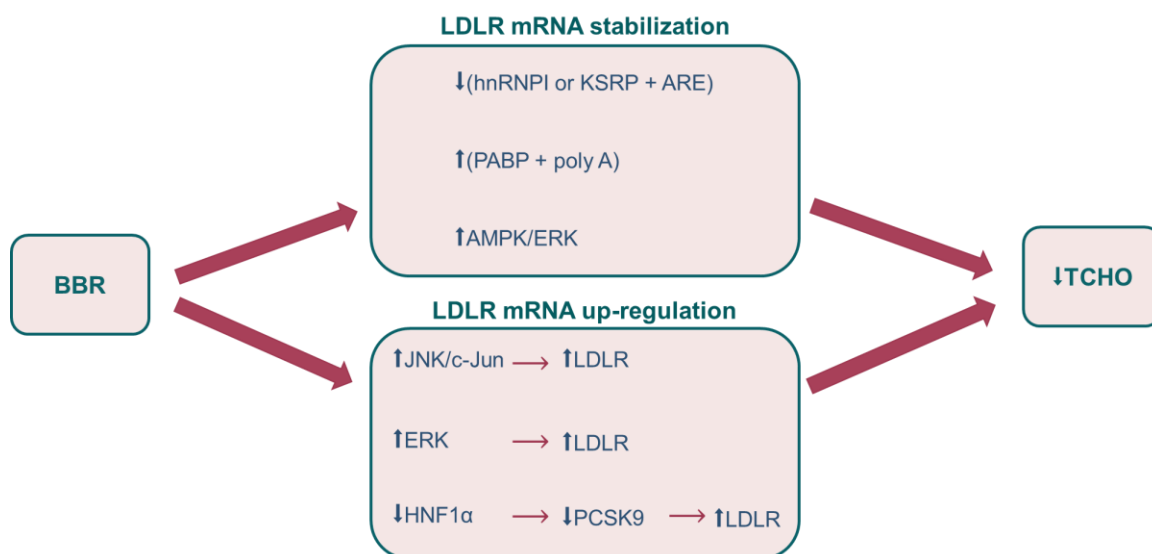


**Figure 2.3** Cholesterol-lowering activity of BBR.

### *A) LDLR mRNA stabilization*

The 3'-untranslated region (3'-UTR) of mRNA is the section of mRNA located after the translation termination codon. This section has different binding sites including those for regulatory proteins, microRNAs, proteins involved in the localization of the mRNA, as well as the sequence to introduce a poly(A) tail to the end of the mRNA transcript. The 3'-UTR may also contain AU-rich elements (AREs), that cause mRNAs to be degraded rapidly.

The 3'-UTR of human LDLR mRNA has three AREs, and LDLR mRNA stability is regulated by a group of ARE binding proteins, i.e. heterologous nuclear ribonucleoprotein D/I (hnRNP D, hnRNP I)<sup>24</sup> and KH type splicing regulatory protein (KHSRP).<sup>24,25</sup> The binding of these proteins to AREs reduces the expression of LDLR mRNA.

Several studies have shown that BBR stabilizes LDLR protein by hampering the binding between these ARE binding proteins and LDLR-ARE motifs.<sup>24</sup>

Furthermore, *in vitro* experiments demonstrated that BBR significantly promotes binding of the cytoplasmic polyA-binding protein (PABP) to the poly(A) tail of LDLR mRNA, indirectly

increasing the stability of LDLR. In fact, PABP preserves the mRNA from nucleophilic attack thus contributing to its stability.<sup>26</sup> Finally, BBR can also stabilize LDLR mRNA by activating the AMPK/ERK signaling pathway.<sup>5,27</sup>

*B) Upregulation of LDLR mRNA expression*

BBR utilizes multiple pathways to upregulate LDLR mRNA expression i.e. (Figure 2.4):

a) activation of the JNK/c-Jun signaling pathway;<sup>28</sup>

b) inhibition of the expression of PCSK9,<sup>29,30</sup> which is regulated at the transcription level mainly by the hepatocyte nuclear factor 1 $\alpha$  (HNF1 $\alpha$ ).<sup>31,32</sup> BBR reduces the HNF1 $\alpha$  protein levels through the ubiquitin proteasome degradation pathway.<sup>33,34</sup>

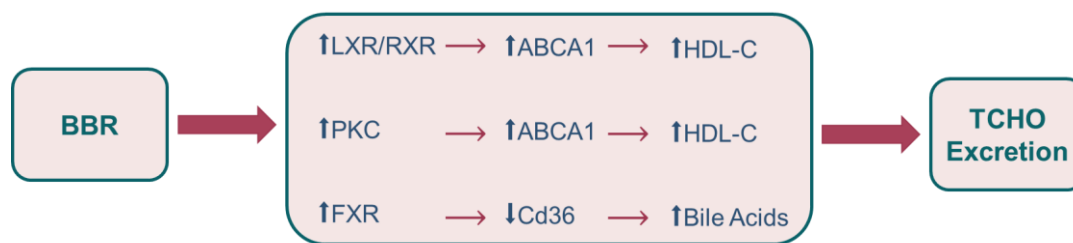


**Figure 2.4** The action of BBR on the excretion of cholesterol.

As shown in Figure 2.4, BBR also increases cholesterol excretion through:

a) upregulation of ABCA1 protein after activation of RXR/LXR and protein kinase C (PKC)<sup>35</sup> pathways;

b) modulation either directly and indirectly of the farnesoid X receptor (FXR), a nuclear receptor for bile acids. It has been reported that BBR inhibits the bile salt hydrolase (BSH), that deconjugates the glycine and taurine from the sterol core of the bile acids. Thus BBR increases the levels of gly/tauro-conjugated bile acids, which in turn activate FXR. The final result is: i) increased expression of ABCA1, ii) reduced uptake of long-chain fatty acids in the liver and iii) increased efflux of cholesterol.<sup>36,37</sup>

**2.3 Other pharmacological properties of BBR**

In addition to its cholesterol-lowering activity, BBR has antitumor, antioxidant, anti-inflammatory, hypoglycemic and neuroprotective activities. Furthermore, it has antibacterial and antifungal properties, but the mechanism of action has not yet been clarified.<sup>38</sup>

**2.3.1 Anticancer activity**

Berberine inhibits cell proliferation by modulating various processes, such as cell cycle, apoptosis and cellular autophagy, as well as the development of metastases (Figure 2.5).

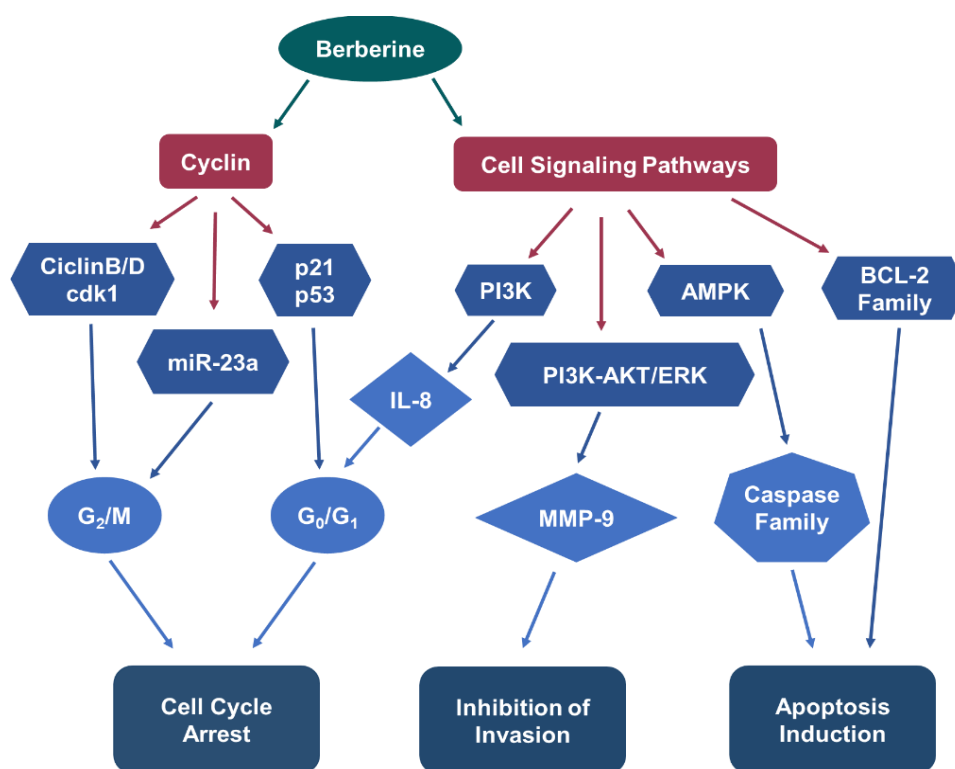


**Figure 2.5** Molecular mechanisms underlying the antitumor activity of BBR.

BBR induces cell cycle arrest at the G0/G1 and G2/M phase,<sup>39,40</sup> by upregulation of tumor suppressor factors such as p21, p53 and p27, and downregulation of cyclins D1, D2, E, and cyclin-dependent kinases Cdk2, Cdk4, and Cdk6.<sup>41-43</sup> In addition, berberine may influence cell cycle through regulation of the retinoblastoma protein (Rb), and increase the expression of miR-23a, which could enhance berberine-induced G2/M cell cycle arrest (Figure 2.5).

Moreover, BBR promotes apoptosis through different pathways i.e. activation of proapoptotic caspases, downregulation of antiapoptotic proteins.<sup>41,44,45</sup>

Recently, it has also been seen that BBR can selectively bind with G-quadruplex DNA structures and inhibit telomerase activity.<sup>46</sup> In addition, it significantly promotes mRNA expression of the antiproliferative factors FoxO1 and FoxO3a, Janus Kinase 2 (JAK2), phosphoinositide 3-kinase (PI3K), activator protein-1 (AP-1), NF-kappaB.<sup>47-52</sup>

Finally, BBR favors autophagy either by phosphorylation of JNK kinase and targeting the AMPK/mTOR/ULK1 pathway, and inhibits the development of metastases by limiting the expression of MMP-2 and MMP-9 and by reducing the expression of the transcription factor snail-1 (Figure 2.5).<sup>53</sup>

### ***2.3.2 Antioxidant and anti-inflammatory activities***

In *vitro* studies evidenced that BBR counteracts oxidative stress by increasing several antioxidant defense e.g. SOD (superoxide dismutase), GSH (glutathione) and GSH-Px (glutathione peroxidase) (Figure 2.6).

The mechanism of action probably involves the upregulation of sirtuin 1 (SIRT1), that elevates the transcriptional activity FOXO proteins, which target genes encoding antioxidant enzymes (Figure 2.6).<sup>54</sup>

Another possible mechanism is the inhibition via AMPK of nicotinamide adenine dinucleotide phosphate (NADPH) oxidase, one of the major producers of ROS in the body.<sup>55</sup>

Moreover, BBR could increase the expression of uncoupling protein 2 (UCP2) and induce the nuclear factor erythroid 2 (NF-E2)-related factor 2 (Nrf2) pathway, both involved in the reduction of oxidative stress.<sup>56</sup>

BBR has also an interesting anti-inflammatory activity, probably related to its ability to modulate both the signaling pathways of mitogen-activated protein kinase (MAPK) and NF-Kb

## Chapter 2

(Figure 2.6). The latter is a protein complex functioning as a transcription factor, that under normal conditions in the cytoplasm is in its inactive form through interaction with inhibitory molecules belonging to the I $\kappa$ B family.<sup>57</sup> In response to specific stimuli (inflammatory cytokines, bacterial and viral products, various types of stress), I $\kappa$ B molecules undergo phosphorylation on two critical serine residues, Ser176 and Ser181. This modification allows their polyubiquitination and destruction by the proteasome. Consequently, NF- $\kappa$ B is activated, enters the nucleus and stimulates the transcription of various genes that participate in the immune and inflammatory response.<sup>57</sup>

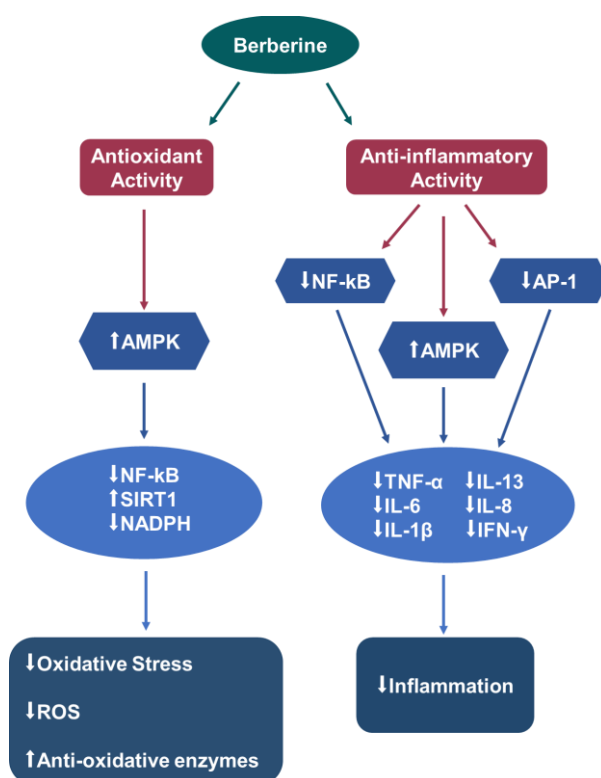


**Figure 2.6** Antioxidant and anti-inflammatory activities of BBR.

BBR inhibits the phosphorylation of Ser181 and consequently promote the stability of the NF- $\kappa$ B/I $\kappa$ B- $\alpha$  complex, thus avoiding the activation of the inflammatory response.<sup>56</sup>

BBR could inhibit NF- $\kappa$ B by suppressing Rho GTPase and through PPAR $\gamma$  activation; finally, BBR can inhibit the transcription factor AP-1 (Activator protein-1) which like NF- $\kappa$ B plays a critical role for the development of inflammation.<sup>56</sup>

### 2.3.3 Hypoglycemic activity

The hypoglycemic activity of BBR was first observed in 1986 and results were very similar to that of metformin, a drug used to treat type 2 diabetes mellitus.<sup>58</sup>

BBR regulates glucose metabolism through several mechanisms (Figure 2.7): 1) increased secretion and sensitivity of insulin; 2) activation of AMPK pathway; 3) modulation of gut microbiota; 4) inhibition of gluconeogenesis in the liver; 5) stimulation of glycolysis in peripheral tissue cells and 6) increased levels of the glucose transporter1 (GLUT1).<sup>59,60</sup>

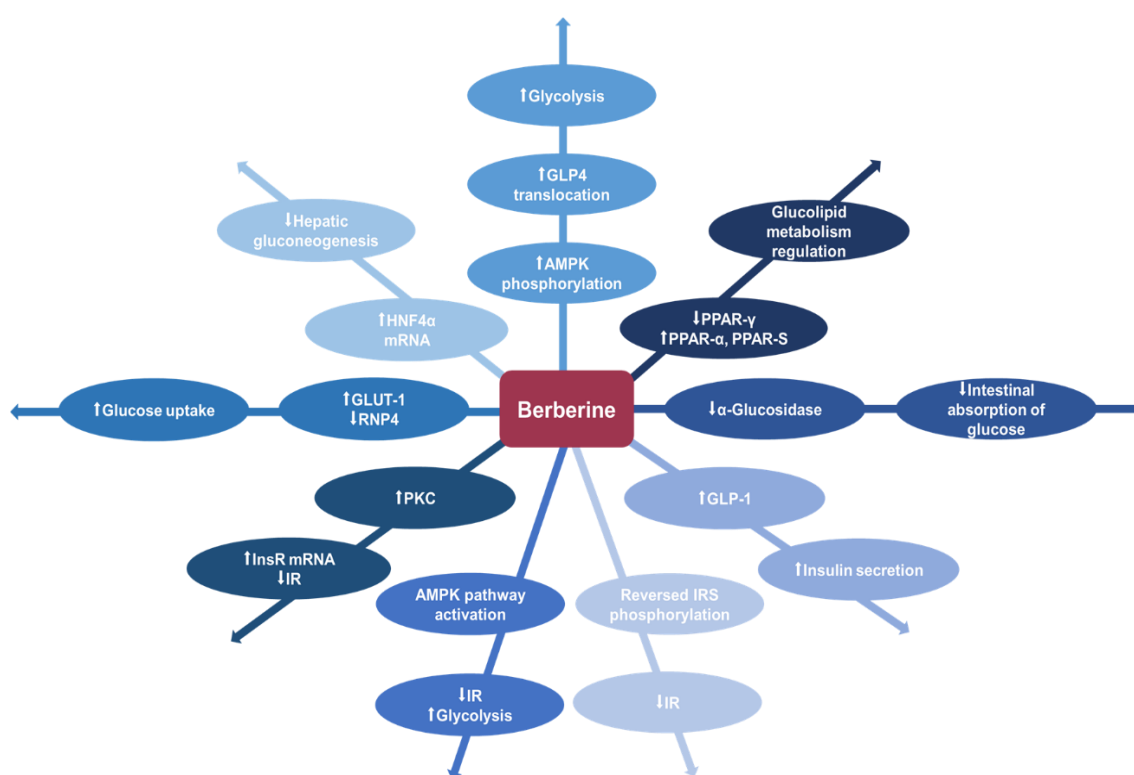


**Figure 2.7** Effects of berberine on glycometabolism.

In addition, *in vitro* BBR decreases the expression either of peroxisome proliferator-activated receptor  $\gamma$  (PPAR $\gamma$ ) or of fatty acid transferase, thus inhibiting fatty acid uptake and improving free fatty acid-induced insulin resistance.<sup>60</sup> Finally, BBR enhances the activity of GLP-1 receptors and limits the absorption of glucose in the gastrointestinal tract, by inhibiting  $\alpha$ -glucosidase, an enzyme that allows the breakdown of carbohydrates into monosaccharides.<sup>61,62</sup>

## Chapter 2

### 2.3.4 Neuroprotective activity

Berberine also has potent neuroprotective properties and may play an important role in the treatment of neurodegenerative diseases such as Alzheimer's disease (AD), Parkinson's disease (PD) and Huntington's disease (HD).

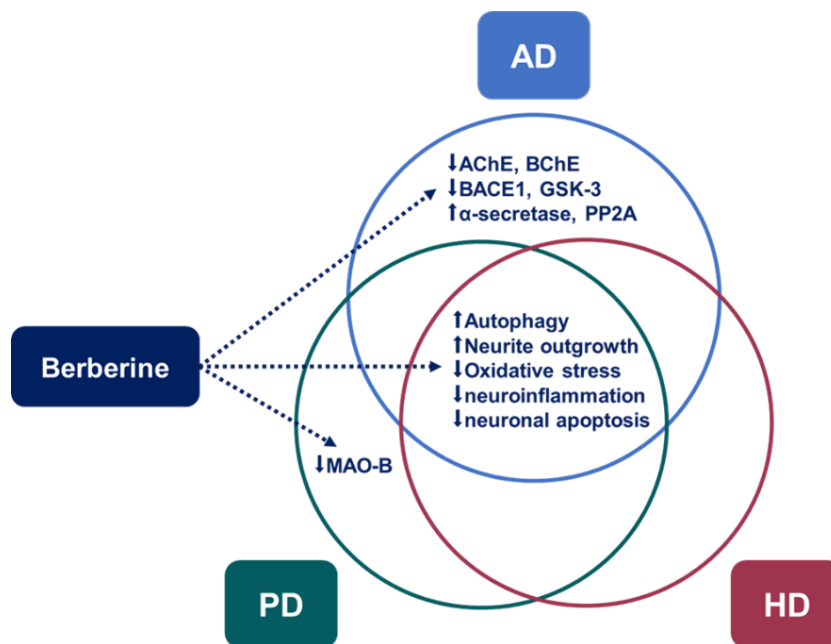


**Figure 2.8** BBR's effects on neurodegenerative diseases.

BBR is able to cross the blood-brain barrier (BBB) and can modulate several targets implicated in neurodegeneration. In fact, it can inhibit proteins such as acetylcholinesterase (AChE), butyrylcholinesterase (BChE),  $\beta$ -site amyloid precursor protein cleaving enzyme 1 (BACE1), glycogen synthase kinase-3 (GSK-3) and monoamine oxidase-B (MAO-B), and activate  $\alpha$ -secretase and protein phosphatase 2A (PP2A).<sup>63</sup>

BBR significantly decreases intracellular oxidative stress<sup>64</sup> by attenuating neuroinflammation,<sup>65,66</sup> and accelerates the elimination of misfolded and aggregated toxic proteins ( $\tau$  protein, amyloid- $\beta$  peptide A $\beta$ ) in neuronal cells.<sup>67-69</sup> Moreover, it reduces several risk factors that can promote cognitive decline (i. e. diabetes, hypercholesterolemia, obesity), and protects neurons from cell death.<sup>70</sup>

#### **2.4. Limitations of BBR and strategies to improve its bioavailability**

Currently, the use of berberine is rather limited and its clinical dosage is relatively high, due to its poor oral bioavailability, which is less than 1%.<sup>71</sup> The low oral bioavailability of BBR is related to several factors: BBR is poorly water soluble, undergoes self-aggregation (which limits its intestinal absorption) as well as significant first pass metabolism, and is substrate of P-glycoprotein and of multidrug resistance-associated protein-1 (MRP1).<sup>72</sup>

Furthermore, BBR can upregulate P-gp, and modulate the activity of some cytochrome P450 isoenzymes, and this may limit its clinical use in patients who concomitantly take other drugs.<sup>73</sup>

BBR is generally well tolerated; the main side effects include: constipation, nausea, cramps and diarrhea. However, at high doses, arterial hypotension, dyspnea, heart damage and gastric lesions can also occur.<sup>73,74</sup>

In order to improve its oral bioavailability, several strategies have been proposed such as:

- co-administration of BBR with absorption enhancers such as sodium caprate, chitosan and sodium deoxycholate, which increase BBR solubility and permeability in the intestinal mucosa; in particular, sodium caprate also inhibits BBR self-aggregation and P-gp functionality;<sup>74</sup>
- synthesis of BBR organic acid salts: it has been shown that the bioavailability of berberine fumarate and berberine succinate can be increased respectively by 1,278 and 1,313-fold, compared to BBR hydrochloride;<sup>75</sup>
- concomitant administration of plant polyphenols and others natural extracts, such as *Silybum Marianum* extract, acting as P-gp inhibitors;<sup>76</sup>
- development of new formulations including microemulsions, micellar systems or nanoparticles. Dan *et al.* realized BBR-MgAl monolayer hydrotalcite as a kind of novel drug delivery system, which greatly increased the bioavailability of BBR. Gia *et al.* reported that BBR loaded into solid polymer particles with  $\beta$ -cyclodextrin as a vector,

## **Chapter 2**

had a bioavailability of about 50%.<sup>77</sup> Xiong *et al.* developed a set of nanocrystals modified with Brij-S20 (BS20) to improve intestinal absorption of BBR, with a 404.1% increase in bioavailability compared to pure BBR.<sup>78</sup> Finally, Elsheikh *et al.* used new cremochylomicrons, and after treatment both the absorption rate and the amount of BBR-cremochylomicrons were twice as high.<sup>79</sup>

However, the realization of synthetic or semisynthetic BBR analogues could be a valid alternative to overcome its pharmacokinetic drawbacks, prevent drugs incompatibilities, and improve its pharmacological activity.

**References**

1. Grycová, L.; Dostál, J.; Marek, R. Quaternary protoberberine alkaloids. *Phytochemistry* **2007**, *68*(2), 150–175. doi: 10.1016/j.phytochem.2006.10.004
2. Birdsall, T. C.; Kelly, G. S. Berberine: therapeutic potential of an alkaloid found in several medicinal plants. *Sci. Rev. Altern. Med.* **1997**, *2*(2), 94-103.
3. Neag, M. A.; Mocan, A.; Echeverría, J.; Pop, R. M.; Bocsan, C. I.; Crişan, G.; Buzoianu, A. D. Berberine: botanical occurrence, traditional uses, extraction methods, and relevance in cardiovascular, metabolic, hepatic, and renal disorders. *Front. Pharmacol.* **2018**, *9*, 557. doi: 10.3389/fphar.2018.00557
4. Ren, L. H.; Vasil'ev, A. V.; Orkehov, A. N.; Tertov, V. V.; Tutel'ian, V. A. Evaluation of the antiatherosclerotic properties of natural compounds of plant origin on cell cultures of the human aortic intima. *Farmakol. Toksikol.* **1989**, *52*(5), 44–46. PMID: 2599077
5. Kong, W.; Wei, J.; Abidi, P.; Lin, M.; Inaba, S.; Li, C.; Wang, Y.; Wang, Z.; Si, S.; Pan, H.; Wang, S.; Wu, J.; Wang, Y.; Li, Z.; Liu, J.; Jiang, J. D. Berberine is a novel cholesterol-lowering drug working through a unique mechanism distinct from statins. *Nat. Med.* **2004**, *10*(12), 1344–1351. doi: 10.1038/nm1135
6. Wang, Y.; Jia, X.; Ghanam, K.; Beaurepaire, C.; Zidichouski, J.; Miller, L. Berberine and plant stanols synergistically inhibit cholesterol absorption in hamsters. *Atherosclerosis* **2010**, *209*(1), 111–117. doi: 10.1016/j.atherosclerosis.2009.08.050
7. Wang, Y.; Yi, X.; Ghanam, K.; Zhang, S.; Zhao, T.; Zhu, X. Berberine decreases cholesterol levels in rats through multiple mechanisms, including inhibition of cholesterol absorption. *Metab. Clin. Exp.* **2014**, *63*(9), 1167–1177. doi: 10.1016/j.metabol.2014.05.013
8. Kim, W. S.; Lee, Y. S.; Cha, S. H.; Jeong, H. W.; Choe, S. S.; Lee, M. R.; Oh, G. T.; Park, H. S.; Lee, K. U.; Lane, M. D.; Kim, J. B. Berberine improves lipid dysregulation in obesity by controlling central and peripheral AMPK activity. *Am. J. Physiol. Endocrinol. Metab.* **2009**, *296*(4), E812–E819. doi: 10.1152/ajpendo.90710.2008
9. Jia, X.; Chen, Y.; Zidichouski, J.; Zhang, J.; Sun, C.; Wang, Y. Co-administration of berberine and plant stanols synergistically reduces plasma cholesterol in rats. *Atherosclerosis* **2008**, *201*(1), 101–107. doi: 10.1016/j.atherosclerosis.2008.03.008
10. Zhang, Q.; Xiao, X.; Feng, K.; Wang, T.; Li, W.; Yuan, T.; Sun, X.; Sun, Q.; Xiang, H.; Wang, H. Berberine moderates glucose and lipid metabolism through multipathway mechanism. *Evid. Based Complementary Altern. Med.* **2011**, *2011*, 924851. doi: 10.1155/2011/924851
11. He, K.; Kou, S.; Zou, Z.; Hu, Y.; Feng, M.; Han, B.; Li, X.; Ye, X. Hypolipidemic effects of alkaloids from *Rhizoma Coptidis* in diet-induced hyperlipidemic hamsters. *Planta Med.* **2016**, *82*(8), 690–697. doi: 10.1055/s-0035-1568261

## **Chapter 2**

12. Sanders, M. J.; Grondin, P. O.; Hegarty, B. D.; Snowden, M. A.; Carling, D. Investigating the mechanism for AMP activation of the AMP-activated protein kinase cascade. *Eur. J. Biochem.* **2007**, *403*(1), 139–148. doi: 10.1042/BJ20061520
13. Turner, N.; Li, J. Y.; Gosby, A.; To, S. W.; Cheng, Z.; Miyoshi, H.; Taketo, M. M.; Cooney, G. J.; Kraegen, E. W.; James, D. E.; Hu, L. H.; Li, J.; Ye, J. M. Berberine and its more biologically available derivative, dihydroberberine, inhibit mitochondrial respiratory complex I: a mechanism for the action of berberine to activate AMP-activated protein kinase and improve insulin action. *Diabetes* **2008**, *57*(5), 1414–1418. doi: 10.2337/db07-1552
14. Hardie, D. G.; Ross, F. A.; Hawley, S. A. AMPK: a nutrient and energy sensor that maintains energy homeostasis. *Nat. Rev. Mol. Cell Biol.* **2012**, *13*(4), 251–262. doi: 10.1038/nrm3311
15. Zhang, Z.; Zhang, H.; Li, B.; Meng, X.; Wang, J.; Zhang, Y.; Yao, S.; Ma, Q.; Jin, L.; Yang, J.; Wang, W.; Ning, G. Berberine activates thermogenesis in white and brown adipose tissue. *Nat. Commun.* **2014**, *5*, 5493. doi: 10.1038/ncomms6493
16. Wang, Q.; Zhang, M.; Liang, B.; Shirwany, N.; Zhu, Y.; Zou, M. H. Activation of AMP-activated protein kinase is required for berberine-induced reduction of atherosclerosis in mice: the role of uncoupling protein 2. *PLoS One* **2011**, *6*(9), e25436. doi: 10.1371/journal.pone.0025436
17. Xue, B.; Kahn, B. B. AMPK integrates nutrient and hormonal signals to regulate food intake and energy balance through effects in the hypothalamus and peripheral tissues. *J. Physiol.* **2006**, *574*(Pt 1), 73–83. doi: 10.1113/jphysiol.2006.113217
18. Inoue, I.; Itoh, F.; Aoyagi, S.; Tazawa, S.; Kusama, H.; Akahane, M.; Mastunaga, T.; Hayashi, K.; Awata, T.; Komoda, T.; Katayama, S. Fibrate and statin synergistically increase the transcriptional activities of PPARalpha/RXRalpha and decrease the transactivation of NFkappaB. *Biochem. Biophys. Res. Commun.* **2002**, *290*(1), 131–139. doi: 10.1006/bbrc.2001.6141
19. Zou, Y.; Du, H.; Yin, M.; Zhang, L.; Mao, L.; Xiao, N.; Ren, G.; Zhang, C.; Pan, J. Effects of high dietary fat and cholesterol on expression of PPAR alpha, LXR alpha, and their responsive genes in the liver of apoE and LDLR double deficient mice. *Mol. Cell. Biochem.* **2009**, *323*(1-2), 195–205. doi: 10.1007/s11010-008-9982-3
20. Jiang, D.; Wang, D.; Zhuang, X.; Wang, Z.; Ni, Y.; Chen, S.; Sun, F. Berberine increases adipose triglyceride lipase in 3T3-L1 adipocytes through the AMPK pathway. *Lipids Health Dis.* **2016**, *15*(1), 214. doi: 10.1186/s12944-016-0383-4
21. Hao, M.; Li, Y.; Liu, L.; Yuan, X.; Gao, Y.; Guan, Z.; Li, W. The design and synthesis of a novel compound of berberine and baicalein that inhibits the efficacy of lipid accumulation in 3T3-L1 adipocytes. *Bioorg. Med. Chem.* **2017**, *25*(20), 5506–5512. doi: 10.1016/j.bmc.2017.08.013
22. Choi, B. H.; Ahn, I. S.; Kim, Y. H.; Park, J. W.; Lee, S. Y.; Hyun, C. K.; Do, M. S. Berberine reduces the expression of adipogenic enzymes and inflammatory molecules of 3T3-L1 adipocyte. *Exp. Mol. Med.* **2006**, *38*(6), 599–605. doi: 10.1038/emm.2006.71

23. Xia, X.; Yan, J.; Shen, Y.; Tang, K.; Yin, J.; Zhang, Y.; Yang, D.; Liang, H.; Ye, J.; Weng, J. Berberine improves glucose metabolism in diabetic rats by inhibition of hepatic gluconeogenesis. *PLoS One* **2011**, *6*(2), e16556. doi: 10.1371/journal.pone.0016556
24. Li, H.; Chen, W.; Zhou, Y.; Abidi, P.; Sharpe, O.; Robinson, W. H.; Kraemer, F. B.; Liu, J. Identification of mRNA binding proteins that regulate the stability of LDL receptor mRNA through AU-rich elements. *J. Lipid Res.* **2009**, *50*(5), 820–831. doi: 10.1194/jlr.M800375-JLR200
25. Pan, R.; Cai, W., Sun, J.; Yu, C.; Li, P.; Zheng, M. Inhibition of KHSRP sensitizes colorectal cancer to 5-fluorouracil through miR-501-5p-mediated ERRF1 mRNA degradation. *J. Cell. Physiol.* **2020**, *235*(2), 1576–1587. doi: 10.1002/jcp.29076
26. Behm-Ansmant, I.; Gatfield, D.; Rehwinkel, J.; Hilgers, V.; Izaurralde, E. A conserved role for cytoplasmic poly(A)-binding protein 1 (PABPC1) in nonsense-mediated mRNA decay. *EMBO Rep.* **2007**, *26*(6), 1591–1601. doi: 10.1038/sj.emboj.7601588
27. Abidi, P.; Zhou, Y.; Jiang, J. D.; Liu, J. Extracellular signal-regulated kinase-dependent stabilization of hepatic low-density lipoprotein receptor mRNA by herbal medicine berberine. *Arterioscler. Thromb. Vasc. Biol.* **2005**, *25*(10), 2170–2176. doi: 10.1161/01.ATV.0000181761.16341.2b
28. Lee, S.; Lim, H. J.; Park, J. H.; Lee, K. S.; Jang, Y.; Park, H. Y. Berberine-induced LDLR up-regulation involves JNK pathway. *Biochem. Biophys. Res. Commun.* **2007**, *362*(4), 853–857. doi: 10.1016/j.bbrc.2007.08.060
29. Lagace, T. A. PCSK9 and LDLR degradation: regulatory mechanisms in circulation and in cells. *Curr. Opin. Lipidol.* **2014**, *25*(5), 387–393. doi: 10.1097/MOL.0000000000000114
30. Qian, Y. W.; Schmidt, R. J.; Zhang, Y.; Chu, S.; Lin, A.; Wang, H.; Wang, X.; Beyer, T. P.; Bensch, W. R.; Li, W.; Ehsani, M. E.; Lu, D.; Konrad, R. J.; Eacho, P. I.; Moller, D. E.; Karathanasis, S. K.; Cao, G. Secreted PCSK9 downregulates low density lipoprotein receptor through receptor-mediated endocytosis. *J. Lipid Res.* **2007**, *48*(7), 1488–1498. doi: 10.1194/jlr.M700071-JLR200
31. Li, H.; Dong, B.; Park, S. W.; Lee, H. S.; Chen, W.; Liu, J. Hepatocyte nuclear factor 1alpha plays a critical role in PCSK9 gene transcription and regulation by the natural hypocholesterolemic compound berberine. *J. Biol. Chem.* **2009**, *284*(42), 28885–28895. doi: 10.1074/jbc.M109.052407
32. Momtazi, A. A.; Banach, M.; Pirro, M.; Katsiki, N.; Sahebkar, A. Regulation of PCSK9 by nutraceuticals. *Pharmacol. Res.* **2017**, *120*, 157–169. doi: 10.1016/j.phrs.2017.03.023
33. Dong, B.; Li, H.; Singh, A. B.; Cao, A.; Liu, J. Inhibition of PCSK9 transcription by berberine involves down-regulation of hepatic HNF1 $\alpha$  protein expression through the ubiquitin-proteasome degradation pathway. *J. Biol. Chem.* **2015**, *290*(7), 4047–4058. doi: 10.1074/jbc.M114.597229
34. Zhou, Y.; Cao, S.; Wang, Y.; Xu, P.; Yan, J.; Bin, W.; Qiu, F.; Kang, N. Berberine metabolites could induce low density lipoprotein receptor up-regulation to exert lipid-lowering effects in human hepatoma cells. *Fitoterapia* **2014**, *92*, 230–237. doi: 10.1016/j.fitote.2013.11.010

## **Chapter 2**

35. Liang, H.; Wang, Y. Berberine alleviates hepatic lipid accumulation by increasing ABCA1 through the protein kinase C $\delta$  pathway. *Biochem. Biophys. Res.* **2018**, *498*(3), 473–480. doi: 10.1016/j.bbrc.2018.03.003
36. Sun, R.; Yang, N.; Kong, B.; Cao, B.; Feng, D.; Yu, X.; Ge, C.; Huang, J.; Shen, J.; Wang, P.; Feng, S.; Fei, F.; Guo, J.; He, J.; Aa, N.; Chen, Q.; Pan, Y.; Schumacher, J. D.; Yang, C. S.; Guo, G. L.; Wang, G. Orally administered berberine modulates hepatic lipid metabolism by altering microbial bile acid metabolism and the intestinal FXR signaling pathway. *Mol. Pharmacol.* **2017**, *91*(2), 110–122. doi: 10.1124/mol.116.106617
37. Tian, Y.; Cai, J.; Gui, W.; Nichols, R. G.; Koo, I.; Zhang, J.; Anitha, M.; Patterson, A. D. Berberine directly affects the gut microbiota to promote intestinal farnesoid X receptor activation. *Drug Metab. Dispos.* **2019**, *47*(2), 86–93. doi: 10.1124/dmd.118.083691
38. Dhamgaye, S.; Devaux, F.; Vandeputte, P.; Khandelwal, N. K.; Sanglard, D.; Mukhopadhyay, G.; Prasad, R. Molecular mechanisms of action of herbal antifungal alkaloid berberine, in *Candida albicans*. *PLoS One* **2014**, *9*(8), e104554. doi: 10.1371/journal.pone.0104554
39. Eo, S. H.; Kim, J. H.; Kim, S. J. Induction of G<sub>2</sub>/M arrest by berberine via activation of PI3K/Akt and p38 in human chondrosarcoma cell line. *Cancer Res.* **2014**, *22*(3), 147–157. doi:10.3727/096504015X14298122915583
40. Gu, M.; Xu, J.; Han, C.; Kang, Y.; Liu, T.; He, Y.; Huang, Y.; Liu, C. Effects of berberine on cell cycle, DNA, reactive oxygen species, and apoptosis in L929 murine fibroblast cells. *Evid. Based Complementary Altern. Med.* **2015**, *2015*, 796306. doi: 10.1155/2015/796306
41. Li, L.; Wang, X.; Sharvan, R.; Gao, J.; Qu, S. Berberine could inhibit thyroid carcinoma cells by inducing mitochondrial apoptosis, G<sub>0</sub>/G<sub>1</sub> cell cycle arrest and suppressing migration via PI3K-AKT and MAPK signaling pathways. *Biomed. Pharmacother.* **2017**, *95*, 1225–1231. doi: 10.1016/j.biopha.2017.09.010
42. Mantena, S. K.; Sharma, S. D.; Katiyar, S. K. Berberine, a natural product, induces G<sub>1</sub>-phase cell cycle arrest and caspase-3-dependent apoptosis in human prostate carcinoma cells. *Mol. Cancer Ther.* **2006**, *5*(2), 296–308. doi: 10.1158/1535-7163.MCT-05-0448
43. Zheng, F.; Tang, Q.; Wu, J.; Zhao, S.; Liang, Z.; Li, L.; Wu, W.; Hann, S. p38 $\alpha$  MAPK-mediated induction and interaction of FOXO3a and p53 contribute to the inhibited-growth and induced-apoptosis of human lung adenocarcinoma cells by berberine. *J. Exp. Clin. Cancer Res.* **2014**, *33*(1), 36. doi: 10.1186/1756-9966-33-36
44. Hwang, J. M.; Kuo, H. C.; Tseng, T. H.; Liu, J. Y.; Chu, C. Y. Berberine induces apoptosis through a mitochondria/caspases pathway in human hepatoma cells. *Arch. Toxicol.* **2006**, *80*(2), 62–73. doi: 10.1007/s00204-005-0014-8
45. Yang, X.; Huang, N. Berberine induces selective apoptosis through the AMPK-mediated mitochondrial/caspase pathway in hepatocellular carcinoma. *Mol. Med. Rep.* **2013**, *8*(2), 505–510. doi: 10.3892/mmr.2013.1506

46. Franceschin, M.; Rossetti, L.; D'Ambrosio, A.; Schirripa, S.; Bianco, A.; Ortaggi, G.; Savino, M.; Schultes, C.; Neidle, S. Natural and synthetic G-quadruplex interactive berberine derivatives. *Bioorg. Med. Chem. Lett.* **2006**, *16*(6), 1707–1711. doi: 10.1016/j.bmcl.2005.12.001
47. Mahata, S.; Bharti, A. C.; Shukla, S.; Tyagi, A.; Husain, S. A.; Das, B. C. Berberine modulates AP-1 activity to suppress HPV transcription and downstream signaling to induce growth arrest and apoptosis in cervical cancer cells. *Mol. Cancer* **2011**, *10*, 39. doi: 10.1186/1476-4598-10-39
48. Fu, L.; Chen, W.; Guo, W.; Wang, J.; Tian, Y.; Shi, D.; Zhang, X.; Qiu, H.; Xiao, X.; Kang, T.; Huang, W.; Wang, S.; Deng, W. Berberine targets AP-2/hTERT, NF- $\kappa$ B/COX-2, HIF-1 $\alpha$ /VEGF and cytochrome-c/caspase signaling to suppress human cancer cell growth. *PLoS One* **2013**, *8*(7), e69240. doi: 10.1371/journal.pone.0069240
49. Wu, C. M.; Li, T. M.; Tan, T. W.; Fong, Y. C.; Tang, C. H. Berberine reduces the metastasis of chondrosarcoma by modulating the  $\alpha\beta$ 3 integrin and the PKC  $\delta$ , c-Src, and AP-1 signaling pathways. *Evid.-Based Complementary Altern. Med.* **2013**, *2013*, 423164. doi: 10.1155/2013/423164
50. Belanova, A.; Beseda, D.; Chmykhalo, V.; Stepanova, A.; Belousova, M.; Khrenkova, V.; Gavalas, N.; Zolotukhin, P. Berberine effects on NF $\kappa$ B, HIF1A and NFE2L2/AP-1 pathways in HeLa cells. *Anti-Cancer Agents Med. Chem.* **2019**, *19*(4), 487–501. doi: 10.2174/1871520619666181211121405
51. El-Zeftawy, M.; Ghareeb, D.; El-Bealy, E. R.; Saad, R.; Mahmoud, S.; Elguindy, N.; El-Kott, A. F.; El-Sayed, M. Berberine chloride ameliorated PI3K/Akt-p/SIRT-1/PTEN signaling pathway in insulin resistance syndrome induced in rats. *J. Food Biochem.* **2019**, *43*(12), e13049. doi: 10.1111/jfbc.13049
52. Kim, S.; You, D.; Jeong, Y.; Yu, J.; Kim, S. W.; Nam, S. J.; Lee, J. E. Berberine down-regulates IL-8 expression through inhibition of the EGFR/MEK/ERK pathway in triple-negative breast cancer cells. *Phytomedicine* **2018**, *50*, 43–49. doi: 10.1016/j.phymed.2018.08.004
53. Wang, Y.; Liu, Y.; Du, X.; Ma, H.; Yao, J. The anti-cancer mechanisms of berberine: a review. *Cancer Manag. Res.* **2020**, *12*, 695–702. doi: 10.2147/CMAR.S242329
54. Van der Horst, A.; Tertoolen, L. G.; de Vries-Smits, L. M.; Frye, R. A.; Medema, R. H.; Burgering, B. M. FOXO4 is acetylated upon peroxide stress and deacetylated by the longevity protein hSir2 (SIRT1). *J. Biol. Chem.* **2004**, *279*(28), 28873–28879. doi: 10.1074/jbc.M401138200
55. Sarna, L. K.; Wu, N.; Hwang, S. Y.; Siow, Y. L. Berberine inhibits NADPH oxidase mediated superoxide anion production in macrophages. *Can. J. Physiol. Pharmacol.* **2010**, *88*(3), 369–378. doi: 10.1139/Y09-136
56. Li, Z.; Geng, Y. N.; Jiang, J. D.; Kong, W. J. Antioxidant and anti-inflammatory activities of berberine in the treatment of diabetes mellitus. *Evid.-Based Complementary Altern. Med.* **2014**, *2014*, 289264. doi: 10.1155/2014/289264
57. Israël, A. The IKK complex, a central regulator of NF-kappaB activation. *Cold Spring Harb. Perspect. Biol.* **2010**, *2*(3), a000158. doi: 10.1101/cshperspect.a000158

## **Chapter 2**

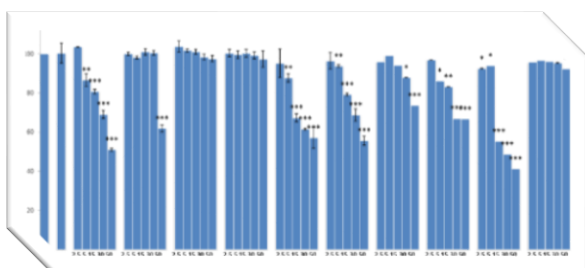
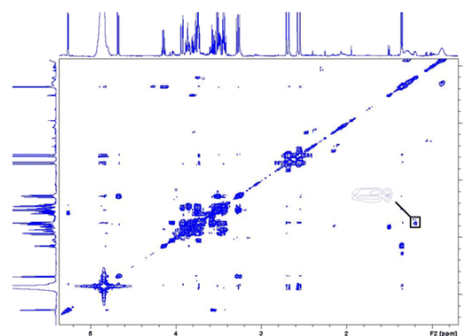
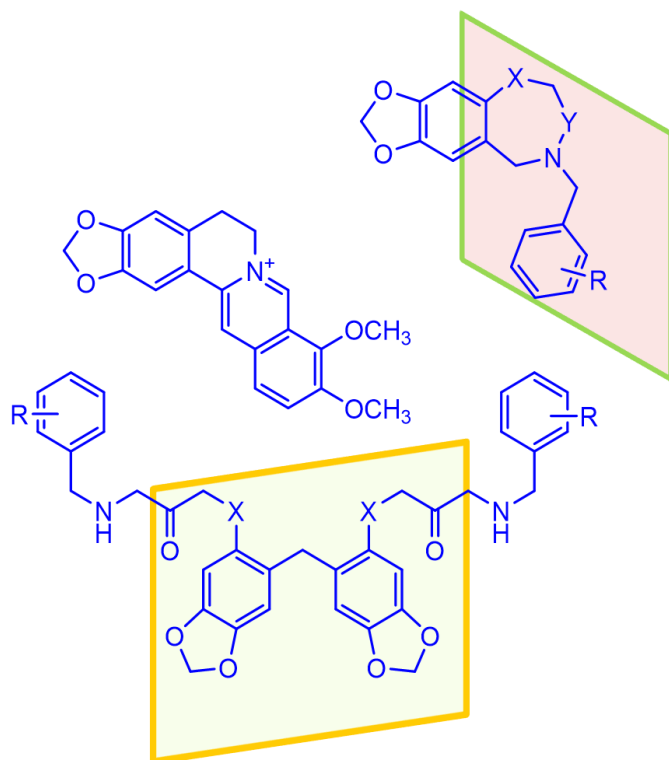
58. Chang, W.; Chen, L.; Hatch, G. M. Berberine as a therapy for type 2 diabetes and its complications: From mechanism of action to clinical studies. *Biochem. Cell Biol.* **2015**, *93*(5), 479–486. doi: 10.1139/bcb-2014-0107
59. Kong, W. J.; Zhang, H.; Song, D. Q.; Xue, R.; Zhao, W.; Wei, J.; Wang, Y. M.; Shan, N.; Zhou, Z. X.; Yang, P.; You, X. F.; Li, Z. R.; Si, S. Y.; Zhao, L. X.; Pan, H. N.; Jiang, J. D. Berberine reduces insulin resistance through protein kinase C-dependent up-regulation of insulin receptor expression. *Metab. Clin. Exp.* **2009**, *58*(1), 109–119. doi: 10.1016/j.metabol.2008.08.013
60. Chen, Y.; Li, Y.; Wang, Y.; Wen, Y.; Sun, C. Berberine improves free-fatty-acid-induced insulin resistance in L6 myotubes through inhibiting peroxisome proliferator-activated receptor gamma and fatty acid transferase expressions. *Metab. Clin. Exp.* **2009**, *58*(12), 1694–1702. doi: 10.1016/j.metabol.2009.06.009
61. Kim, S. H.; Shin, E. J.; Kim, E. D.; Bayaraa, T.; Frost, S. C.; Hyun, C. K. Berberine activates GLUT1-mediated glucose uptake in 3T3-L1 adipocytes. *Biol. Pharm. Bull.* **2007**, *30*(11), 2120–2125. doi: 10.1248/bpb.30.2120
62. Zhang, W.; Xu, Y. C.; Guo, F. J.; Meng, Y.; Li, M. L. Anti-diabetic effects of cinnamaldehyde and berberine and their impacts on retinol-binding protein 4 expression in rats with type 2 diabetes mellitus. *Chin. Med. J.* **2008**, *121*(21), 2124–2128.
63. Fan, D.; Liu, L.; Wu, Z.; Cao, M. Combating neurodegenerative diseases with the plant alkaloid berberine: molecular mechanisms and therapeutic potential. *Curr. Neuropharmacol.* **2019**, *17*(6), 563–579. doi:10.2174/1570159X16666180419141613
64. Lin, M. T.; Beal, M. F. Mitochondrial dysfunction and oxidative stress in neurodegenerative diseases. *Nature* **2006**, *443*(7113), 787–795. doi: 10.1038/nature05292
65. Akiyama, H.; Barger, S.; Barnum, S.; Bradt, B.; Bauer, J.; Cole, G. M.; Cooper, N. R.; Eikelenboom, P.; Emmerling, M.; Fiebich, B. L.; Finch, C. E.; Frautschy, S.; Griffin, W. S.; Hampel, H.; Hull, M.; Landreth, G.; Lue, L.; Mrak, R.; Mackenzie, I. R.; McGeer, P. L.; Wyss-Coray, T. Inflammation and Alzheimer's disease. *Neurobiol. Aging* **2000**, *21*(3), 383–421. doi: 10.1016/s0197-4580(00)00124-x
66. Heneka, M. T.; Carson, M. J.; El Khoury, J.; Landreth, G. E.; Brosseron, F.; Feinstein, D. L.; Jacobs, A. H.; Wyss-Coray, T.; Vitorica, J.; Ransohoff, R. M.; Herrup, K.; Frautschy, S. A.; Finsen, B.; Brown, G. C.; Verkhratsky, A.; Yamanaka, K.; Koistinaho, J.; Latz, E.; Halle, A.; Petzold, G. C.; Kummer, M. P. Neuroinflammation in Alzheimer's disease. *Lancet Neurol.* **2015**, *14*(4), 388–405. doi: 10.1016/S1474-4422(15)70016-5
67. Hardy, J.; Selkoe, D. J. The amyloid hypothesis of Alzheimer's disease: progress and problems on the road to therapeutics. *Science* **2002**, *297*(5580), 353–356. doi: 10.1126/science.1072994
68. Turab Naqvi, A. A.; Hasan, G. M.; Hassan, M. I. Targeting tau hyperphosphorylation via kinase inhibition: strategy to address Alzheimer's disease. *Curr. Top. Med. Chem.* **2020**, *20*(12), 1059–1073. doi: 10.2174/1568026620666200106125910

69. Ittner, L. M.; Götz, J. Amyloid- $\beta$  and tau--a toxic pas de deux in Alzheimer's disease. *Nat. Rev. Neurosci.* **2011**, *12*(2), 65–72. doi: 10.1038/nrn2967
70. Di Paolo, G.; Kim, T. W. Linking lipids to Alzheimer's disease: cholesterol and beyond. *Nat. Rev. Neurosci.* **2011**, *12*(5), 284–296. doi: 10.1038/nrn3012
71. Liu, Y. T.; Hao, H. P.; Xie, H. G.; Lai, L.; Wang, Q.; Liu, C. X.; Wang, G. J. Extensive intestinal first-pass elimination and predominant hepatic distribution of berberine explain its low plasma levels in rats. *Drug Metab. Dispos.* **2010**, *38*(10), 1779–1784. doi: 10.1124/dmd.110.033936
72. Chen, W.; Miao, Y. Q.; Fan, D. J.; Yang, S. S.; Lin, X., Meng, L. K.; Tang, X. Bioavailability study of berberine and the enhancing effects of TPGS on intestinal absorption in rats. *AAPS PharmSciTech* **2011**, *12*(2), 705–711. doi: 10.1208/s12249-011-9632-z
73. Guo, Y.; Chen, Y.; Tan, Z. R.; Klaassen, C. D.; Zhou, H. H. Repeated administration of berberine inhibits cytochromes P450 in humans. *Eur. J. Clin. Pharmacol.* **2012**, *68*(2), 213–217. doi:10.1007/s00228-011-1108-2
74. Fan, D.; Wu, X.; Dong, W.; Sun, W.; Li, J.; Tang, X. Enhancement by sodium caprate and sodium deoxycholate of the gastrointestinal absorption of berberine chloride in rats. *Drug Dev. Ind. Pharm.* **2013**, *39*(9), 1447–1456. doi:10.3109/03639045.2012.723219
75. Cui, H. X.; Hu, Y. N.; Li, J. W.; Yuan, K.; Guo, Y. Preparation and evaluation of antidiabetic agents of berberine organic acid salts for enhancing the bioavailability. *Molecules* **2018**, *24*(1), 103. doi:10.3390/molecules24010103
76. Di Pierro, F.; Putignano, P.; Villanova, N.; Montesi, L.; Moscatiello, S.; Marchesini, G. Preliminary study about the possible glycemic clinical advantage in using a fixed combination of *Berberis aristata* and *Silybum marianum* standardized extracts versus only *Berberis aristata* in patients with type 2 diabetes. *Clin. Pharmacol.: Adv. Appl.* **2013**, *5*, 167–174. doi:10.2147/CPAA.S54308
77. Jia, J.; Zhang, K.; Zhou, X.; Zhou, D.; Ge, F. Precise dissolution control and bioavailability evaluation for insoluble drug berberine via a polymeric particle prepared using supercritical CO<sub>2</sub>. *Polymers* **2018**, *10*(11), 1198. doi: 10.3390/polym10111198
78. Xiong, W.; Sang, W.; Linghu, K. G.; Zhong, Z. F.; Cheang, W. S.; Li, J.; Hu, Y. J.; Yu, H.; Wang, Y. T. Dual-functional Brij-S20-modified nanocrystal formulation enhances the intestinal transport and oral bioavailability of berberine. *Int. J. Nanomedicine* **2018**, *13*, 3781–3793. doi: 10.2147/IJN.S163763
79. Elsheikh, M. A.; Elnaggar, Y.; Hamdy, D. A.; Abdallah, O. Y. Novel cremochylomicrons for improved oral bioavailability of the antineoplastic phytochemistry berberine chloride: optimization and pharmacokinetics. *Int. J. Pharm.* **2018**, *535*(1-2), 316–324. doi: 10.1016/j.ijpharm.2017.11.023



# Chapter 3

## Development of Berberine Analogues





### 3.1 Background

BBR is currently used in many dietary supplements (e.g. Eulipid®, Berberol®, Pantavis®, Armolipid®, Diabetyn®) for its hypoglycemic and lipid-lowering properties.

To date berberine scaffold has been extensively investigated mainly to generate new antibacterial,<sup>1-3</sup> anticancer,<sup>4-6</sup> and hypoglycemic agents.<sup>7,8</sup> On the contrary, there are few research studies on the structural modifications required to increase its hypolipidemic activity.

A possible reason for this is that, despite a number of studies evidencing that BBR is involved in many interconnected pathways, a specific molecular target has not been identified yet. This has considerably limited a comprehensive SAR analysis of BBR analogues. On the other hand, from a chemical point of view, introduction of some functional groups and substituents at specific positions of BBR scaffold could be very challenging.

The structure-activity relationships (SARs) of BBR have been limited with E aromatic ring first. Jian-Dong Jiang *et al.* reported that two vicinal methoxy groups at the 10- and 11- position (compound **2**, pseudoberberine, Figure 3.1) promoted an increased expression of LDLR of 1.6 times compared to BBR.<sup>9</sup>

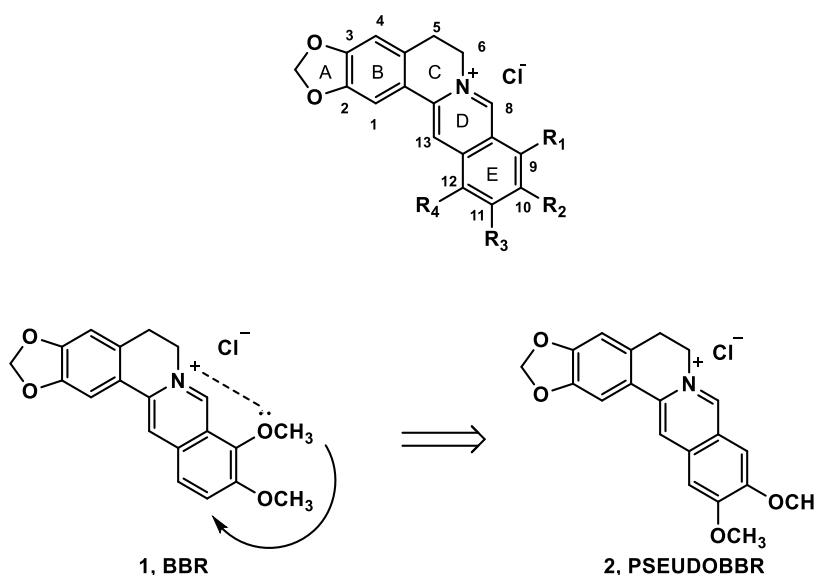


**Figure 3.1** Structure of berberine **1** and pseudoberberine **2**.

### Chapter 3

The authors speculated that a possible electrostatic effect between *N*-7 and methoxy group at the C-9 position of BBR could reduce the electropositivity of the quaternary ammonium ion, which seems an essential structural requirement for the cholesterol-lowering activity<sup>9</sup> (Figure 3.1). On the other hand, the tetrahydrogenated analogues of **1** and **2** had much lower activity on the LDLR expression compared with their parent compounds. This could be associated not only with the conversion of the quaternary ammonium moiety into the tertiary amine (with related loss of the positive charge at this position), but also with a significant configuration change<sup>10</sup> (Figure 3.2). Indeed, after hydrogenation the planar structure of **1** and **2** could be converted into a bended structure at pseudo-trans ring junction between C and D rings, altering the interaction with their putative target(s).

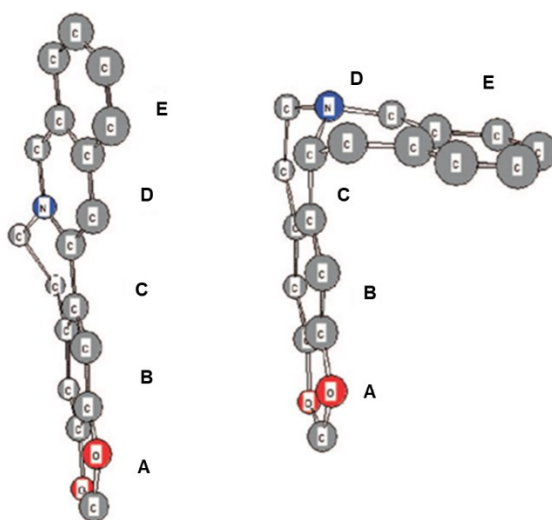


**Figure 3.2** Planar structure of BBR and folded structure of its reduced analog.<sup>10</sup>

Further SAR analysis on E ring of **1** indicated that:

- replacement of the methoxy group at the C-9 of **1** with OH or halogen causes a loss of activity;
- introduction of a methoxy groups at the C-12 generates a partial loss of activity probably due to steric hindrance;

- c) replacement of the methoxy group at the C-10 position with an OH (with or without a methoxy group at the C-9) is tolerated, while substitution at the C-10 with bulky alkoxy substituents causes partial loss of activity;
- d) the absence of substituents on the E ring reduces the activity.

The same research group evaluated also semisynthetic analogues of **1** obtained by treatment of **1** with phloroglucinol in H<sub>2</sub>SO<sub>4</sub>. This reaction gave the 2,3-dihydroxy analogue of **1**, that was substituted with different alkyl/aryl halides at 3- and at 2- and 3- positions. All synthesized analogues partially or completely lost their activity on LDLR expression. Furthermore, substitution of the 1,3-dioxol ring (ring A) with 1,4-dioxane ring also caused a loss of activity.<sup>10</sup>

Finally, the introduction of electron donor groups (methyl, ethyl, propyl, butyl, hexyl or benzyl) at the *N*-7 or C-13 positions considerably reduces the activity. This significant impact on the potency could be associated either to electron donor properties of these groups, that might reduce the electropositivity of quaternary nitrogen, or their steric hindrance.

Overall, this study highlights that the quaternary nitrogen and the planar structure are both crucial factors for the activity; furthermore, electronic nature (electron donor or electron-acceptor), and size of substituents at C-2, C-3, C-13 and *N*-7 of the lead **1** may influence the activity as a consequence of steric and/or electronic effects.<sup>10-12</sup>

However, subsequent SAR studies of BBR analogues were not consistent with these results. Indeed, Song *et al.* reported a series of BBR analogues bearing fatty acids with different lengths at the C-9 position, and compound **3** (Figure 3.3), bearing a 14-carbon fatty acid at the C-9 position was the most promising of this series. It showed potent lipid-lowering activity and good safety in a rat model, reducing TCHO (total cholesterol) and LDL cholesterol by 35.8% and 45.5%, respectively.<sup>13</sup>

Moreover, in 2015, Nechepurenko *et al.* described a small set of BBR analogues containing a reduced D ring, and one of them bearing a sulfonyl groups at the C-9 position (**4**, Figure 3.3)

### Chapter 3

showed a pronounced hypocholesterolemic activity in a rat model, lowering TCHO and triglyceride by 33% and 25% respectively.<sup>14</sup>

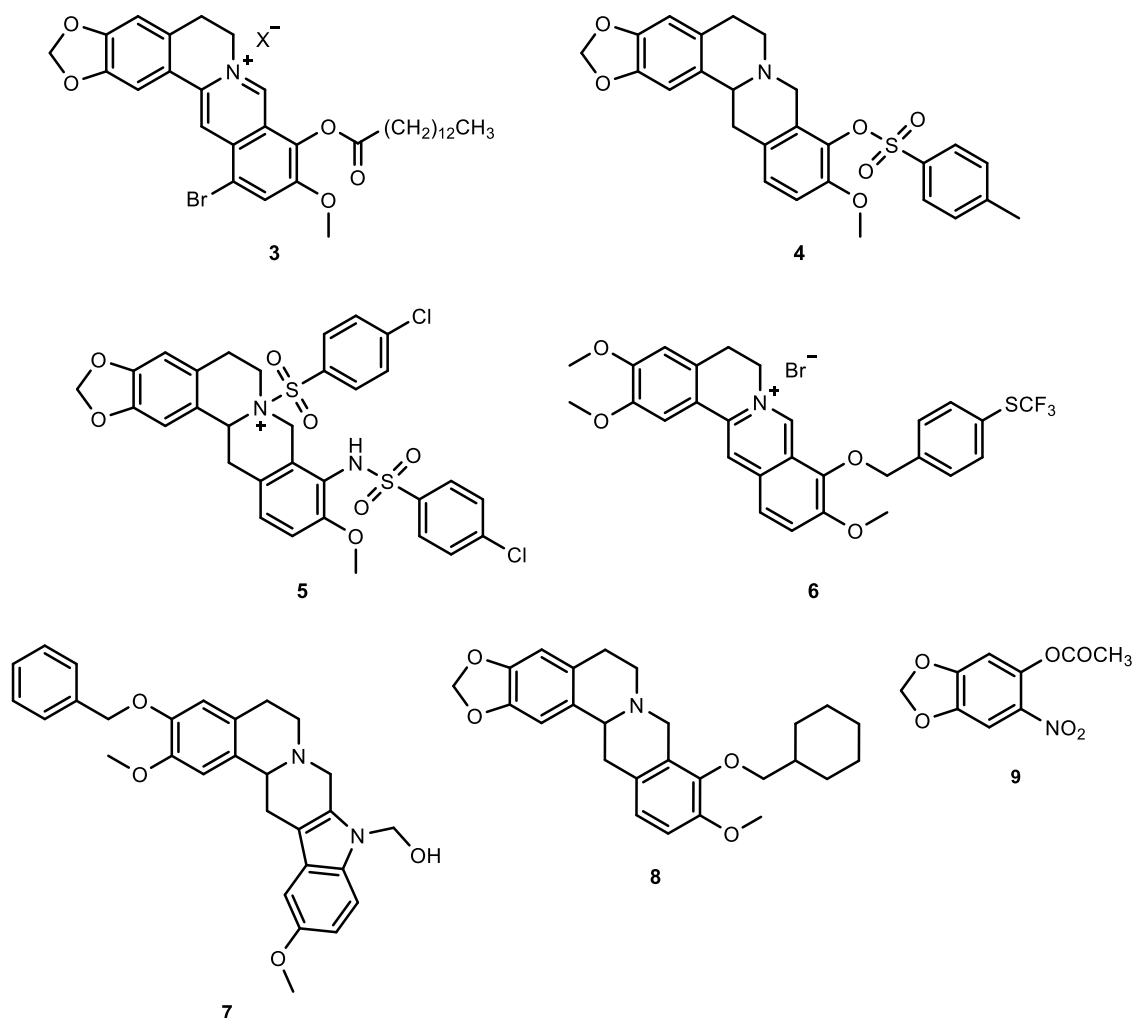


**Figure 3.3** Representative BBR analogues.

Recently, Lin-Guo Zhao *et al.* identified a 7,9-disulfatetrahydroberberine (**5**, Figure 3.3) as a promising new lipid-lowering lead compound, with inhibition rate (at 10  $\mu\text{M}$ ) against total cholesterol and triglycerides over 60% and 70% respectively.<sup>15</sup>

Song *et al.* in 2021 reported a set of BBR analogues and evaluated their ability to promote a down-regulation of PCSK9.<sup>16</sup> Compound **6** (Figure 3.3), bearing two methoxy groups at C-2 and C-3, showed  $\text{IC}_{50}$  value of  $9.5 \pm 0.5 \mu\text{M}$ , better than that of BBR.

In the same year, Chenglin Wu *et al.* described the synthesis and the hypolipidemic activity of a small library of tetrahydroprotoberberine (THPB) analogues, in which an indole system replaced the aromatic ring E of THPB. Compound **7** (Figure 3.3) was the most active THPB analogue; in particular, it induced downregulation of PCSK9 protein ( $IC_{50} = 1.34 \mu\text{mol/L}$ ), reduction of LDL levels (LDL uptake rate = 2.37 fold *vs* control) and reduction of PCSK9 mRNA expression ( $IC_{50} = 1.10 \mu\text{mol/L}$ ) more efficiently than berberine (PCSK9 mRNA  $IC_{50} = 8.04 \mu\text{mol/L}$ , LDL uptake rate = 1.38 fold *vs* control).<sup>17</sup>

Recently, Xiaojun Xu *et al.* synthesized three different THPB series that were evaluated for their ability to promote proteasomal degradation of SREBPs. Compound **8** (Figure 3.3) showed good downregulation effects on TCHO and TG.<sup>18</sup>

Finally, simplified derivatives of BBR (e.g. compound **9**, Figure 3.3) have also been described in the literature for their ability to increase the expression of LDLR receptors.<sup>19,20</sup>

It should be emphasized that in these compounds all structural requirements believed to be crucial for the lipid-lowering activity of BBR on the basis of first SAR analysis have not been retained. Indeed, these data indicate that a bulky substituent is tolerated at C-9 and N-7 (e.g. compounds **3-6**, Figure 3.3), a positive charge at N-7 is not strictly required (e.g. compounds **4, 7, 8**), ring A could be opened, and at C-3 or C-9 position a bulky substituent could be introduced (e.g. compounds **6, 7**, Figure 3.3). Furthermore, also more structurally simplified BBR analogues may serve as lipid lowering agents (e.g. compound **9**, Figure 3.3).

However, on the basis of reported data it is difficult to elaborate a rational structure-activity relationship (SAR) since the molecular mechanism of these compounds has not been deep investigated. Furthermore, we noticed that some reports lack important data (e.g. solubility, cell permeability and/or cytotoxicity), which can be useful to establish whether these analogues improve or not some pharmacokinetic/pharmacodynamic aspects compared to BBR.

## Chapter 3

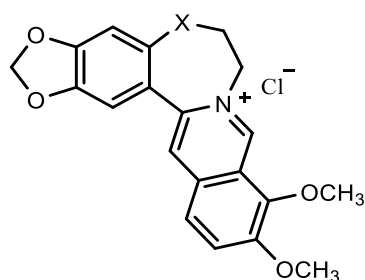
### 3.2 Aim of the work

This PhD project describes the design, synthesis, and biological evaluation of a small library of BBR analogues, designed in order to:

- improve the pharmacokinetic profile of the lead compound (e.g. solubility, cell permeability);
- extend SAR analysis to better define the minimum structural requirements for the lipid-lowering activity of BBR;
- enhance the lipid-lowering efficacy and reduce toxicity compared to the lead compound.

At the beginning of my PhD, I focused on the synthesis of **1** (BBR) and its analogue **1a** (Figure 3.4), in which a seven-membered oxazepine ring replaces the six-membered ring C of BBR.

This structural modification might prevent or reduce self-aggregation tendency of BBR, one of the main reasons for its poor bioavailability, and affect its hypolipidemic activity. This tetracycle-modified derivative of BBR was not described in the literature when we decide to synthesize it, while it was reported that **1b** (analogue of **1a**) had good anticancer<sup>21</sup> and hypoglycemic activity.<sup>22</sup> However, **1b** has not been evaluated as a hypolipidemic agent, hence it is not possible to establish whether the enlargement of C ring may affect this activity.



**1a**, X = O

**1b**, X = CH<sub>2</sub>

**Figure 3.4** Structure of BBR analogues **1a,b**.

### 3.3 Synthesis of BBR and 1a

Berberine (BBR) was synthesized according to the synthetic procedure reported by Luis M. Mori-Quiroz *et al.*<sup>23</sup> with minor modifications (Scheme 3.1). Briefly, the commercially available 3-(benzo[d][1,3]dioxol-5-yl)propanoic acid **2** was converted to the corresponding amide **3** using di-*tert*-butyldicarbonate (Boc)<sub>2</sub>O in the presence of NH<sub>4</sub>HCO<sub>3</sub> and pyridine. The amide **3** was reacted with (bis(trifluoroacetoxy)iodo)benzene (PIFA) to give the amine **4** by Hofmann rearrangement under mild conditions. Then, the amine **4** was converted to the tetrahydroisoquinoline **5** via Pictet–Spengler reaction in the presence of 2,2-dimethoxyacetaldehyde. Subsequently, the intermediate **5** was submitted to a reductive amination with 2,3-dimethoxybenzaldehyde and NaBH<sub>3</sub>CN to furnish the tertiary amine **6**, that underwent a Friedel-Craft alkoxyalkylation by reaction with triflic acid (TfOH). This reaction produced the intermediate **7**, which generated lambertine **8** (not isolated) after elimination of the methoxy group. Finally, crude lambertine **8** was directly oxidated using iodine and sodium acetate to give BBR in good yield.

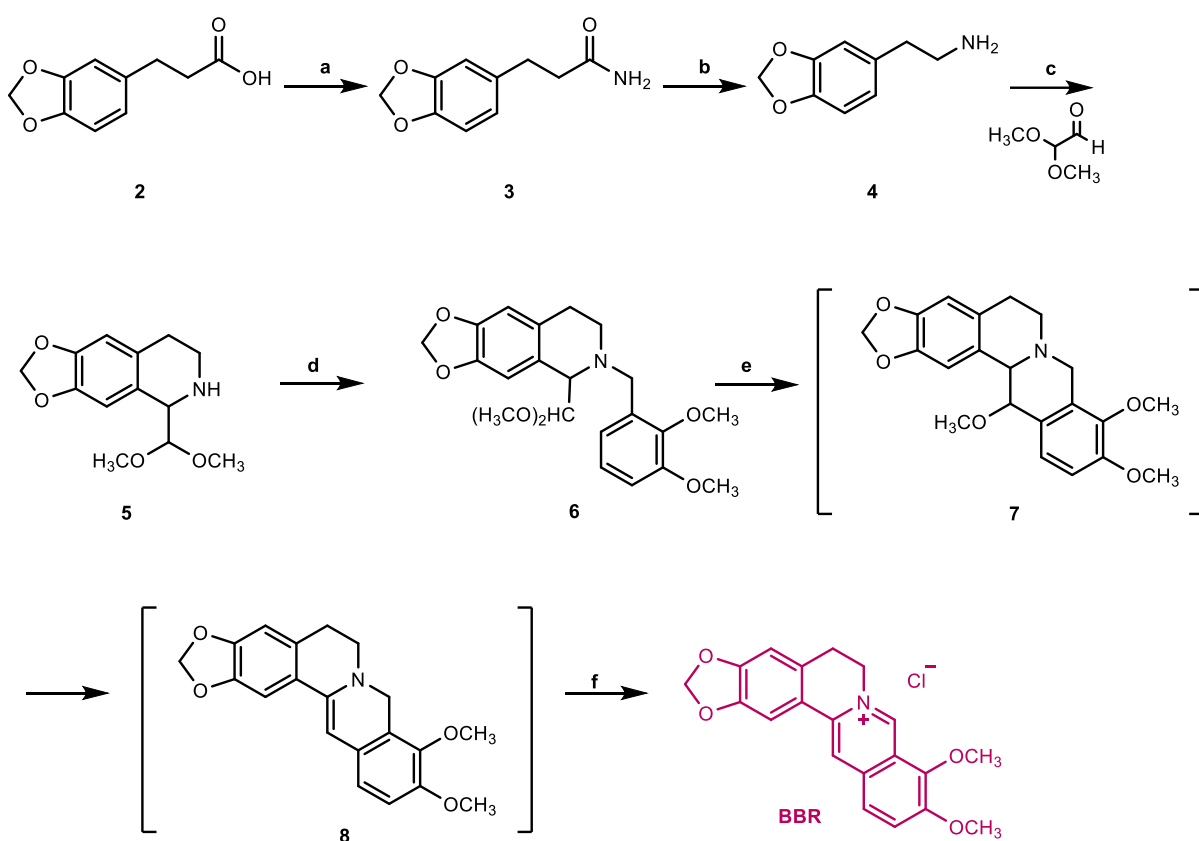
In Scheme 3.2 the synthesis of **1a** is described. The critical intermediate **11** was synthesized by two different approaches. In the first one (Scheme 3.2, A) sesamol **9** was reacted with 2-bromoacetamide to afford the amide **10**, which in turn was reduced using LiAlH<sub>4</sub> to render amine **11** in 48.2% yield over 2 steps. Alternatively, sesamol **9** was reacted with 2-((*tert*-butoxycarbonyl)amino)ethyl methanesulfonate **12** to generate **13**, which was deprotected in the presence of trifluoroacetic acid (TFA) to give amine **11** in 79.2% yield over two steps. The 2-((*tert*-butoxycarbonyl)amino)ethyl methanesulfonate **12** was easily obtained starting from 2-aminoethanol **14**, which was converted to the *N*-Boc derivative **15** using (Boc)<sub>2</sub>O and NaI as a catalyst<sup>24</sup> (Scheme 3.2, B). Then, mesylation of **15** with methanesulfonyl chloride and TEA as a base provided compound **12** in good yield.

### Chapter 3

The amine **11** was reacted via Pictet-Spengler reaction with 2,2-dimethoxyacetaldehyde and TFA to give the benzoxazepine **16**, which in turn furnished the amine **17** by reductive amination in the presence of 2,3-dimethoxybenzaldehyde and  $\text{NaBH}_3\text{CN}$  (Scheme 3.2, C). Unfortunately, efforts to obtain **1a** from **17** using the same synthetic procedure employed for BBR (e.g. oxidation using iodine and sodium acetate) failed.

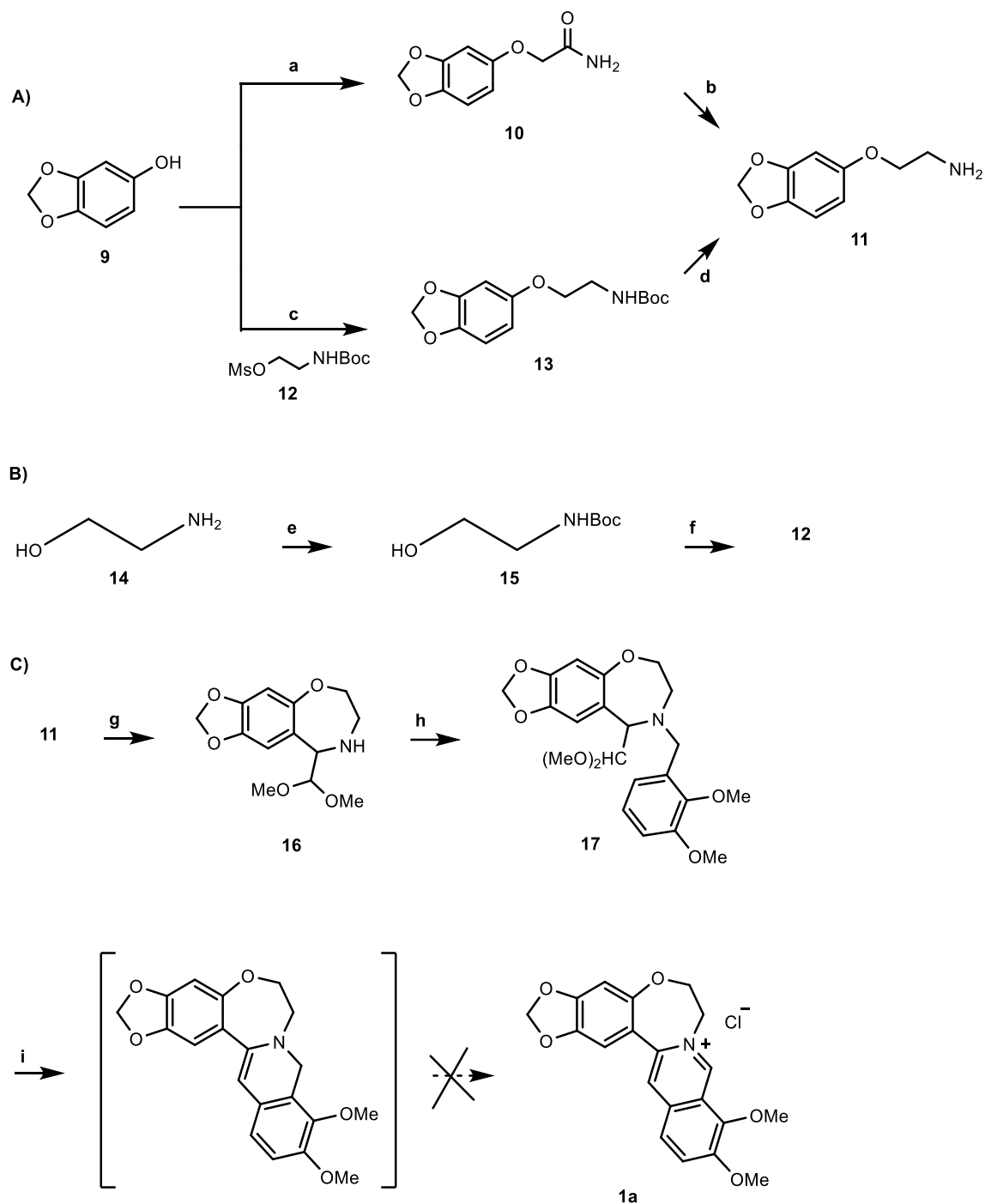
However, Wu Yong *et al.* in October 2020 published a patent, which described the synthesis of **1a** employing a different synthetic approach.<sup>25</sup>

#### Scheme 3.1



**Reagents and conditions:** a)  $\text{NH}_4\text{HCO}_3$ , dry pyridine,  $(\text{Boc})_2\text{O}$ , dry dioxane, rt, 12h; b) PIFA, pyridine,  $\text{CH}_3\text{CN}/\text{EtOAc}/\text{H}_2\text{O}$  (2:2:1), rt, 12h; c) dry DCM, anhydrous  $\text{MgSO}_4$ , rt, 2h, then TFA, rt, 2h; d) 2,3-dimethoxybenzaldehyde,  $\text{NaBH}_3\text{CN}$ , AcOH, dry MeOH, rt, 24h; e) TfOH, dry DCM,  $0^\circ\text{C}$  to rt, 2h; f)  $\text{CH}_3\text{COONa}$ ,  $\text{I}_2$ , EtOH, rt, 1h.

Scheme 3.2



**Reagents and conditions:** a)  $\text{BrCH}_2\text{CONH}_2$ ,  $\text{Cs}_2\text{CO}_3$ , DMF, rt, 24h; b)  $\text{LiAlH}_4$ , dry THF,  $0^\circ\text{C}$  to rt, 2.5h; c)  $\text{Cs}_2\text{CO}_3$ , DMF,  $60^\circ\text{C}$ , overnight; d) TFA, DCM, rt, 1h; e)  $(\text{Boc})_2\text{O}$ , NaI, THF,  $0^\circ\text{C}$  to rt, 1h; f)  $\text{CH}_3\text{SO}_2\text{Cl}$ , dry DCM, dry TEA,  $0^\circ\text{C}$  to rt, 4h; g) 2,2-dimethoxyacetaldehyde, dry DCM, anhydrous  $\text{MgSO}_4$ , rt, 2h, then TFA, rt, 2h; h) 2,3-dimethoxybenzaldehyde,  $\text{NaBH}_3\text{CN}$ , AcOH, dry MeOH, rt, 24h; i) TfOH, dry DCM,  $0^\circ\text{C}$  to rt, 2h, then  $\text{I}_2$ ,  $\text{CH}_3\text{COONa}$ , EtOH, rt, 1h.

### **3.4 Synthesis of structurally simplified BBR analogues**

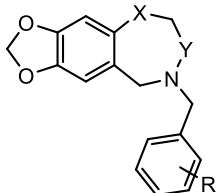
As previously reported (see paragraph 3.1), recent SAR studies of BBR analogues highlighted that:

- a) the quaternary nitrogen is not necessary (compounds **4**, **7-9**, Figure 3.3);
- b) structural simplifications of the lead are possible (compound **9**, Figure 3.3);
- c) enlargement of C ring of BBR does not compromise its anticancer and hypoglycemic activities, rather it can improve them (e.g. compound **1b**, Figure 3.4).

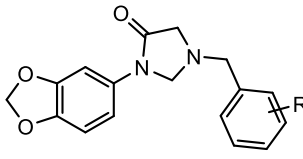
Thus, we thought that also an appropriate combination of some of these structural modifications could retain/improve main BBR pharmacological properties including its hypolipidemic one.

With this in mind, we designed a small library of structurally simplified BBR analogues based on well known privileged scaffolds such as benzo(di)azepinone, benzoxazepine, benzoxazepinone, 4-imidazolidinone and tetrahydroisoquinoline scaffolds, which also enable for a wide chemical space exploration and a more comprehensive SAR analysis (compounds **18a-l**, **19a-c**, **20a-e**, Table 3.1).

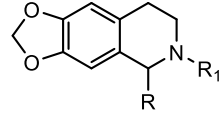
Table 3.1



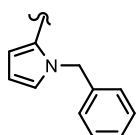
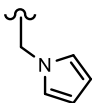
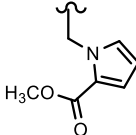
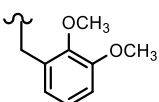
**18a-l**



**19a-c**



**20a-e**

Cpd	X	Y	R	R <sub>1</sub>
<b>18a</b>	CH <sub>2</sub>	C=O	2,3-dimethoxy	-
<b>18b</b>	CH <sub>2</sub>	C=O	4-OCH <sub>3</sub>	-
<b>18c</b>	CH <sub>2</sub>	C=O	4-Cl	-
<b>18d</b>	CH <sub>2</sub>	C=O	3-CF <sub>3</sub>	-
<b>18e</b>	CH <sub>2</sub>	C=O	H	-
<b>18f</b>	CH <sub>2</sub>	C=O	3-Br	-
<b>18g</b>	O	C=O	2,3-dimethoxy	-
<b>18h</b>	O	C=O	2,5-dimethoxy	-
<b>18i</b>	O	C=O	3,4-dimethoxy	-
<b>18j</b>	O	C=O	4-OCH <sub>3</sub>	-
<b>18k</b>	NH	C=O	2,3-dimethoxy	-
<b>18l</b>	O	CH <sub>2</sub>	2,3-dimethoxy	-
<b>19a</b>	-	-	4-methoxy	-
<b>19b</b>	-	-	2,4-dimethoxy	-
<b>19c</b>	-	-	2,3-dimethoxy	-
<b>20a</b>	-	-		H
<b>20b</b>	-	-	benzyl	H
<b>20c</b>	-	-		H
<b>20d</b>	-	-		H
<b>20e</b>	-	-	H	

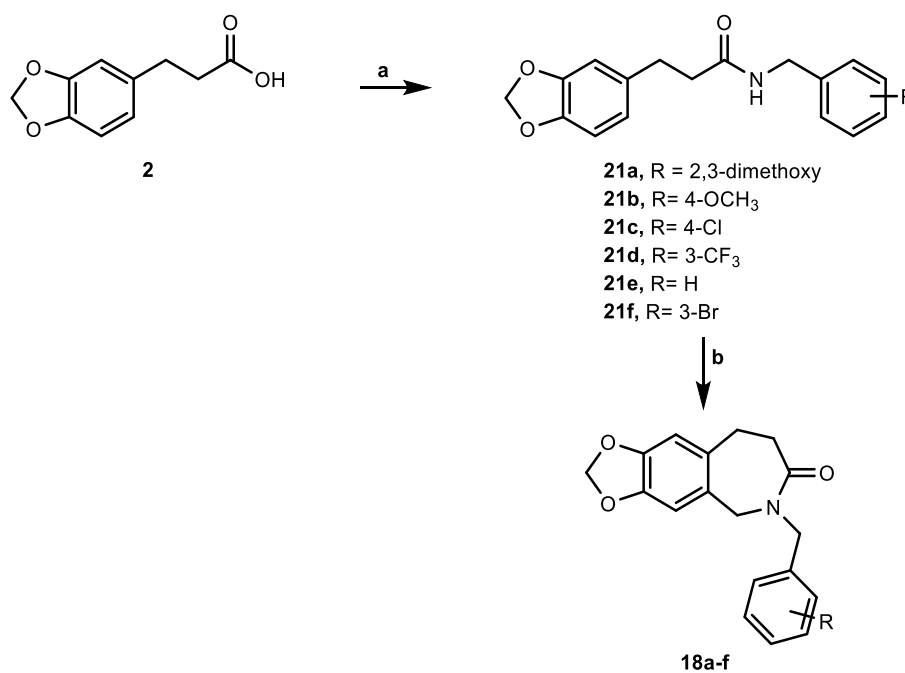
## Chapter 3

### 3.4.1 Synthesis of 18a-l, 19a-c and 20a-e

Benzazepinones **18a-f** were obtained in two synthetic steps as reported in Scheme 3.3. The commercially available 3-(benzo[d][1,3]dioxol-5-yl)propanoic acid **2** was converted into amides **21a-f** by coupling with the appropriate amine in the presence of HOBT (1-hydroxybenzotriazole), HBTU (*N,N,N',N'*-Tetramethyl-O-(benzotriazol-1-yl)uronium tetrafluoroborate) as coupling reagents and DIPEA (*N,N*-diisopropylethylamine) as a base.

Then amides **21a-f** were cyclized to the target compounds **18a-f** following the synthetic procedure described by Masahiro So *et al.*,<sup>26</sup> in the presence of paraformaldehyde and TFA in dichloroethane as a solvent and at room temperature.

Scheme 3.3



**Reagents and conditions:** a) HOBT, HBTU, DIPEA, DMF, appropriate amine, rt, overnight; b) dry ClCH<sub>2</sub>CH<sub>2</sub>Cl, paraformaldehyde, TFA, rt, 5h.

The authors applied this synthetic approach to a small set of 2-benzazepinones derivatives, and indicated two plausible reaction mechanisms for the cyclization including: a) Pictet–Spengler-type intramolecular Friedel–Crafts reaction (path A), and b) Friedel–Craft hydroxymethylation followed by dehydration (path B) (Figure 3.5).

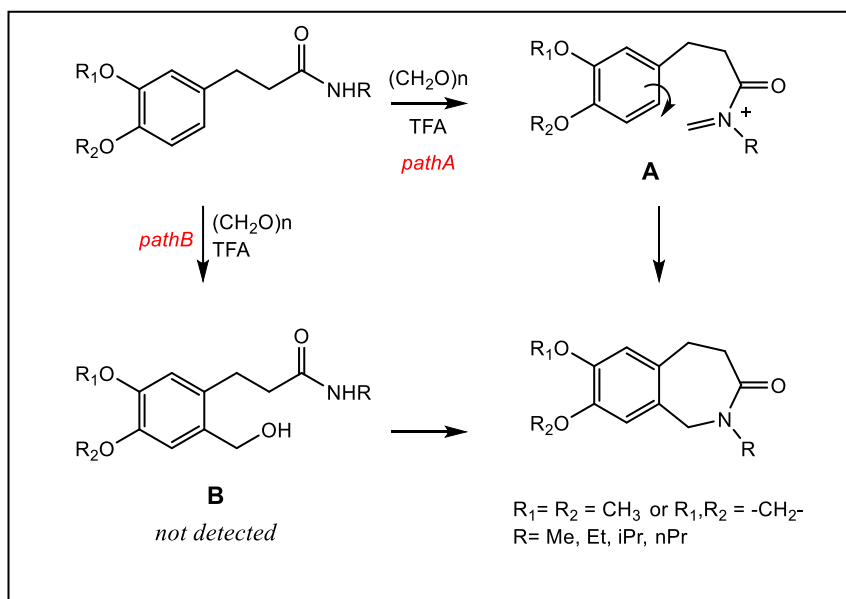


**Figure 3.5** Plausible reaction mechanism proposed by Masahiro So et al.<sup>26</sup>

The authors never detected the intermediate B (Figure 3.5), thus, despite the Pictet–Spengler reaction is not commonly applied to amides cyclization, path A seems the most plausible one.

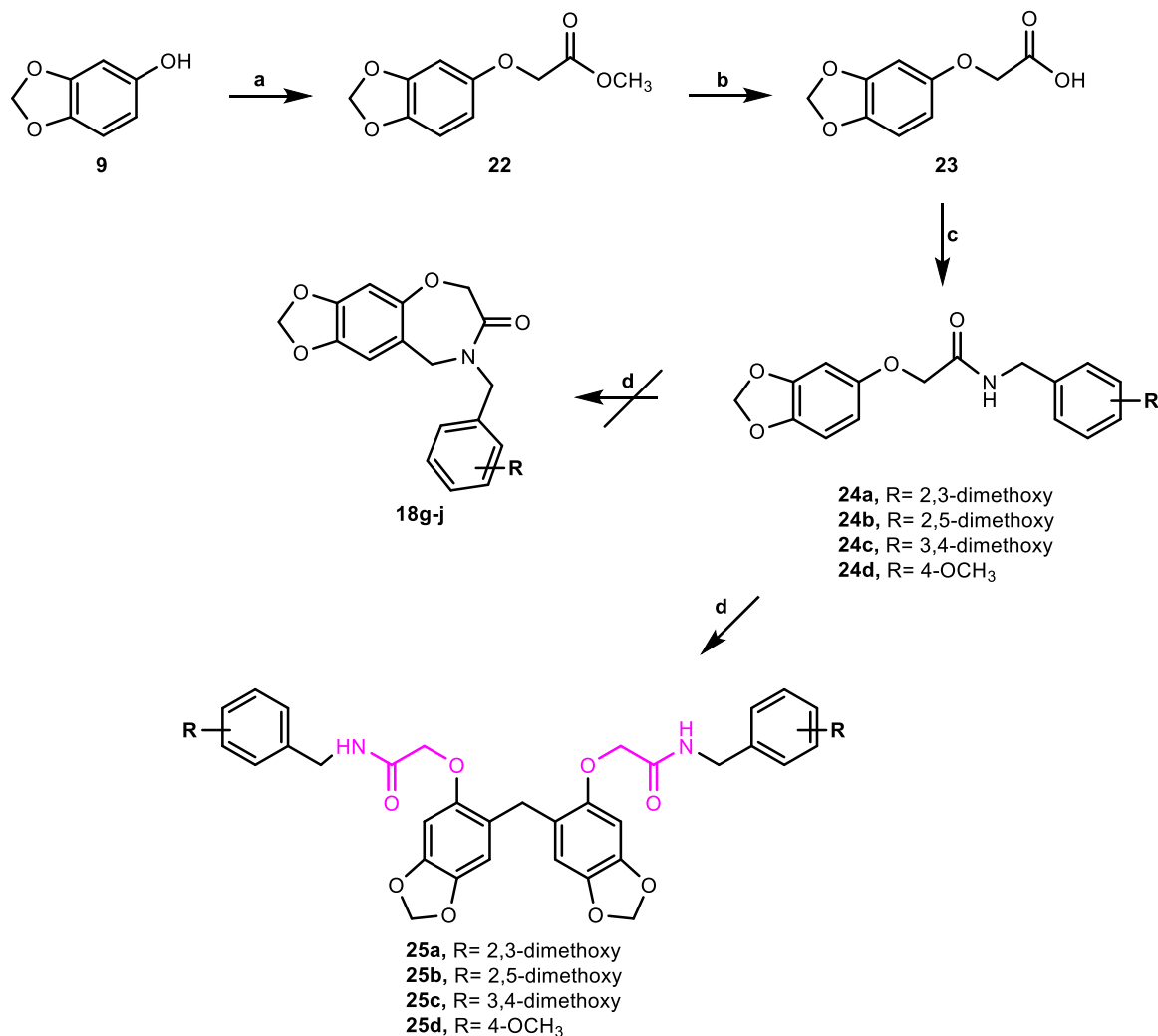
The authors also noticed that the cyclization occurs in good yield and with high regioselectivity when two electron-donating substituents are on the benzofused ring and one of them is in the *p*-position of the cyclized aromatic carbon. On the contrary, the presence of only one electron-donating group generates the corresponding benzazepinone derivative in low yield (<30%). However, they reported only the cyclization of *N*-alkyl substituted amides, and did not assess how this reaction may be affected by the presence of variously substituted *N*-aryl/heteroaryl groups.

This reaction was investigated by us also to obtain benzoxazepinones **18g-j** (Scheme 3.4) and the benzodiazepinone **18k** (Scheme 3.5). The critical intermediates **24a-d** were obtained starting from sesamol **9** that was reacted with methyl 2-bromoacetate to give the ester **22**, which in turn was hydrolyzed to the corresponding acid **23** (Scheme 3.4). The latter was coupled with appropriate amine in the presence of HOBT, HBTU as coupling reagents and DIPEA as a base to furnish **24a-d** in good yields. However, the next cyclization step did not occur. This reaction

### Chapter 3

was also performed in different reaction conditions (i.e.  $\text{CH}_2\text{Cl}_2$ ,  $\text{CH}_2\text{O}$  37 wt.% in  $\text{H}_2\text{O}$ , dry  $\text{MgSO}_4$ , TFA,  $90^\circ\text{C}$ , sealed tube), and in all cases only dimeric compounds **25a-d** were isolated.

#### Scheme 3.4



**Reagents and conditions:** a)  $\text{Cs}_2\text{CO}_3$ ,  $\text{BrCH}_2\text{COOCH}_3$ , DMF, rt, overnight; b) 4N NaOH, MeOH, reflux, 2h; c) HOBt, HBTU, DIPEA, DMF, appropriate amine, rt, 12h; d)  $\text{CH}_2\text{O}$  37 wt.% in  $\text{H}_2\text{O}$ , dry DCM, anhydrous  $\text{MgSO}_4$ , rt, 2h, then TFA,  $90^\circ\text{C}$ , 4h, sealed tube.

In Figure 3.6 the structural characterization of **25a** by 1D and 2D NMR ( $^1\text{H}$ ,  $^{13}\text{C}$ DEPTQ, COSY, HMBC, HSQC) has been reported (see also Appendix).

The results of both mono- and bi-dimensional NMR experiments suggested that the described reaction allowed to the dimerization of the starting reagent through one molecule of the electrophilic reagent formaldehyde. Indeed, in the range 7.0-6.0 ppm of the  $^1\text{H}$  NMR

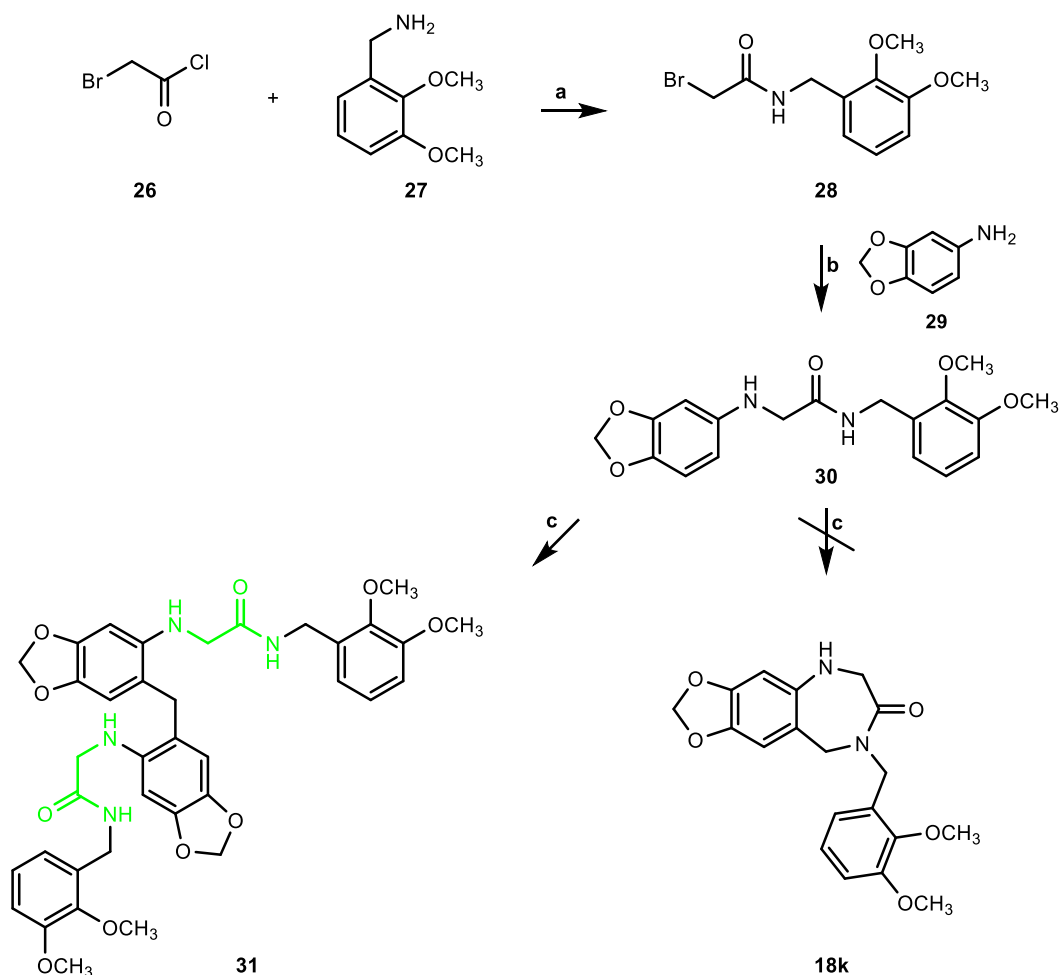


### Chapter 3

formula of  $[\text{C}_{37}\text{H}_{39}\text{N}_2\text{O}_{12}]^+$  ( $\text{MH}^+$  703.2425 uma), the final molecule should have the structure depicted in Figure 3.6.

Similar result was obtained also starting from the amide **30**. The latter was synthesized by a convergent approach (Scheme 3.5), starting from 2-bromoacetyl chloride **26**, that was coupled with 2,3-dimethoxybenzylamine **27** in the presence of TEA (triethylamine) as a base to give the amide **28**. Thus **28** was reacted with amine **29** to furnish the arylaminoamide **30**. Subsequent reaction with formaldehyde and TFA did not provide the desired compound **18k**, but the dimer **31**.

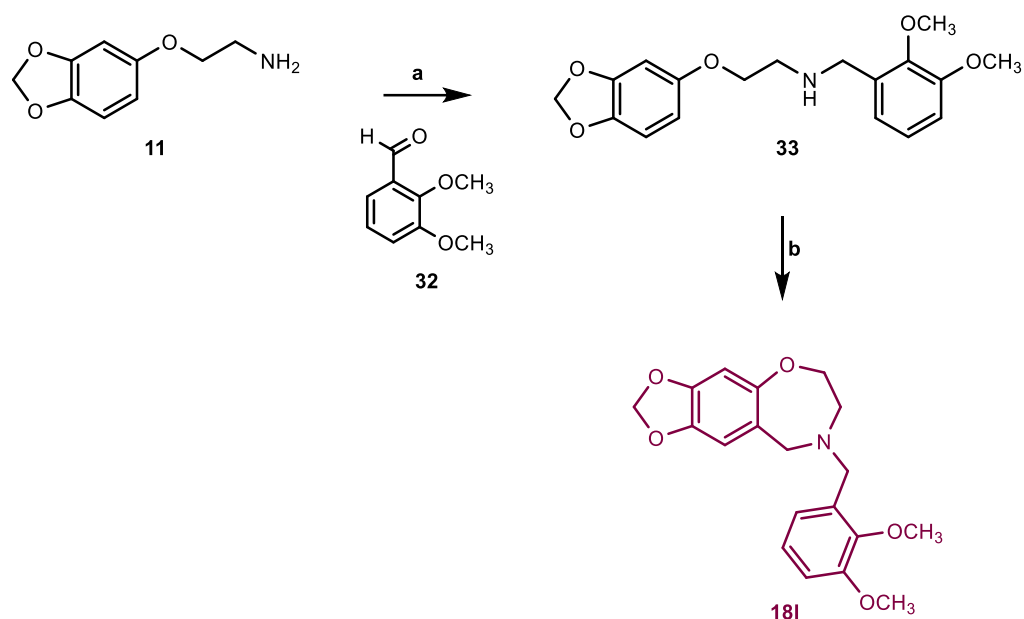
Scheme 3.5



**Reagents and conditions:** a) dry DCM, dry TEA, from 0°C to rt, 12h; b)  $\text{K}_2\text{CO}_3$ , KI, 2-butanone, rt, overnight; c) sealed tube,  $\text{CH}_2\text{O}$  37 wt.% in  $\text{H}_2\text{O}$ , dry DCM, anhydrous  $\text{MgSO}_4$ , rt, 2h, then TFA, 90°C, 4h.

In Scheme 3.6 the synthesis of **18I** is described. Briefly, amine **11** was submitted to reductive amination with 2,3-dimethoxybenzaldehyde **32** and NaBH<sub>4</sub> to furnish amine **33**, which underwent subsequent cyclization via Pictet-Spengler reaction in the presence of formaldehyde and TFA.

Scheme 3.6

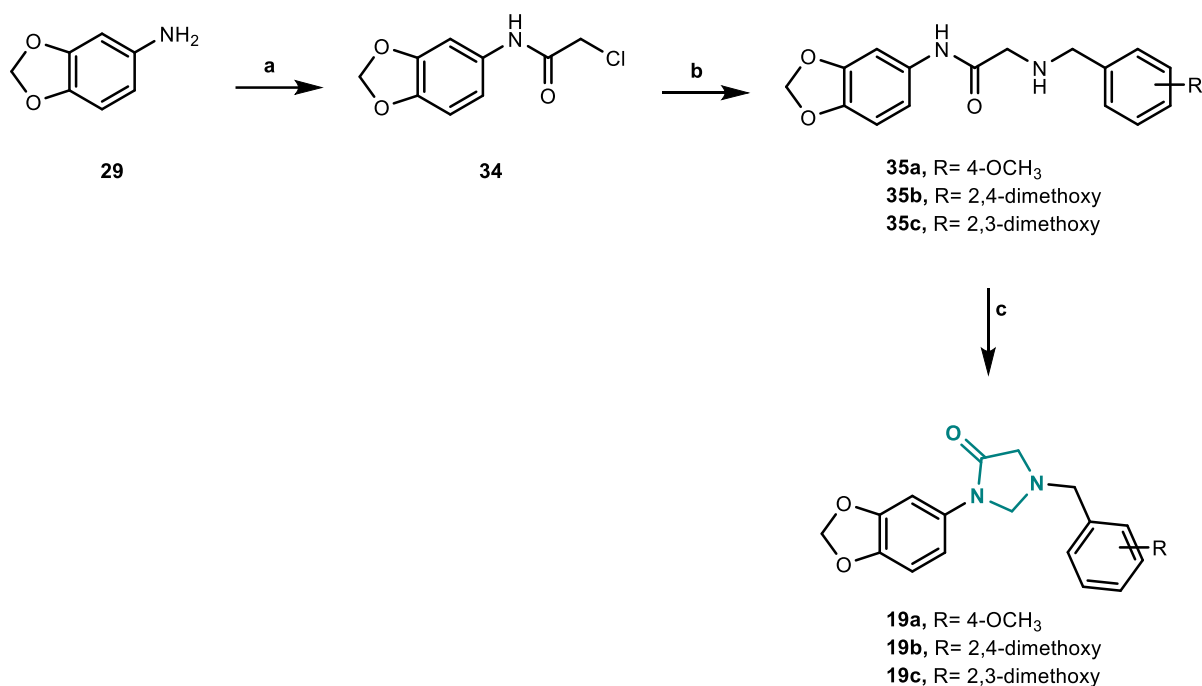


**Reagents and conditions:** a) anhydrous MgSO<sub>4</sub>, dry MeOH, AcOH, rt, 2h, then NaBH<sub>4</sub>, rt, 2h; b) sealed tube, CH<sub>2</sub>O 37 wt.% in H<sub>2</sub>O, dry DCM, anhydrous MgSO<sub>4</sub>, rt, 2h, then TFA, 90°C, 4h.

In Scheme 3.7 the synthesis of 4-imidazolidinone derivatives **19a-c** is reported. The benzo[d][1,3]dioxol-5-amine **29** was reacted with 2-chloroacetyl chloride to give the  $\alpha$ -chloramide **34**, which underwent nucleophilic substitution with appropriate benzylamine to afford  $\alpha$ -aminoamides **35a-c**. Then, the desired 4-imidazolidinone derivatives **19a-c** were obtained by cyclocondensation of **35a-c** in the presence of formaldehyde and TFA. This is an unusual approach to synthesize 4-imidazolidinones, and only few examples based on this procedure have been reported in literature until now.<sup>27</sup>

## Chapter 3

### Scheme 3.7

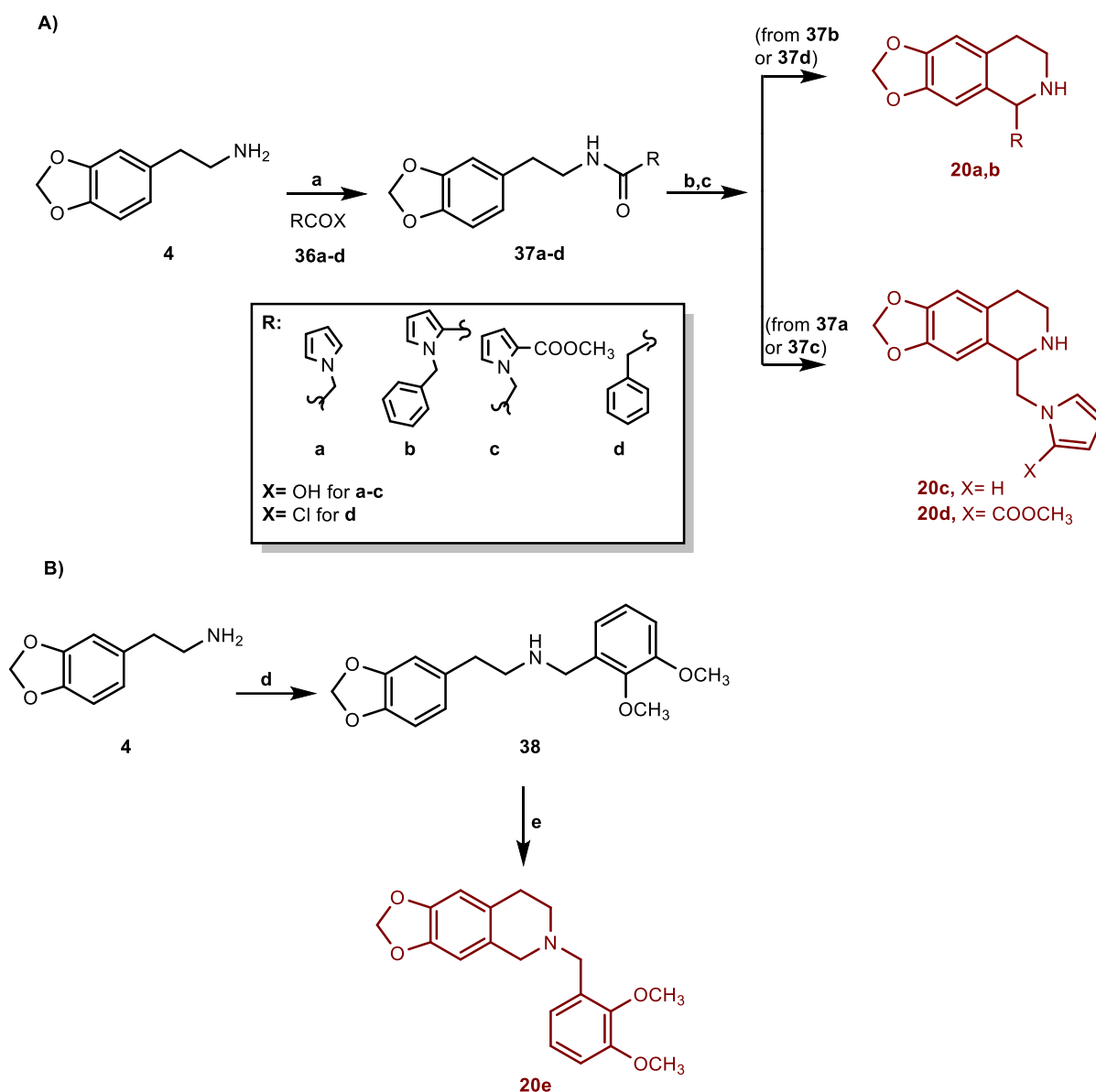


**Reagents and conditions:** a)  $\text{ClCOCH}_2\text{Cl}$ , dry TEA, dry DCM,  $0^\circ\text{C}$  to rt, 2h; b) appropriate amine,  $\text{K}_2\text{CO}_3$ , DMF, rt, 24h; c)  $\text{CH}_2\text{O}$  37 wt.% in  $\text{H}_2\text{O}$ , anhydrous  $\text{MgSO}_4$ , rt, 2h, then TFA,  $90^\circ\text{C}$ , 4h.

The synthesis of **20a-c** was carried out as described in Scheme 3.8. Amine **4** was coupled with **36a-d** using OxymaPure<sup>®</sup> (2-cyano-2-(hydroxyimino)acetate) and EDAC (*N*-(3-dimethylaminopropyl)-*N'*-ethylcarbodiimide) as coupling reagents, and DIPEA as a base (Scheme 3.8, A) to furnish **37a-d**. The cyclization of **37a-d** to the corresponding final compounds **20a-d** was accomplished in two steps. First the intermediates **37a-d** in the presence of  $\text{POCl}_3$  were involved in a Bischler-Napieralski reaction to give the corresponding dihydroisoquinolines (not isolated) which, after work up, were directly reduced to tetrahydroisoquinolines **20a-d** by sodium borohydride (Scheme 3.8, A).<sup>28</sup>

Amine **4** was also reacted with 2,3-dimethoxybenzaldehyde and  $\text{NaBH}_4$  to give amine **38** that was converted to **20e** by Pictet-Spengler reaction with formaldehyde and TFA (Scheme 3.8, B).

Scheme 3.8



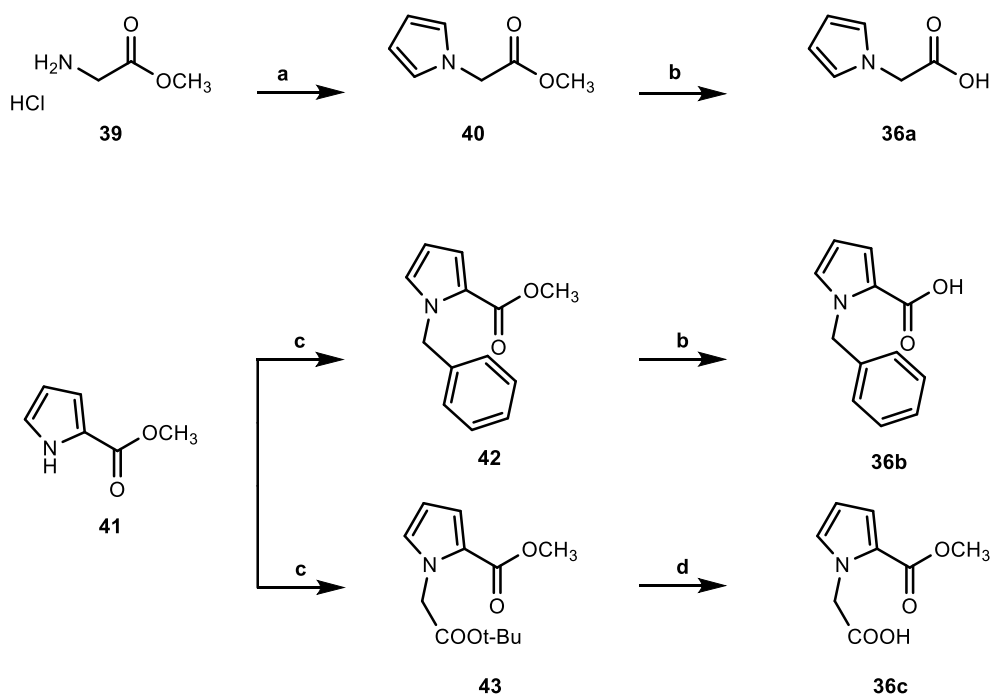
**Reagents and conditions:** a) OxymaPure<sup>®</sup>, EDAC, DIPEA, DMF, rt, 12h, and 2-(1H-pyrrol-1-yl)acetic acid **36a** (for **37a**), or 1-benzyl-1H-pyrrole-2-carboxylic **36b** (for **37b**), or 2-(2-(methoxycarbonyl)-1H-pyrrol-1-yl)acetic acid **36c** (for **37c**), or dry TEA, dry DCM, rt, 1.5h and phenylacetyl chloride **36d** (for **37d**); b) POCl<sub>3</sub>, dry CH<sub>3</sub>CN, reflux, 1h; c) NaBH<sub>4</sub>, dry MeOH, from 0°C to rt, 2h; d) 2,3-dimethoxybenzaldehyde, AcOH, dry MeOH, anhydrous MgSO<sub>4</sub>, rt, 2h, then NaBH<sub>4</sub>, rt, 2h; e) CH<sub>2</sub>O 37 wt.% in H<sub>2</sub>O, dry DCM, anhydrous MgSO<sub>4</sub>, rt, 2h, then TFA, 90°C, 4h.

Acids **36a-c** were synthesized as reported in Scheme 3.9. Glycine methyl ester hydrochloride **39** underwent a modified Clauson-Kaas reaction<sup>29</sup> to provide the pyrrole derivative **40**, which was hydrolyzed to the corresponding acid **36a**.

### Chapter 3

Acids **36b,c** were obtained by hydrolysis of the corresponding ester **42** and **43** respectively, which in turn were synthesized starting from commercially available pyrrole derivative **41**, by *N*-alkylation with benzyl bromide for **42**, and *tert*-butyl 2-bromoacetate for **43**.

Scheme 3.9



**Reagents and conditions:** a) 2,5-dimethoxytetrahydrofuran,  $\text{CH}_3\text{COONa}$ ,  $\text{H}_2\text{O}/\text{DCM}$  (1:2), overnight; b) 4N NaOH, rt, 1h; c) benzyl bromide, NaOH 50% w/v in  $\text{H}_2\text{O}$ , TBAH, DCM, rt, 12h (for **42**), or  $\text{BrCH}_2\text{COOtBu}$ , NaH (60% dispersion in mineral oil), dry DMF, from  $0^\circ\text{C}$  to rt, 1h (for **43**); d) TFA, DCM, rt, 2h.

### 3.5 Biological evaluation

#### 3.5.1 Cell Viability Assay

Compounds **18a-c**, **18l**, **19c**, **24a**, **31** and **25a,b** were evaluated for their cytotoxicity on HepG2 and HaCaT cell lines, using BBR as reference compound (Figures 3.7, 3.8, Tables 3.2, 3.3). HepG2 derives from a human hepatoblastoma, and is a common cell line used for screening lipid-lowering agents, as well as in drug discovery and hepatotoxicity studies since it shares the same function of lipid metabolism as normal hepatocyte metabolism. HaCaT cells are immortalized human keratinocytes, endowed with high capacity to differentiate and proliferate *in vitro*.

Cell viability was evaluated using the MTT assay procedure, which measures the level of mitochondrial dehydrogenase activity using the yellow 3-(4,5-dimethyl-2-thiazolyl)-2,5-diphenyl-2H-tetrazolium bromide (MTT) as substrate. The assay is based on the redox ability of living mitochondria to convert dissolved MTT into insoluble purple formazan. Briefly, for cell viability test, an initial concentration of 3.8 mg/mL in DMSO was prepared for the given substances; the final concentrations (2.5, 5, 15, 30 and 50 µg/mL) administered to cells were obtained in the growth medium selected for each cell line. After treatment for 24, 48 and 72 hours, at the ends of the selected experimental times, MTT stock solution (5 mg/mL) was added to all wells of an assay (25 µL per 100 µL medium), and plates were incubated at 37°C for 4 hours. Next, cells were lysed and the dark blue crystals dissolved with 100 µL of a solution containing 50% (v/v) *N,N*-dimethylformamide, 20% (w/v) SDS with an adjusted pH of 4.5. The optical density (OD) of each well was measured with a microplate spectrophotometer (Titertek Multiskan MCC/340) equipped with a 620 nm filter. HepG2 and HaCaT cells viability in response to treatment with tested compounds was calculated as: % viable cells = [OD (550 nm-690 nm) substances/OD (550 nm-690 nm) negative control] × 100. DMSO 0.1% v/v was used as technical control.

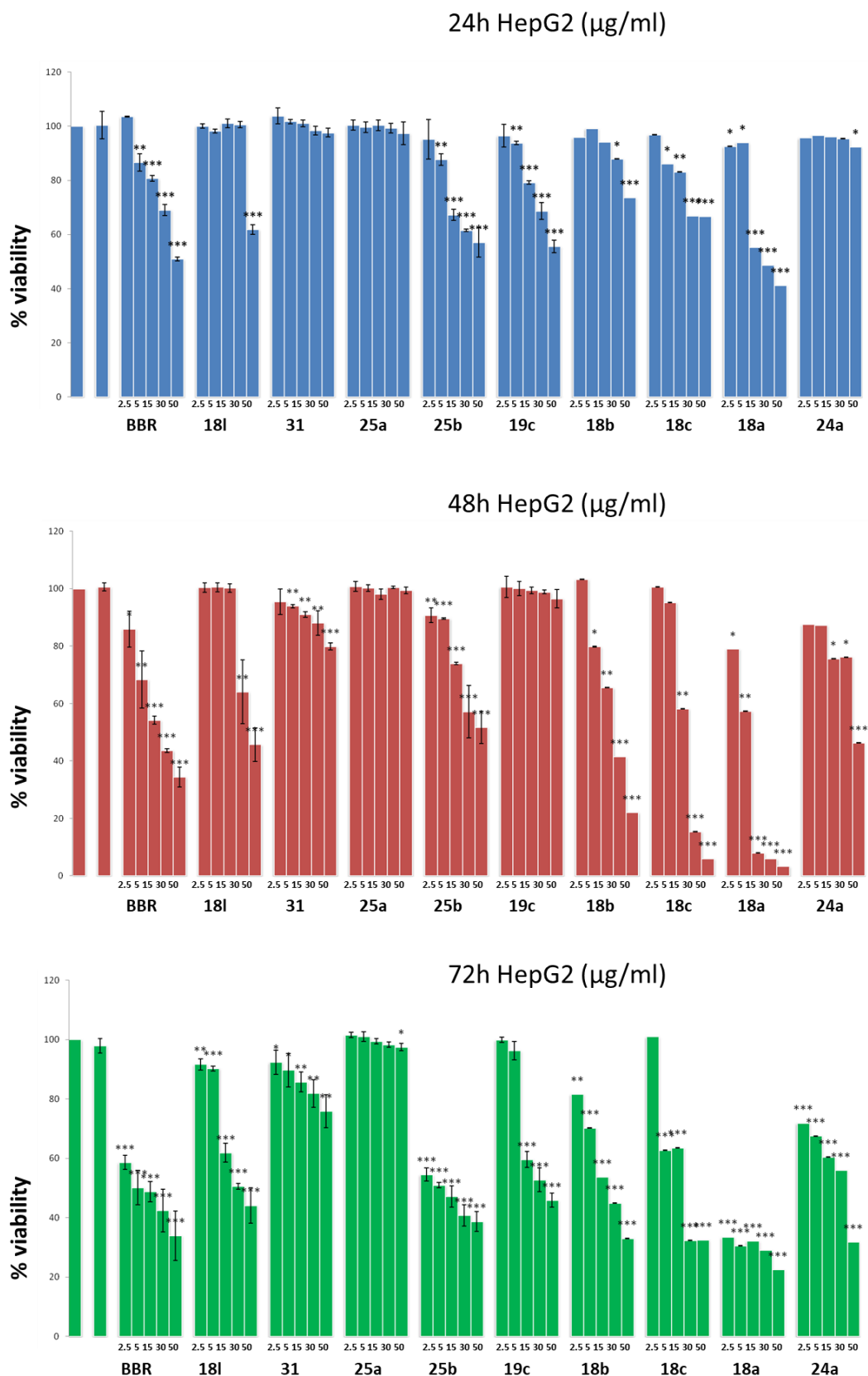


**Figure 3.7** HepG2 cell viability evaluated by MTT assay after treatment for 24, 48 and 72h with title compounds (18a-c, 18l, 19c, 24a, 31, 25a,b and BBR) at final concentration of 2.5, 5, 15, 30 and 50  $\mu\text{g/ml}$ . DMSO 0.1% v/v was used as technical control.

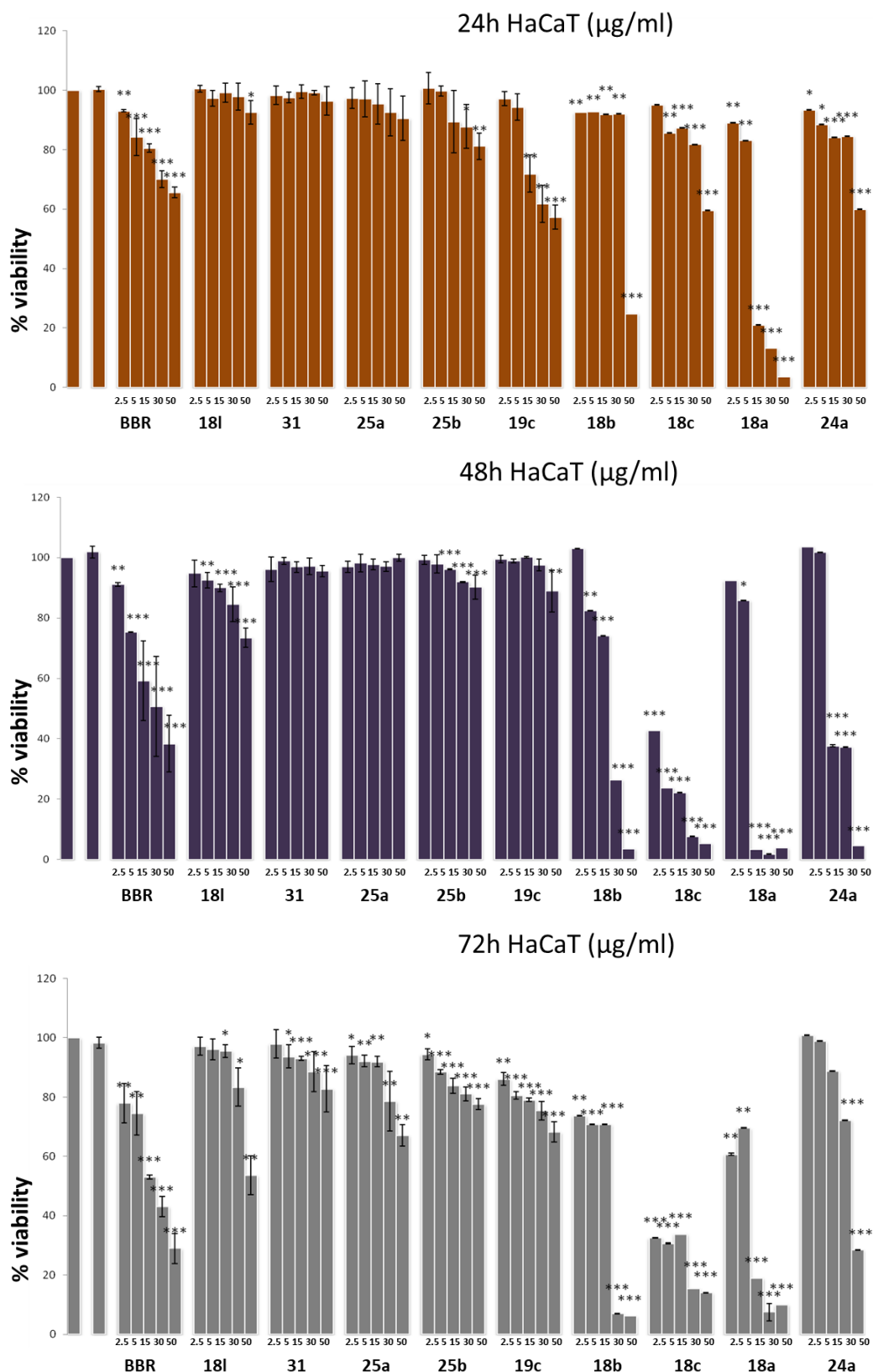


**Figure 3.8** HaCaT cell viability evaluated by MTT assay after treatment for 24, 48 and 72h with title compounds (18a-c, 18l, 19c, 24a, 31, 25a,b and BBR) at final concentration of 2.5, 5, 15, 30 and 50  $\mu\text{g/mL}$ ; DMSO 0.1% v/v was used as technical control.

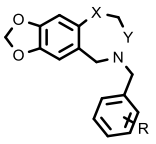
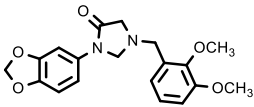
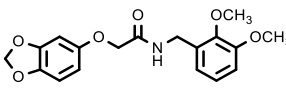
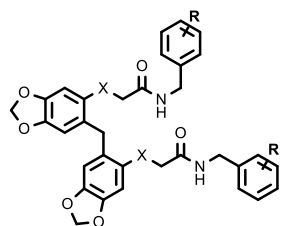
### Chapter 3

On HepG2 cell line, the benzazepinone derivatives **18a-c** exhibited a cytotoxic activity higher than that of our reference compound, with IC<sub>50</sub> values in a low micromolar range (Table 3.2).

On HaCaT cell line compounds **18b** and **18c** bearing an electron-donor and an electron-withdrawing group respectively at the para position of pendent benzyl moiety, were less cytotoxic compared to **18a**. Moreover, replacement of the benzazepinone ring with a benzoxazepine ring reduced cytotoxicity on both cell lines (**18l** vs **18a**, Tables 3.2, 3.3). Introduction of a 4-imidazolidinone ring gave rise to **19c** which showed an antiproliferative activity similar to that of BBR after 24h of treatment (Tables 3.2, 3.3).

Interestingly, IC<sub>50</sub> value of **19a** after 48h of treatment was significantly higher than that observed after 24h and 72h of treatment on both cell lines. The reason for this behavior is currently under investigation.

**Table 3.2** IC<sub>50</sub> (μM) values of tested compounds evaluated on HepG2 cell line

	Cpd	X	Y	R	<sup>a</sup> IC <sub>50</sub> 24h	<sup>a</sup> IC <sub>50</sub> 48h	<sup>a</sup> IC <sub>50</sub> 72h
	<b>BBR</b>	-	-	-	134.1±19.7	75.9±5.9	35.9±5.8
	<b>18a</b>	CH <sub>2</sub>	C=O	2,3-dimethoxy	11.8±0.2	5.7±0.3	13.2±0.4
	<b>18b</b>	CH <sub>2</sub>	C=O	4-OCH <sub>3</sub>	35.3±0.4	11.0±1.1	10.8±0.6
	<b>18c</b>	CH <sub>2</sub>	C=O	4-Cl	20.7±0.4	9.5±0.5	10.5±0.6
	<b>18l</b>	O	CH <sub>2</sub>	2,3-dimethoxy	234.1±17.7	134.1±6.3	109.6±20.3
	<b>19c</b>	-	-	-	151.6±3.0	1818.9±31.6	109.2±3.7
	<b>24a</b>	-	-	-	260.7±0.4	16.8±0.6	11.0±0.5
	<b>25a</b>	O	-	2,3-dimethoxy	1278.5±16.0	1252.0±9.0	867.9±7.9
	<b>25b</b>	O	-	2,5-dimethoxy	73.9±2.4	66.0±2.5	13.4±1.9
	<b>31</b>	NH	-	2,3-dimethoxy	627.3±11.6	212.4±16.4	182.2±33.2

<sup>a</sup>Compound concentration required to reduce cell proliferation by 50%, as determined by the MTT assay; data represent mean values (±SD) for three independent determinations. The statistical relevance was evaluated vs not treated cells though two-tailed t-test comparing two variables. Differences were considered significant if  $p < 0.05$  (\*),  $p < 0.01$  (\*\*),  $p < 0.001$  (\*\*\*)

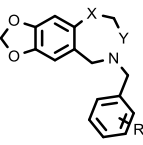
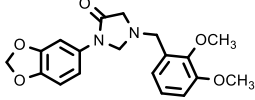
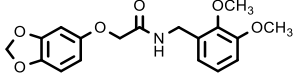
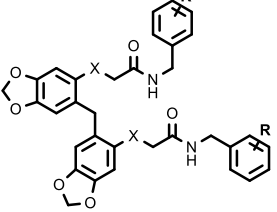
The dimer **25a** showed no appreciable cytotoxic activity against both cell lines (Figure 3.7, 3.8, Table 3.2, 3.3) at higher dose used; on the contrary, a significant antiproliferative activity was observed after 48 and 72h of treatment with its monomer **24a**.

The dimer analogue **31** was more cytotoxic on HepG2 cell line compared to **25a**, but less cytotoxic on HaCaT cell line.

Interestingly, shifting the methoxy group from C-3 to C-5 (**25b** vs **25a**) markedly reduced cell viability (Tables, 3.2, 3.3).

Following these results, compounds **18l**, **25a** and **31** were selected to assess their ability to reduce total cholesterol and triglycerides levels on HepG2 cells.

**Table 3.3**  $IC_{50}$  ( $\mu M$ ) values of tested compounds evaluated on HaCaT cell line

	Cpd	X	Y	R	<sup>a</sup> IC <sub>50</sub> 24h	<sup>a</sup> IC <sub>50</sub> 48h	<sup>a</sup> IC <sub>50</sub> 72
	<b>BBR</b>	-	-	-	201.1±33.8	90.8±26.9	69.6±6.2
	<b>18a</b>	CH <sub>2</sub>	C=O	2,3-dimethoxy	45.0±0.6	38.6±0.6	19.5±1.0
	<b>18b</b>	CH <sub>2</sub>	C=O	4-OCH <sub>3</sub>	131.8±0.5	74.9±1.0	55.0±0.9
	<b>18c</b>	CH <sub>2</sub>	C=O	4-Cl	214.8±1.2	73.5±0.5	107.3±0.9
	<b>18l</b>	O	CH <sub>2</sub>	2,3-dimethoxy	1133.9±44.9	313.0±50.0	174.2±6.3
	<b>19c</b>	-	-	-	144.3±6.6	687.9±31.1	228.0±29.5
	<b>24a</b>	-	-	-	212.8±1.0	69.3±1.6	84.9±1.4
	<b>25a</b>	O	-	2,3-dimethoxy	1877.1±45.3	1603.7±13.2	256.7±28.7
	<b>25b</b>	O	-	2,5-dimethoxy	178.2±41.8	364.7±12.8	145.3±13.2
	<b>31</b>	NH	-	2,3-dimethoxy	2383.7±18.2	1998.9±16.6	234.7±34.2

<sup>a</sup>Compound concentration required to reduce cell proliferation by 50%, as determined by the MTT assay; data represent mean values ( $\pm$ SD) for three independent determinations. The statistical relevance was evaluated vs not treated cells though two-tailed *t*-test comparing two variables. Differences were considered significant if  $p < 0.05$  (\*),  $p < 0.01$  (\*\*),  $p < 0.001$  (\*\*\*)

## 3.5.2 Quantification of TCHO and TG

HepG2 cells were grown in high-glucose Dulbecco's modified Eagle's medium (DMEM) supplemented with 10% fetal bovine serum (FBS), 100 U/mL penicillin, and 100 µg/mL streptomycin and propagated at 37°C in a humidified atmosphere containing 5% CO<sub>2</sub> in air.

Compounds **18l**, **25a**, and **31** were dissolved in DMSO to make stock solutions; the final concentrations (5, 10 and 30 µM) administered to cells were obtained in the growth medium. BBR was used as reference compound, and given its cytotoxicity on HepG2 cells, was evaluated only at 5 and 10µM. The final concentration of the vehicle in the solution never exceeded 0.1%.

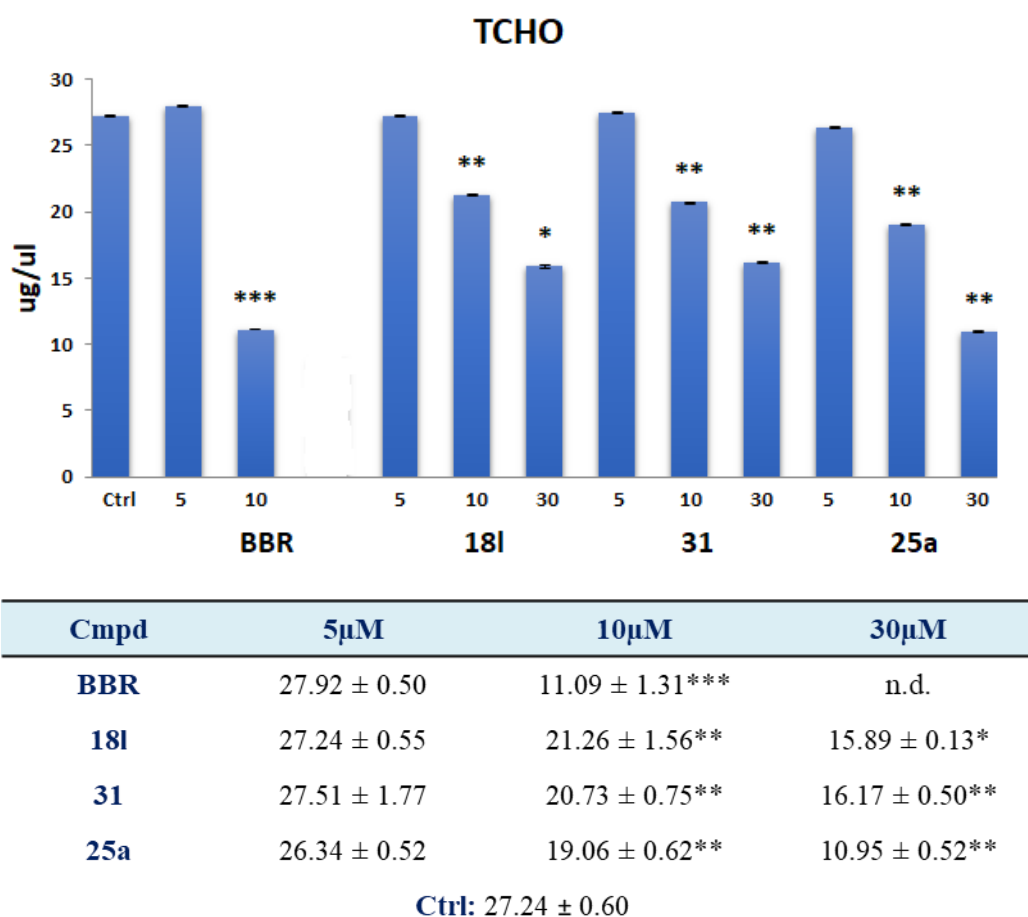


**Figure 3.9** Evaluation of TCHO levels in HepG2 cells after treatment for 48h with title compounds at indicated final concentrations (µM). DMSO 0.1% v/v was used as technical control. Data represent mean values (±SD) of triplicate determinations from two independent experiments. The statistical relevance was evaluated vs not treated cells though two-tailed t-test comparing two variables. Differences were considered significant if  $p < 0.05$  (\*),  $p < 0.01$  (\*\*),  $p < 0.001$  (\*\*\*)

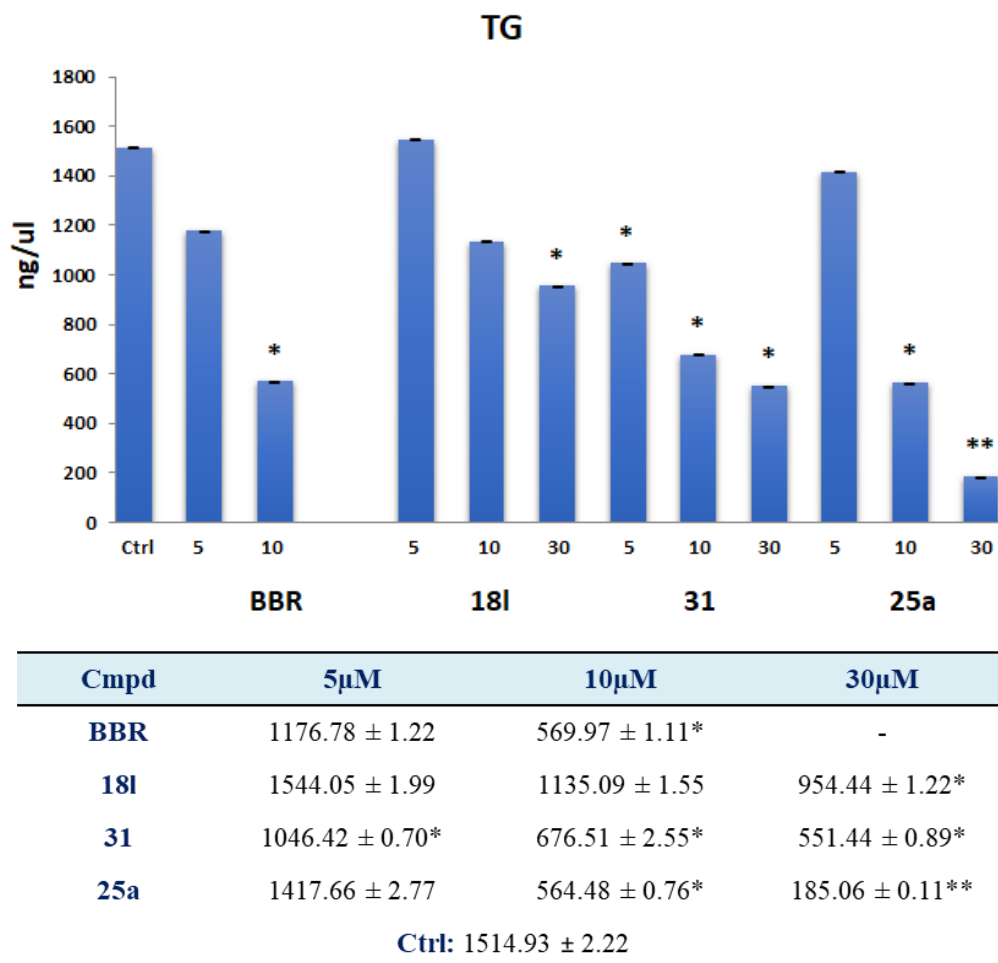


**Figure 3.10** Evaluation of TG levels in HepG2 cells after treatment for 48h with title compounds at indicated final concentrations ( $\mu\text{M}$ ). DMSO 0.1% v/v was used as technical control. Data represent mean values ( $\pm\text{SD}$ ) of triplicate determinations from two independent experiments. The statistical relevance was evaluated vs not treated cells though two-tailed *t*-test comparing two variables. Differences were considered significant if  $p < 0.05$  (\*),  $p < 0.01$  (\*\*),  $p < 0.001$  (\*\*\*)

After 48h of treatment, cells were lysed, and cell lysates were used to measure the levels of total cholesterol (TCHO) and triglycerides (TG), using an assay kit directly (MAK045 for TCHO, and MAK266 for TG, from MERK), following manufacturer's instructions.

All tested compounds at 10 $\mu\text{M}$  were less effective than BBR at reducing TCHO (Figure 3.9) A significant inhibition rate of about 60% against total cholesterol was observed for **25a** at 30 $\mu\text{M}$ . Benzoxazepine **18I** at 10 $\mu\text{M}$  showed a modest inhibitory activity against TG compared to dimers **31** and **25a**, which in turn at 10 $\mu\text{M}$  exhibited inhibition rate similar to that of BBR (55% and 63% for **31** and **25a** respectively vs 62% of BBR, Figure 3.10). Interestingly,

### Chapter 3

compound **25a** at 30 $\mu$ M displayed an extremely high inhibitory rate compared to its analogue **31** (88% of **25a** vs 64% of **31**, Figure 3.10), suggesting that the introduction of an H-donor group at positions 3,3' can reduce the lipid-lowering activity of this class of derivatives.

#### 3.5.3 Real-time Quantitative Reverse Transcription PCR (qRT-PCR) analysis

Compounds **18l** and **31** were evaluated on HepG2 cells to assess by qRT-PCR their ability to modulate LDLR expression after 48h of treatment at 10 $\mu$ M, using BBR as reference compound. As shown in Figure 3.11, both tested compounds were able to increase LDLR expression, although **18l** was less effective with respect to both **31** and BBR.

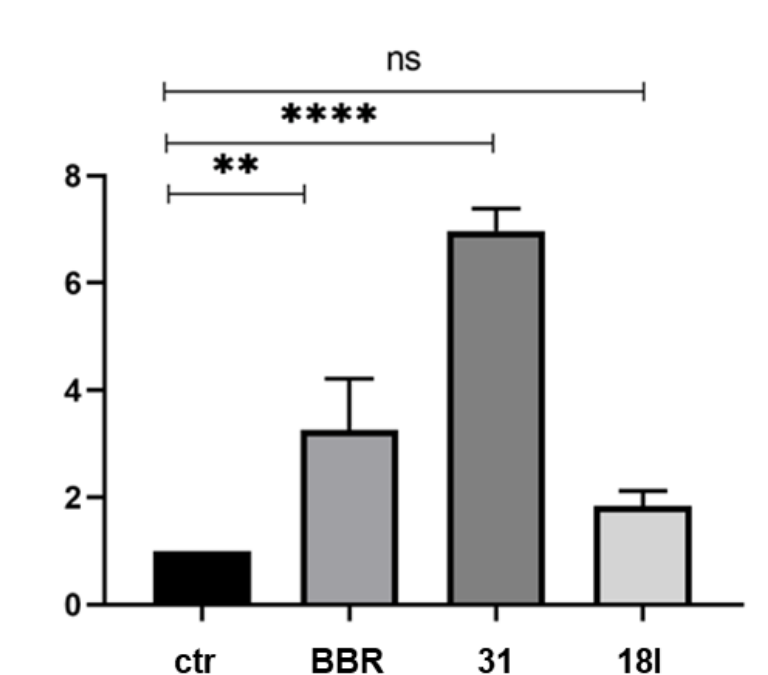


**Figure 3.11** Statistical analyses were performed with GraphPad Prism 6.0. Data are expressed as the mean  $\pm$  SEM, and differences were considered significant at  $p \leq 0.05$  with ranks \*  $p < 0.05$ , \*\*  $p < 0.01$ , \*\*\*  $p < 0.001$ , \*\*\*\*  $p < 0.0001$  ( $n = 2$ ).

Compounds **18l** and **31** are not structurally related since **18l** is a benzoxazepine derivative and **31** is a dimeric bis-amide. Thus a deeper investigation is needed to assess whether these two compounds share the same molecular mechanism.

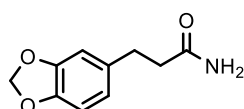
### 3.6 Experimental section

#### 3.6.1 General

$^1\text{H}$  and  $^{13}\text{C}$  NMR spectra were recorded at 400 and 101 MHz respectively, using a Bruker Avance 400 MHz spectrometer. Splitting patterns are described as singlet (s), doublet (d), triplet (t), quartet (q), quintuplet (qt), and broad (br). Mass spectra were obtained by electrospray ionization (ESIMS) using a Thermo Finnigan LCQ Deca XP Max ion-trap mass spectrometer equipped with Xcalibur software and an LTQ Orbitrap XL mass spectrometer (Thermo Fisher Scientific, San Jose, CA, USA) operating in either positive or negative ionization mode. The Orbitrap mass analyzer was calibrated according to the manufacturer's directions using a mixture of caffeine, methionine-arginine-phenylalanine-alanine-acetate (MRFA), and Ultramark 1621 in a solution of acetonitrile, methanol, and acetic acid. Chromatographic separations were performed on silica gel (Kieselgel 40, 0.040–0.063 mm, Merck). Reactions and product mixtures were routinely monitored by thin-layer chromatography (TLC) on Merck 0.2 mm precoated silica (60 F254) aluminum sheets, with visualization by irradiation with a UV lamp. Yields refer to purified products and are not optimized. All starting materials, reagents, and solvents (reagent grade) were purchased from Sigma-Aldrich and used without further purification.

#### 3.6.2 Synthesis of BBR and 17

##### 3-(Benzo[d][1,3]dioxol-5-yl)propanamide **3**

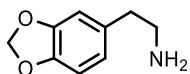


To a solution of 3-(benzo[d][1,3]dioxol-5-yl)propanoic acid **2** (1.0 g, 5.15 mmol) in dry dioxane (25 mL), dry pyridine (0.25 mL, 3.09 mmol),  $(\text{Boc})_2\text{O}$  (1.46 g, 6.69 mmol) and  $\text{NH}_4\text{HCO}_3$  (0.529 g, 6.69 mmol) were added. The resulting mixture was stirred at room temperature for 12h. The solvent was removed under reduced pressure, and the residue was

### Chapter 3

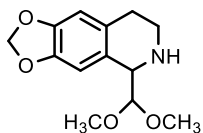
taken up in EtOAc and washed with H<sub>2</sub>O (2x20 mL) and brine (2x20 mL). The organic phase was dried over anhydrous Na<sub>2</sub>SO<sub>4</sub>, filtered and solvent was removed under vacuum. The residue was purified by flash chromatography (SiO<sub>2</sub>, EtOAc/*n*-hexane 8:2 as eluent) to give the title compound as a white solid. Yield: 87%. <sup>1</sup>HNMR (CDCl<sub>3</sub>) δ: 2.52 (t, 2H, *J*= 8.0 Hz), 2.92 (t, 2H, *J*= 8.0 Hz), 5.40 (brs, 2H), 5.95 (s, 2H), 6.67-6.78 (m, 3H).

#### 2-(Benzo[d][1,3]dioxol-5-yl)ethan-1-amine **4**



To a solution of **3** (0.485 g, 2.51 mmol) in EtOAc/CH<sub>3</sub>CN/H<sub>2</sub>O (2:2:1, 15 mL), pyridine (1.0 mL, 12.6 mmol) and [bis(trifluoroacetoxy)iodo]benzene (PIFA) (2.16 g, 5.02 mmol) were added, and the mixture was stirred at room temperature for 12h. Then Na<sub>2</sub>S<sub>2</sub>O<sub>3</sub> (20% 6.3 mL, 5.02 mmol) was added, and the mixture was stirred for 30 min. The organic solvent was removed under reduced pressure, and the residue was taken up in EtOAc and washed with 1M NaOH (2x20 mL) and brine (2x20 mL). The organic layer was washed with brine, dried over anhydrous Na<sub>2</sub>SO<sub>4</sub>, filtered and concentrated under reduced pressure. The crude material was purified by flash chromatography (SiO<sub>2</sub>, EtOAc 100%, then EtOAc/MeOH/NH<sub>4</sub>OH 9:1:0.2 as eluent) to give the title compound as a pale yellow solid. Yield: 90%. <sup>1</sup>HNMR (CDCl<sub>3</sub>) δ: 2.84 (t, 2H, *J*= 8.0 Hz), 3.10 (t, 2H, *J*= 8.0 Hz), 5.90 (s, 2H), 6.63 (m, 2H), 6.72 (m, 1H). HRMS (ESI) *m/z* [M+H]<sup>+</sup> calcd for [C<sub>9</sub>H<sub>12</sub>NO<sub>2</sub>]<sup>+</sup> 166.0862, found 166.0861.

#### 5-(Dimethoxymethyl)-5,6,7,8-tetrahydro-[1,3]dioxolo[4,5-*g*]isoquinoline **5**



To a solution of 2-(benzo[d][1,3]dioxol-5-yl)ethan-1-amine **4** (0.445 g, 2.69 mmol) in dry dichloromethane (14 mL) 2,2-dimethoxyacetaldehyde (60 wt.% in H<sub>2</sub>O, 0.841 g, 8.08 mmol) was added, followed by addition of anhydrous MgSO<sub>4</sub> (6.00 g, 4.98 mmol). The resulting mixture was stirred at room temperature for 2h, and then filtered through a pad of celite. The residue was washed with dry DCM (3x10 mL), and the organic phase was concentrated under

vacuum to  $\approx$  15 mL. Trifluoroacetic acid (6.0 mL, 0.0783 mmol) was added, and the resulting mixture was stirred at room temperature for 2h, then washed with water (3x15 mL). The combined aqueous phases were basified with 50% NaOH (pH  $\approx$  9) and extracted with EtOAc (3x20 mL). The combined organic phases were dried over dry Na<sub>2</sub>SO<sub>4</sub>, filtered and solvent was removed under reduced pressure. After purification by flash chromatography (SiO<sub>2</sub>, EtOAc/MeOH 9:1, then DCM/MeOH 9:1 as eluent), the title compound was obtained as a yellow oil. Yield: 75%. <sup>1</sup>HNMR (CDCl<sub>3</sub>)  $\delta$ : 2.73 (t, 2H,  $J$ = 5.9 Hz), 2.92-2.98 (m, 1H), 3.18-3.24 (m, 1H), 3.29 (brs, 1H), 3.43 (s, 6H), 3.96 (d, 1H,  $J$ = 5.8 Hz), 4.43 (d, 1H,  $J$ = 5.8 Hz), 5.89 (s, 2H), 6.55 (s, 1H), 6.88 (s, 1H).

*6-(2,3-Dimethoxybenzyl)-5-(dimethoxymethyl)-5,6,7,8-tetrahydro-[1,3]dioxolo[4,5-g]isoquinoline 6*



To a solution of **5** (0.463 g, 1.84 mmol) in dry MeOH (5 mL) 2,3-dimethoxybenzaldehyde (0.337 g, 2.03 mmol), acetic acid (0.221 g, 3.69 mmol) and sodium cyanoborohydride (0.586 g, 2.77 mmol) were added, and the resulting mixture was stirred at room temperature for 24h. Then the mixture was basified with 4N NaOH (pH  $\approx$  9), and methanol was removed under reduced pressure. The residue was taken up with DCM; the organic phase was dried (Na<sub>2</sub>SO<sub>4</sub>), filtered, and solvent was removed under vacuum. After purification by flash chromatography (SiO<sub>2</sub>, *n*-hexane/EtOAc 7:3 as eluent), the title compound was obtained as a yellow oil. Yield: 68%. <sup>1</sup>HNMR (CDCl<sub>3</sub>)  $\delta$ : 2.49-2.54 (m, 1H), 2.78-2.91 (m, 2H), 3.21-3.27 (m, 1H), 3.32 (s, 6H), 3.70 (d, 1H,  $J$ = 5.0 Hz), 3.73 (d, 1H, overlapped), 3.76 (s, 3H), 3.83 (d, 1H, overlapped), 3.86 (s, 3H), 4.39 (d, 1H,  $J$ = 5.0 Hz), 5.89 (m, 2H), 6.56 (s, 1H), 6.79 (s, 1H), 6.83 (dd, 1H,  $J$ = 8.0, 1.6 Hz), 7.03 (t, 1H,  $J$ = 7.9 Hz), 7.10 (d, 1H,  $J$ = 7.7 Hz).

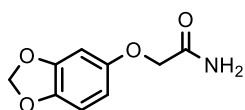
*9,10-Dimethoxy-5,6-Dihydro-[1,3]dioxolo[4,5-g]isoquinolino[3,2a]isoquinolin-7-ium chloride 1 (BBR)*

### Chapter 3



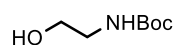
To a solution of **6** (0.289 g, 0.720 mmol) in dry DCM (15 mL), cooled to 0°C, triflic acid (0.324 g, 2.16 mmol) was added dropwise. The resulting mixture was stirred for 10 min, then was allowed to warm to room temperature and stirred in these conditions for 2h. The mixture was taken up in DCM, and washed with a saturated solution of NaHCO<sub>3</sub> (3x15 mL). The organic phase was dried over dry Na<sub>2</sub>SO<sub>4</sub>, filtered, and solvent was removed under reduced pressure. The residue was diluted with ethanol (5 mL), and sodium acetate (0.0738 g, 0.9 mmol) was added followed by a solution of iodine (0.183 g, 0.72 mmol) in ethanol (1 mL). After 1h, a solution of Na<sub>2</sub>S<sub>2</sub>O<sub>3</sub> (10 wt.% in H<sub>2</sub>O, 30 mL) was added, and the mixture was stirred for 15 min. Then organic solvent was removed under reduced pressure, and a 20% NaOH solution (10 mL) was added to the resulting residue. The mixture was stirred at room temperature for 10 min, and then washed with DCM (3x15 mL). The combined organic phases were washed with 1N HCl (3x15 mL). The combined aqueous phases were concentrated under reduced pressure. The resulting residue was purified by flash chromatography (SiO<sub>2</sub>, DCM then DCM/MeOH 9:1 as eluent) to give the title compound as a yellow solid. Yield: 88%. <sup>1</sup>HNMR (DMSO-d<sub>6</sub>) δ: 3.21 (t, 2H, *J*= 6.2 Hz), 4.07 (s, 3H), 4.10 (s, 3H), 4.95 (t, 2H, *J*= 6.3 Hz), 6.18 (s, 2H), 7.09 (s, 1H), 7.81 (s, 1H), 8.02 (d, 1H, *J*= 9.1 Hz), 8.21 (d, 1H, *J*= 9.1 Hz), 8.97 (s, 1H), 9.91 (s, 1H); <sup>13</sup>CNMR (DMSO-d<sub>6</sub>) δ: 26.8, 55.7, 57.6, 62.4, 102.6, 105.9, 108.9, 120.7, 120.9, 121.9, 124.0, 127.3, 131.2, 133.5, 138.0, 144.1, 145.9, 148.2, 150.3, 150.9. HRMS (ESI) *m/z* [M+H]<sup>+</sup> calcd for [C<sub>20</sub>H<sub>18</sub>NO<sub>4</sub>]<sup>+</sup> 336.1230, found 336.1220.

#### *2-(Benzo[d][1,3]dioxol-5-yloxy)acetamide 10*



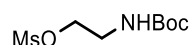
To a solution of sesamol **9** (0.50 g, 3.62 mmol) in DMF (5 mL) Cs<sub>2</sub>CO<sub>3</sub> (3.54 g, 0.211 mol) was added, and the resulting mixture was stirred at room temperature for 30 min, then 2-bromoacetamide (0.749 g, 5.43 mmol) was added. After 24h the mixture was diluted with a saturated solution of NaHCO<sub>3</sub> (20 mL) and EtOAc (30 mL). The layers were separated, and the organic phase was dried over dry Na<sub>2</sub>SO<sub>4</sub>, filtered and solvent was removed under reduced pressure. The resulting residue was purified by flash chromatography (SiO<sub>2</sub>, EtOAc/*n*-hexane 8:2 as eluent) to give the title compound as a white solid. Yield: 86%. <sup>1</sup>HNMR (CDCl<sub>3</sub>) δ: 4.42 (s, 2H), 5.70 (brs, 2H), 5.94 (s, 2H), 6.34 (dd, 1H, *J*= 8.5, 2.6 Hz), 6.51 (d, 1H, *J*= 2.6 Hz), 6.72 (d, 1H, *J*= 8.5 Hz).

*tert*-Butyl (2-hydroxyethyl)carbamate **15**



To a mixture of 2-aminoethan-1-ol **14** (2.50 g, 40.9 mmol) and NaI (6.13 g, 40.9 mmol) in THF (20 mL), cooled to 0°C, a solution of (Boc)<sub>2</sub>O (10.72 g, 49.11 mmol) in THF (25 mL) was added dropwise. The resulting mixture was allowed to warm to room temperature and stirred in these conditions for 1h, then solvent was removed under reduced pressure. The residue was taken up in EtOAc and washed with 5% Na<sub>2</sub>S<sub>2</sub>O<sub>3</sub> (2x15 mL). The organic layer was dried over dry Na<sub>2</sub>SO<sub>4</sub>, filtered and solvent was removed under reduced pressure. The resulting solid was enough pure to be used in the next step without further purification. <sup>1</sup>HNMR CDCl<sub>3</sub> δ: 1.43 (s, 9H), 3.27 (q, 2H, *J*= 5.4 Hz), 3.68 (q, 2H, *J*= 5.2 Hz), 5.02 (brs, 1H).

2-((*tert*-Butoxycarbonyl)amino)ethyl methanesulfonate **12**

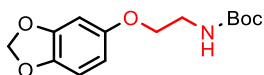


To a solution of **15** (2.50 g, 15.5 mmol) in dry DCM (15 mL) cooled to 0°C, dry TEA (1.96 g, 19.4 mmol) was added followed by dropwise addition of methanesulfonyl chloride (2.13 g, 18.6 mmol). The resulting mixture was allowed to warm to room temperature for 4h, then diluted with DCM, and washed with saturated solution of NaHCO<sub>3</sub> (3x15 mL) and brine (2x20 mL). The organic phase was dried over anhydrous Na<sub>2</sub>SO<sub>4</sub>, filtered and concentrated under

### Chapter 3

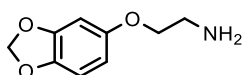
reduced pressure. The crude material was purified by flash chromatography (SiO<sub>2</sub>, EtOAc/*n*-hexane 7:3 as eluent) to give the title compound as a white solid. Yield: 94%. <sup>1</sup>HNMR (CDCl<sub>3</sub>) δ: 1.45 (s, 9H), 3.04 (s, 3H), 3.49 (m, 2H), 4.29 (t, *J*= 5.1 Hz, 2H), 4.95 (brs, 1H).

#### *tert*-Butyl (2-(benzo[d][1,3]dioxol-5-yloxy)ethyl)carbamate **13**



To a solution of sesamol **9** (0.700 g, 48.5 mmol) in DMF (7 mL), Cs<sub>2</sub>CO<sub>3</sub> (2.37 g, 72.7 mmol) and 2-((*tert*-butoxycarbonyl)amino)ethyl methanesulfonate **12** (0.0131 g, 54.6 mmol) were added, and the mixture was stirred at 60°C overnight. The reaction mixture was diluted with NaOH 1M and washed with EtOAc (2x25 mL). The combined organic layers were dried over anhydrous Na<sub>2</sub>SO<sub>4</sub>, filtered and concentrated under reduced pressure. The crude material was purified by flash chromatography (SiO<sub>2</sub>, *n*-hexane/EtOAc 1:1 as eluent) to give the title compound as a pale yellow oil. Yield: 88%. <sup>1</sup>HNMR (CDCl<sub>3</sub>) δ: 1.45 (s, 9H), 3.46-3.50 (m, 2H), 3.93 (t, 2H, *J*= 5.1 Hz), 4.98 (brs, 1H), 5.90 (s, 2H), 6.30 (dd, 1H, *J*= 8.5, 2.5 Hz), 6.47 (d, 1H, *J*= 2.5 Hz), 6.69 (d, 1H, *J*= 8.5 Hz). <sup>13</sup>CNMR (CDCl<sub>3</sub>) δ: 28.7, 40.5, 68.4, 79.8, 98.4, 101.5, 106.0, 108.3, 142.2, 148.6, 154.4, 156.2.

#### 2-(Benzo[d][1,3]dioxol-5-yloxy)ethan-1-amine **11**

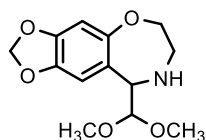


*Route A*) 2-(benzo[d][1,3]dioxol-5-yloxy)acetamide **10** (1.0 g, 5.12 mmol) was dissolved in dry THF (15 mL), and the solution was cooled to 0°C, then LiAlH<sub>4</sub> (15.37 mL, 1M in THF) was slowly added. The mixture was stirred for 10 min, then was allowed to warm to room temperature. After 2.5h the reaction mixture was cooled with ice bath and EtOAc (~20 mL) was carefully added to destroy the excess of LiAlH<sub>4</sub>. The resulting suspension was filtered through a pad of celite, and the residue was washed with EtOAc (3x15 mL). The combined organic phases were dried over anhydrous Na<sub>2</sub>SO<sub>4</sub>, filtered and concentrated under vacuum.

The residue was purified by flash chromatography (SiO<sub>2</sub>, EtOAc/MeOH 8:2 as eluent) to give the title compound as a colorless oil. Yield: 56%.

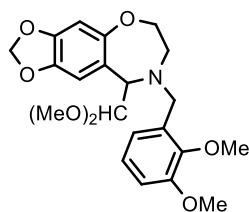
*Route B*) To a solution of *tert*-butyl (2-(benzo[d][1,3]dioxol-5-yloxy)ethyl)carbamate **13** (0.394 g, 1.42 mmol) in DCM (10 mL), trifluoroacetic acid (1.08 mL, 14.2 mmol) was added, and the mixture was stirred at room temperature for 1h. The organic solvent was removed under reduced pressure, and the residue was taken up in EtOAc and washed with Na<sub>2</sub>CO<sub>3</sub> saturated solution. The organic layer was dried over Na<sub>2</sub>SO<sub>4</sub>, filtered and concentrated under vacuum to give the title compound as a colorless oil. Yield: 90%. <sup>1</sup>HNMR (CDCl<sub>3</sub>) δ: 3.04 (t, 2H, *J*= 5.2 Hz), 3.92 (t, 2H, *J*= 5.2 Hz), 5.91 (s, 2H), 6.33 (dd, 1H, *J*= 8.5, 2.5 Hz), 6.50 (d, 1H, *J*= 2.5 Hz), 6.70 (d, 1H, *J*= 8.5 Hz).

*9-(Dimethoxymethyl)-6,7,8,9-tetrahydro [1,3]dioxolo[4',5':4,5]benzo[1,2-f][1,4]oxazepine 16*



The title compound was synthesized starting from 2-(benzo[d][1,3]dioxol-5-yloxy)ethan-1-amine **11** (0.359 g, 1.98 mmol), following the same procedure reported for **5**. After purification by flash chromatography (SiO<sub>2</sub>, EtOAc/MeOH 8:2 as eluent) **16** was obtained as a yellow oil. Yield: 87%. <sup>1</sup>HNMR (CDCl<sub>3</sub>) δ: 3.18-3.23 (m, 2H), 3.24 (s, 3H), 3.37-3.43 (m, 2H), 3.49 (s, 3H), 3.93-4.18 (m, 3H), 5.92 (q, 2H, *J*= 1.5 Hz), 6.55 (s, 1H), 6.72 (s, 1H). <sup>13</sup>CDEPTQ (CDCl<sub>3</sub>) δ: 48.0, 54.2, 55.8, 61.9, 74.4, 101.3, 103.2, 104.0, 109.1, 126.0, 143.3, 146.8, 154.3. HRMS (ESI) *m/z* [M+H]<sup>+</sup> calcd for [C<sub>13</sub>H<sub>18</sub>NO<sub>5</sub>]<sup>+</sup> 268.1185 found 268.1178.

*8-(2,3-Dimethoxybenzyl)-9-(dimethoxymethyl)-6,7,8,9-tetrahydro-[1,3]dioxolo[4',5':4,5]benzo[1,2-f][1,4]oxazepine 17*

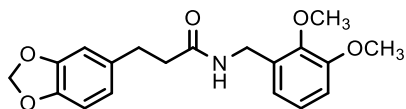


### Chapter 3

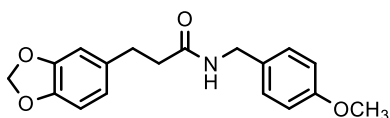
The title compound was synthesized starting from 9-(dimethoxymethyl)-6,7,8,9-tetrahydro-[1,3]dioxolo[4',5':4,5]benzo[1,2-f][1,4]oxazepine **16** (0.417 g, 1.56 mmol), and following the same procedure reported for **6**. After purification by flash chromatography (SiO<sub>2</sub>, *n*-hexane/EtOAc 7:3 as eluent) **17** was obtained as a white solid. Yield: 40%. <sup>1</sup>HNMR (CDCl<sub>3</sub>) δ: 2.83 (d, 1H, *J*= 15.4 Hz), 3.16 (s, 3H), 3.35 (s, 3H), 3.52 (m, 1H), 3.60 (d, 1H, *J*= 13.8 Hz), 3.71 (d, 1H, overlapped), 3.76 (s, 3H), 3.84 (s, 3H), 3.89 (d, 1H, overlapped), 4.00-4.03 (m, 2H), 5.09 (d, 1H, *J*= 8.2 Hz), 5.94 (s, 2H), 6.55 (s, 1H), 6.60 (s, 1H), 6.80-6.83 (m, 1H), 6.99-7.03 (m, 2H). HRMS (ESI) *m/z* [M+H]<sup>+</sup> calcd for [C<sub>22</sub>H<sub>28</sub>NO<sub>7</sub>]<sup>+</sup> 418.1860, found 418.1863, [M+Na]<sup>+</sup> calcd for [C<sub>22</sub>H<sub>27</sub>NO<sub>7</sub>Na]<sup>+</sup> 440.1680, found 440.1681.

#### 3.6.3 Synthesis of 18a-f

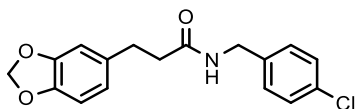
##### 3-(Benzo[d][1,3]dioxol-5-yl)-N-(2,3-dimethoxybenzyl)propanamide **21a**



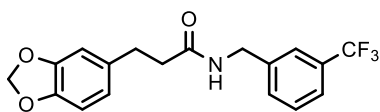
To a solution of 3-(benzo[d][1,3]dioxol-5-yl)propanoic acid **2** (0.300 g, 1.54 mmol) in DMF (3 mL) stirred at room temperature, HOBT (0.313 g, 2.32 mmol), HBTU (0.879 g, 2.32 mmol) and DIPEA (0.299 g, 2.32 mmol) were added. After 20 min, 2,3-dimethoxybenzylamine (0.387 g, 2.32 mmol) was added, and the mixture was stirred overnight. Then solvent was removed under reduced pressure and the residue was taken up in EtOAc and washed with a saturated solution of NaHCO<sub>3</sub> (2x25 mL), brine (2x20 mL) and 2N HCl (2x25 mL). The organic phase was dried over anhydrous Na<sub>2</sub>SO<sub>4</sub>, filtered, and solvent was removed under reduced pressure. The residue was purified by flash chromatography (SiO<sub>2</sub>, EtOAc/*n*-hexane 7:3 as eluent) to give the title compound as a white solid. Yield: 93%. <sup>1</sup>HNMR (CDCl<sub>3</sub>) δ: 2.44 (t, 2H, *J*= 8.3 Hz), 2.90 (t, 2H, *J*= 8.3 Hz), 3.85 (s, 3H), 3.89 (s, 3H), 4.44 (d, 2H, *J*= 5.7 Hz), 5.93 (s, 2H), 6.64 (m, 1H), 6.67 (m, 2H), 6.81 (dd, 1H, *J*= 7.7, 1.5 Hz), 6.88 (dd, 1H, *J*= 8.2, 1.5 Hz), 7.02 (t, 1H, *J*= 7.9 Hz).

3-(Benzo[d][1,3]dioxol-5-yl)-N-(4-methoxybenzyl)propanamide **21b**

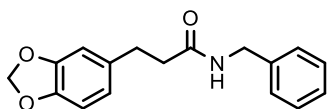
Starting from **2** (0.300 g, 1.54 mmol) and 4-methoxybenzylamine (0.318 g, 2.32 mmol) the compound **21b** was obtained as a white solid following the same procedure described for **21a**. Yield: 89%. <sup>1</sup>HNMR (CDCl<sub>3</sub>) δ: 2.46 (t, 2H, *J* = 7.5 Hz), 2.91 (t, 2H, *J* = 7.5 Hz), 3.79 (s, 3H), 4.33 (d, 2H, *J* = 5.6 Hz), 5.67 (brs, 1H), 5.93 (s, 2H), 6.64-6.74 (m, 3H), 6.85 (d, 2H, *J* = 8.6 Hz), 7.11 (d, 2H, *J* = 8.6 Hz). <sup>13</sup>CDEPTQ NMR (CDCl<sub>3</sub>) δ: 31.5, 38.8, 43.1, 55.3, 100.8, 108.3, 108.8, 114.0, 121.2, 129.1, 139.3, 134.6, 145.9, 147.7, 159.0, 171.7.

3-(Benzo[d][1,3]dioxol-5-yl)-N-(4-chlorobenzyl)propanamide **21c**

Starting from **2** (0.300 g, 1.54 mmol) and 4-chlorobenzylamine (0.328 g, 2.32 mmol) the compound **21c** was obtained as a white solid following the same procedure described for **21a**. Yield: 87%. <sup>1</sup>HNMR (CDCl<sub>3</sub>) δ: 2.50 (t, 2H, *J* = 7.3 Hz), 2.94 (t, 2H, *J* = 7.35 Hz), 4.40 (d, 2H, *J* = 5.5 Hz), 5.95 (s, 2H), 6.65-6.75 (m, 3H), 7.10 (d, 2H, *J* = 8.3 Hz), 7.27 (d, 2H, *J* = 8.3 Hz). HRMS (ESI) *m/z* [M+H]<sup>+</sup> calcd for [C<sub>17</sub>H<sub>17</sub>ClNO<sub>3</sub>]<sup>+</sup> 318.0891, found 318.0891.

3-(Benzo[d][1,3]dioxol-5-yl)-N-(3-(trifluoromethyl)benzyl)propanamide **21d**

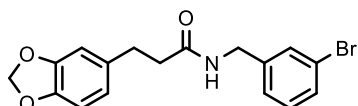
Starting from **2** (0.300 g, 1.54 mmol) and 3-(trifluoromethyl)benzylamine (0.406 g, 2.32 mmol) the compound **21d** was obtained as a white solid following the same procedure described for **21a**. Yield: 76%. <sup>1</sup>HNMR (CDCl<sub>3</sub>) δ: 2.59 (t, 2H, *J* = 7.4 Hz), 2.95 (t, 2H, *J* = 7.4 Hz), 4.49 (d, 2H, *J* = 5.9 Hz), 5.67 (s, 2H), 6.65-6.76 (m, 3H), 7.36-7.49 (m, 3H), 7.55 (d, 1H, *J* = 7.8 Hz).

3-(Benzo[d][1,3]dioxol-5-yl)-N-benzylpropanamide **21e**

### Chapter 3

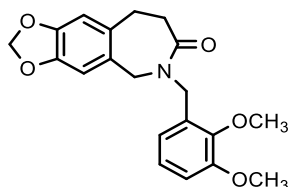
Starting from **2** (0.300 g, 1.54 mmol) and benzylamine (0.248 g, 2.32 mmol) the compound **21e** was obtained as a white solid following the same procedure described for **21a**. Yield: 85%. <sup>1</sup>HNMR (CDCl<sub>3</sub>) δ: 2.50 (t, 2H, *J* = 7.5 Hz), 2.94 (t, 2H, *J* = 7.5 Hz), 4.42 (s, 2H), 5.94 (s, 2H), 6.67 (dd, 1H, *J* = 7.9 Hz, 1.7 Hz), 6.72 (d, 1H, *J* = 1.7 Hz), 6.74 (d, 1H, 7.9 Hz), 7.18 (m, 2H), 7.29-7.35 (m, 4H).

#### *3-(Benzo[d][1,3]dioxol-5-yl)-N-(3-bromobenzyl)propanamide 21f*



Starting from **2** (0.300 g, 1.54 mmol) and 3-bromobenzylamine (0.512 g, 2.32 mmol) the compound **21f** was obtained as a white solid following the same procedure described for **21a**. Yield: 76%. <sup>1</sup>HNMR (CDCl<sub>3</sub>) δ: 3.50 (t, 2H, *J* = 7.4 Hz), 2.91 (t, 2H, *J* = 7.4 Hz), 4.38 (d, 2H, *J* = 5.8 Hz), 5.94 (s, 2H), 6.64-6.76 (m, 3H), 7.10 (d, 1H, *J* = 7.6 Hz), 7.18 (t, 1H, *J* = 7.8 Hz), 7.34 (brs, 1H), 7.40 (d, 1H, *J* = 7.7 Hz).

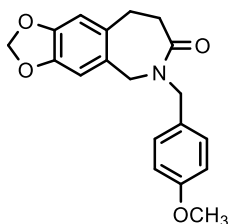
#### *6-(2,3-Dimethoxybenzyl)-5,6,8,9-tetrahydro-7H-[1,3]dioxolo[4',5':4,5]benzo[1,2-c]azepin-7-one 18a*



Paraformaldehyde (0.044 g, 1.46 mmol) and TFA (0.337 mL, 4.40 mmol) were added to a solution of 3-(benzo[d][1,3]dioxol-5-yl)-N-(2,3-dimethoxybenzyl)propanamide **21a** (0.230, 0.293 mmol) in dry ClCH<sub>2</sub>CH<sub>2</sub>Cl (5 mL), and the reaction mixture was stirred at room temperature for 5h. The solvent was removed under reduced pressure, and the resulting residue was taken up in dichloromethane and washed with a saturated solution of NaHCO<sub>3</sub> (15 mL) and brine (2x20 mL). The organic phase was dried over anhydrous Na<sub>2</sub>SO<sub>4</sub>, filtered, and solvent was removed under vacuo. The crude residue was purified by flash chromatography (SiO<sub>2</sub>, *n*-hexane/EtOAc 7:3 as eluent) to give **18a** as a white solid. Yield: 54%. <sup>1</sup>HNMR (CDCl<sub>3</sub>) δ: 2.94 (t, 2H, *J* = 8.2 Hz), 3.09 (t, 2H, *J* = 8.2 Hz), 3.84 (s, 3H), 3.88 (s, 3H), 4.31 (s, 2H), 4.72 (s, 2H),

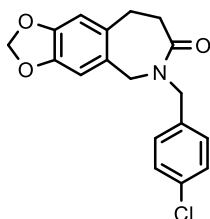
5.90 (s, 2H), 6.38 (s, 1H), 6.60 (s, 1H), 6.82-6.85 (m, 2H), 6.99 (t, 1H,  $J=7.9$  Hz).  $^{13}\text{CDEPTQ}$  NMR ( $\text{CDCl}_3$ )  $\delta$ : 29.0, 33.9, 44.3, 50.8, 55.8, 60.9, 101.0, 109.0, 110.0, 111.6, 121.6, 124.2, 128.0, 131.0, 131.3, 145.3, 147.2, 147.5, 152.6, 173.3. HRMS (ESI)  $m/z$   $[\text{M}+\text{H}]^+$  calcd for  $[\text{C}_{20}\text{H}_{22}\text{NO}_5]^+$  356.1492, found 356.1519.

*6-(4-Methoxybenzyl)-5,6,8,9-tetrahydro-7H-[1,3]dioxolo[4',5':4,5]benzo[1,2-c]azepin-7-one*  
**18b**



Starting from 3-(benzo[d][1,3]dioxol-5-yl)-*N*-(4-methoxybenzyl)propanamide **21b** (0.187 g, 0.597 mmol) compound **18b** was obtained as a white solid following the same procedure described for **18a**. Yield: 68%.  $^1\text{HNMR}$  ( $\text{CDCl}_3$ )  $\delta$ : 2.97 (t, 2H,  $J=8.3$  Hz), 3.11 (t, 2H,  $J=8.3$  Hz), 3.82 (s, 3H), 4.28 (s, 2H), 4.61 (s, 2H), 5.92 (s, 2H), 6.32 (s, 1H), 6.63 (s, 1H), 6.85 (d, 2H,  $J=8.6$  Hz), 7.17 (d, 2H,  $J=8.6$  Hz).  $^{13}\text{CDEPTQ}$  NMR ( $\text{CDCl}_3$ )  $\delta$ : 28.9, 33.9, 49.9, 50.8, 55.3, 101.0, 108.9, 110.1, 114.0, 127.7, 129.2, 129.5, 131.3, 145.4, 147.3, 159.1, 173.4. HRMS (ESI)  $m/z$   $[\text{M}+\text{H}]^+$  calcd for  $[\text{C}_{19}\text{H}_{20}\text{NO}_4]^+$  326.1387, found 326.1387.

*6-(4-Chlorobenzyl)-5,6,8,9-tetrahydro-7H-[1,3]dioxolo[4',5':4,5]benzo[1,2-c]azepin-7-one*  
**18c**

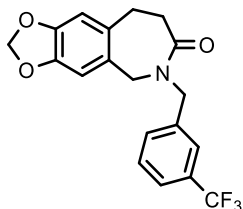


Starting from 3-(benzo[d][1,3]dioxol-5-yl)-*N*-(4-chlorobenzyl)propanamide **21c** (0.346 g, 1.09 mmol) compound **18c** was obtained as a white solid following the same procedure described for **18a**. Yield: 63%.  $^1\text{HNMR}$  ( $\text{CDCl}_3$ )  $\delta$ : 2.97 (t, 2H,  $J=8.3$  Hz), 3.11 (t, 2H,  $J=8.3$  Hz), 4.29 (s, 2H), 4.63 (s, 2H), 5.92 (s, 3H), 6.32 (s, 1H), 6.63 (s, 1H), 7.16 (d, 2H,  $J=8.4$  Hz), 7.27 (d, 2H,  $J=8.4$  Hz).  $^{13}\text{CDEPTQ}$  NMR ( $\text{CDCl}_3$ )  $\delta$ : 28.9, 33.9, 50.0, 51.3, 101.1, 108.8, 110.1,

### Chapter 3

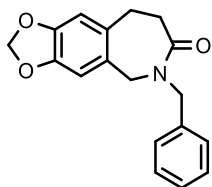
127.5, 128.7, 129.4, 131.2, 133.3, 135.9, 145.5, 147.4, 173.4. HRMS (ESI)  $m/z$   $[M+H]^+$  calcd for  $[C_{18}H_{17}ClNO_3]^+$  330.0891, found 330.0922.

6-(3-(Trifluoromethyl)benzyl)-5,6,8,9-tetrahydro-7H-[1,3]dioxolo[4',5':4,5]benzo[1,2-c]azepin-7-one **18d**



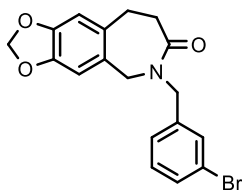
Starting from 3-(benzo[d][1,3]dioxol-5-yl)-*N*-(3-(trifluoromethyl)benzyl)propanamide **21d** (0.303 g, 0.863 mmol) compound **18d** was obtained as a white solid following the same procedure described for **18a**. Yield: 48%.  $^1H$ NMR ( $CDCl_3$ )  $\delta$ : 2.97 (t, 2H,  $J=7.4$  Hz), 3.11 (t, 2H,  $J=7.4$  Hz), 4.27 (s, 2H), 4.72 (s, 2H), 5.88 (s, 2H), 6.25 (s, 1H), 6.61 (s, 1H), 7.40 (m, 3H), 7.48 (m, 1H).  $^{13}C$ DEPTQ NMR ( $CDCl_3$ )  $\delta$ : 28.9, 33.8, 50.3, 51.6, 101.1, 108.7, 110.1, 124.0 (q,  $J_{CF}=273.7$  Hz), 124.3 (q,  $J_{CF}=3.7$  Hz), 126.6 (q,  $J_{CF}=3.6$  Hz), 127.5, 129.0, 130.7 (q,  $J_{CF}=32.3$  Hz), 131.1, 131.3, 138.4, 145.5, 147.4, 173.5. HRMS (ESI)  $m/z$   $[M+H]^+$  calcd for  $[C_{19}H_{17}F_3NO_3]^+$  364.1155, found 364.1185.

6-Benzyl-5,6,8,9-tetrahydro-7H-[1,3]dioxolo[4',5':4,5]benzo[1,2-c]azepin-7-one **18e**



Starting from 3-(benzo[d][1,3]dioxol-5-yl)-*N*-benzylpropanamide **21e** (0.165 g, 0.583 mmol), compound **18e** was obtained as a white solid following the same procedure described for **18a**. Yield: 52%.  $^1H$ NMR ( $CDCl_3$ )  $\delta$ : 2.99 (t, 2H,  $J=7.4$  Hz), 3.13 (t, 2H,  $J=7.4$  Hz), 4.30 (s, 2H), 4.68 (s, 2H), 5.91 (s, 2H), 6.32 (s, 1H), 6.64 (s, 1H), 7.23-7.35 (m, 5H).  $^{13}C$ DEPTQ NMR ( $CDCl_3$ )  $\delta$ : 29.0, 34.0, 50.5, 51.0, 101.0, 108.9, 110.1, 127.5, 127.7, 128.1, 128.6, 131.3, 137.2, 145.4, 147.3, 173.4. HRMS (ESI)  $m/z$   $[M+H]^+$  calcd for  $[C_{18}H_{18}NO_3]^+$  296.1281, found 296.1307.

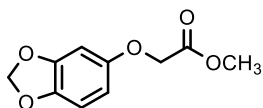
6-(3-Bromobenzyl)-5,6,8,9-tetrahydro-7H-[1,3]dioxolo[4',5':4,5]benzo[1,2-c]azepin-7-one  
**18f**



Starting from 3-(benzo[d][1,3]dioxol-5-yl)-*N*-benzylpropanamide **21f** (0.300 g, 0.828 mmol) compound **18f** was obtained as a white solid following the same procedure described for **18a**. Yield: 90%. <sup>1</sup>HNMR (CDCl<sub>3</sub>) δ: 2.99 (t, 2H, *J*= 7.4 Hz), 3.12 (t, 2H, *J*= 7.1 Hz), 4.30 (s, 2H), 4.60 (s, 2H), 5.93 (s, 2H), 6.33 (s, 1H), 6.65 (s, 1H), 7.15-7.20 (m, 2H), 7.35 (m, 1H), 7.40 (m, 1H). <sup>13</sup>CDEPTQ NMR (CDCl<sub>3</sub>) δ: 28.9, 33.9, 50.0, 51.4, 101.1, 108.8, 110.2, 122.7, 126.6, 127.5, 130.1, 130.6, 131.0, 131.2, 139.7, 145.5, 147.4, 173.4. HRMS (ESI) *m/z* [M+H]<sup>+</sup> calcd for [C<sub>18</sub>H<sub>16</sub>BrNO<sub>3</sub>Na]<sup>+</sup> 396.0206, found 396.0244.

### 3.6.4 Synthesis of 25a-d

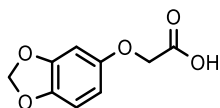
#### Methyl 2-(benzo[d][1,3]dioxol-5-yloxy)acetate **22**



To a solution of sesamol **9** (2.00 g, 14.5 mmol) in DMF (10 mL), Cs<sub>2</sub>CO<sub>3</sub> (11.79 g, 37.0 mmol) and methyl 2-bromoacetate (4.43 g, 29.0 mmol) were added and the resulting mixture was stirred at room temperature overnight. Then the mixture was diluted with EtOAc (20 mL) and washed with H<sub>2</sub>O. The organic layer was dried over anhydrous Na<sub>2</sub>SO<sub>4</sub>, filtered and concentrated under reduced pressure to give the title compound as a white solid. The latter was enough pure to be used in the next step without further purification. Yield: 97%. <sup>1</sup>HNMR (CDCl<sub>3</sub>) δ: 3.77 (s, 3H), 4.53 (s, 2H), 5.89 (s, 2H), 6.28 (dd, 1H, *J*= 8.7, 2.1 Hz), 6.50 (d, 1H, *J*= 2.2 Hz), 6.66 (d, 1H, *J*= 8.5 Hz).

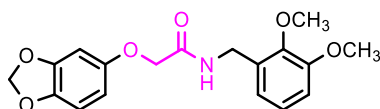
#### 2-(Benzo[d][1,3]dioxol-5-yloxy)acetic acid **23**

### Chapter 3

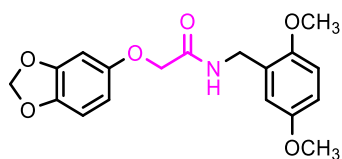


To a solution of methyl 2-(benzo[d][1,3]dioxol-5-yloxy)acetate **22** (1.99 g, 8.87 mmol) in MeOH (20 mL) 4N NaOH (1.77 g, 44.3 mmol) was added, and the resulting mixture was refluxed for 2h. The organic solvent was removed under reduced pressure and 6N HCl (pH  $\approx$  3) was added. The resulting mixture was extracted with EtOAc (3x20 mL). The collected organic phases were dried over anhydrous Na<sub>2</sub>SO<sub>4</sub>, filtered and concentrated under vacuum, to give a white solid that was used in the next step without other purification. Yield: quantitative. <sup>1</sup>HNMR (DMSO-*d*<sub>6</sub>)  $\delta$ : 4.58 (s, 2H), 5.97 (s, 2H), 6.34 (dd, 1H, *J*= 8.5, 2.6 Hz), 6.63 (d, 1H, *J*= 2.6 Hz), 6.80 (d, 1H, *J*= 8.5 Hz). HRMS (ESI) *m/z* [M-H]<sup>-</sup> calcd for [C<sub>9</sub>H<sub>7</sub>O<sub>5</sub>]<sup>-</sup> 195.0299, found 195.0297.

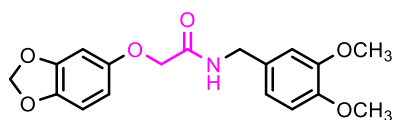
#### 2-(Benzo[d][1,3]dioxol-5-yloxy)-*N*-(2,3-dimethoxybenzyl)acetamide **24a**



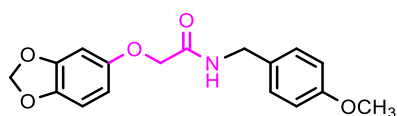
To a solution of 2-(benzo[d][1,3]dioxol-5-yloxy)acetic acid **23** (0.500 g, 2.55 mmol) in DMF (5 mL) HOBT (0.517 g, 3.82 mmol), HBTU (1.45 g, 3.82 mmol) and DIPEA (0.494 g, 3.82 mmol) were added, and the resulting mixture was stirred at room temperature for 20 min. Then 2,3-dimethoxybenzylamine (0.639 g, 3.82 mmol) was added and the mixture was stirred 12h. Solvent was removed under vacuo, and the residue was taken up in EtOAc and washed with NaHCO<sub>3</sub> saturated solution (2x20 mL), brine (20 mL), and 2M HCl (2x25 mL). The organic phase was dried over anhydrous Na<sub>2</sub>SO<sub>4</sub>, filtered and solvent was removed under reduced pressure. The crude residue was purified by flash chromatography (SiO<sub>2</sub>, *n*-hexane/EtOAc 1:1 as eluent) to give **24a** as a white solid. Yield: 88%. <sup>1</sup>HNMR CDCl<sub>3</sub>  $\delta$ : 3.87 (s, 3H), 3.88 (s, 3H, overlapped), 4.43 (s, 2H), 4.55 (s, 2H), 5.93 (s, 2H), 6.31 (dd, 1H, *J*= 8.5, 2.6 Hz), 6.49 (d, 1H, *J*= 2.6 Hz), 6.69 (d, 1H, *J*= 8.5 Hz), 6.87-6.90 (m, 2H), 7.00-7.04 (m, 2H).

2-(Benzo[d][1,3]dioxol-5-yloxy)-N-(2,5-dimethoxybenzyl)acetamide **24b**

The title compound was obtained as a white solid following the same procedure reported for **24a**. Yield: 76%.  $^1\text{H}$ NMR  $\text{CDCl}_3$   $\delta$ : 3.75 (s, 3H), 3.79 (s, 3H), 4.42 (s, 2H), 4.49 (d, 2H,  $J$ = 6.1 Hz), 5.93 (s, 2H), 6.29 (dd, 1H,  $J$ = 8.5, 2.6 Hz), 6.47 (d, 1H,  $J$ = 2.6 Hz), 6.69 (d, 1H,  $J$ = 8.5 Hz), 6.81 (m, 2H), 6.87 (m, 1H), 7.10 (brs, 1H).

2-(Benzo[d][1,3]dioxol-5-yloxy)-N-(3,4-dimethoxybenzyl)acetamide **24c**

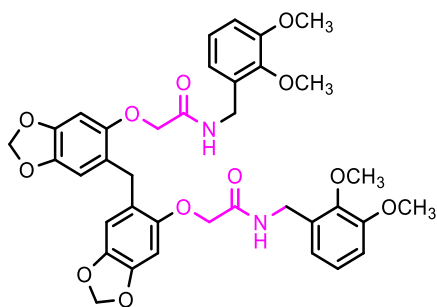
The title compound was obtained as a white solid following the same procedure reported for **24a**. Yield: 83%.  $^1\text{H}$ NMR ( $\text{CDCl}_3$ )  $\delta$ : 3.83 (s, 3H), 3.85 (s, 3H), 4.44 (s, 2H), 4.45 (d, 2 H, overlapped), 5.90 (s, 2H), 6.29 (dd, 1H,  $J$ = 8.5, 2.6 Hz), 6.46 (d, 1H,  $J$ = 2.6 Hz), 6.68 (d, 1H,  $J$ = 8.5 Hz), 6.79-6.81 (m, 3H), 6.83 (brs, 1H).  $^{13}\text{C}$ DEPTQ NMR ( $\text{CDCl}_3$ )  $\delta$ : 42.8, 55.8, 55.9, 68.3, 98.2, 101.3, 105.9, 108.0, 111.1, 111.2, 120.0, 130.3, 142.6, 148.4, 148.5, 149.1, 152.5, 168.0. HRMS (ESI)  $m/z$   $[\text{M}+\text{H}]^+$  calcd for  $[\text{C}_{18}\text{H}_{20}\text{NO}_6]^+$  346.1280, found 346.1279.

2-(Benzo[d][1,3]dioxol-5-yloxy)-N-(4-methoxybenzyl)acetamide **24d**

The title compound was obtained as a white solid following the same procedure reported for **24a**. Yield: 89%.  $^1\text{H}$ NMR ( $\text{CDCl}_3$ )  $\delta$ : 3.80 (s, 3H), 4.45 (s, 2H), 4.47 (d, 2H,  $J$ = 5.9 Hz overlapped), 5.93 (s, 2H), 6.31 (dd, 1H,  $J$ = 8.5, 2.6 Hz), 6.47 (d, 1H,  $J$ = 2.5 Hz), 6.70 (d, 1H,  $J$ = 8.5 Hz), 6.80 (brs, 1H), 6.87 (d, 2H,  $J$ = 8.6 Hz), 7.21 (d, 2H,  $J$ = 8.6 Hz).  $^{13}\text{C}$ DEPTQ NMR ( $\text{CDCl}_3$ )  $\delta$ : 42.8, 55.6, 68.7, 98.6, 101.8, 106.3, 108.4, 114.5, 125.5, 130.1, 143.1, 148.8, 152.9, 159.5, 168.4.

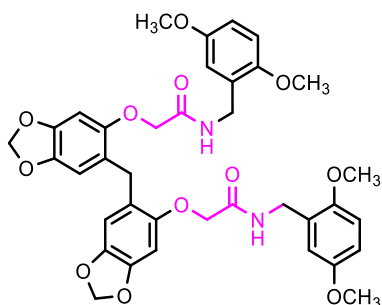
2,2'-((Methylenebis(benzo[d][1,3]dioxole-6,5-diyl))bis(oxy))bis(N-(2,3-dimethoxybenzyl)acetamide) **25a**

### Chapter 3



Formaldehyde 37 wt.% in H<sub>2</sub>O (0.325 ml, 4.33 mmol) was added to a solution of amide **24a** (0.300 g, 0.869 mmol) and anhydrous MgSO<sub>4</sub> (0.400 g, 3.32 mmol) in dry dichloromethane (25 mL) in a sealed tube, and the resulting mixture was stirred at room temperature for 2h. Then TFA (0.133 mL, 1.74 mmol) was added and the mixture was heated at 90°C for 4h. Then, after cooling to room temperature, the mixture was washed with a saturated solution of NaHCO<sub>3</sub> (2x20 mL), and brine (20 mL). The organic solvent was removed under reduced pressure, and the residue was purified by flash chromatography (SiO<sub>2</sub>, EtOAc/*n*-hexane 4:1 as eluent) After recrystallization from EtOAc/*n*-hexane the title compound **25a** was obtained as a white solid. Yield: 73%. <sup>1</sup>HNMR (CDCl<sub>3</sub>) δ: 3.77 (s, 6H), 3.79 (brs, 2H), 3.83 (s, 6H), 4.32 (s, 4H), 4.44 (d, 4H, *J*= 6.0 Hz), 5.86 (s, 4H), 6.38 (s, 2H), 6.48 (s, 2H), 6.73 (d, 2H, *J*= 7.6 Hz), 6.79 (t, 2H, *J*= 6.1 Hz), 6.83 (d, 2H, *J*= 8.2 Hz), 6.95 (m, 2H). <sup>13</sup>CDEPTQ NMR CDCl<sub>3</sub> δ: 30.7, 38.7, 56.1, 60.9, 69.0, 96.5, 101.7, 110.1, 112.4, 121.1, 121.3, 124.4, 131.6, 142.6, 147.0, 147.5, 149.9, 153.0, 168.2. HRMS (ESI) *m/z* [M+H]<sup>+</sup> calcd for [C<sub>37</sub>H<sub>39</sub>N<sub>2</sub>O<sub>12</sub>]<sup>+</sup> 703.2497, found 703.2491.

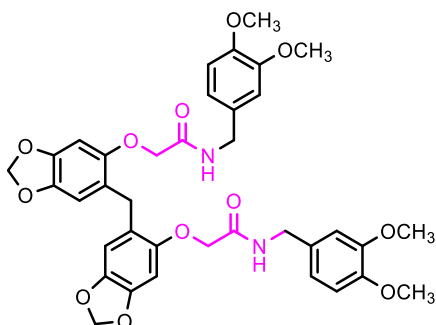
2,2'-((Methylenebis(benzo[d][1,3]dioxole-6,5-diyl))bis(oxy))bis(*N*-(2,5-dimethoxybenzyl)acetamide) **25b**



The title compound was obtained as a white solid following the same procedure reported for **25a**. Yield: 51%. <sup>1</sup>HNMR (CDCl<sub>3</sub>) δ: 3.70 (s, 6H), 3.74 (s, 6H), 3.82 (s, 2H), 4.33 (s, 4H), 4.42

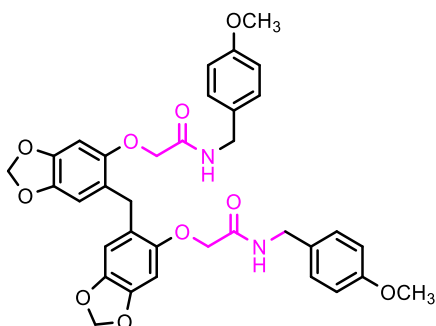
(d, 4H,  $J = 6.1$  Hz), 5.88 (s, 4H), 6.38 (s, 2H), 6.51 (s, 2H), 6.74-6.80 (m, 6H), 6.88 (brt, 2H,  $J = 6.1$  Hz). HRMS (ESI)  $m/z$   $[M+H]^+$  calcd for  $[C_{37}H_{38}N_2O_{12}Na]^+$  725.2317, found 725.2355.

2,2'-((Methylenebis(benzo[d][1,3]dioxole-6,5-diyl))bis(oxy))bis(*N*-(3,4-dimethoxybenzyl)acetamide) **25c**



The title compound was obtained as a white solid following the same procedure reported for **25a**. Yield: 48%.  $^1\text{H NMR}$  ( $\text{CDCl}_3$ )  $\delta$ : 3.72 (s, 2H), 3.81 (s, 6H), 3.86 (s, 6H), 4.33 (s, 4H), 4.35 (d, 4H,  $J = 5.9$  Hz), 5.86 (s, 4H), 6.37 (s, 2H), 6.48 (s, 2H), 6.50 (brt, 2H,  $J = 2.1$  Hz), 6.71 (m, 2H), 6.78 (d, 4H,  $J = 8.7$  Hz). HRMS (ESI)  $m/z$   $[M+H]^+$  calcd for  $[C_{37}H_{38}N_2O_{12}Na]^+$  725.2317, found 725.2363.

2,2'-((Methylenebis(benzo[d][1,3]dioxole-6,5-diyl))bis(oxy))bis(*N*-(4-methoxybenzyl)acetamide) **25d**

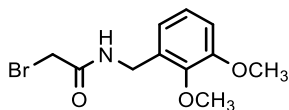


The title compound was obtained as a white solid following the same procedure reported for **25a**. Yield: 49%.  $^1\text{H NMR}$  ( $\text{CDCl}_3$ )  $\delta$ : 3.70 (s, 2H), 3.78 (s, 6H), 4.29 (s, 4H), 4.34 (d, 4H,  $J = 5.9$  Hz), 5.87 (s, 4H), 6.36 (s, 2H), 6.45 (m, 2H), 6.47 (s, 2H), 6.82 (d, 4H,  $J = 8.7$  Hz), 7.09 (d, 4H,  $J = 8.6$  Hz).  $^{13}\text{C DEPTQ NMR}$  ( $\text{CDCl}_3$ )  $\delta$ : 31.0, 42.7, 55.6, 69.0, 96.6, 101.7, 110.2, 114.4, 121.2, 129.1, 130.1, 142.7, 147.1, 149.8, 159.4, 168.2. HRMS (ESI)  $m/z$   $[M+H]^+$  calcd for  $[C_{35}H_{35}N_2O_{10}]^+$  643.2286, found 643.2277.

## Chapter 3

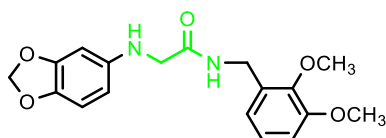
### 3.6.5 Synthesis of 31

#### 2-Bromo-*N*-(2,3-dimethoxybenzyl)acetamide **28**



To a solution of bromoacetyl chloride **26** (0.500 g, 3.18 mmol) in dry dichloromethane (3 mL), cooled to 0°C, dry TEA (0.483 g, 4.77 mmol) and 2,3-dimethoxybenzylamine **27** (0.531 g, 3.18 mmol) were added, and the resulting mixture was allowed to room temperature. After 12h, a saturated solution of NaHCO<sub>3</sub> (25 mL) was added, then the layers were separated, and the organic phase was washed with brine (2x20 mL), dried over anhydrous Na<sub>2</sub>SO<sub>4</sub>, filtered, and solvent was removed under reduced pressure. The resulting residue was purified by flash chromatography (SiO<sub>2</sub>, *n*-hexane/EtOAc 9:1 as eluent) to give the title compound as a white solid. Yield: 76%. <sup>1</sup>HNMR (CDCl<sub>3</sub>) δ: 3.91 (s, 3H), 3.92 (s, 2H), 3.93 (s, 3H), 4.52 (d, 2H, *J*= 5.8 Hz), 6.91 (m, 2H), 7.06 (t, 1H, *J*= 7.9 Hz). HRMS (ESI) *m/z* [M+H]<sup>+</sup> calcd for [C<sub>11</sub>H<sub>14</sub>BrNO<sub>3</sub>Na]<sup>+</sup> 310.0049, found 310.0052.

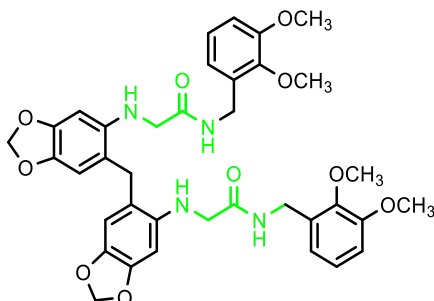
#### 2-(Benzo[d][1,3]dioxol-5-ylamino)-*N*-(2,3-dimethoxybenzyl)acetamide **30**



To a solution of benzo[d][1,3]dioxol-5-amine **29** (0.250 g, 1.82 mmol) in 2-butanone (5 mL), 2-bromo-*N*-(2,3-dimethoxybenzyl)acetamide **28**, K<sub>2</sub>CO<sub>3</sub> (0.377 g, 2.73 mmol) and KI (0.453 g, 2.73 mmol) were added. The resulting mixture was stirred at room temperature overnight. Solvent was removed under vacuo, and the residue was taken up in EtOAc and washed with brine (2x20 mL) and 1N HCl (20 mL). The organic phase was dried over anhydrous Na<sub>2</sub>SO<sub>4</sub>, filtered and the solvent was removed under reduced pressure. The crude residue was purified by flash chromatography (SiO<sub>2</sub>, EtOAc/*n*-hexane 8:2 as eluent) to give the title compound as a white solid. Yield: 74%. <sup>1</sup>HNMR (CDCl<sub>3</sub>) δ: 3.74 (d, 2H, *J*= 4.7 Hz), 3.79 (s, 3H), 3.85 (m, 4H), 4.49 (d, 2H, *J*= 5.9 Hz), 5.86 (s, 2H), 6.01 (dd, 1H, *J*= 8.2, 2.2 Hz), 6.22 (d, 1H, *J*= 2.2

Hz), 6.64 (d, 1H,  $J = 8.3$  Hz), 6.82-6.85 (m, 2H), 6.99 (m, 1H), 7.09 (brs, 1H). HRMS (ESI)  $m/z$   $[M+H]^+$  calcd for  $[C_{18}H_{21}N_2O_5]^+$  345.1445, found 345.1440.

2,2'-((Methylenebis(benzo[d][1,3]dioxole-6,5-diyl))bis(azanediyl))bis(N-(2,3-dimethoxybenzyl)acetamide) **31**

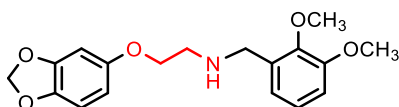


The title compound was obtained following the procedure reported for **25a** as a white solid.

Yield: 67%.  $^1\text{H NMR}$  ( $\text{CDCl}_3$ )  $\delta$ : 3.58 (s, 2H), 3.73 (d, 4H,  $J = 4.9$  Hz), 3.76 (s, 6H), 3.83 (s, 6H), 4.07 (brt, 2H,  $J = 5.4$  Hz), 4.44 (d, 4H,  $J = 5.9$  Hz), 5.82 (s, 4H), 6.21 (s, 2H), 6.46 (s, 2H), 6.75 (dd, 2H,  $J = 7.7, 1.5$  Hz), 6.82 (dd, 2H,  $J = 8.3, 1.5$  Hz), 6.86 (brt, 2H,  $J = 6.0$  Hz), 6.96 (t, 2H,  $J = 7.9$  Hz).  $^{13}\text{C DEPTQ NMR}$  ( $\text{CDCl}_3$ )  $\delta$ : 33.0, 36.9, 49.2, 55.9, 60.7, 95.2, 100.9, 109.8, 112.1, 116.1, 121.2, 124.3, 131.7, 140.2, 140.6, 147.2, 147.5, 152.7, 170.3. HRMS (ESI)  $m/z$   $[M+H]^+$  calcd for  $[C_{37}H_{41}N_4O_{10}]^+$  701.2817, found 701.2783.

### 3.6.6 Synthesis of 18l

2-(Benzo[d][1,3]dioxol-5-yloxy)-N-(2,3-dimethoxybenzyl)ethan-1-amine **33**

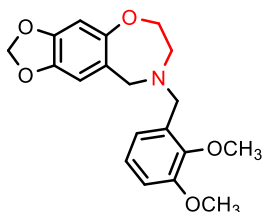


To a solution of 2-(benzo[d][1,3]dioxol-5-yloxy)ethan-1-amine **11** (0.286 g, 1.58 mmol) in dry MeOH (5 mL), anhydrous  $\text{MgSO}_4$  (1g, 8.31 mmol), acetic acid (0.190 g, 3.16 mmol) and 2,3-dimethoxybenzaldehyde **32** (0.289 g, 1.74 mmol) were added. The mixture was stirred at room temperature for 2h, then  $\text{NaBH}_4$  (0.239 g, 6.31 mmol) was added portionwise. The mixture was stirred at room temperature for another 2h. Then, the solvent was removed in vacuo, and the residue was taken up in EtOAc and washed with 1N NaOH (2x20 mL) and brine

### Chapter 3

(2x15 mL). The organic layer was dried over anhydrous Na<sub>2</sub>SO<sub>4</sub>, filtered and concentrated under reduced pressure. The residue was purified by flash chromatography (SiO<sub>2</sub>, EtOAc 100% as eluent) to give the title compound as a pale yellow oil. Yield: 56%. <sup>1</sup>HNMR (CDCl<sub>3</sub>) δ: 3.00 (t, 2H, *J*= 5.3 Hz), 3.87-3.93 (m, 8H), 4.03 (t, 2H; *J*= 5.2 Hz), 5.92 (s, 2H), 6.33 (dd, 1H, *J*= 8.5, 2.5 Hz), 6.50 (d, 1H, *J*= 2.5 Hz), 6.70 (d, 1H, *J*= 8.5 Hz), 6.88 (dd, 1H, *J*= 8.1, 1.6 Hz), 6.94 (dd, 1H, *J*= 7.7, 1.6 Hz), 7.05 (t, 1H, *J*= 7.9 Hz). <sup>13</sup>CDEPTQ NMR (CDCl<sub>3</sub>) δ: 52.9, 56.1, 58.3, 58.8, 71.3, 101.6, 103.1, 110.1, 115.6, 122.7, 124.1, 125.1, 133.0, 143.3, 147.2, 148.1, 153.1, 155.3. HRMS (ESI) *m/z* [M+H]<sup>+</sup> calcd for [C<sub>18</sub>H<sub>22</sub>NO<sub>5</sub>]<sup>+</sup> 332.1498, found 332.1491.

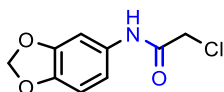
8-(2,3-Dimethoxybenzyl)-6,7,8,9-tetrahydro-[1,3]dioxolo[4',5':4,5]benzo[1,2-*f*][1,4]oxazepine **18l**



The synthesis of **18l** was carried out starting from **33** (0.210 g, 0.634 mmol) and following the same procedure described for **25a**. After purification by flash chromatography (SiO<sub>2</sub>, EtOAc/MeOH 9:1 as eluent) **18l** was obtained as a colorless oil. Yield: 63%. <sup>1</sup>HNMR (CDCl<sub>3</sub>) δ: 3.02 (m, 2H), 3.65 (s, 2H), 3.75 (s, 2H), 3.78 (s, 3H), 3.86 (s, 3H), 4.04 (m, 2H), 5.91 (s, 2H), 6.54 (s, 1H), 6.56 (s, 1H), 6.84 (dd, 1H, *J*= 7.8, 1.9 Hz), 6.97-7.05 (m, 2H). <sup>13</sup>CDEPTQ NMR (CDCl<sub>3</sub>) δ: 52.5, 55.7, 57.9, 58.4, 60.8, 70.9, 101.2, 102.7, 109.7, 111.2, 122.3, 123.8, 124.7, 132.6, 143.0, 146.8, 147.7, 152.7, 154.9. HRMS (ESI) *m/z* [M+H]<sup>+</sup> calcd for [C<sub>19</sub>H<sub>22</sub>NO<sub>5</sub>]<sup>+</sup> 344.1498, found 344.1496.

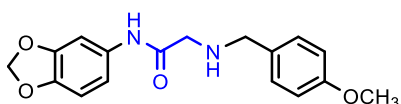
#### 3.6.7 Synthesis of 19a-c

*N*-(Benzo[*d*][1,3]dioxol-5-yl)-2-chloroacetamide **34**



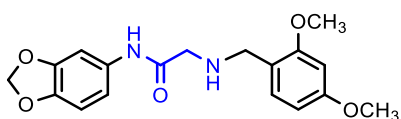
To a solution of benzo[d][1,3]dioxol-5-amine **29** (3.65 g, 26.6 mmol) and dry TEA (3.23 g, 31.9 mmol) in dry dichloromethane (15 mL), cooled to 0°C, chloroacetyl chloride (3.60 g, 31.9 mmol) was added dropwise. The mixture was allowed to room temperature and stirred for 2h. Then, organic solvent was removed under vacuo, and the residue was taken up in EtOAc and washed with a saturated solution of NaHCO<sub>3</sub> (2x30 mL), and brine (2x20 mL). The organic phase was dried over anhydrous Na<sub>2</sub>SO<sub>4</sub>, filtered and evaporated under vacuo. The crude residue was purified by flash chromatography (SiO<sub>2</sub>, *n*-hexane/EtOAc 8:2 as eluent) to give the title compound as a colorless oil. Yield: 28%. <sup>1</sup>HNMR (DMSO-d<sub>6</sub>) δ: 4.24 (s, 2H), 6.03 (s, 2H), 6.91 (d, 1H, *J*= 8.4 Hz), 7.00 (dd, 1H, *J*= 8.4, 2.1 Hz), 7.31 (d, 1H, *J*= 2.1 Hz), 10.2 (s, 1H).

*N*-(Benzo[d][1,3]dioxol-5-yl)-2-((4-methoxybenzyl)amino)acetamide **35a**



To a solution of 4-methoxybenzylamine (0.482 g, 3.51 mmol) and K<sub>2</sub>CO<sub>3</sub> (0.485 g, 3.51 mmol) in dry DMF (3 mL), a solution of **34** (0.500 g, 2.34 mmol) in dry DMF (5 mL) was added, and the mixture was stirred at room temperature overnight. Then, the mixture was diluted with a saturated solution of NaHCO<sub>3</sub>, and washed with EtOAc (2x25 mL). The combined organic phases were dried over anhydrous Na<sub>2</sub>SO<sub>4</sub>, filtered and solvent was removed under vacuo. The resulting residue was purified by flash chromatography (SiO<sub>2</sub>, EtOAc/*n*-hexane 3:1 as eluent) to furnish **35a** as a white solid. Yield: 75%. <sup>1</sup>HNMR (CDCl<sub>3</sub>) δ: 2.09 (s, 2H), 3.78 (s, 2H), 3.39 (brs, 1H), 3.80 (s, 3H), 5.94 (s, 2H), 6.74 (d, 1H, *J*= 8.3 Hz), 6.84 (dd (1H, *J*= 8.4, 2.1 Hz), 6.89 (d, 2H, *J*= 8.6 Hz), 7.24 (d, 2H, *J*= 8.6 Hz), 7.28 (d, 1H, *J*= 2.2 Hz). HRMS (ESI) *m/z* [M+H]<sup>+</sup> calcd for [C<sub>17</sub>H<sub>19</sub>N<sub>2</sub>O<sub>4</sub>]<sup>+</sup> 315.1345, found 315.1344.

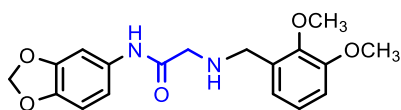
*N*-(Benzo[d][1,3]dioxol-5-yl)-2-((2,4-dimethoxybenzyl)amino)acetamide **35b**



### Chapter 3

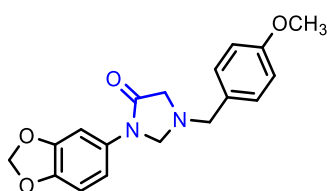
Starting from 2,4-dimethoxybenzylamine (0.240 g, 1.30 mmol) the title compound was obtained as a colorless oil following the same procedure described for **35a**. Yield 76%. <sup>1</sup>HNMR (CDCl<sub>3</sub>) δ: 2.05 (brs, 1H), 3.33 (s, 2H), 3.72 (s, 2H), 3.80 (s, 3H), 3.81 (s, 3H), 5.93 (s, 2H), 6.43 (dd, 1H, *J* = 8.1, 2.4 Hz), 6.47 (d, 1H, *J* = 2.4 Hz), 6.74 (d, 1H, *J* = 8.3 Hz), 6.86 (dd, 1H, *J* = 8.3, 2.1 Hz), 7.08 (d, 2H, *J* = 8.1 Hz), 7.29 (d, 1H, *J* = 2.1 Hz), 9.40 (s, 1H). HRMS (ESI) *m/z* [M+H]<sup>+</sup> calcd for [C<sub>18</sub>H<sub>21</sub>N<sub>2</sub>O<sub>5</sub>]<sup>+</sup> 345.1450, found 345.1457.

#### *N*-(Benzo[*d*][1,3]dioxol-5-yl)-2-((2,3-dimethoxybenzyl)amino)acetamide **35c**



Starting from 2,3-dimethoxybenzylamine (0.180 g, 1.07 mmol) the title compound was obtained as a colorless oil following the same procedure described for **35a**. Yield: 56%. <sup>1</sup>HNMR (CDCl<sub>3</sub>) δ: 3.38 (s, 2H), 3.78 (s, 2H), 3.85 (s, 3H), 3.88 (s, 3H), 3.91 (s, 1H), 5.94 (s, 2H), 6.75 (d, 1H, *J* = 8.3 Hz), 6.84 (dd, 1H, *J* = 7.5, 1.5 Hz), 6.90 (dd, 1H, *J* = 8.3, 1.5 Hz), 6.93 (dd, 1H, *J* = 8.3, 2.1 Hz), 7.02-7.06 (m, 1H), 7.36 (d, 1H, *J* = 2.1 Hz), 9.41 (brs, 1H). <sup>13</sup>CDEPTQ NMR (CDCl<sub>3</sub>) δ: 49.9, 52.5, 55.9, 61.0, 101.3, 102.3, 108.2, 112.5, 112.6, 122.1, 124.3, 132.5, 132.8, 144.1, 147.7, 147.9, 153.0, 169.7.

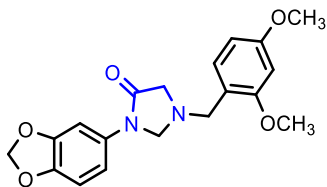
#### 3-(Benzo[*d*][1,3]dioxol-5-yl)-1-(4-methoxybenzyl)imidazolidin-4-one **19a**



Starting from **35a** (0.276 g, 0.875 mmol) compound **19a** was synthesized following the same procedure described for **25a**. After purification by flash chromatography (SiO<sub>2</sub>, EtOAc/*n*-hexane 4:1 as eluent) the title compound was obtained as a white solid. Yield: 92%. <sup>1</sup>HNMR CDCl<sub>3</sub> δ: 3.46 (s, 2H), 3.75 (s, 2H), 3.80 (s, 3H), 4.45 (s, 2H), 6.73 (d, 1H, *J* = 1.9 Hz), 6.74 (s, 1H), 6.88 (d, 2H, *J* = 8.6 Hz), 7.22 (d, 1H, *J* = 1.9 Hz), 7.26 (d, 2H, *J* = 8.6 Hz). <sup>13</sup>CDEPTQ NMR (CDCl<sub>3</sub>) δ: 55.2, 57.1, 58.4, 71.9, 101.3, 102.4, 108.0, 112.6, 114.0, 128.8, 129.8, 131.7, 144.7,

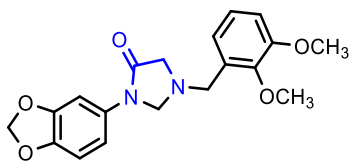
147.9, 159.2, 169.9. HRMS (ESI)  $m/z$   $[M+Na]^+$  calcd for  $[C_{18}H_{18}N_2O_4Na]^+$  349.1159, found 349.1192.

*3-(Benzo[d][1,3]dioxol-5-yl)-1-(2,4-dimethoxybenzyl)imidazolidin-4-one 19b*



Starting from **35b** (0.156 g, 0.45 mmol) the title compound was obtained as a white solid following the same procedure described for **25a**. Yield: 20%.  $^1\text{H}$ NMR ( $\text{CDCl}_3$ )  $\delta$ : 3.50 (s, 2H), 3.79 (s, 2H), 3.80 (s, 3H), 3.81 (s, 3H), 4.52 (s, 2H), 5.94 (s, 2H), 6.46-6.49 (m, 2H), 6.72-6.77 (m, 2H), 7.19-7.21 (m, 2H).  $^{13}\text{C}$ DEPTQ NMR ( $\text{CDCl}_3$ )  $\delta$ : 52.3, 55.4, 55.5, 57.1, 70.9, 98.7, 101.3, 102.4, 104.2, 108.0, 112.6, 117.3, 131.2, 131.9, 144.7, 147.9, 158.7, 160.6, 170.3. HRMS (ESI)  $m/z$   $[M+H]^+$  calcd for  $[C_{19}H_{21}N_2O_5]^+$  357.1450, found 357.1478.

*3-(Benzo[d][1,3]dioxol-5-yl)-1-(2,3-dimethoxybenzyl)imidazolidin-4-one 19c*

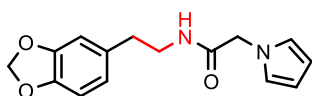


Starting from **35c** (0.325 g, 0.94 mmol) the title compound was obtained as a white solid following the same procedure described for **25a**. Yield: 82%.  $^1\text{H}$ NMR ( $\text{CDCl}_3$ )  $\delta$ : 3.52 (s, 2H), 3.85 (s, 3H), 3.87 (s, 2H), 3.88 (s, 3H), 4.51 (s, 2H), 5.95 (s, 2H), 6.76 (d, 2H,  $J=1.3$  Hz), 6.88 (dd, 1H,  $J=8.1, 1.6$  Hz), 6.98 (dd, 1H,  $J=7.7, 1.6$  Hz), 7.06 (t, 1H,  $J=7.9$  Hz), 7.23 (t, 1H,  $J=1.3$  Hz).  $^{13}\text{C}$ DEPTQ NMR ( $\text{CDCl}_3$ )  $\delta$ : 52.6, 55.8, 57.3, 60.9, 71.0, 101.3, 102.5, 108.0, 112.0, 112.7, 122.0, 124.1, 130.6, 131.8, 144.8, 147.6, 147.9, 152.9, 170.1. HRMS (ESI)  $m/z$   $[M+H]^+$  calcd for  $[C_{19}H_{21}N_2O_5]^+$  357.1450, found 357.1432.

### 3.6.8 Synthesis of 20a-e

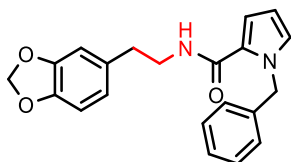
*N-(2-(Benzo[d][1,3]dioxol-5-yl)ethyl)-2-(1H-pyrrol-1-yl)acetamide 37a*

### Chapter 3



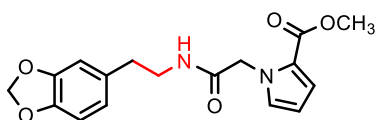
To a solution of 2-(1H-pyrrol-1-yl)acetic acid **36a** (0.129 g, 1.03 mmol) in DMF (5 mL), OxymePure<sup>®</sup> (0.179 g, 1.24 mmol), EDAC (0.237 g, 1.24 mmol) and DIPEA (0.215 mL, 2.24 mmol) were added, and the mixture was stirred at room temperature for 15 min. Then **4** (0.204 g, 1.24 mmol) was added, and after 12h the solvent was removed under vacuum. The residue was taken up in DCM and washed with a saturated solution of NaHCO<sub>3</sub> (2x15 mL), brine (2x15 mL). The organic solvent was dried over anhydrous Na<sub>2</sub>SO<sub>4</sub>, filtered and concentrated under vacuo. After purification by column chromatography (SiO<sub>2</sub>, EtOAc/*n*-hexane 7:3 as eluent) the title compound was obtained as a pale yellow oil. Yield: 20%. <sup>1</sup>HNMR (CDCl<sub>3</sub>) δ: 2.62 (t, 2H, *J*= 6.8 Hz), 3.39 (q, 2H, *J*= 6.6 Hz), 4.55 (s, 2H), 5.94 (s, 2H), 6.21 (t, 2H, *J*= 2.1 Hz), 6.47 (dd, 1H, *J*= 7.9, 1.7 Hz), 6.54 (d, 1H, *J*= 1.7 Hz), 6.56 (t, 2H, *J*= 2.1 Hz), 6.70 (d, 1H, *J*= 7.9 Hz). HRMS (ESI) *m/z* [M+H]<sup>+</sup> calcd for [C<sub>15</sub>H<sub>17</sub>N<sub>2</sub>O<sub>3</sub>]<sup>+</sup> 273.1239, found 273.1241.

#### *N*-(2-(Benzo[d][1,3]dioxol-5-yl)ethyl)-1-benzyl-1H-pyrrole-2-carboxamide **37b**



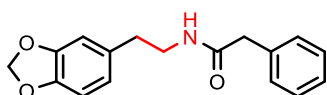
Starting from 1-benzyl-1H-pyrrole-2-carboxylic acid **36b** (0.200 g, 0.993 mmol) compound **37b** was obtained as a colorless oil following the same procedure reported for **37a**. Yield: 42%. <sup>1</sup>HNMR CDCl<sub>3</sub> δ: 2.74 (t, 2H, *J*= 6.8 Hz), 3.53 (q, 2H, *J*= 6.6 Hz), 5.60 (s, 2H), 5.84 (brs, 1H), 5.93 (s, 2H), 6.10 (dd, 1H, *J*= 3.9, 2.6 Hz), 6.44 (dd, 1H, *J*= 3.9, 1.7 Hz), 6.59 (dd, 1H, *J*= 7.5, 1.7 Hz), 6.66 (d, 1H, *J*= 1.7 Hz), 6.73 (d, 1H, *J*= 7.9 Hz), 6.79 (dd, 1H, *J*= 2.6, 1.7 Hz), 7.12 (m, 2H), 7.29 (m, 3H). HRMS (ESI) *m/z* [M+H]<sup>+</sup> calcd for [C<sub>21</sub>H<sub>21</sub>N<sub>2</sub>O<sub>3</sub>]<sup>+</sup> 349.1547, found 349.1550.

#### *Methyl 1*-(2-((2-(benzo[d][1,3]dioxol-5-yl)ethyl)amino)-2-oxoethyl)-1H-pyrrole-2-carboxylate **37c**



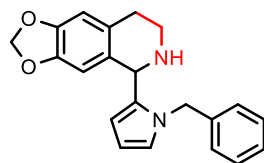
Starting from 2-(2-(methoxycarbonyl)-1H-pyrrol-1-yl)acetic acid **36c** (0.170 g, 0.75 mmol) compound **37c** was obtained as a white solid following the same procedure reported for **37a**. Yield: 57%. <sup>1</sup>HNMR CDCl<sub>3</sub> δ: 2.64 (t, 2H, *J*= 6.8 Hz), 3.42 (t, 2H, *J*= 6.5 Hz), 3.80 (s, 3H), 4.89 (s, 2H), 5.82 (brs, 1H), 5.93 (s, 2H), 6.20 (dd, 1H, *J*= 4.1, 2.7 Hz), 6.46 (dd, 1H, *J*= 7.8, 1.7 Hz); 6.54 (d, 1H, *J*=1.7 Hz), 6.68 (d, 1H, *J*=7.9 Hz), 6.86 (t, 1H, *J*= 2.2 Hz), 6.99 (dd, 1H, *J*= 4.0, 1.7 Hz). HRMS (ESI) *m/z* [M+Na]<sup>+</sup> calcd for [C<sub>17</sub>H<sub>18</sub>N<sub>2</sub>O<sub>5</sub>Na]<sup>+</sup> 353.1108, found 353.1104.

*N*-(2-(Benzo[*d*][1,3]dioxol-5-yl)ethyl)-2-phenylacetamide **37d**



To a solution of phenylacetyl chloride **36d** (0.129 g, 0.833 mmol) in dry DCM (3 mL), dry TEA (0.140 g, 1.39 mmol) and amine **4** (0.0917 g, 0.555 mmol) were added, and the resulting mixture was stirred at room temperature for 1.5h. Then, the mixture was diluted with H<sub>2</sub>O (10 mL) and extracted with DCM (2x10 mL). The combined organic phases were dried over anhydrous Na<sub>2</sub>SO<sub>4</sub>, filtered and concentrated under reduced pressure. The residue was purified by column chromatography (SiO<sub>2</sub>, *n*-hexane/EtOAc 7:3 as eluent) to give **37d** as a white solid. Yield: 54%. <sup>1</sup>HNMR (CDCl<sub>3</sub>) δ: 2.63 (t, 2H, *J*= 6.8 Hz), 3.40 (q, 2H, *J*= 6.5 Hz), 3.53 (s, 2H), 5.32 (brs, 1H), 5.92 (s, 2H), 6.44 (dd, 1H, *J*= 7.9, 1.7 Hz), 6.53 (d, 1H, *J*= 1.7 Hz), 6.66 (d, 1H, *J*= 7.9 Hz), 7.18 (m, 2H), 7.31 (m, 3H).

5-(1-Benzyl-1H-pyrrol-2-yl)-5,6,7,8-tetrahydro-[1,3]dioxolo[4,5-*g*]isoquinoline **20a**

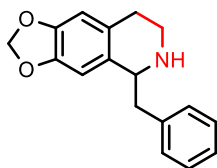


To a solution of **37a** (0.461 g, 1.32 mmol) in dry CH<sub>2</sub>CN (5 mL), POCl<sub>3</sub> (0.743 mL, 7.97 mmol) was added and the resulting mixture was heated at reflux for 1h. Then, the mixture was

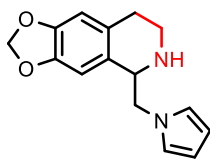
### Chapter 3

allowed to room temperature, quenched with 2N NaOH (pH  $\approx$  9), and volatiles were removed under vacuo. The residue was taken up in DCM (15 mL) and washed with brine (2x10 mL); the organic solvent was dried over anhydrous Na<sub>2</sub>SO<sub>4</sub>, filtered and concentrated under vacuo. Then the residue was diluted with dry MeOH (5 mL), the resulting mixture was cooled to 0°C and NaBH<sub>4</sub> (0.500, 13.2 mmol) was added portionwise. After 2h, the mixture was quenched with a saturated solution of NH<sub>4</sub>Cl and extracted with EtOAc (2x25 mL). The organic phase was washed with brine (2x15 mL), dried over anhydrous Na<sub>2</sub>SO<sub>4</sub>, filtered and concentrated under vacuo. The residue was purified by column chromatography (SiO<sub>2</sub>, *n*-hexane/EtOAc 7:3 as eluent) to give the title compound **20a** as a colorless oil. Yield: 53%. <sup>1</sup>HNMR (CDCl<sub>3</sub>)  $\delta$ : 2.65 (m, 1H), 2.80 (m, 1H), 2.92 (m, 1H), 3.17 (m, 1H), 4.98 (s, 1H), 5.10 (d, 1H, *J*= 16.0 Hz), 5.29 (d, 1H, *J*= 16.0 Hz), 5.82 (m, 2H), 5.86 (dd, 1H, *J*= 3.5, 1.8 Hz), 6.08 (t, 1H, *J*= 3.1 Hz), 6.22 (s, 1H), 6.51 (s, 1H), 6.65 (dd, 1H, *J*= 2.8, 1.8), 6.99 (d, 2H, *J*= 6.7 Hz), 7.20-7.29 (m, 4H). <sup>13</sup>CDEPTQ NMR (CDCl<sub>3</sub>)  $\delta$ : 29.6, 41.2, 50.5, 54.3, 100.5, 106.7, 107.7, 108.3, 110.3, 122.7, 126.6, 127.1, 128.2, 128.5, 130.1, 134.2, 138.9, 145.4, 146.0. HRMS (ESI) *m/z* [M+H]<sup>+</sup> calcd for [C<sub>21</sub>H<sub>21</sub>N<sub>2</sub>O<sub>2</sub>]<sup>+</sup> 333.1603, found 333.1599.

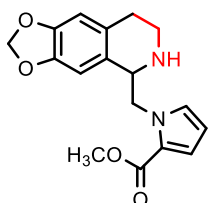
#### *5-Benzyl-5,6,7,8-tetrahydro-[1,3]dioxolo[4,5-g]isoquinoline 20b*



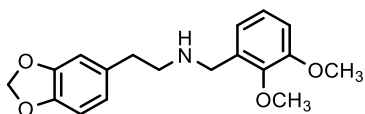
The title compound was obtained following the same procedure described for **20a** as a colorless oil. Yield: 42%. <sup>1</sup>HNMR (CDCl<sub>3</sub>)  $\delta$ : 2.64-2.79 (m, 2H), 2.84-2.90 (m, 2H), 3.15-3.21 (m, 2H), 4.11 (dd, 1H, *J*= 10.1, 3.8 Hz), 5.91 (m, 2H), 6.57 (s, 1H), 6.72 (s, 1H), 7.23-7.27 (m, 3H), 7.31-7.35 (m, 2H). <sup>13</sup>CDEPTQ NMR (CDCl<sub>3</sub>)  $\delta$ : 30.0, 40.5, 42.7, 57.3, 100.6, 106.2, 108.9, 126.5, 128.4, 128.6, 129.3, 131.7, 139.0, 145.7, 145.9. HRMS (ESI) *m/z* [M+H]<sup>+</sup> calcd for [C<sub>17</sub>H<sub>18</sub>NO<sub>2</sub>]<sup>+</sup> 268.1337, found 268.1332.

5-((1*H*-Pyrrol-1-yl)methyl)-5,6,7,8-tetrahydro-[1,3]dioxolo[4,5-*g*]isoquinoline **20c**

The title compound was obtained following the same procedure described for **20a** as a white solid. Yield: 58%. <sup>1</sup>HNMR (CDCl<sub>3</sub>) δ: 2.71 (m, 2H), 3.08 (m, 1H), 4.09 (m, 2H), 4.26 (m, 2H), 5.94 (s, 2H), 6.20 (brt, 2H, *J*= 2.1 Hz), 6.57 (s, 1H), 6.61 (s, 1H), 6.71 (brt, 2H, *J*= 2.0 Hz). HRMS (ESI) *m/z* [M+H]<sup>+</sup> calcd for [C<sub>15</sub>H<sub>17</sub>N<sub>2</sub>O<sub>2</sub>]<sup>+</sup> 257.1284, found 257.1281.

Methyl 1-((5,6,7,8-tetrahydro-[1,3]dioxolo[4,5-*g*]isoquinolin-5-yl)methyl)-1*H*-pyrrole-2-carboxylate **20d**

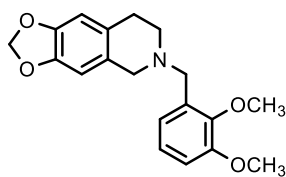
The title compound was obtained following the same procedure described for **20a** as a colorless oil. Yield: 49%. <sup>1</sup>HNMR (CDCl<sub>3</sub>) δ: 2.77 (m, 2H), 3.04 (m, 1H), 3.16 (m, 1H), 3.85 (s, 3H), 4.18 (m, 2H), 4.40 (m, 1H), 4.94 (dd, 1H, *J*= 13.8, 3.3 Hz), 5.92 (m, 2H), 6.16 (dd, 1H, *J*= 4.0, 2.6 Hz), 6.58 (s, 1H), 6.89 (s, 1H), 6.91 (t, 1H, *J*= 2.2 Hz), 7.02 (dd, 1H, *J*= 4.0, 1.8 Hz). HRMS (ESI) *m/z* [M+H]<sup>+</sup> calcd for [C<sub>17</sub>H<sub>19</sub>N<sub>2</sub>O<sub>4</sub>]<sup>+</sup> 315.1339, found 315.1339.

2-(Benzo[*d*][1,3]dioxol-5-yl)-*N*-(2,3-dimethoxybenzyl)ethan-1-amine **38**

The title compound was obtained starting from 2-(benzo[*d*][1,3]dioxol-5-yl)ethan-1-amine **4** (0.280 g, 1.69 mmol), following the same procedure reported for **33**. After purification by flash chromatography (SiO<sub>2</sub>, EtOAc/MeOH 9:1 as eluent), compound **38** was obtained as a white solid. Yield: 80%. <sup>1</sup>HNMR (CDCl<sub>3</sub>) δ: 2.79 (m, 2H), 2.88 (m, 2H), 3.39 (brs, 1H), 3.80 (s, 3H), 3.86 (s, 3H), 3.93 (s, 2H), 5.91 (s, 2H), 6.61-6.64 (m, 2H), 6.71 (d, 1H, *J*= 7.8 Hz), 6.83-6.92 (m, 2H), 7.01 (t, 1H, *J*= 8.2 Hz).

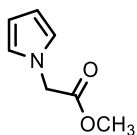
### Chapter 3

#### 6-(2,3-Dimethoxybenzyl)-5,6,7,8-tetrahydro-[1,3]dioxolo[4,5-g]isoquinoline **20e**



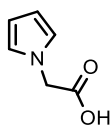
The title compound was obtained starting from **38** (0.342 g, 1.08 mmol), following the same procedure described for **25a**. White solid. Yield: 56%. <sup>1</sup>HNMR (CDCl<sub>3</sub>) δ: 2.71-2.83 (m, 4H), 3.60 (s, 2H), 3.75 (s, 2H), 3.87 (s, 3H), 3.90 (s, 3H), 5.89 (s, 2H), 6.49 (s, 1H), 6.58 (s, 1H), 6.88 (dd, 1H, *J*= 7.6, 2.1 Hz), 7.03-7.11 (m, 2H). <sup>13</sup>CDEPTQ NMR (CDCl<sub>3</sub>) δ: 29.3, 50.7, 55.7, 56.0, 56.1, 60.9, 100.5, 106.5, 108.4, 111.2, 122.5, 123.8, 127.4, 128.0, 132.2, 145.6, 145.9, 147.8, 152.8. HRMS (ESI) *m/z* [M+H]<sup>+</sup> calcd for [C<sub>19</sub>H<sub>22</sub>NO<sub>4</sub>]<sup>+</sup> 328.1543, found 328.1567.

#### Methyl 2-(1H-pyrrol-1-yl)acetate **40**



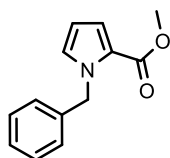
A solution of 2,5-dimethoxytetrahydrofuran (0.734 g, 5.55 mmol) in H<sub>2</sub>O (7 mL), degassed and kept under inert atmosphere (N<sub>2</sub>), was heated at reflux for 2h, then was allowed to room temperature and a mixture of glycine methyl ester hydrochloride (0.500 g, 6.67 mmol) and AcONa (1.31g, 15.9 mmol) in H<sub>2</sub>O/DCM (15 mL, 1:2) was added. The resulting mixture was stirred at room temperature overnight, protected from light, then was diluted with DCM (15 mL) and washed brine (15 mL). The layers were separated, and the organic phase was dried over anhydrous Na<sub>2</sub>SO<sub>4</sub>, filtered and concentrated under vacuo. The crude residue was purified by flash chromatography (SiO<sub>2</sub>, EtOAc as eluent) to give the title compound as a yellow oil. Yield: 25%. <sup>1</sup>HNMR (CDCl<sub>3</sub>) δ: 3.79 (s, 3H), 4.67 (s, 2H), 6.23 (t, 2H, *J*= 2.1 Hz), 6.69 (t, 2H, *J*= 2.1 Hz).

#### 2-(1H-Pyrrol-1-yl)acetic acid **36a**



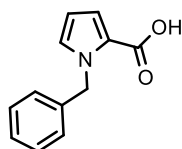
To a solution of methyl 2-(1H-pyrrol-1-yl)acetate **40** (0.300 g, 2.16 mmol) in MeOH (5 mL), NaOH (0.090 g, 2.25 mmol) was added and the resulting mixture was stirred at room temperature for 1h. Solvent was removed under vacuo and the residue was treated with 2N HCl (pH  $\approx$ 3) and extracted with EtOAc (3x15 mL). The combined organic phases were dried over Na<sub>2</sub>SO<sub>4</sub>, filtered and concentrated under vacuo to give **36a**, that was used in the next step without other purification. <sup>1</sup>HNMR (CDCl<sub>3</sub>)  $\delta$ : 4.72 (s, 2H), 6.25 (t, 2H,  $J$ = 2.1 Hz), 6.69 (t, 2H,  $J$ = 2.1 Hz). HRMS (ESI)  $m/z$  [M+H]<sup>+</sup> calcd for [C<sub>6</sub>H<sub>8</sub>NO<sub>2</sub>]<sup>+</sup> 126.0549, found 126.0550.

*Methyl 1-benzyl-1H-pyrrole-2-carboxylate* **42**



To a solution of methyl 1H-pyrrole-2-carboxylate **41** (0.500 g, 3.99 mmol) in DCM (15 mL), NaOH 50% w/v in H<sub>2</sub>O (8 mL) and TBAH (0.500 mL) were added, and the mixture was vigorously stirred at room temperature for 1h. Then a solution of benzyl bromide (1.18 g, 6.87 mmol) in DCM (5 mL) was added dropwise. After 12h, the phases were separated, the organic layer was washed with brine (2x15 mL), and 1N HCl (2x25 mL). The organic solvent was dried over anhydrous Na<sub>2</sub>SO<sub>4</sub>, filtered and concentrated under reduced pressure. The residue was purified by flash chromatography (SiO<sub>2</sub>, *n*-hexane/EtOAc 8:2 as eluent) to furnish **42** as a pale yellow oil. Yield: 60%. <sup>1</sup>HNMR (CDCl<sub>3</sub>)  $\delta$ : 3.77 (s, 3H), 5.57 (s, 2H), 6.19 (dd, 1H,  $J$ = 4.0, 2.6 Hz), 6.89 (t, 1H,  $J$ = 2.6 Hz), 7.01 (dd, 1H,  $J$ = 3.9, 1.8 Hz), 7.11 (d, 2H,  $J$ = 8.0 Hz), 7.23-7.33 (m, 3H).

*1-Benzyl-1H-pyrrole-2-carboxylic acid* **36b**

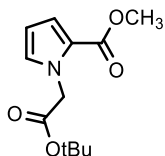


Starting from **42** (0.380 g, 1.76 mmol) the title compound was obtained as an amorphous solid following the same procedure used for **36a**. Yield: 78%. <sup>1</sup>HNMR (DMSO-*d*<sub>6</sub>)  $\delta$ : 5.59 (s,

### Chapter 3

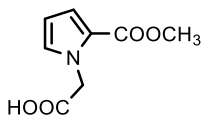
2H), 6.18 (t, 1H,  $J= 3.2$  Hz), 7.11 (d, 2H,  $J= 7.5$  Hz), 7.25-7.41 (m, 4H).  $^{13}\text{C}$ NMR ( $\text{DMSO-d}_6$ )  $\delta$ : 52.1, 109.2, 119.1, 123.3, 127.8, 128.3, 129.6, 130.7, 140.4, 163.0.

#### *Methyl 1-(2-(tert-butoxy)-2-oxoethyl)-1H-pyrrole-2-carboxylate 43*



To a solution of methyl 1H-pyrrole-2-carboxylate **41** (0.500 g, 3.99 mmol) in dry THF (5 mL) cooled to 0°C, NaH (60 wt.% dispersion in mineral oil, 0.240 g, 5.99 mmol) was added portionwise. Then after 20 min *tert*-butyl bromoacetate (0.935 g, 4.79 mmol) was added, and the resulting mixture was allowed to room temperature. After 1h, the solvent was removed under reduced pressure, and the resulting residue was taken up in EtOAc (20 mL), and washed with 0.5N HCl (15 mL), and brine. The organic phase was dried on anhydrous  $\text{Na}_2\text{SO}_4$ , filtered and solvent was removed under vacuo. The residue was purified by flash chromatography ( $\text{SiO}_2$ , *n*-hexane/EtOAc 4:1 as eluent) to give the title compound as a colorless oil. Yield: 63%.  $^1\text{H}$ NMR ( $\text{CDCl}_3$ )  $\delta$ : 1.48 (s, 9H), 3.78 (s, 3H), 4.91 (s, 2H), 6.17 (dd, 1H,  $J= 4.0, 2.6$  Hz), 6.79 (t, 1H,  $J= 2.6$  Hz), 6.98 (dd, 1H,  $J= 4.0, 1.8$  Hz).

#### *2-(2-(Methoxycarbonyl)-1H-pyrrol-1-yl)acetic acid 36c*



To a solution of **43** (0.060 g, 0.25 mmol) in DCM (1 mL), TFA (0.5 mL) was added and the mixture was stirred at room temperature for 2h. The solvent was removed under reduced pressure, to give **36c** as an oil, that was used in the next step without further purification. Yield: 89%.  $^1\text{H}$ NMR ( $\text{CDCl}_3$ )  $\delta$ : 3.77 (s, 3H), 4.99 (s, 2H), 6.19 (m, 1H), 6.83 (m, 1H), 6.99 (m, 1H).

### **3.6.9 Cell viability assay**

HaCaT cell line (Human immortalized keratinocytes) was purchased from CLS Cell Lines Service GmbH and was maintained in Dulbecco's modified Eagle's medium (DMEM) with 10% fetal bovine serum (FBS).

HepG2 cells (Human immortalized cells of hepatocellular carcinoma) were obtained from ATCC (HB-8065™) and cultured in MEM with 15% FBS.

All the media were supplemented with antibiotics (10000 U/mL penicillin and 10 mg/mL streptomycin), cells were stained at 37°C in 5% CO<sub>2</sub> -95% air humidified atmosphere and were serially passed at 70-80% confluence.

### **3.6.10 RNA isolation and reverse transcription-PCR (RT-PCR)**

HepG2 cells were homogenized in 0.5 mL TRI Reagent® (Sigma-Aldrich, Germany). RNA isolation was performed according to the manufacturer's protocol. Total RNA was quantified using NanoDrop ND-1000 Spectrophotometer (Thermo Scientific) and RNA samples with a 260/280 nm ratio between 1.9 and 2.1 were selected for further analysis. cDNA was obtained from 1µg RNA/sample using QuantiTect Reverse Transcription Kit (Qiagen, Germany). Then, the quantitative expression of the selected gene was evaluated. To this aim the primer pair was designed using Primer3 software (<https://primer3.ut.ee/>).

### **3.6.11 Quantitative Reverse Transcription PCR (qRT-PCR)**

Quantitative expression of the selected gene was analyzed by RT-qPCR, using the iQ5 Real time PCR Detection System (Bio-Rad). We used the only primer pairs validated by qualitative RT-PCR analyses. PCR reactions were carried out in a total volume of 15µL using 10ng of cDNA, 4 pmol of each primer and 7.5µL 2x Luna Universal qPCR Master mix (New England BioLabs). Cycling parameters were as follows: one cycle at 95°C for 3 min and 40 two-step

### **Chapter 3**

cycles at 95°C for 10s and at 60°C for 30s. Samples were run in triplicates, using 96-wells qPCR microplates (Bio-Rad). All quantifications were normalized to the expression of GAPDH. Values of cycle threshold (Ct) obtained in quantification were used for the calculations of fold changes in mRNA abundance according to the  $2^{-\Delta\Delta Ct}$  method<sup>30</sup>.

## References

1. Yang, Y.; Ye, X. L.; Li, X. G.; Zhen, J.; Zhang, B.; Yuan, L. Synthesis and antimicrobial activity of 8-alkylberberine derivatives with a long aliphatic chain. *Planta Med.* **2007**, *73*(6), 602–604. doi: 10.1055/s-2007-967180
2. Wang, L. J.; Ye, X. L.; Chen, Z.; Li, X. G.; Sun, Q. L.; Zhang, B. S.; Cao, X. G.; Yu, G.; Niu, X. H. Synthesis and antimicrobial activity of 3-octyloxy-8-alkyljatrorrhizine derivatives. *J. Asian Nat. Prod. Res.* **2009**, *11*(4), 365–370. doi: 10.1080/10286020902727447
3. Liu, Y. X.; Xiao, C. L.; Wang, Y. X.; Li, Y. H.; Yang, Y. H.; Li, Y. B.; Bi, C. W.; Gao, L. M.; Jiang, J. D.; Song, D. Q. Synthesis, structure-activity relationship and in vitro anti-mycobacterial evaluation of 13-n-octylberberine derivatives. *Eur. J. Med. Chem.* **2012**, *52*, 151–158. doi: 10.1016/j.ejmech.2012.03.012
4. Ma, Y.; Ou, T. M.; Tan, J. H.; Hou, J. Q.; Huang, S. L.; Gu, L. Q.; Huang, Z. S. Quinolino-benzo-[5, 6]-dihydroisoquinolium compounds derived from berberine: a new class of highly selective ligands for G-quadruplex DNA in c-myc oncogene. *Eur. J. Med. Chem.* **2011**, *46*(5), 1906–1913. doi: 10.1016/j.ejmech.2011.02.020
5. Lo, C. Y.; Hsu, L. C.; Chen, M. S.; Lin, Y. J.; Chen, L. G.; Kuo, C-D.; Wu, J-Y. Synthesis and anticancer activity of a novel series of 9-O-substituted berberine derivatives: a lipophilic substitute role. *Bioorg. Med. Chem. Lett.* **2013**, *23*(1), 305–309. doi: 10.1016/j.bmcl.2012.10.098
6. Pierpaoli, E.; Damiani, E.; Orlando, F.; Lucarini, G.; Bartozzi, B.; Lombardi, P.; Salvatore, C.; Geroni, C.; Donati, A.; Provinciali, M. Antiangiogenic and antitumor activities of berberine derivative NAX014 compound in a transgenic murine model of HER2/neu-positive mammary carcinoma. *Carcinogenesis* **2015**, *36*(10), 1169–1179. doi: 10.1093/carcin/bgv103
7. Bian, X.; He, L.; Yang, G. Synthesis and antihyperglycemic evaluation of various protoberberine derivatives. *Bioorg. Med. Chem. Lett.* **2006**, *16*(5), 1380–1383. doi: 10.1016/j.bmcl.2005.11.045
8. Wang, D. M.; Wei, J. Z.; Fan, B. Y.; Liu, Q.; Zhu, H. B.; Shen, Z. F.; Wu, S. Synthesis and biological evaluation of tetrahydrooptisine quaternary ammonium compounds. *Acta Pharm. Sin.* **2012**, *47*(12), 1640–1645. PMID: 23460970
9. Yang, P.; Song, D. Q.; Li, Y. H.; Kong, W. J.; Wang, Y. X.; Gao, L. M.; Liu, S. Y.; Cao, R. Q.; Jiang, J. D. Synthesis and structure-activity relationships of berberine analogues as a novel class of low-density-lipoprotein receptor up-regulators. *Bioorg. Med. Chem. Lett.* **2008**, *18*(16), 4675–4677. doi: 10.1016/j.bmcl.2008.07.005
10. Li, Y. H.; Yang, P.; Kong, W. J.; Wang, Y. X.; Hu, C. Q.; Zuo, Z. Y.; Wang, Y. M.; Gao, H.; Gao, L. M.; Feng, Y. C.; Du, N. N.; Liu, Y.; Song, D. Q.; Jiang, J. D. Berberine analogues as a novel class of the low-density-lipoprotein receptor up-regulators: synthesis, structure-activity relationships, and cholesterol-lowering efficacy. *J. Med. Chem.* **2009**, *52*(2), 492–501. doi: 10.1021/jm801157z
11. Wang, Y. X.; Wang, Y. P.; Zhang, H.; Kong, W. J.; Li, Y. H.; Liu, F.; Gao, R. M.; Liu, T.; Jiang, J. D.; Song, D. Q. Synthesis and biological evaluation of berberine analogues as novel up-regulators for both low-density-lipoprotein receptor and insulin receptor. *Bioorg. Med. Chem. Lett.* **2009**, *19*(21), 6004–6008. doi: 10.1016/j.bmcl.2009.09.059

### Chapter 3

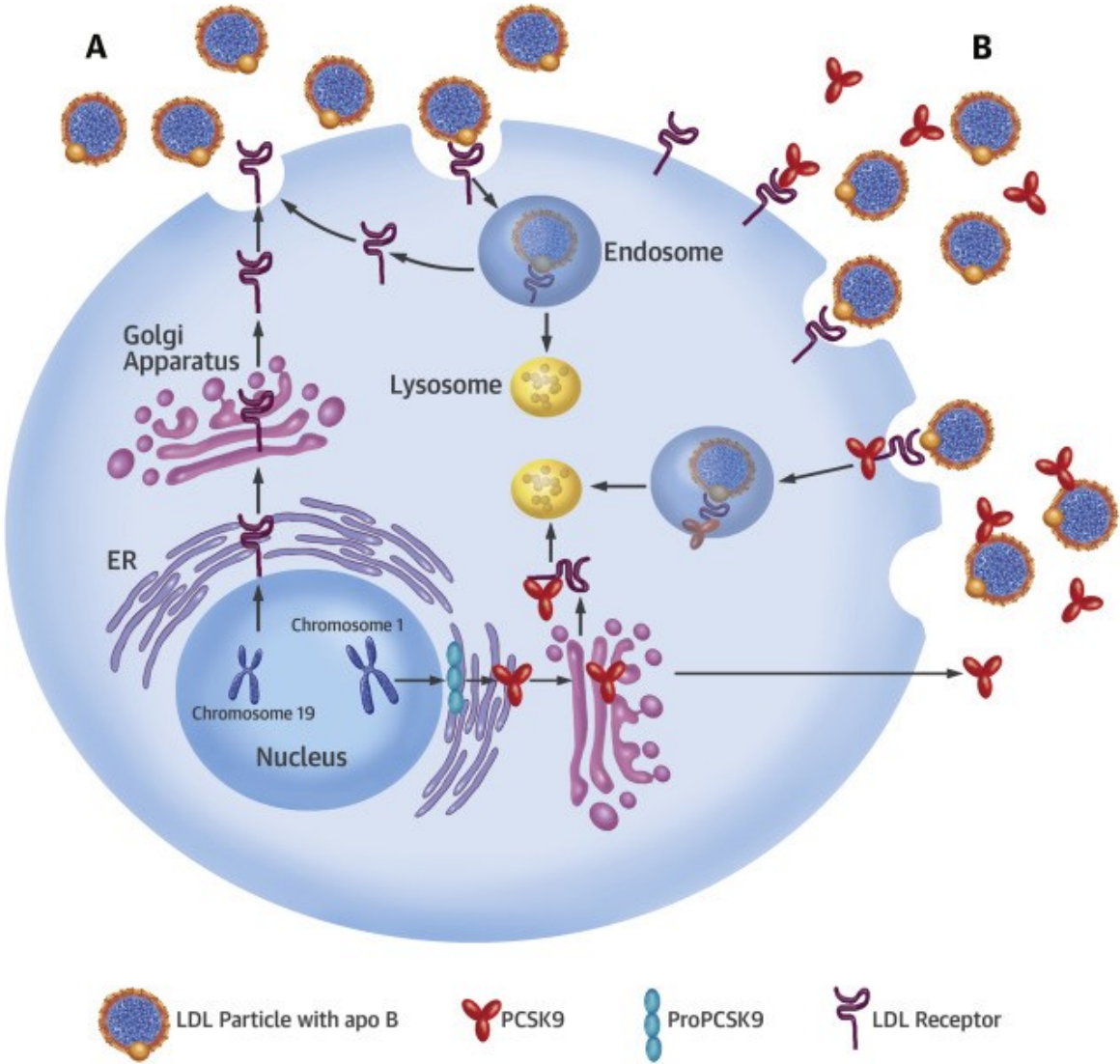
12. Wang, Y. X.; Kong, W. J.; Li, Y. H.; Tang, S.; Li, Z.; Li, Y. B.; Shan, Y. Q.; Bi, C. W.; Jiang, J. D.; Song, D. Q. Synthesis and structure-activity relationship of berberine analogues in LDLR up-regulation and AMPK activation. *Bioorg. Med. Chem.* **2012**, *20*(22), 6552–6558. doi: 10.1016/j.bmc.2012.09.029
13. Li, Y. H.; Li, Y.; Yang, P.; Kong, W. J.; You, X. F.; Ren, G.; Deng, H. B.; Wang, Y. M.; Wang, Y. X.; Jiang, J. D.; Song, D. Q. Design, synthesis, and cholesterol-lowering efficacy for prodrugs of berberrubine. *Bioorg. Med. Chem.* **2010**, *18*(17), 6422–6428. doi: 10.1016/j.bmc.2010.06.106
14. Nechepurenko, I.; Boyarskikh, U.; Khvostov, M.; Baev, D.; Komarova, N.; Filipenko, M.; Tolstikova, T.; Salakhutdinov, N. Hypolipidemic berberine derivatives with a reduced aromatic ring C. *Chem. Nat. Compd.* **2015**, *51*(5), 916-922. doi: 10.1007/s10600-015-1447-9
15. Li, D. D.; Yu, P.; Wang, Z. Z.; Xiao, W.; Zhou, X. H.; Zhao, L. G. Discovery of 7,9-disulfatetrahydroberberine as novel lipid-lowering agents. *ACS Omega* **2020**, *5*(48), 30836–30848. doi: 10.1021/acsomega.0c03253
16. Fan, T. Y.; Yang, Y. X.; Zeng, Q. X.; Wang, X. L.; Wei, W.; Guo, X. X.; Zhao, L. P.; Song, D. Q.; Wang, Y. X.; Wang, L.; Hong, B. Structure-activity relationship and biological evaluation of berberine derivatives as PCSK9 down-regulating agents. *Bioorg. Chem.* **2021**, *113*, 104994. doi: 10.1016/j.bioorg.2021.104994
17. Wu, C.; Xi, C.; Tong, J.; Zhao, J.; Jiang, H.; Wang, J.; Wang, Y.; Liu, H. Design, synthesis, and biological evaluation of novel tetrahydroprotoberberine derivatives (THPBs) as proprotein convertase subtilisin/kexin type 9 (PCSK9) modulators for the treatment of hyperlipidemia. *Acta Pharm. Sin. B* **2019**, *9*(6), 1216–1230. doi: 10.1016/j.apsb.2019.06.006
18. Ge, H.; Zhang, W.; Yuan, K.; Xue, H.; Cheng, H.; Chen, W.; Xie, Y.; Zhang, J.; Xu, X.; Yang, P. Design, synthesis, and biological evaluation of novel tetrahydroprotoberberine derivatives to reduce SREBPs expression for the treatment of hyperlipidemia. *Eur. J. Med. Chem.* **2021**, *221*, 113522. doi: 10.1016/j.ejmech.2021.113522
19. Ying, Z.; Desikan, R.; Xu, X.; Maiseyeu, A.; Liu, C.; Sun, Q.; Ziouzenkova, O.; Parthasarathy, S.; Rajagopalan, S. Modified methylenedioxyphenol analogs lower LDL cholesterol through induction of LDL receptor expression. *J. Lipid Res.* **2012**, *53*(5), 879–887. doi: 10.1194/jlr.M022806
20. Parthasarathy, S.; Rajagopalan, S.; Rajagopal, D.; Novel methylenedioxy phenolic compounds and their use to treat disease. Patent WO2010017323A1, February 11, **2010**.
21. Zhongzhen, Y.; Xin, C.; Weijian, L.; Guo-Bo, L.; Yong, W. Total synthesis and evaluation of B-homo palmatine and berberine derivatives as p300 histone acetyltransferase inhibitors. *Eur. J. Org. Chem.* **2018**, *2018*, 1041-1052. doi:10.1002/ejoc.201701693
22. Wu, Y.; Haili, L.; Weijian, G. M. The synthesis of high B rings jamaicin and palmatine derivative and as hypoglycemic purposes. Patent CN108101902B, May 15, **2020**.
23. Mori-Quiroz, L. M.; Hedrick, S. L.; De Los Santos, A. R.; Clift, M. D. A unified strategy for the syntheses of the isoquinolinium alkaloids berberine, coptisine, and jatrorrhizine. *Org. Lett.* **2018**, *20*(14), 4281–4284. doi: 10.1021/acs.orglett.8b01702
24. Senthil, P.; Selvaraj, S. Sodium iodide as a novel, chemoselective and highly efficient catalyst for N-tert-butoxy carbonylation of amines at room temperature. *J. Chem. Pharm. Res.* **2016**, *8*, 510-518.

25. Zhu, W.; Miao, Z.; Li, B.; Song, S.; Xu, Z.; Zhang, Y. Cai, T.; Chen, K. Seven-element-ring berberine analogue, pharmaceutical composition thereof, preparation method and usage. Patent WO2016138882A1, September 09, **2016**.
26. So, M.; Kotake, T.; Matsuura, K.; Inui, M.; Kamimura, A. Concise synthesis of 2-benzazepine derivatives and their biological activity. *J. Org. Chem.* **2012**, *77*(8), 4017–4028. doi: 10.1021/jo300380z
27. Fu-Lin Chen, K. S. An exception of Eschweiler-Clarke methylation: cyclocondensation of  $\alpha$ -amino amides with formaldehyde and formic acid. *Chem. Heterocycl. Compd.* **2005**, *41*, 697-700. doi:10.1002/CHIN.200509105
28. Bala, M.; Verma, P.K.; Kumar, N.; Singh, B.; Direct waste-free synthesis of amides from nonactivated carboxylic acids and amines: application to the synthesis of tetrahydroisoquinolines. *Synth. Commun.* **2015**, *45*, 847-856 doi:10.1080/00397911.2014.984853
29. Gourlay, B.S.; Molesworth, P. P.; Ryan, J. H.; Smith, J. A. A new and high-yielding synthesis of unstable pyrroles via a modified Clauson-Kaas reaction. *Tetrahedron Lett.* **2006**, *47*(5), 799-801.
30. Livak, K. J.; Schmittgen, T. D. Analysis of relative gene expression data using real-time quantitative PCR and the  $2^{-\Delta\Delta C(T)}$  method. *Methods* **2001**, *25*(4), 402–408. doi: 10.1006/meth.2001.1262



# Chapter 4

## PCSK9: a New Target for Fighting Hypercholesterolemia





#### **4.1 PCSK9 and its role in cardiovascular diseases**

Proprotein convertase subtilisin/kexin type 9 (PCSK9), initially named Neural Apoptosis Regulated Convertase 1 (NARC1), is a soluble protease discovered in 2003. It is the ninth member of the serine secretory proteinase family called pro-protein convertase (PC),<sup>1,2</sup> and is highly expressed in the liver, and, to a lesser extent, in the intestine, adipose tissue, pancreas, kidneys and vascular cells.<sup>3-7</sup>

Circulating levels of PCSK9 biologically increase in the late night and decrease in the late afternoon,<sup>8</sup> and are influenced by multiple factors including body mass index (BMI), plasma cholesterol and triglyceride levels, blood pressure, age and sex.<sup>9,10</sup>

Targeting PCSK9 is an interesting new approach to reduce hyperlipidemia and related risk of cardiovascular diseases. In support of its key role in this field, there is the discovery that various gain-of-function (GOF) mutations of PCSK9<sup>11,12</sup> are associated with significant elevations of plasma LDL; on the contrary, several loss-of-function (LOF) mutations of PCSK9<sup>13,14</sup> protect against hypercholesterolemia and cardiovascular risk.

PCSK9 regulates lipoprotein metabolism by several mechanisms including:

- binding with many protein partners (e.g. LDLR, CAP1, c-IAP1, VLDL receptor, apoER2, DAP1, LRP1 and proteins present in the functional plasma membrane microdomains (so-called lipid rafts);
- modulation of gene expression of many factors promoting CVDs.<sup>15</sup>

Currently, two full human mAbs PCSK9 inhibitors, alirocumab and evolocumab, have been approved by the US FDA and EMA.<sup>16</sup> However, PCSK9 monoclonal antibodies require once- or twice-monthly subcutaneous injections and their manufacturing process is expensive, increasing the cost of therapy. Thus, development of new inhibitors of PCSK9 with effectiveness of cost and ease of administration is strongly encouraged.

## Chapter 4

### 4.2 PCSK9 gene and structure

The human *PCSK9* gene is located at chromosome 1p32 and consists of 11 introns and 12 exons that encode a 692-amino acids full-length PCSK9 (preproPCSK9), that later undergoes post-translational modifications to form a 62 kDa mature protein.<sup>17</sup> PreproPCSK9 includes five segments: a signal peptide (aa 1–30), an *N*-terminal prodomain (aa 31–152), a catalytic domain (aa 153–404), a *C*-terminal cys-his-rich domain (aa 455–692), that can be further divided into three modules, namely M1, M2 and M3, and a small peptide (also known as the hinge region (aa 405–454),<sup>18</sup> that serves as a link between the catalytic and *C*-terminal domains.

There are two types of circulating PCSK9: mature and furin-cleaved. The maturation process of PCSK9 requires three steps. The first event occurs in the endoplasmic reticulum (ER), where preproPCSK9 is converted into proPCSK9 by eliminating the signal peptide (SP). Then proPCSK9 undergoes to autocatalytic cleavage to form a 62 kDa mature PCSK9 domain and a 13 kDa prodomain. The latter noncovalently binds to the catalytic domain of PCSK9, forming the PCSK9–prodomain heterodimer, which has the correct folding necessary for PCSK9 transportation from the ER to the Golgi apparatus and to be protected from interaction with others enzymes, especially furin, during this intracellular movement (Figure 4.1).<sup>19</sup>

In the Golgi apparatus the PCSK9–prodomain heterodimer undergoes glycosylation and interacts with sortilin, which facilitates its secretion into the circulation. Interestingly, enzymatic activity of PCSK9 is not required for LDL receptor binding and LDL receptor degradation.

Normally, mature PCSK9 has its pro-domain non-covalently attached; however, it can be cleaved by the membrane-bound proprotein convertase furin (and to a lesser extent by the proprotein convertase PC5/6A) at the Arg<sup>218</sup>-Gln<sup>219</sup> peptide bond, given rise to a smaller heterodimer (55 + 13kDa), that is no longer able to promote LDLR degradation.<sup>19,20</sup>

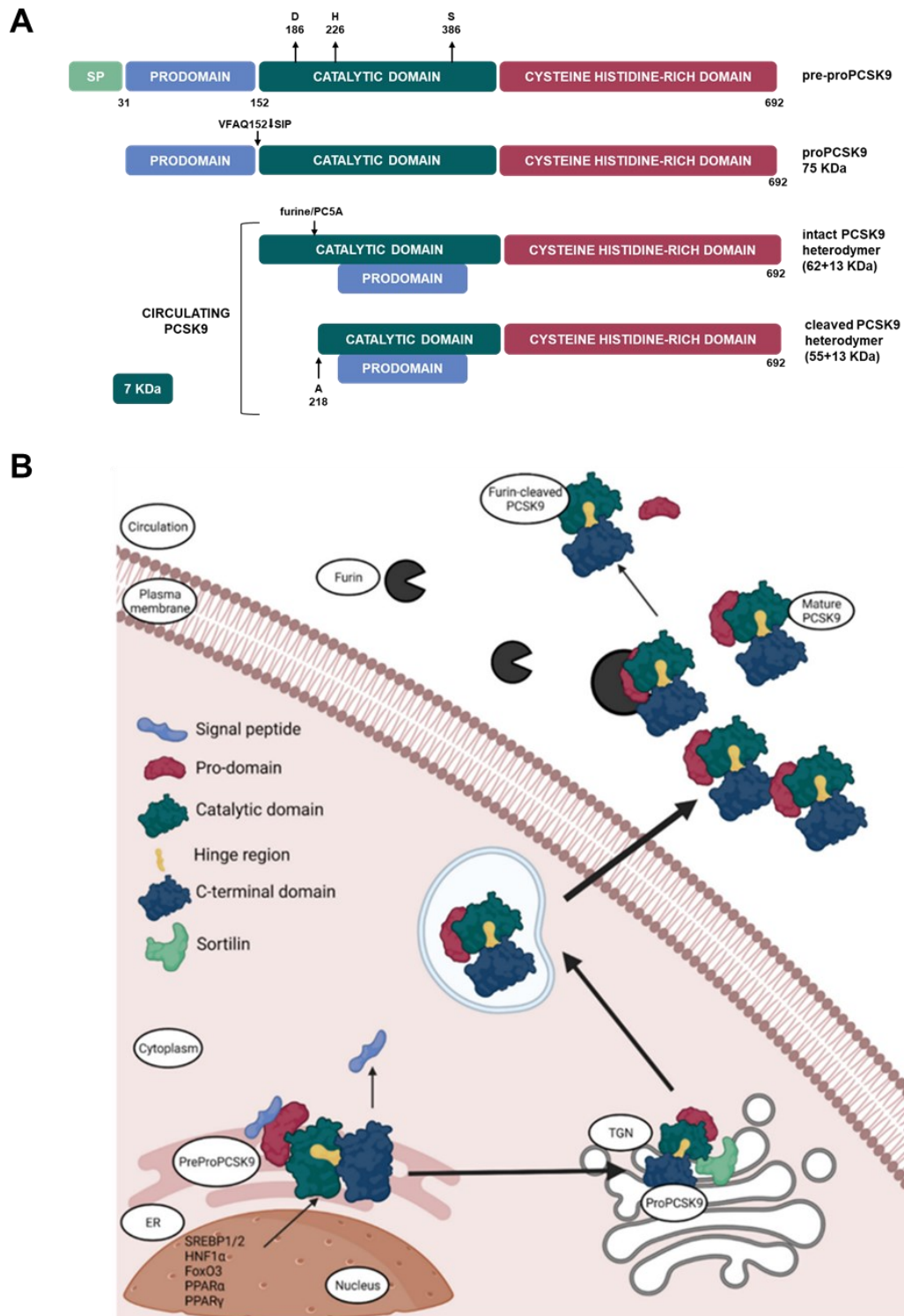


**Figure 4.1** A) Processing of *pre-proPCSK9* leading to *PCSK9* mature form; B) synthesis and secretion of *PCSK9*.<sup>21</sup>

The expression of the *PCSK9* gene is regulated by various transcription factors and cofactors such as sterol-response element binding protein (SREBP1/2), hepatocyte nuclear factor 1 $\alpha$  (HNF1 $\alpha$ ), forkhead box O3 (FoxO3), and peroxisome proliferator-activated receptor  $\alpha$  and  $\gamma$

## Chapter 4

(PPAR $\alpha$  and PPAR $\gamma$ ). In particular, the PCSK9 promoter contains a region, named Sterol Regulatory Element (SRE)<sup>22</sup> to which SREBP1/2 can bind.<sup>18</sup> Low cholesterol concentrations upregulates SREBP1/2 expression, that in turn increases PCSK9 levels in circulation.<sup>23</sup>

However, recent evidences suggest that the primary positive regulator of PCSK9 is HNF1 $\alpha$ , which bind to a site located next to the SRE site in the promoter region.<sup>22</sup> On the contrary FoxO3 suppresses PCSK9 expression recruiting sirtuins 6 and inhibiting HNF1 $\alpha$ -mediated upregulation of PCSK9.<sup>24</sup> Sirtuins 1 and 6 and histone deacetylases are also known to suppress SREBP2 expression in the liver.<sup>23,25</sup> Finally, PPAR $\gamma$  increases the gene expression of PCSK9 while PPAR $\alpha$  decreases it.<sup>2</sup>

### 4.3 PCSK9 polymorphisms

The identification of PCSK9 variants has been crucial in studying its role in hypercholesterolemia and related CVDs.<sup>13,26-33</sup> To date several loss-of-function mutations have been identified providing protection against coronary artery disease.<sup>23,34,35</sup>

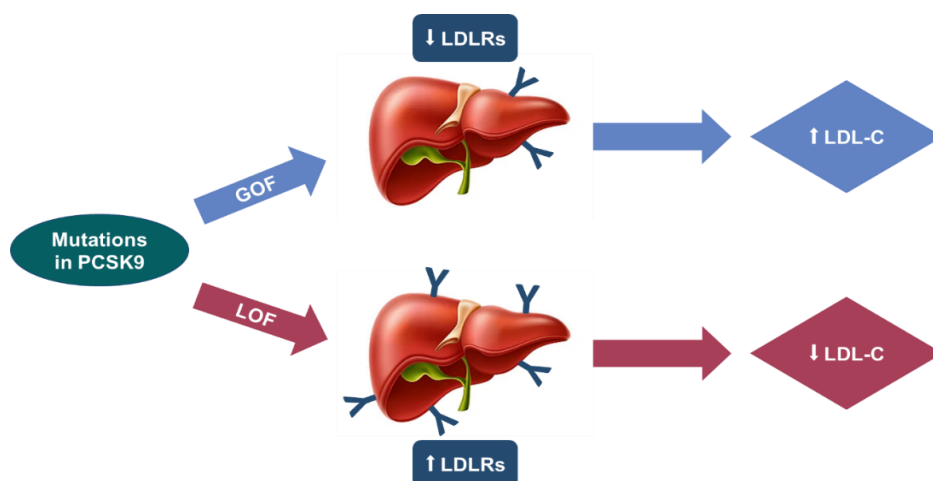


**Figure 4.2** Loss- and gain-of-function mutation in PCSK9.<sup>35</sup>

LOF mutations can affect the secretory pathway of PCSK9 or are correlated with an increase in proteolysis<sup>36-38</sup> and a lowering of the levels of lipoprotein(a).<sup>39,40</sup> Additionally, some variants (e.g. W428X, A443T and R434W) generate misfolded and non-functional PCSK9.<sup>41</sup>

The PCSK9 gene also undergoes gain-of-function mutations leading to hypercholesterolemia and premature atherosclerosis.<sup>23,42</sup> For instance, the D374Y and S127R mutations improve the affinity of PCSK9 towards LDLR and increase the concentration of ApoB100-containing atherogenic lipoprotein particles (such as LDL, VLDL, IDL).<sup>36,37,43-45</sup>

Interestingly, some variants of PCSK9 (e.g. S127R, A245T and R272Q) show both LOF and GOF mutations (Figure 4.2).<sup>46-50</sup>

#### **4.4 PCSK9-LDLR binding**

The LDLR-mediated endocytic pathway of LDL is critical for the maintenance of the cholesterol homeostasis. After binding of LDL-C to the LDLR, the resulting complex is endocytosed in the hepatocytes, then LDL-C is degraded in the lysosome into lipids and amino acids, while LDLR is transported back to the cell surface, where it can bind to LDL-C again.

This process of internalization and recycling back of the receptor to the plasma membrane is interrupted by PCSK9, which acts as a molecular chaperone to assist the lysosomal degradation of LDLR in hepatocytes.<sup>51</sup>

The LDL receptor is structured in:

- *extracellular domain* consisting in: a) a ligand-binding domain (1-292 residues), located at the *N*-terminus of the protein; b) a so-called epidermal growth factor (EGF) precursor homology domain (293-699), which contains two cysteine-rich EGF-like domains (EGF-A and EGF-B) separated from a third EGF repeat (EGF-C) by a  $\beta$ -propeller domain; c) an oligosaccharide-rich domain (residues 700-758), which is a threonine- and serine-rich region;
- *membrane-spanning domain* (residues 759-781);
- *cytoplasmic domain* (residues 782-832), important for receptor clustering in clathrin coated pits and for internalization of the receptor.<sup>52,53</sup>

## Chapter 4

The ligand-binding domain interacts with ApoB100 of LDL; this binding is favored at a neutral pH, when extracellular domain of LDLR adopts a linear open conformation.<sup>54</sup>

Then the complex receptor/ligand is internalized via clathrin-coated pits and delivered to endosomes.<sup>55</sup> Here the low pH induces a conformational switch from an open to a closed form of the LDLR, thus promoting the discharge of bound LDL that is delivered to lysosomes for degradation, while LDLR is recycled back to the cell surface<sup>54, 55</sup> (pathway 1, Figure 4.3).

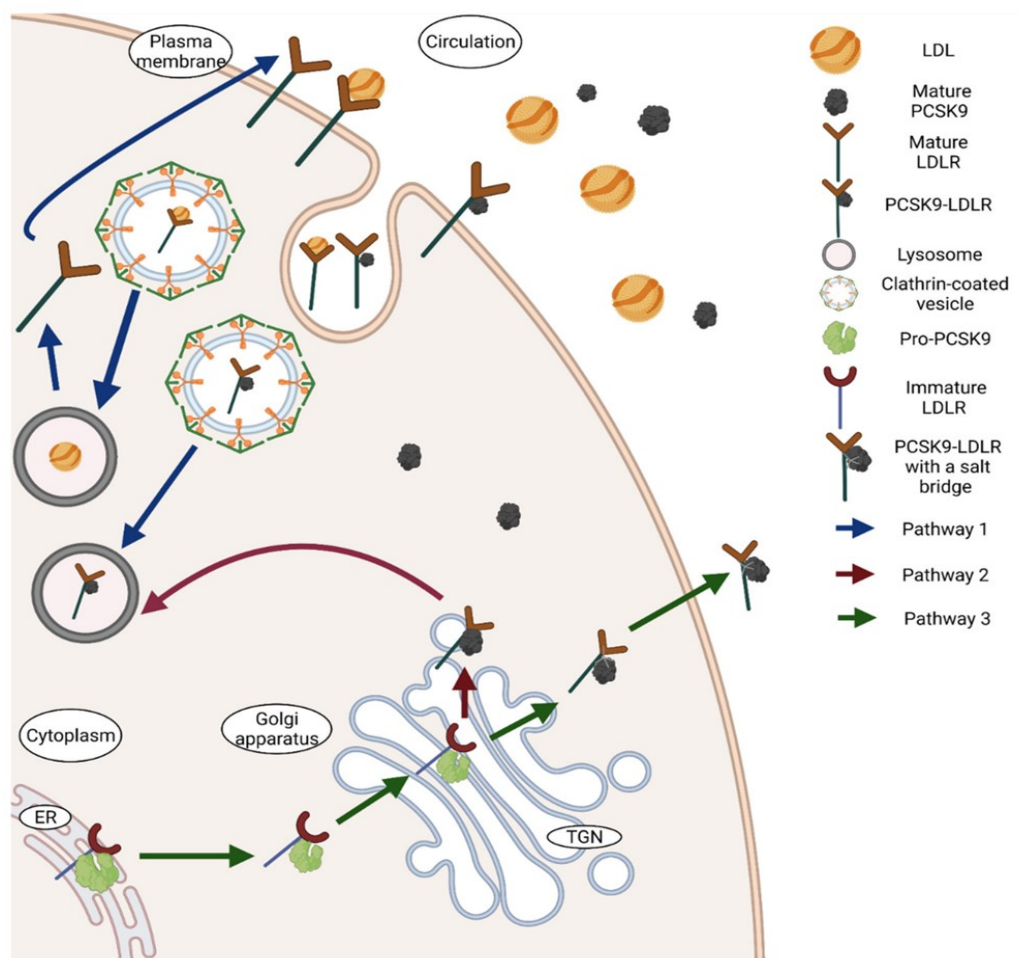


**Figure 4.3** Interactions between PCSK9 and LDLR.<sup>21</sup>

The interaction between PCSK9 and LDLR involves the catalytic domain of PCSK9 and the EGF-A domain of LDLR. Interestingly, Shoudong *et al.* reported that replacement of Leu at position 318 in the EGF-A of LDLR with Asp (as it is in VLDLR), markedly reduced PCSK9 binding to the receptor, indicating the important role of this residue in PCSK9 binding.<sup>56</sup>

Several lines of evidence demonstrate that PCSK9/LDLR complex enters cells via clathrin-coated pits. Knockdown of clathrin heavy chain significantly reduces PCSK9-promoted LDLR degradation in human hepatoma-derived cell lines, Huh7 and HepG2 cell.<sup>57-59</sup> Conversely, Jang *et al.* reported that knockdown of clathrin heavy chain did not affect PCSK9-promoted LDLR degradation in HepG2 cells; instead, the authors found that the PCSK9/LDLR complex entered cells via caveolae-dependent endocytosis.<sup>60</sup> The reasons for this discrepancy are unclear. However, it is of note that different approaches were used in these studies.<sup>58,60</sup>

The PCSK9/LDLR interaction is affected by pH changes as well as calcium concentrations.<sup>61,62</sup> Indeed, it has been observed that PCSK9 binds to the LDLR receptor with a much higher affinity at the endosomal acidic pH than at the neutral pH.<sup>63</sup> This increased affinity is generated by an interaction between the ligand-binding domain of the LDLR and the C-terminal domain of the mature PCSK9,<sup>51</sup> causing LDLR to not unfold and therefore it isn't recycled back to the cell surface.<sup>36,64</sup>

PCSK9 also facilitates intracellular degradation of mature LDLR present in the Golgi or Trans-Golgi complex, before it reaches the cell surface<sup>23</sup> (pathway 2, Figure 4.3), redirecting it to the lysosomes for degradation. Unlike the extracellular degradation of LDLR, this intracellular degradation involves the catalytic activity of PCSK9.<sup>23</sup>

Finally, the pre-proPCSK9 can interact with the precursor of LDLR in non-destructive way (pathway 3, Figure 4.3), acting as a chaperone to transport the precursor form of the LDLR from the ER to the Golgi apparatus wherein LDLR matures.<sup>23,65</sup> This interaction is also advantageous for the auto-catalytic cleavage and thus for the maturation of the pre-pro-PCSK9.

Furthermore, the mature PCSK9 can help LDLR to be released by the cell.<sup>65</sup> However, this chaperone activity is not critical for the transportation of LDLR to the cell membrane since it happens also in the absence of PCSK9.<sup>65</sup>

## Chapter 4

### 4.5 PCSK9 inhibition strategies

Currently, the inhibition of the PCSK9/LDLR interaction by peptidomimetics or small molecules is the most common strategy pursued to inhibit PCSK9 as will be discussed in detail in Chapter 5.

Another validated strategy is the suppression of PCSK9 expression; in this regard, several natural substances (including berberine (Chapter 2), quercetin-3- $\beta$ -D-glucoside,<sup>66</sup> curcumin,<sup>67</sup> polydatin,<sup>68</sup> tanshinone IIA,<sup>69</sup> and hanabiratakeli A,<sup>70</sup> Figure 4.4) evidenced an inhibitory activity against PCSK9 mRNA expression, mainly by lowering levels of HNF-1 $\alpha$  and/or SREBP2, key transactivators involved in the regulation of PCSK9 gene expression.<sup>23,71,72</sup>

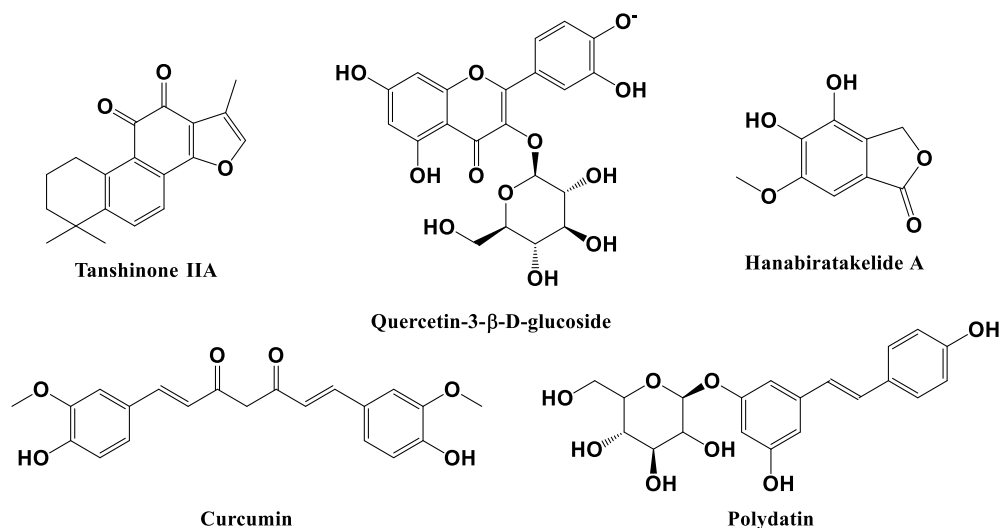


**Figure 4.4** Chemical structure of some natural PCSK9-expression modulators.

These plant derived natural products usually have a multitarget action and alongside a lipid-lowering action, they also show hypoglycemic, antioxidant, anti-inflammatory properties that are useful for therapeutic intervention in patients with complex diseases such as metabolic disorders.

Gene silencing with small nucleic acid molecules, i.e. antisense oligonucleotides (ASOs) (e.g. ISIS-405879/BMS-844421, SPC5001, CiVi007),<sup>73</sup> and small interfering RNAs (siRNAs)<sup>74</sup> targeting the PCSK9 mRNA, is another proposed approach.

Inclisiran (Figure 4.5), a first-in-class siRNA that specifically targets PCSK9 within the liver, is a synthetic double-stranded RNA that contains modified nucleotides, and is conjugated to triantennary *N*-acetylgalactosamine carbohydrates (GalNAc). The GalNAc moiety of inclisiran binds to the asialoglycoprotein receptor that is selectively expressed on the surface of hepatocyte and facilitates the receptor-mediated endocytosis of the drug.<sup>75,76</sup>

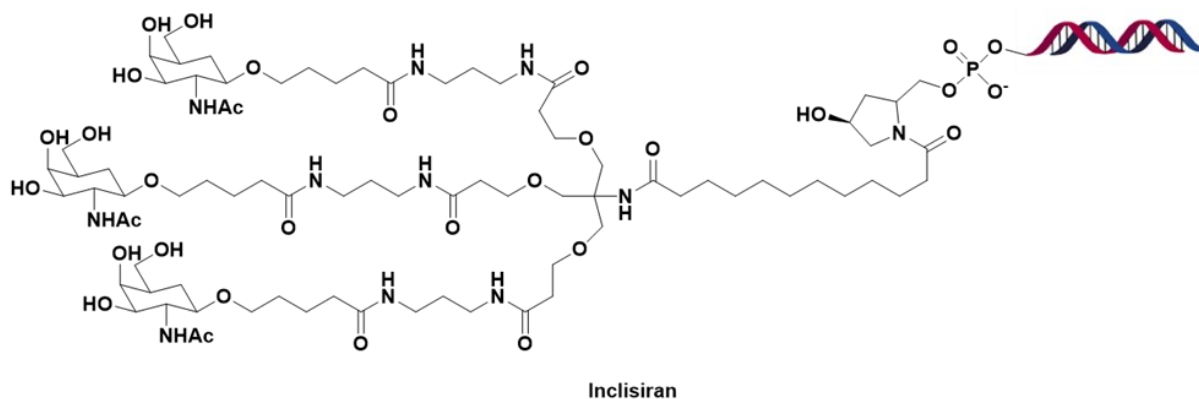


**Figure 4.5** Chemical structure of the siRNA inhibitor inclisiran.

Inclisiran has a good safety profile and a prolonged duration of action, and its cost/effectiveness ratio is more favorable than that of evolocumab and alirocumab.<sup>77</sup>

Recently, liver heparan sulfate proteoglycans (HSPG) have been found to act as co-receptors for PCSK9.<sup>78</sup> Indeed, the PCSK9 prodomain can interact with HSPGs and this binding facilitates the subsequent PCSK9:LDLR complex formation. Accordingly, mAbs, specifically directed against the HSPG binding site, and mimetics of heparin or heparan sulfate (e.g. suramin, dextran sulfate and S-dC-36, Figure 4.6), have been developed as inhibitors of PCSK9.<sup>78</sup>

CRISPR-Cas9 platform is an innovative technology that has yielded promising results for lowering total cholesterol levels targeting PCSK9. CRISPR-associated systems (Cas) use the Cas9 (CRISPR-Cas9) nuclease derived from bacteria, such as *Streptococcus pyogenes* or *Staphylococcus aureus*, that binds to DNA and causes double-stranded breaks with the goal of introducing LOF mutations into the endogenous PCSK9 gene *in vivo*. However, extensive

## Chapter 4

research work is still required to develop CRISPR technology, because of the relatively high frequency of off-target effects, and potential immunogenicity.<sup>79-81</sup>

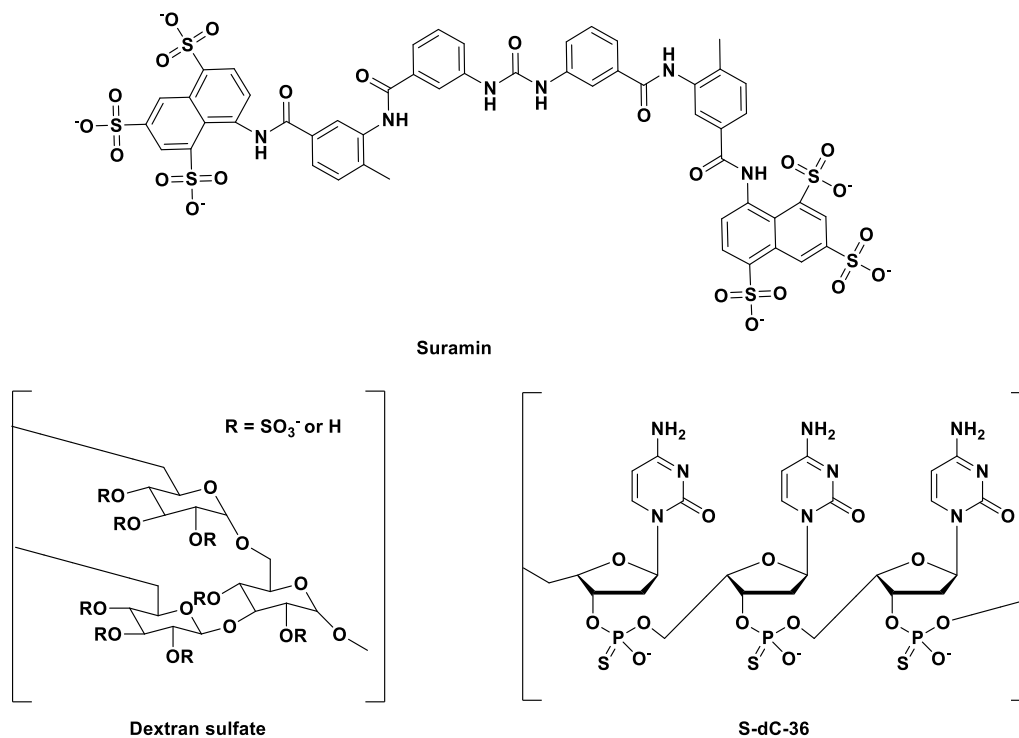


**Figure 4.6** Structures of heparin mimetics PCSK9 inhibitors.

Finally, several peptide-based vaccines are under development to neutralize PCSK9. For example, Pan *et al.* used a peptide virus-like particle (VLP) vaccine targeting PCSK9 in mouse models and noticed an increased expression of LDLR in the liver without detectable immune damage.<sup>82</sup> Galabova *et al.* reported antigenic short peptides (approximately 8-13 residues) able to induce the production of high-affinity mAbs against PCSK9, decreasing LDL-C levels by up to 50%. These peptides mimic parts of the *N*-terminus of mature human PCSK9,<sup>83</sup> and the most promising one (AFFITTOPE<sup>®</sup>), formulated into AT04A vaccine, is currently in Phase I clinical trial.<sup>84</sup>

**References**

1. Seidah, N. G.; Benjannet, S.; Wickham, L.; Marcinkiewicz, J.; Jasmin, S. B.; Stifani, S.; Basak, A.; Prat, A.; Chretien, M. The secretory proprotein convertase neural apoptosis-regulated convertase 1 (NARC-1): liver regeneration and neuronal differentiation. *Proc. Natl. Acad. Sci. U.S.A.* **2003**, *100*(3), 928–933. doi: 10.1073/pnas.0335507100
2. Ragusa, R.; Basta, G.; Neglia, D.; De Caterina, R.; Del Turco, S.; Caselli, C. PCSK9 and atherosclerosis: looking beyond LDL regulation. *Eur. J. Clin. Invest.* **2021**, *51*(4), e13459. doi: 10.1111/eci.13459
3. Leblond, F.; Seidah, N. G.; Précourt, L. P.; Delvin, E.; Dominguez, M.; Levy, E. Regulation of the proprotein convertase subtilisin/kexin type 9 in intestinal epithelial cells. *Am. J. Physiol. Gastrointest.* **2009**, *296*(4), G805–G815. doi: 10.1152/ajpgi.90424.2008
4. Langhi, C.; Le May, C.; Gmyr, V.; Vandewalle, B.; Kerr-Conte, J.; Krempf, M.; Pattou, F.; Costet, P.; Cariou, B. PCSK9 is expressed in pancreatic delta-cells and does not alter insulin secretion. *Biochem. Biophys. Res. Commun.* **2009**, *390*(4), 1288–1293. doi: 10.1016/j.bbrc.2009.10.138
5. Wolf, A.; Kutsche, H. S.; Schreckenber, R.; Weber, M.; Li, L.; Rohrbach, S.; Schulz, R.; Schlüter, K. D. Autocrine effects of PCSK9 on cardiomyocytes. *Basic Res. Cardiol.* **2020**, *115*(6), 65. doi: 10.1007/s00395-020-00824-w
6. Artunc, F. Kidney-derived PCSK9—a new driver of hyperlipidemia in nephrotic syndrome? *Kidney Int.* **2020**, *98*(6), 1393–1395. doi: 10.1016/j.kint.2020.07.027
7. O'Connell, E. M.; Lohoff, F. W. Proprotein convertase subtilisin/kexin type 9 (PCSK9) in the brain and relevance for neuropsychiatric disorders. *Front. Neurosci.* **2020**, *14*, 609. doi: 10.3389/fnins.2020.00609
8. Persson, L.; Cao, G.; Ståhle, L.; Sjöberg, B. G.; Troutt, J. S.; Konrad, R. J.; Gälman, C.; Wallén, H.; Eriksson, M.; Hafström, I.; Lind, S.; Dahlin, M.; Amark, P.; Angelin, B.; Rudling, M. Circulating proprotein convertase subtilisin kexin type 9 has a diurnal rhythm synchronous with cholesterol synthesis and is reduced by fasting in humans. *Arterioscler. Thromb. Vasc. Biol.* **2010**, *30*(12), 2666–2672. doi: 10.1161/ATVBAHA.110.214130
9. Cui, Q.; Ju, X.; Yang, T.; Zhang, M.; Tang, W.; Chen, Q.; Hu, Y.; Haas, J. V.; Troutt, J. S.; Pickard, R. T.; Darling, R.; Konrad, R. J.; Zhou, H.; Cao, G. Serum PCSK9 is associated with multiple metabolic factors in a large Han Chinese population. *Atherosclerosis*, **2010**, *213*(2), 632–6. doi: 10.1016/j.atherosclerosis.2010.09.027
10. Ferri, N.; Ruscica, M.; Coggi, D.; Bonomi, A.; Amato, M.; Frigerio, B.; Sansaro, D.; Ravani, A.; Veglia, F.; Capra, N.; Lupo, M. G.; Macchi, C.; Castelnovo, S.; Savonen, K.; Silveira, A.; Kurl, S.; Giral, P.; Pirro, M.; Strawbridge, R. J.; Gigante, B. Improve study group sex-specific predictors of PCSK9 levels in a European population: the improve study. *Atherosclerosis* **2020**, *309*, 39–46. doi: 10.1016/j.atherosclerosis.2020.07.014
11. Yuan, F.; Guo, L.; Park, K. H.; Woollard, J. R.; Taek-Geun, K.; Jiang, K.; Melkamu, T.; Zang, B.; Smith, S. L.; Fahrenkrug, S. C.; Kolodgie, F. D.; Lerman, A.; Virmani, R.; Lerman, L. O.; Carlson, D. F. Ossabaw pigs with a PCSK9 gain-of-function mutation develop accelerated coronary atherosclerotic lesions: a novel model for preclinical studies. *J. Am. Heart Assoc.* **2018**, *7*(6), e006207. doi: 10.1161/JAHA.117.006207

## **Chapter 4**

12. Abifadel, M.; Guerin, M.; Benjannet, S.; Rabès, J. P.; Le Goff, W.; Julia, Z.; Hamelin, J.; Carreau, V.; Varret, M.; Bruckert, E.; Bonnefont-Rousselot, D.; Chapman, J.; Carrié, A.; Michel, J. B.; Prat, A.; Seidah, N. G.; Boileau, C. Identification and characterization of new gain-of-function mutations in the PCSK9 gene responsible for autosomal dominant hypercholesterolemia. *Atherosclerosis* **2012**, *223*(2), 394–400. doi: 10.1016/j.atherosclerosis.2012.04.006
13. Fasano, T.; Cefalù, A. B.; Di Leo, E.; Noto, D.; Pollaccia, D.; Bocchi, L.; Valenti, V.; Bonardi, R.; Guardamagna, O.; Aversa, M.; Tarugi, P. A novel loss of function mutation of PCSK9 gene in white subjects with low-plasma low-density lipoprotein cholesterol. *Arterioscler. Thromb. Vasc. Biol.* **2007**, *27*(3), 677–681. doi: 10.1161/01.ATV.0000255311.26383.2f
14. Small, A. M.; Huffman, J. E.; Klarin, D.; Lynch, J. A.; Assimes, T.; DuVall, S.; Sun, Y. V.; Shere, L.; Natarajan, P.; Gaziano, M.; Rader, D. J.; Wilson, P.; Tsao, P. S.; Chang, K. M.; Cho, K.; O'Donnell, C. J.; Casas, J. P.; Damrauer, S. M. PCSK9 loss of function is protective against extra-coronary atherosclerotic cardiovascular disease in a large multi-ethnic cohort. *PLoS One* **2020**, *15*(11), e0239752. doi: 10.1371/journal.pone.0239752
15. Liu, X.; Suo, R.; Chan, C.; Liu, T.; Tse, G.; Li, G. The immune functions of PCSK9: local and systemic perspectives. *J. Cell. Physiol.* **2019**, *234*(11), 19180–19188. doi: 10.1002/jcp.28612
16. White, C. M. Therapeutic potential and critical analysis of the PCSK9 monoclonal antibodies evolocumab and alirocumab. *Ann. Pharmacother.* **2015**, *49*(12), 1327-35. doi: 10.1177/1060028015608487
17. Seidah, N. G.; Prat, A. The proprotein convertases are potential targets in the treatment of dyslipidemia. *J. Mol. Med.* **2007**, *85*(7), 685–696. doi: 10.1007/s00109-007-0172-7
18. Wiciński, M.; Żak, J.; Malinowski, B.; Popek, G.; Grzešek, G. PCSK9 signaling pathways and their potential importance in clinical practice. *EPMA J.* **2017**, *8*(4), 391–402. doi: 10.1007/s13167-017-0106-6
19. Seidah, N. G.; Prat, A. The biology and therapeutic targeting of the proprotein convertases. *Nat. Rev. Drug Discov.* **2012**, *11*(5), 367–383. doi: 10.1038/nrd3699
20. Barale, C.; Melchionda, E.; Morotti, A.; Russo, I. PCSK9 biology and its role in atherothrombosis. *Int. J. Mol. Sci.* **2021**, *22*(11), 5880. doi: 10.3390/ijms22115880
21. Sundararaman, S. S.; Döring, Y.; van der Vorst, E. P. C. PCSK9: a multi-faceted protein that is involved in cardiovascular biology. *Biomedicines* **2021**, *9*(7), 793. doi: 10.3390/biomedicines9070793
22. Nishikido, T.; Ray, K. K. Targeting the peptidase PCSK9 to reduce cardiovascular risk: implications for basic science and upcoming challenges. *Br. J. Pharmacol.* **2021**, *178*(11), 2168–2185. doi: 10.1111/bph.14851
23. Schulz, R.; Schlüter, K. D.; Laufs, U. Molecular and cellular function of the proprotein convertase subtilisin/kexin type 9 (PCSK9). *Basic Res. Cardiol.* **2015**, *110*(2), 4. doi: 10.1007/s00395-015-0463-z
24. Tao, R.; Xiong, X.; DePinho, R. A.; Deng, C. X.; Dong, X. C. FoxO3 transcription factor and Sirt6 deacetylase regulate low density lipoprotein (LDL)-cholesterol homeostasis via control of the proprotein convertase subtilisin/kexin type 9 (PCSK9) gene expression. *J. Biol. Chem.* **2013**, *288*(41), 29252–29259. doi: 10.1074/jbc.M113.481473
25. Goettsch, C.; Kjolby, M.; Aikawa, E. Sortilin and its multiple roles in cardiovascular and metabolic diseases. *Arterioscler. Thromb. Vasc. Biol.* **2018**, *38*(1), 19–25. doi: 10.1161/ATVBAHA.117.310292

26. Lu, H.; Howatt, D. A.; Balakrishnan, A.; Graham, M. J.; Mullick, A. E.; Daugherty, A. Hypercholesterolemia induced by a PCSK9 gain-of-function mutation augments angiotensin II-induced abdominal aortic aneurysms in C57BL/6 mice-brief report. *Arterioscler. Thromb. Vasc. Biol.* **2016**, *36*(9), 1753–1757. doi: 10.1161/ATVBAHA.116.307613
27. Zhao, Z.; Tuakli-Wosornu, Y.; Lagace, T. A.; Kinch, L.; Grishin, N. V.; Horton, J. D.; Cohen, J. C.; Hobbs, H. H. Molecular characterization of loss-of-function mutations in PCSK9 and identification of a compound heterozygote. *Am. J. Hum. Genet.* **2006**, *79*(3), 514–523. doi: 10.1086/507488
28. El Khoury, P.; Elbitar, S.; Ghaleb, Y.; Khalil, Y. A.; Varret, M.; Boileau, C.; Abifadel, M. PCSK9 mutations in familial hypercholesterolemia: from a groundbreaking discovery to anti-PCSK9 therapies. *Curr. Atheroscler. Rep.* **2017**, *19*(12), 49. doi: 10.1007/s11883-017-0684-8
29. Lee, C. J.; Lee, Y.; Park, S.; Kang, S. M.; Jang, Y.; Lee, J. H.; Lee, S. H. Rare and common variants of ApoB and PCSK9 in Korean patients with extremely low low-density lipoprotein-cholesterol levels. *PLoS One* **2017**, *12*(10), 0186446. doi: 10.1371/journal.pone.0186446
30. Hopkins, P. N.; Krempf, M.; Bruckert, E.; Donahue, S.; Yang, F.; Zhang, Y.; Di Cioccio, A. T. Pharmacokinetic and pharmacodynamic assessment of alirocumab in patients with familial hypercholesterolemia associated with proprotein convertase subtilisin/kexin type 9 gain-of-function or apolipoprotein B loss-of-function mutations. *J. Clin. Lipidol.* **2019**, *13*(6), 970–978. doi: 10.1016/j.jacl.2019.10.007
31. Kaya, E.; Kayıkçıoğlu, M.; Tetik Vardarlı, A.; Eroğlu, Z.; Payzın, S.; Can, L. PCSK 9 gain-of-function mutations (R496W and D374Y) and clinical cardiovascular characteristics in a cohort of Turkish patients with familial hypercholesterolemia. *Anatol. J. Cardiol.* **2017**, *18*(4) doi: 10.14744/AnatolJCardiol.2017.7654
32. Poirier, S.; Hamouda, H. A.; Villeneuve, L.; Demers, A.; Mayer, G. Trafficking dynamics of PCSK9-induced LDLR degradation: focus on human PCSK9 mutations and C-terminal domain. *PLoS One* **2016**, *11*(6), e0157230. doi: 10.1371/journal.pone.0157230
33. Eroğlu, Z.; Tetik Vardarlı, A.; Düzgün, Z.; Gündüz, C.; Bozok Çetintaş, V.; Kayıkçıoğlu, M. Case-control study on PCSK9 R496W (rs374603772) and D374Y (rs137852912) mutations in Turkish patients with primary dyslipidemia. *Anatol. J. Cardiol.* **2018**, *19*(5), 334–340. doi: 10.14744/AnatolJCardiol.2018.86648
34. Benjannet, S.; Rhinds, D.; Hamelin, J.; Nassoury, N.; Seidah, N. G. The proprotein convertase (PC) PCSK9 is inactivated by furin and/or PC5/6A: functional consequences of natural mutations and post-translational modifications. *J. Biol. Chem.* **2006**, *281*(41), 30561–30572. doi: 10.1074/jbc.M606495200
35. Cohen, J. C.; Boerwinkle, E.; Mosley, T. H. Jr.; Hobbs, H. H. Sequence variations in PCSK9, low LDL, and protection against coronary heart disease. *N. Engl. J. Med.* **2006**, *354*(12), 1264–1272. doi: 10.1056/NEJMoa054013
36. Glerup, S.; Schulz, R.; Laufs, U.; Schlüter, K. D. Physiological and therapeutic regulation of PCSK9 activity in cardiovascular disease. *Basic Res. Cardiol.* **2017**, *112*(3), 32. doi: 10.1007/s00395-017-0619-0
37. Shyamala, N.; Gundapaneni, K. K.; Galimudi, R. K.; Tupurani, M. A.; Padala, C.; Puranam, K.; Kupsal, K.; Kummari, R.; Gantala, S. R.; Nallamala, K. R.; Sahu, S. K.; Hanumanth, S. R. PCSK9 genetic (rs11591147) and epigenetic (DNA methylation) modifications associated with PCSK9

## **Chapter 4**

expression and serum proteins in CAD patients. *J. Gene Med.* **2021**, 23(8), e3346. doi: 10.1002/jgm.3346

38. Benn, M.; Tybjaerg-Hansen, A.; Nordestgaard, B. G. Low LDL cholesterol by PCSK9 variation reduces cardiovascular mortality. *J. Am. Coll. Cardiol.* **2019**, 73(24), 3102–3114. doi: 10.1016/j.jacc.2019.03.517

39. Langsted, A.; Nordestgaard, B. G.; Benn, M.; Tybjaerg-Hansen, A.; Kamstrup, P. R. PCSK9 R46L loss-of-function mutation reduces lipoprotein(a), LDL cholesterol, and risk of aortic valve stenosis. *J. Clin. Endocrinol. Metab.* **2016**, 101(9), 3281–3287. doi: 10.1210/jc.2016-1206

40. Bayona, A.; Arrieta, F.; Rodríguez-Jiménez, C.; Cerrato, F.; Rodríguez-Nóvoa, S.; Fernández-Lucas, M.; Gómez-Coronado, D.; Mata, P. Loss-of-function mutation of PCSK9 as a protective factor in the clinical expression of familial hypercholesterolemia: a case report. *Medicine* **2020**, 99(34), e21754. doi: 10.1097/MD.00000000000021754

41. Holla, Ø. L.; Laerdahl, J. K.; Strøm, T. B.; Tveten, K.; Cameron, J.; Berge, K. E.; Leren, T. P. Removal of acidic residues of the prodomain of PCSK9 increases its activity towards the LDL receptor. *Biochem. Biophys. Res. Commun.* **2011**, 406(2), 234–238. doi: 10.1016/j.bbrc.2011.02.023

42. Fan, D.; Yancey, P. G.; Qiu, S.; Ding, L.; Weeber, E. J.; Linton, M. F.; Fazio, S. Self-association of human PCSK9 correlates with its LDLR-degrading activity. *Biochemistry* **2008**, 47(6), 1631-9. doi: 10.1021/bi7016359

43. Ouguerram, K.; Chetiveaux, M.; Zair, Y.; Costet, P.; Abifadel, M.; Varret, M.; Boileau, C.; Magot, T.; Krempf, M. Apolipoprotein B100 metabolism in autosomal-dominant hypercholesterolemia related to mutations in PCSK9. *Arterioscler. Thromb. Vasc. Biol.* **2004**, 24(8), 1448–1453. doi: 10.1161/01.ATV.0000133684.77013.88

44. Norata, G. D.; Garlaschelli, K.; Grigore, L.; Raselli, S.; Tramontana, S.; Meneghetti, F.; Artali, R.; Noto, D.; Cefalù, A. B.; Buccianti, G.; Averna, M.; Catapano, A. L. Effects of PCSK9 variants on common carotid artery intima media thickness and relation to ApoE alleles. *Atherosclerosis* **2010**, 208(1), 177–182. doi: 10.1016/j.atherosclerosis.2009.06.023

45. Ferreira, J. P.; Xhaard, C.; Lamiral, Z.; Borges-Canha, M.; Neves, J. S.; Dandine-Roulland, C.; LeFloch, E.; Deleuze, J. F.; Bacq-Daian, D.; Bozec, E.; Girerd, N.; Boivin, J. M.; Zannad, F.; Rossignol, P. PCSK9 Protein and rs562556 polymorphism are associated with arterial plaques in healthy middle-aged population: the STANISLAS cohort. *J. Am. Heart Assoc.* **2020**, 9(7), e014758. doi: 10.1161/JAHA.119.014758

46. Lallanne, F.; Lambert, G.; Amar, M. J.; Chétiveaux, M.; Zaïr, Y.; Jarnoux, A. L.; Ouguerram, K.; Friburg, J.; Seidah, N. G.; Brewer, H. B.; Jr, Krempf, M.; Costet, P. Wild-type PCSK9 inhibits LDL clearance but does not affect ApoB-containing lipoprotein production in mouse and cultured cells. *Lipid Res.* **2005**, 46(6), 1312–1319. doi: 10.1194/jlr.M400396-JLR200

47. Cameron, J.; Holla, O. L.; Laerdahl, J. K.; Kulseth, M. A.; Ranheim, T.; Rognes, T.; Berge, K. E.; Leren, T. P. Characterization of novel mutations in the catalytic domain of the PCSK9 gene. *J. Intern. Med.* **2008**, 263(4), 420–431. doi: 10.1111/j.1365-2796.2007.01915.x

48. Shapiro, M. D.; Fazio, S. PCSK9 and atherosclerosis - lipids and beyond. *J. Atheroscler. Thromb.* **2017**, 24(5), 462–472. doi: 10.5551/jat.RV17003

49. Abifadel, M.; Varret, M.; Rabès, J. P.; Allard, D.; Ouguerram, K.; Devillers, M.; Cruaud, C.; Benjannet, S.; Wickham, L.; Erlich, D.; Derré, A.; Villéger, L.; Farnier, M.; Beucler, I.; Bruckert, E.; Chambaz, J.; Chanu, B.; Lecerf, J. M.; Luc, G.; Moulin, P.; Boileau, C. Mutations in PCSK9 cause autosomal dominant hypercholesterolemia. *Nat. Genet.* **2003**, *34*(2), 154–156. doi: 10.1038/ng1161
50. Kathiresan, S. A PCSK9 missense variant associated with a reduced risk of early-onset myocardial infarction. *N. Engl. J. Med.* **2008**, *358*(21), 2299–2300. doi: 10.1056/NEJMc0707445
51. Lagace, T. A. PCSK9 and LDLR degradation: regulatory mechanisms in circulation and in cells. *Curr. Opin. Lipidol.* **2014**, *25*(5), 387–393. doi: 10.1097/MOL.0000000000000114
52. Springer, T. A. An extracellular beta-propeller module predicted in lipoprotein and scavenger receptors, tyrosine kinases, epidermal growth factor precursor, and extracellular matrix components. *J. Mol. Biol.* **1998**, *283*(4), 837–62 doi; 10.1006/jmbi.1998.2115
53. Jeon, H.; Meng, W.; Takagi, J.; Eck, M. J.; Springer, T. A.; Blacklow, S. C. Implications for familial hypercholesterolemia from the structure of the LDL receptor YWTD-EGF domain pair. *Nat. Struct. Biol.* **2001**, *8*(6), 499–504. doi: 10.1038/88556
54. Rudenko, G.; Henry, L.; Henderson, K.; Ichtchenko, K.; Brown, M. S.; Goldstein, J. L.; Deisenhofer, J. Structure of the LDL receptor extracellular domain at endosomal pH. *Science* **2002**, *298*(5602), 2353–2358. doi: 10.1126/science.1078124
55. Brown, M. S.; Goldstein, J. L. A receptor-mediated pathway for cholesterol homeostasis. *Science* **1986**, *232*(4746), 34–47. doi: 10.1126/science.3513311
56. Guo, S.; Xia, X. D.; Gu, H. M.; Zhang, D. W. Proprotein convertase subtilisin/kexin-type 9 and lipid metabolism. *Adv. Exp. Med. Biol.* **2020**, *1276*, 137–156. doi: 10.1007/978-981-15-6082-8\_9
57. Wang, Y.; Huang, Y.; Hobbs, H. H.; Cohen, J. C. Molecular characterization of proprotein convertase subtilisin/kexin type 9-mediated degradation of the LDLR. *J. Lipid Res.* **2012**, *53*(9), 1932–1943. doi: 10.1194/jlr.M028563
58. Romagnuolo, R.; Scipione, C. A.; Boffa, M. B.; Marcovina, S. M.; Seidah, N. G.; Koschinsky, M. L. Lipoprotein(a) catabolism is regulated by proprotein convertase subtilisin/kexin type 9 through the low density lipoprotein receptor. *J. Biol. Chem.* **2015**, *290*(18), 11649–11662. doi: 10.1074/jbc.M114.611988
59. Nassoury, N.; Blasiolo, D. A.; Tebon Oler, A.; Benjannet, S.; Hamelin, J.; Poupon, V.; McPherson, P. S.; Attie, A. D.; Prat, A.; Seidah, N. G. The cellular trafficking of the secretory proprotein convertase PCSK9 and its dependence on the LDLR. *Traffic* **2007**, *8*(6), 718–732. doi: 10.1111/j.1600-0854.2007.00562.x
60. Jang, H. D.; Lee, S. E.; Yang, J.; Lee, H. C.; Shin, D.; Lee, H.; Lee, J.; Jin, S.; Kim, S.; Lee, S. J.; You, J.; Park, H. W.; Nam, K. Y.; Lee, S. H.; Park, S. W.; Kim, J. S.; Kim, S. Y.; Kwon, Y. W.; Kwak, S. H.; Yang, H. M.; Kim, H. S. Cyclase-associated protein 1 is a binding partner of proprotein convertase subtilisin/kexin type-9 and is required for the degradation of low-density lipoprotein receptors by proprotein convertase subtilisin/kexin type-9. *Eur. Heart J.* **2020**, *41*(2), 239–252. doi: 10.1093/eurheartj/ehz566
61. Davis, C. G.; Goldstein, J. L.; Südhof, T. C.; Anderson, R. G.; Russell, D. W.; Brown, M. S. Acid-dependent ligand dissociation and recycling of LDL receptor mediated by growth factor homology region. *Nature* **1987**, *326*(6115), 760–765. doi: 10.1038/326760a0

## **Chapter 4**

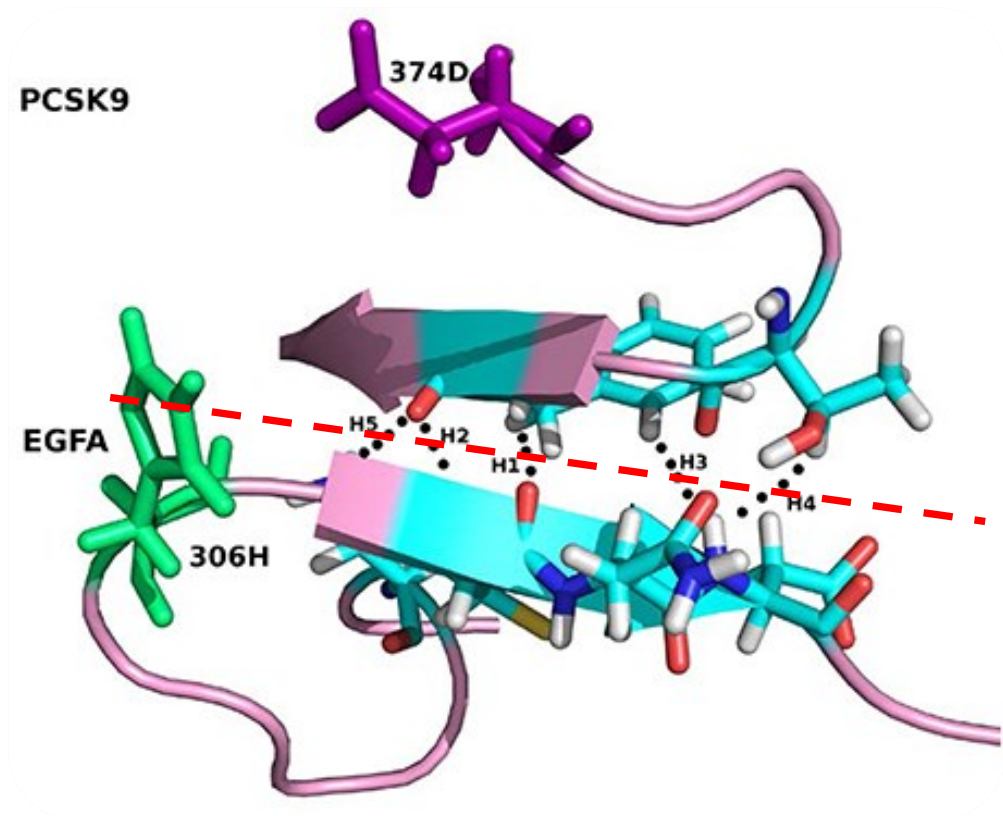
62. Cunningham, D.; Danley, D. E.; Geoghegan, K. F.; Griffor, M. C.; Hawkins, J. L.; Subashi, T. A.; Varghese, A. H.; Ammirati, M. J.; Culp, J. S.; Hoth, L. R.; Mansour, M. N.; McGrath, K. M.; Seddon, A. P.; Shenolikar, S.; Stutzman-Engwall, K. J.; Warren, L. C.; Xia, D.; Qiu, X. Structural and biophysical studies of PCSK9 and its mutants linked to familial hypercholesterolemia. *Nat. Struct. Mol. Biol.* **2007**, *14*(5), 413–419. doi: 10.1038/nsmb1235
63. Zhang, D. W.; Lagace, T. A.; Garuti, R.; Zhao, Z.; McDonald, M.; Horton, J. D.; Cohen, J. C.; Hobbs, H. H. Binding of proprotein convertase subtilisin/kexin type 9 to epidermal growth factor-like repeat A of low density lipoprotein receptor decreases receptor recycling and increases degradation. *J. Biol. Chem.* **2007**, *282*(25), 18602–18612. doi: 10.1074/jbc.M702027200
64. Leren, T. P. Sorting an LDL receptor with bound PCSK9 to intracellular degradation. *Atherosclerosis* **2014**, *237*(1), 76–81. doi: 10.1016/j.atherosclerosis.2014.08.038
65. Strøm, T. B.; Tveten, K.; Leren, T. P. PCSK9 acts as a chaperone for the LDL receptor in the endoplasmic reticulum. *Biochem.* *457*(1), **2014**, 99–105. doi: 10.1042/BJ20130930
66. Mbikay, M.; Sirois, F.; Simoes, S.; Mayne, J.; Chrétien, M. Quercetin-3-glucoside increases low-density lipoprotein receptor (LDLR) expression, attenuates proprotein convertase subtilisin/kexin 9 (PCSK9) secretion, and stimulates LDL uptake by Huh7 human hepatocytes in culture. *FEBS Open Bio* **2014**, *4*, 755–762. doi: 10.1016/j.fob.2014.08.003
67. Panahi, Y.; Ahmadi, Y.; Teymouri, M.; Johnston, T. P.; Sahebkar, A. Curcumin as a potential candidate for treating hyperlipidemia: A review of cellular and metabolic mechanisms. *J. Cell. Physiol.* **2018**, *233*(1), 141–152. doi: 10.1002/jcp.25756
68. Wang, Y.; Ye, J.; Li, J.; Chen, C.; Huang, J.; Liu, P.; Huang, H. Polydatin ameliorates lipid and glucose metabolism in type 2 diabetes mellitus by downregulating proprotein convertase subtilisin/kexin type 9 (PCSK9). *Cardiovasc. Diabetol.* **2016**, *15*, 19. doi: 10.1186/s12933-015-0325-x
69. Chen, H. C.; Chen, P. Y.; Wu, M. J.; Tai, M. H.; Yen, J. H. Tanshinone IIA modulates low density lipoprotein uptake via down-regulation of PCSK9 gene expression in HepG2 cells. *PLoS One* **2016**, *11*(9), e0162414. doi: 10.1371/journal.pone.0162414
70. Bang, S.; Chae, H. S.; Lee, C.; Choi, H. G.; Ryu, J.; Li, W.; Lee, H.; Jeong, G. S.; Chin, Y. W.; Shim, S. H. New aromatic compounds from the fruiting body of *Sparassis crispa* (Wulf.) and their inhibitory activities on proprotein convertase subtilisin/kexin type 9 mRNA expression. *J. Agric. Food Chem.* **2017**, *65*(30), 6152–6157. doi: 10.1021/acs.jafc.7b02657
71. Li, H.; Dong, B.; Park, S. W.; Lee, H. S.; Chen, W.; Liu, J. Hepatocyte nuclear factor 1alpha plays a critical role in PCSK9 gene transcription and regulation by the natural hypocholesterolemic compound berberine. *J. Biol. Chem.* **2009**, *284*(42), 28885–28895. doi: 10.1074/jbc.M109.052407
72. Dong, B.; Wu, M.; Li, H.; Kraemer, F. B.; Adeli, K.; Seidah, N. G.; Park, S. W.; Liu, J. Strong induction of PCSK9 gene expression through HNF1alpha and SREBP2: mechanism for the resistance to LDL-cholesterol lowering effect of statins in dyslipidemic hamsters. *J. Lipid Res.* **2010**, *51*(6), 1486–1495. doi: 10.1194/jlr.M003566
73. Lindholm, M. W.; Elmén, J.; Fisker, N.; Hansen, H. F.; Persson, R.; Møller, M. R.; Rosenbohm, C.; Ørum, H.; Straarup, E. M.; Koch, T. PCSK9 LNA antisense oligonucleotides induce sustained reduction of LDL cholesterol in nonhuman primates. *Mol. Ther.* **2012**, *20*(2), 376–381. doi: 10.1038/mt.2011.260

74. Fitzgerald, K.; Frank-Kamenetsky, M.; Shulga-Morskaya, S.; Liebow, A.; Bettencourt, B. R.; Sutherland, J. E.; Hutabarat, R. M.; Clausen, V. A.; Karsten, V.; Cehelsky, J.; Nochur, S. V.; Kotelianski, V.; Horton, J.; Mant, T.; Chiesa, J.; Ritter, J.; Munisamy, M.; Vaishnav, A. K.; Gollob, J. A.; Simon, A. Effect of an RNA interference drug on the synthesis of proprotein convertase subtilisin/kexin type 9 (PCSK9) and the concentration of serum LDL cholesterol in healthy volunteers: a randomised, single-blind, placebo-controlled, phase 1 trial. *Lancet* **2014**, *383*(9911), 60–68. doi: 10.1016/S0140-6736(13)61914-5
75. Kosmas, C. E.; DeJesus, E.; Morcelo, R.; Garcia, F.; Montan, P. D.; Guzman, E. Lipid-lowering interventions targeting proprotein convertase subtilisin/kexin type 9 (PCSK9): an emerging chapter in lipid-lowering therapy. *Drugs Context* **2017**, *6*, 212511. doi: 10.7573/dic.212511
76. Nair, J. K.; Willoughby, J. L.; Chan, A.; Charisse, K.; Alam, M. R.; Wang, Q.; Hoekstra, M.; Kandasamy, P.; Kell'in, A. V.; Milstein, S.; Taneja, N.; O'Shea, J.; Shaikh, S.; Zhang, L.; van der Sluis, R. J.; Jung, M. E.; Akinc, A.; Hutabarat, R.; Kuchimanchi, S.; Fitzgerald, K.; Manoharan, M. Multivalent *N*-acetylgalactosamine-conjugated siRNA localizes in hepatocytes and elicits robust RNAi-mediated gene silencing. *J. Am. Chem. Soc.* **2014**, *136*(49), 16958–16961. doi: 10.1021/ja505986a
77. Ray, K. K.; Stoekenbroek, R. M.; Kallend, D.; Leiter, L. A.; Landmesser, U.; Wright, R. S.; Wijngaard, P.; Kastelein, J. Effect of an siRNA therapeutic targeting PCSK9 on atherogenic lipoproteins: prespecified secondary end points in ORION 1. *Circulation* **2018**, *138*(13), 1304–1316. doi: 10.1161/CIRCULATIONAHA.118.034710
78. Gustafsen, C.; Olsen, D.; Vilstrup, J.; Lund, S.; Reinhardt, A.; Wellner, N.; Larsen, T.; Andersen, C.; Weyer, K.; Li, J. P.; Seeberger, P. H.; Thirup, S.; Madsen, P.; Glerup, S. Heparan sulfate proteoglycans present PCSK9 to the LDL receptor. *Nat. Commun.* **2017**, *8*(1), 503. doi: 10.1038/s41467-017-00568-7
79. Ding, Q.; Strong, A.; Patel, K. M.; Ng, S. L.; Gosis, B. S.; Regan, S. N.; Cowan, C. A.; Rader, D. J.; Musunuru, K. Permanent alteration of PCSK9 with in vivo CRISPR-Cas9 genome editing. *Circ. Res.* **2014**, *115*(5), 488–492. doi: 10.1161/CIRCRESAHA.115.304351
80. Wang, X.; Raghavan, A.; Chen, T.; Qiao, L.; Zhang, Y.; Ding, Q.; Musunuru, K. CRISPR-Cas9 targeting of PCSK9 in human hepatocytes in vivo—brief report. *Arterioscler. Thromb. Vasc. Biol.* **2016**, *36*(5), 783–786. doi: 10.1161/ATVBAHA.116.307227
81. Thakore, P. I.; Kwon, J. B.; Nelson, C. E.; Rouse, D. C.; Gemberling, M. P.; Oliver, M. L.; Gersbach, C. A. RNA-guided transcriptional silencing in vivo with *S. aureus* CRISPR-Cas9 repressors. *Nat. Commun.* **2018**, *9*(1), 1674. doi: 10.1038/s41467-018-04048-4
82. Pan, Y.; Zhou, Y.; Wu, H.; Chen, X.; Hu, X.; Zhang, H.; Zhou, Z.; Qiu, Z.; Liao, Y. Therapeutic peptide vaccine against PCSK9. *Sci. Rep.* **2017**, *7*(1), 12534. doi: 10.1038/s41598-017-13069-w
83. Galabova, G.; Brunner, S.; Winsauer, G.; Juno, C.; Wanko, B.; Mairhofer, A.; Lührs, P.; Schneeberger, A.; von Bonin, A.; Mattner, F.; Schmidt, W.; Staffler, G. Peptide-based anti-PCSK9 vaccines—an approach for long-term LDLc management. *PLoS One* **2014**, *9*(12), e114469. doi: 10.1371/journal.pone.0114469
84. Landlinger, C.; Pouwer, M. G.; Juno, C.; van der Hoorn, J.; Pieterman, E. J.; Jukema, J. W.; Staffler, G.; Princen, H.; Galabova, G. The AT04A vaccine against proprotein convertase subtilisin/kexin type 9 reduces total cholesterol, vascular inflammation, and atherosclerosis in APOE\*3Leiden.CETP mice. *Eur. Heart J.* **2017**, *38*(32), 2499–2507. doi: 10.1093/eurheartj/ehx260



# Chapter 5

## Development of PCSK9/LDLR Inhibitors





## 5.1 Background

The identification of orally bioavailable PCSK9/LDLR inhibitors represents a valid strategy for the treatment of dyslipidemias.<sup>1</sup> The development of these inhibitors has long been hindered by the poor “druggability” of this target. Indeed, it was difficult to identify the “hot spot” residues that contributed the most to the binding energy between the two proteins, since the interaction zone involved is quite large (about 500 Å), exposed to the solvent and relatively flattened.<sup>2,3</sup> In addition, as for all protein-protein interactions, pockets or grooves suitable for ligand binding are lacking,<sup>4,5</sup> and in general molecular design, drug discovery and development in this field is still a great challenge.<sup>6,7</sup>

PCSK9/LDLR protein-protein interaction (PPI) has been studied based on detailed analysis of crystal structures.<sup>8-10</sup> The interface of PCSK9 consists of a series of hydrophobic amino acid residues centered on Phe379 and surrounded by several polar residues (Figure 5.1).

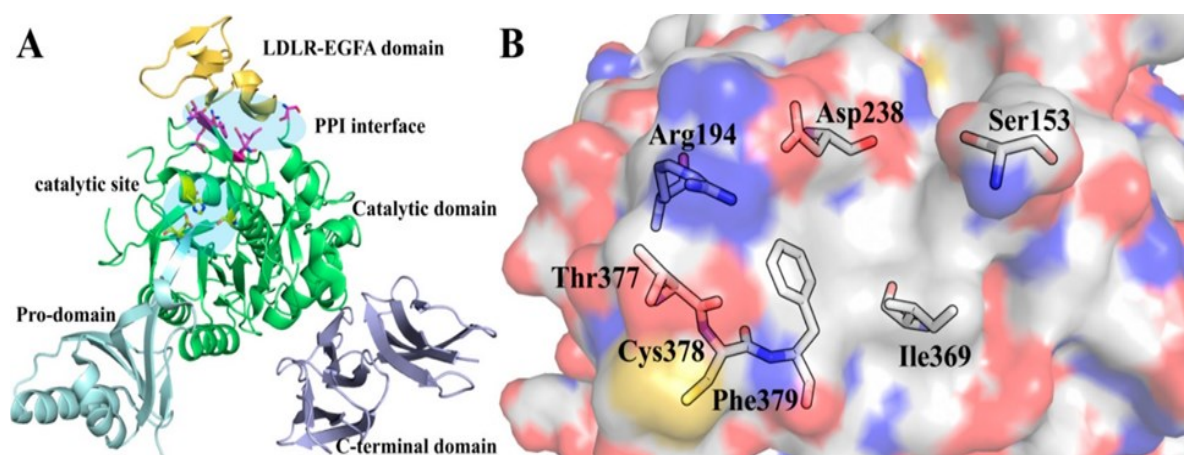


**Figure 5.1** (A) 3D structure model of PCSK9-LDLR complex (PDB ID: 3BPS); (B) Hot spots on PCSK9 surface involved in PCSK9-LDLR PPI<sup>11</sup>.

The direct interactions between PCSK9 and LDLR includes an antiparallel  $\beta$ -sheet-like contact unit, involving residues 377-379 of PCSK9, and 308-310 residues of LDLR-EGF-A domains. In addition, interaction with LDLR-EGF-A domains also requires crucial hydrogen bonds with Ser153, Arg194, and Asp238 residues, as well as hydrophobic interactions with Ile369, Cys378, and Phe379 of the protein partner PCSK9.

## Chapter 5

Currently, only few PCSK9-LDLR inhibitors have been reported in literature including small peptides, peptidomimetics and small molecules.

Among mimetic peptides, short amino acid sequences have been described mimicking domains engaged in PCSK9-LDLR interactions, such as the LDLR-EGF-A domain, the PCSK9 catalytic domain, and the PCSK9 C-terminal domain, including:

- Pep2-8 (Figure 5.2), an optimized short linear peptide (13 residues), identified by screening phage-displayed peptide libraries; this peptide shows potent PCSK9-LDLR PPI inhibitory activity, high PCSK9 binding affinity and promotes restoration of absorption of LDL. As revealed by the X-ray crystal structure of Pep2-8 linked to a truncated C-term form of PCSK9, the peptide adopts a filament-turn-helix conformation, mimicking the secondary structural elements of the EGF-A domain. Indeed, the contact region of Pep2-8 largely overlaps the one contacted by the LDLR EGF-A domain. Therefore, Pep2-8 can be regarded as a competitive inhibitor;<sup>12</sup>
- lupine P5 peptide (Figure 5.2), which inhibits PCSK9-LDLR interaction with IC<sub>50</sub> value of 1.6 μM;<sup>13</sup>
- Cpd7 (Figure 5.2), an *N*-methylimidazole derivative, that was designed starting from the observation that the contact region of PCSK9 and the EGF-A domain of LDLR consists of β strands. This compound consists of multiple C2'-C5'-linked imidazole rings mimicking β-sheet structural motif; it is able to induce a concentration-dependent interruption of the PCSK9-LDLR interaction with an IC<sub>50</sub> value of 11.2 ± 0.2 μM, as well as to increase LDL uptake in HepG2 cells (EC<sub>50</sub> = 6.04 μM);<sup>14</sup>
- MESFPGWNLV(hR)IGLLR peptide (with hR being a homo-arginine residue), a 16-aa linear peptide antagonist of PCSK9 activity, which arose from the discovery by Zhang *et al.* of an *N*-terminal groove in PCSK9, near the PCSK9/EGF-A contact region. This peptide inhibits PCSK9 binding to EGF-A in the TR-FRET assay with an IC<sub>50</sub> value of

8.3  $\mu\text{M}$ , and achieves pharmacologic restoration of LDLR in HepG2 cells by 70% at 75  $\mu\text{M}$ .<sup>15</sup>

- LDL-1dlnr (Figure 5.2), a peptidomimetic compound with PCSK9 micromolar binding affinity, which is able to disrupt the targeted PPI, and increase LDL uptake from the extracellular medium.<sup>16</sup>

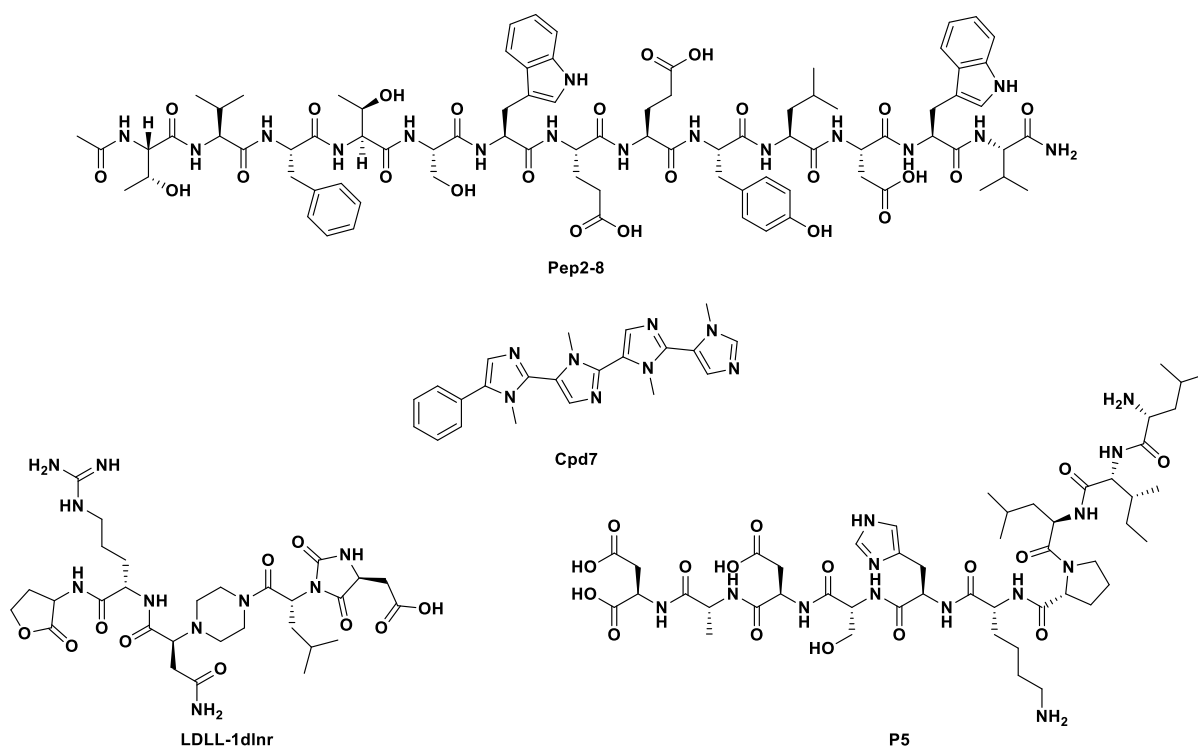


**Figure 5.2** Chemical structures of some reported peptide and peptidomimetic PCSK9 inhibitors.

These examples demonstrate that PCSK9-LDLR PPI can be addressed effectively. In addition, synthetic peptide/peptidomimetic procedures are easier and cheaper than that of mAbs. However, the main drawback is their route of administration; this limit could be bypassed by small molecules, and actually several companies are competing to develop orally available small molecule inhibitors against PCSK9. A number of small molecules have been disclosed in patent applications, but detailed investigations into their mechanism of action are often lacking.<sup>17</sup>

## Chapter 5

Notably, compounds SBC-115,076 and SBC-110,424 (Figure 5.3), which were discovered by PPI surface modeling and virtual high-throughput screening, have been reported as PCSK9 inhibitors and have shown lipid-lowering effects in cell and animal model tests. However, the evidence supporting the direct binding of these compounds to PCSK9 still awaits confirmation, as well as the lack of extensive animal model testing to demonstrate proof of concept, efficacy and safety.<sup>18,19</sup>

Srx Cardio employed a back-scattering interferometry-based assay to evaluate the direct binding to recombinant human PCSK9 for a series of small molecules; among tested compounds, Srx200 (Figure 5.3) showed a  $K_D$  of  $24 \text{ nM} \pm 8 \text{ nM}$ . Interestingly, this result was not confirmed by the DiI-LDL uptake test in HepG2 cells. Indeed, it resulted to be an activator rather than an inhibitor of PCSK9. In the same test the strictly analogue Srx75 (Figure 5.3) reached more than 100% inhibition at  $100 \mu\text{M}$ , suggesting that subtle differences determine if the compound behaves either as an agonist or antagonist.<sup>20</sup>

CB\_36 (Figure 5.3) was found to be a modulator of PCSK9-LDLR interaction *in vitro*. However, additional evidence of its mechanism of action i.e. whether this compound binds to PCSK9 directly, whether its effects are mediated by PCSK9 in a specific-manner, has not been provided.<sup>21</sup>

Rim13 (Figure 5.3), is a tetraimidazole derivative, which turned out to be an inhibitor on the PCSK9-LDLR binding and showed a significant cholesterol-lowering effect on HepG2 cells.<sup>22</sup>

Compound 3f (Figure 5.3) is an analogue of nilotinib; it exhibited PPI disrupting efficacy at nanomolar levels *in vitro*, without inhibitory activity against a panel of tyrosine kinases. However, its binding mode is still to be elucidated experimentally.<sup>23-25</sup>

Recently, Nyrada *et al.* reported a small molecule, NYX-330, able to block the interaction between PCSK9 and LDLR. However, no data has yet been reported and the structure of the compound has not been disclosed.<sup>26</sup>

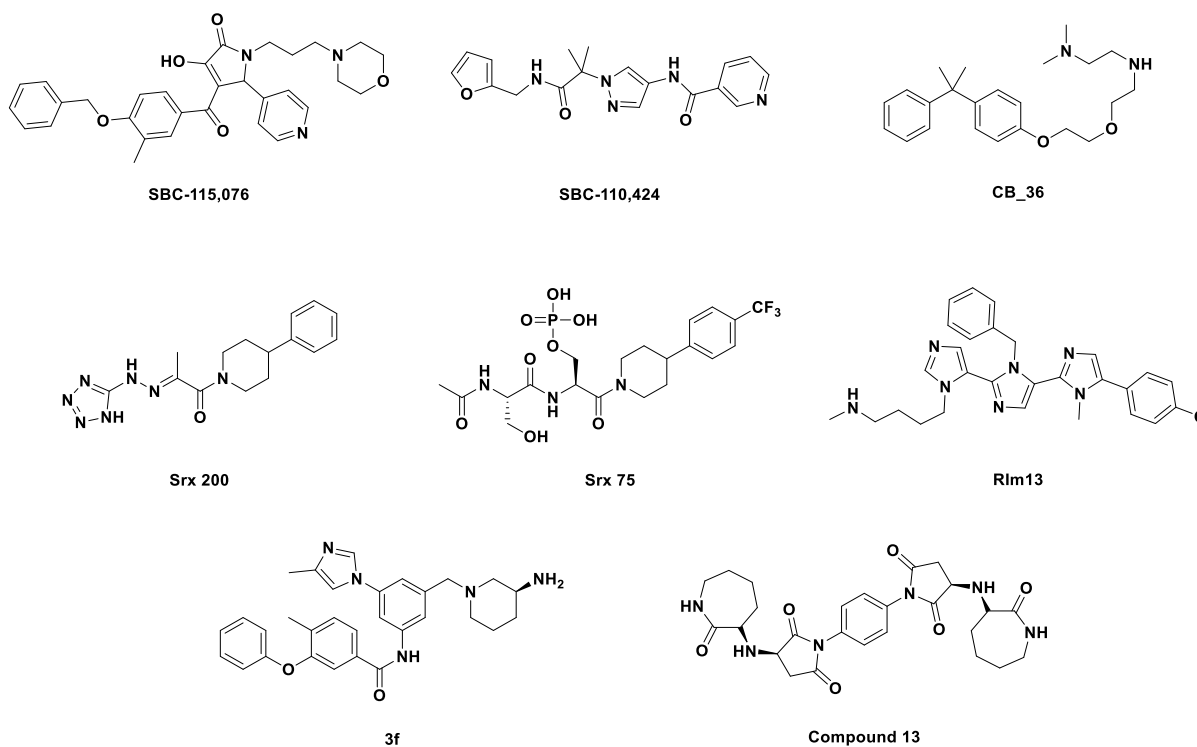


**Figure 5.3** Representative small molecules inhibitors of PCSK9-LDLR PPI.

Finally, Sun *et al.* identified a potential binding pocket on the PCSK9-LDLR PPI interface of PCSK9, which was generated by the induced docking of SBC-115.076. This induced binding pocket was subsequently used for virtual screening to identify novel PCSK9-LDLR PPI small molecule inhibitors. Among the selected compounds, compound 13 (Figure 5.3) showed potent and dose-dependent inhibitory activity against the PCSK9-LDLR interaction in the ELISA test ( $IC_{50} = 7.57 \pm 1.40 \mu M$ ). Furthermore, the results of the cellular study showed that compound 13 could restore to some extent LDL uptake of PCSK9-treated HepG2 cells<sup>11</sup>.

## 5.2 Aim of the work

As a part of my PhD project, I also focused on the development of small molecule inhibitors of the PCSK9/LDLR interaction to mimic the critical residues of LDLR that contribute most to the binding energy with its protein partner PCSK9 (Tables 5.1-5.3).

## Chapter 5

In particular, two series of substituted pyrroles were rationally designed through molecular docking studies, using the crystallographic structure of the peptide Pep2-8 linked to PCSK9 (PDB code: 4NMX) as a reference (Figure 5.4).

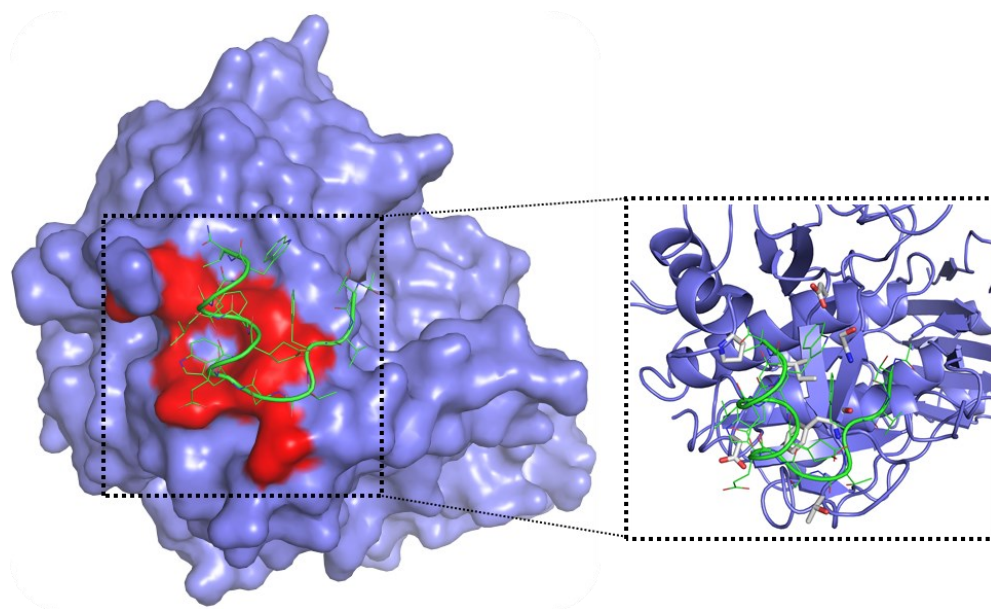


**Figure 5.4** *Crystal structure of the Pep2-8/PCSK9 complex (PDB ID: 4NMX).*

The crystal structure of the peptide inhibitor Pep2-8 bound to PCSK9 at 1.85 Å resolution showed that the peptide adopts a strand-turn-helix conformation.<sup>12</sup> The Pep2-8 contact region on PCSK9 largely overlapped with that contacted by the EGF-A domain of the LDL receptor.

Starting from the structural information available, we examined the PCSK9 site involved in Pep2-8 binding, and envisioned that putative PCSK9 inhibitors could exploit (Figure 5.5):

- a) a hydrophobic pocket sized by Ile369 and Phe379;
- b) at least two negatively charged area, the first one close to Asp367 and Ser381 and the second one close to Asp238 and Thr377.

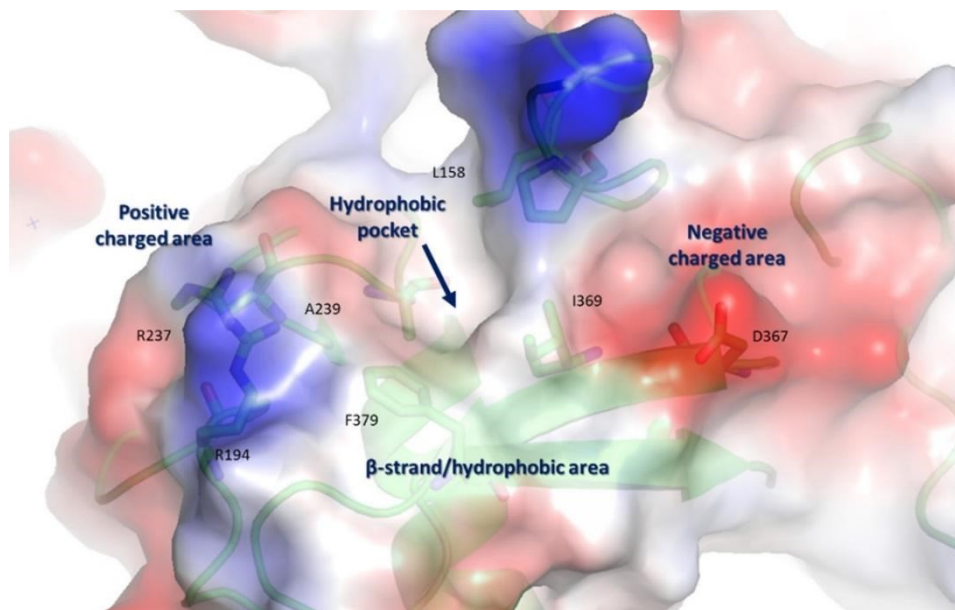


**Figure 5.5** Overview of PCSK9 site involved in the LDLR recognition (adapted from Lammi et al.).<sup>22</sup>

Taking into account this structural information, a small set of compounds was rationally designed starting from the selected scaffolds (Figure 5.6), able to confer a beta turn secondary structure, and bearing different substituents at R2 and R3 (Series I) or R3 (Series II) positions that could show the highest structural complementarity with the biological counterpart and would interact with PCSK9 residues responsible for Pep2-8 binding. Furthermore, a bulky and hydrophobic group was inserted at position R1 (Series I) or R2 (Series II), in order to fill the hydrophobic pocket lined by Ile369 and Phe379 (Tables 5.1-5.3).

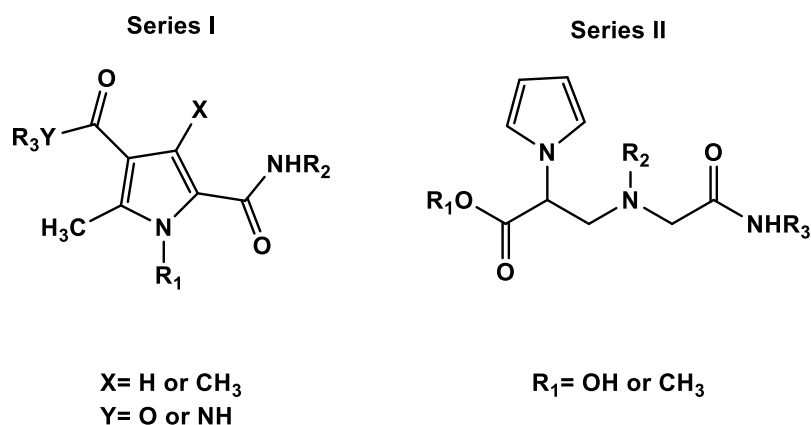


**Figure 5.6** Selected pyrrole scaffolds.

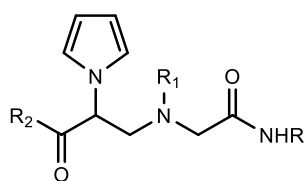
Table 5.1

Cpd	R	R <sub>1</sub>
44a		
44b		
44c		
44d		
44e		
44f		
44g		
44h		
44i		
44j		
44k		
44l		

Table 5.2

Cpd	R	R <sub>1</sub>	
	<b>45a</b>		OCH <sub>2</sub> CH <sub>3</sub>
	<b>45b</b>		OCH <sub>2</sub> CH <sub>3</sub>
	<b>45c</b>		OCH <sub>2</sub> CH <sub>3</sub>
	<b>45d</b>		OH
	<b>45e</b>		OH
	<b>45f</b>		OH
	<b>45g</b>		
	<b>45h</b>		

Table 5.3

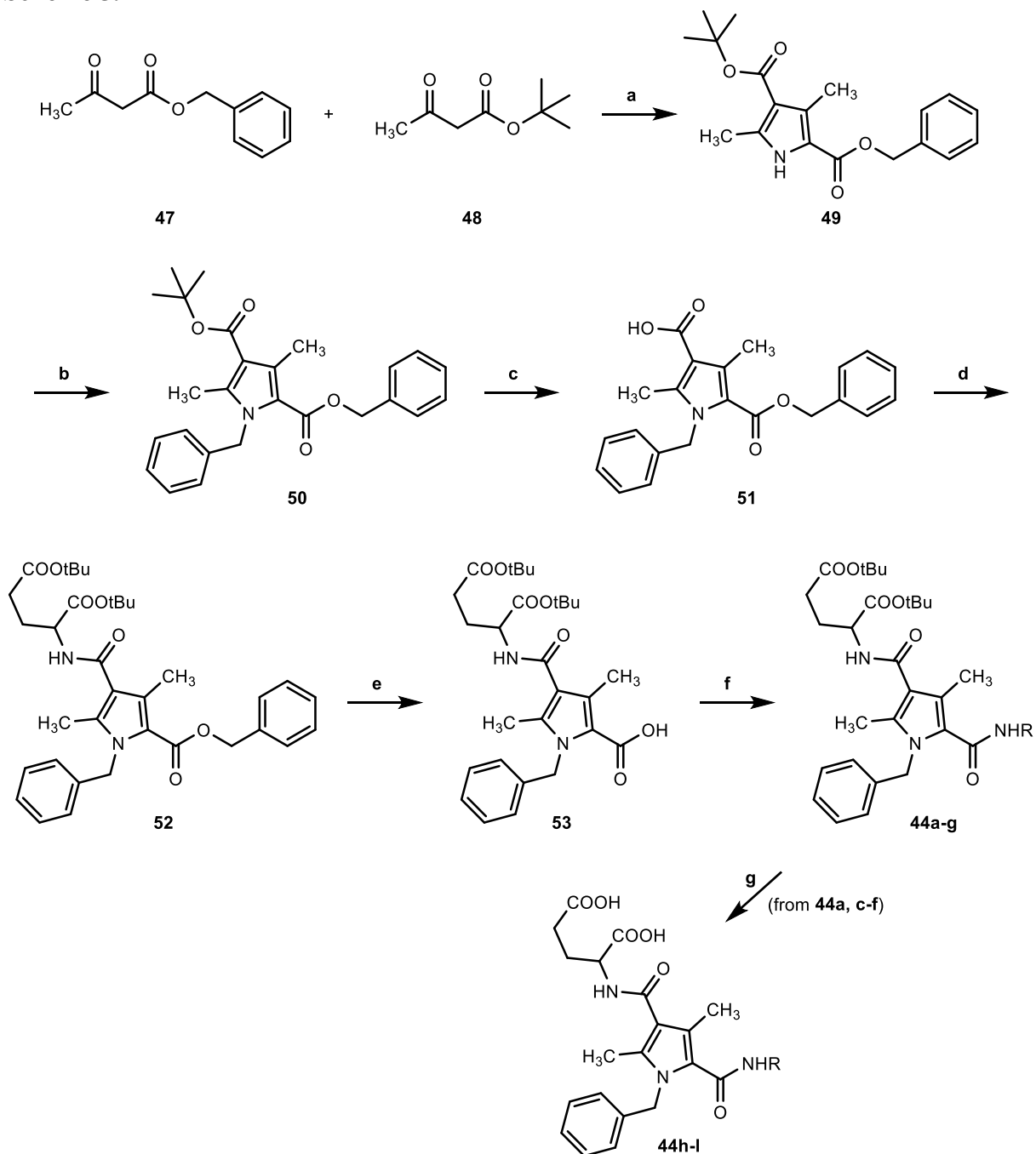


Cpd	R	R <sub>1</sub>	R <sub>2</sub>
46a			OCH <sub>3</sub>
46b			OCH <sub>3</sub>
46c			OCH <sub>3</sub>
46d			OCH <sub>3</sub>
46e			OH

### 5.3 Synthesis

In Schemes 5.1-5.4 the synthesis of final compounds **44a-l**, **45a-h** and **46a-e** is described. The intermediate **49** was obtained by a modified Paal-Knoor reaction between benzyl acetoacetate **47** and *t*-butyl acetoacetate **48** in the presence of NaNO<sub>2</sub> and Zn dust (Scheme 5.1).<sup>27</sup> The pyrrole derivative **49** was *N*-benzylated with benzyl bromide, using a biphasic system (DCM/NaOH 50%), and TBAH (tetrabutylammonium hydroxide) as a phase transfer catalysts. Then, the ester **50** was selectively deprotected in acidic medium (TFA), and the resulting acid **51** was coupled with L-Glu(OtBu)-OtBu HCl to give the amide **52**, which in turn was hydrogenated in the presence of ammonium formate and Pd/C as a catalyst to afford the acid **53**. The latter was coupled with appropriate amine using OxymaPure<sup>®</sup> (2-cyano-2-(hydroxyimino)acetate) and EDAC (3-[(ethylimino)methylidene]amino}-*N,N*-dimethylpropan-1-amine) as coupling reagents, and DIPEA (*N,N*-diisopropylethylamine) as a base to give amides **44a-g**. Compounds **44a**, **c-f** render corresponding acids **44h-l** after *tert*-butyl group cleavage in the presence of TFA (Scheme 5.1).

Scheme 5.1



**Reagents and conditions:** a)  $NaNO_2$ ,  $CH_3COONH_4$ , Zn dust,  $CH_3COOH$ ,  $10^\circ C$  to rt, 12h, then  $70^\circ C$  to  $95^\circ C$ , 4h; b) benzyl bromide, NaOH 50% w/v in  $H_2O$ , TBAH, DCM, rt, 12h; c) TFA, DCM, rt, 0.5h; d) *H-Glu(OtBu)-OtBu*, EDAC, OxymaPure<sup>®</sup>, DIPEA, DMF, rt, 15h; e) Pd/C,  $HCOONH_4$ , dry  $CH_3OH$ , reflux, 2h; f) appropriate amine  $RNH_2$ , EDAC, OxymaPure<sup>®</sup>, DIPEA, DMF, rt, 15h; g) TFA, DCM, rt, 1h.

The synthesis of the pyrrole derivative **60** was accomplished in five steps (Scheme 5.2). Briefly, ( $\pm$ ) serine benzyl ester HCl **54** was reacted with tosyl chloride to afford the sulfonamide **55**, that was converted to dehydro derivative **56** by treatment with  $(Boc)_2O$  (di-*tert*-butyl

## Chapter 5

dicarbonate) in the presence of DMAP (4-dimethylaminopyridine). The intermediate **56** was condensed with ethylacetoacetate **57** in the presence of Cs<sub>2</sub>CO<sub>3</sub> followed by reaction with TFA to provide the pyrrole derivative **58**, that was *N*-benzylated using the same reaction conditions reported for **50**. The resulting ester **59** was hydrogenated with ammonium formate and Pd/C as a catalyst to give the acid **60** in good yield. Hereafter, acid **60**, after activation via acyl chloride, was coupled with appropriate amine to furnish the amides **45a-c**. Subsequent hydrolysis of **45a-c** with NaOH furnished the acids **45d-f**. Compound **45d** was coupled with L-Glu(OtBu)-OtBu HCl to give amide **45g**, that after (Boc)<sub>2</sub>O cleavage furnished **45h**.

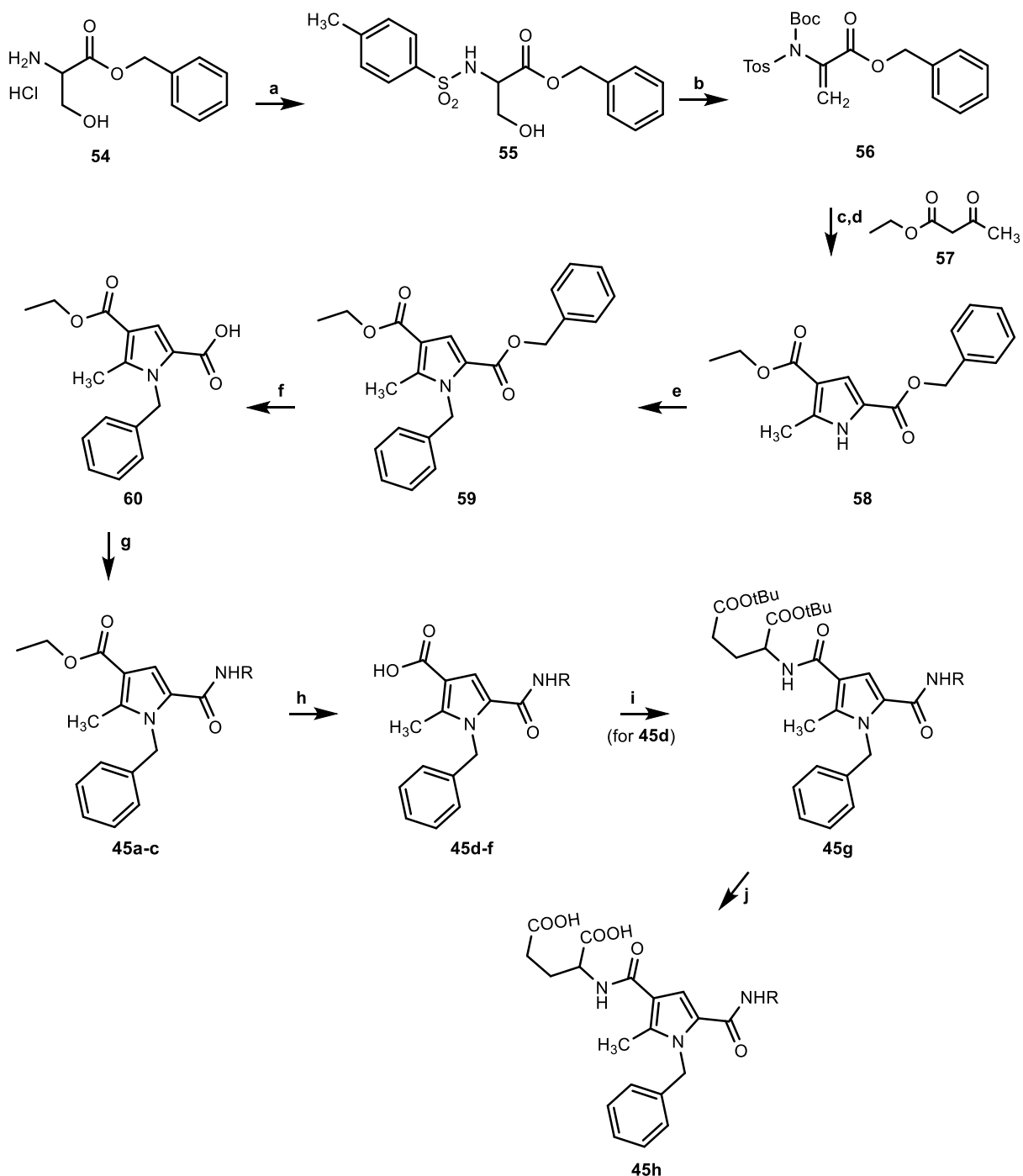
In Scheme 5.3 is described the synthesis of compounds **46a-c**. (±) Serine methyl ester HCl **61** was used as starting material to furnish by Clauson-Kaas reaction the pyrrole derivative **62**, which was converted to its dehydro analogue **63** by reaction with (Boc)<sub>2</sub>O and DMAP (Scheme 5.3, A). Then compound **63** provided amines **66a,b** by aza-Michael addition with benzylamine **64** and glycine benzyl ester **65** respectively, in solvent free conditions at 90°C. Then, pyrrole derivative **66a** was *N*-alkylated with *t*-butyl bromoacetate to give **67**, that after hydrolysis with TFA furnished the corresponding acid **68**. The latter was coupled with appropriate amine using HOBT, HBTU as coupling reagents and DIPEA as a base to give **46a-c** (Scheme 5.3, B).

In Scheme 5.3 is also reported the synthesis of **65**. Glycine HCl **69** was *N*-Boc protected by reaction with (Boc)<sub>2</sub>O and TEA to provide **70**, which in turn was reacted with benzyl bromide in the presence of Cs<sub>2</sub>CO<sub>3</sub> to obtain **71** that rendered **65** after Boc removal with TFA (Scheme 5.4, B).

Finally, the synthesis of compounds **46d,e** was realized as depicted in Schemes 5.4. The intermediate **66b** was *N*-acylated with chloroacetyl chloride to provide **72**. Subsequent nucleophilic substitution of **72** with *N*-Boc-piperazine afforded **73**, that underwent to hydrogenation by ammonium formate and Pd/C as a catalyst to achieve the corresponding acid

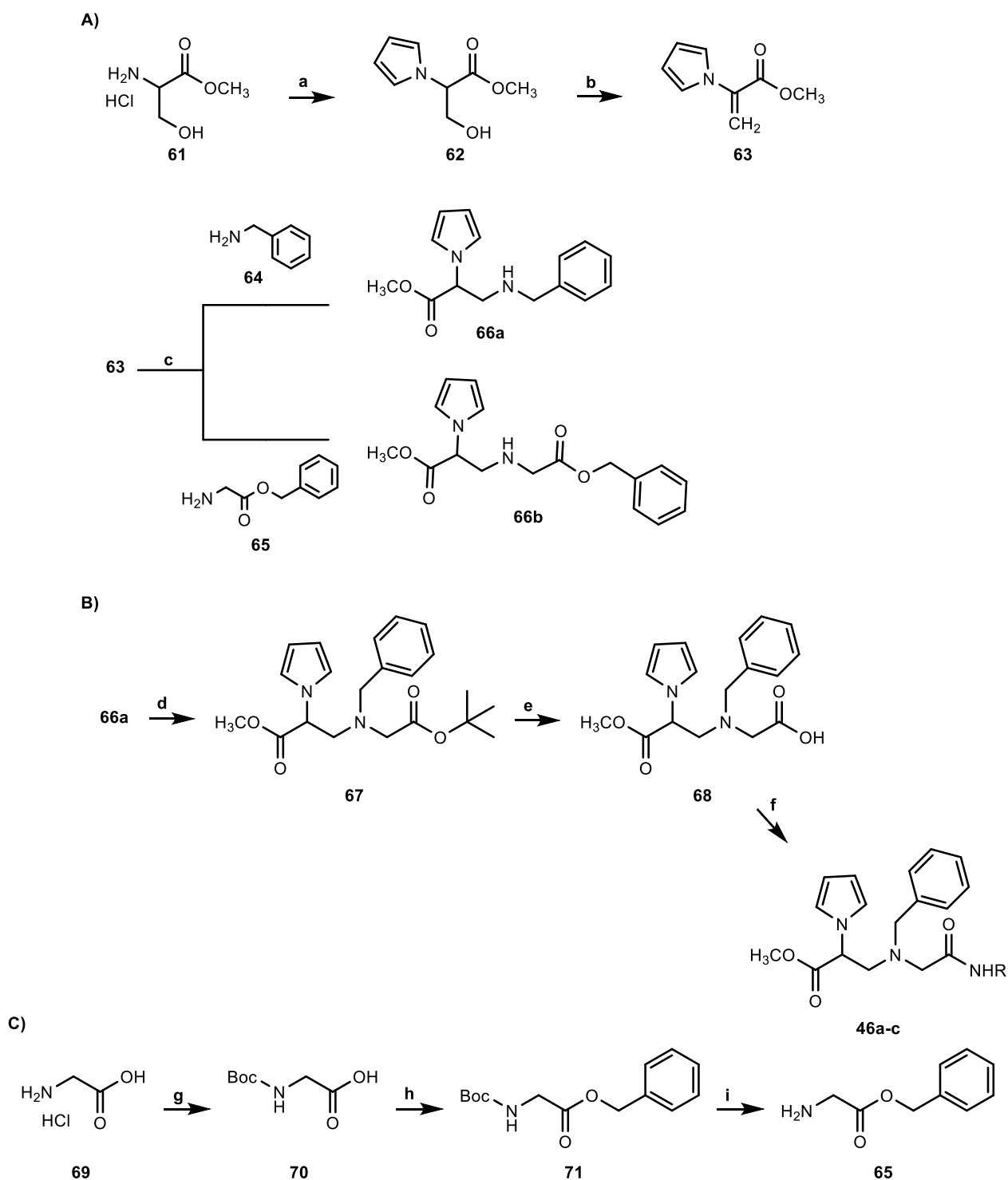
74. The latter was coupled with 4-fluorophenylethylamine to give **46d**, which was hydrolyzed by NaOH to provide **46e** (Scheme 5.4).

Scheme 5.2



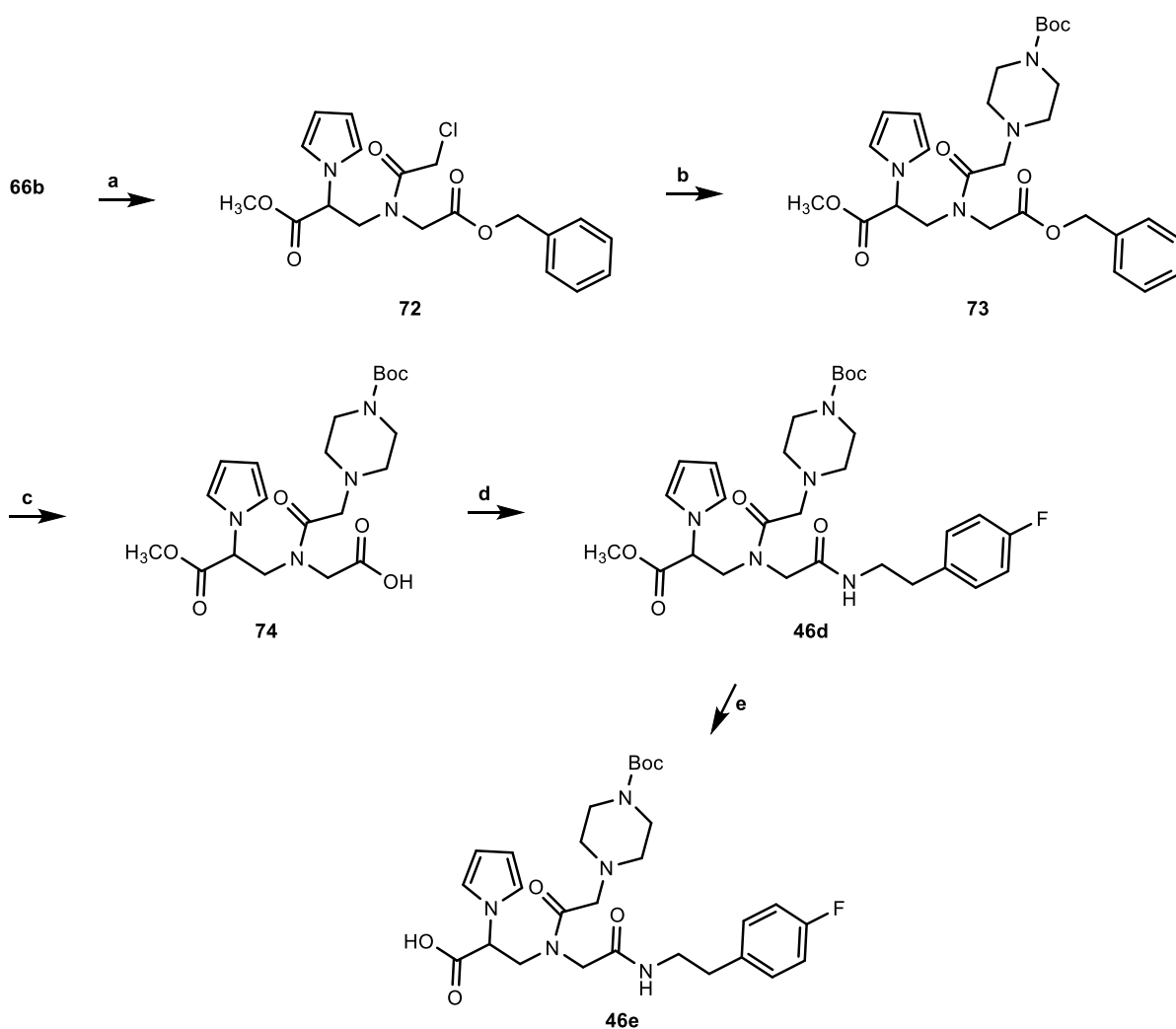
**Reagents and conditions:** a) Tosyl chloride, DCM, TEA, from 0°C to rt, overnight; b) (Boc)<sub>2</sub>O, DMAP, CH<sub>3</sub>CN, rt, 3h; c) Cs<sub>2</sub>CO<sub>3</sub>, dry CH<sub>3</sub>CN, rt, overnight; d) TFA, DCM, rt, 12h; e) benzyl bromide, NaOH 50% w/v in H<sub>2</sub>O, TBAH, DCM, rt, 12h; f) Pd/C, HCOONH<sub>4</sub>, dry CH<sub>3</sub>CH<sub>2</sub>OH, reflux, 0.5h; g) SOCl<sub>2</sub>, dry DCM, dry TEA, appropriate amine RNH<sub>2</sub>, reflux, 3h; h) NaOH 50% w/v in H<sub>2</sub>O, CH<sub>3</sub>CH<sub>2</sub>OH, reflux, 24-48h; i) SOCl<sub>2</sub>, dry DCM, dry TEA, H-Glu(OtBu)-OtBu, reflux, 3h; j) TFA, DCM, rt, 2h.

## Scheme 5.3



**Reagents and conditions:** a) 2,5-dimethoxytetrahydrofuran,  $\text{CH}_3\text{COONa}$ ,  $\text{H}_2\text{O}/\text{DCM}$  (1:2), overnight; b)  $(\text{Boc})_2\text{O}$ , DMAP, dry  $\text{CH}_3\text{CN}$ , rt, 6h; c) solvent free,  $95^\circ\text{C}$ , 5h; d) tert-butyl bromoacetate,  $\text{K}_2\text{CO}_3$ , dry  $\text{CH}_3\text{CN}$ ,  $60^\circ\text{C}$ , 5h then rt, 12h; e) TFA, DCM, rt, 0.5h; f) appropriate amine, DMF, HOBT, HBTU, DIPEA, rt, overnight; g)  $(\text{Boc})_2\text{O}$ , TEA, dioxane/ $\text{H}_2\text{O}$  (1:1), rt, 16h; h)  $\text{Cs}_2\text{CO}_3$ ,  $\text{CH}_3\text{CN}$ , benzyl bromide, rt, 16h; i) TFA, DCM, rt, 1h.

Scheme 5.4



**Reagents and conditions:** (a)  $\text{ClCH}_2\text{COCl}$ , dry TEA, dry DCM, rt, 1.5 h; (b) *N*-Boc-piperazine, TEA,  $\text{CH}_3\text{CN}$ , rt, 1.5h; (c) Pd/C,  $\text{HCOONH}_4$ , dry  $\text{CH}_3\text{OH}$ , reflux, 2.5h; (d) *p*-F( $\text{C}_6\text{H}_4$ ) $\text{CH}_2\text{CH}_2\text{NH}_2$ , HOBT, HBTU, DIPEA, DMF, rt, overnight; (e) 4N NaOH, MeOH, rt, 1.5h

## Chapter 5

### 5.4 Biological evaluation

#### 5.4.1 SPR binding assay

A small set of synthesized derivatives (**44e,f,h-l** and **45h**) was evaluated by Surface Plasmon Resonance (SPR) binding assay to assess their affinity with PCSK9.<sup>28</sup> SPR analysis showed that among tested compounds, **44f** and **45h** efficiently interacted with the immobilized target with  $K_D$  values of  $0.459\pm 0.039$  and  $0.633\pm 0.058$  respectively. Their binding affinity was also greater than that of Pep2-8 ( $K_D = 3.993\pm 0.016$ ), which in turn was consistent with the previously reported value in the literature.<sup>11</sup>

These preliminary results highlight that **44f** and **45h** are promising hits for further *in vitro* studies (e.g. Elisa assay, BODIPY-LDL uptake assay), to confirm their ability to inhibit PCSK9/LDLR interaction. At the same time, these results offer interesting insights for development of new putative PCSK9/LDLR inhibitors. Indeed, it has been demonstrated that *in vitro* wild-type PCSK9 binds LDLR with an approximately 150-fold higher affinity at an acidic endosomal pH ( $K_D = 4.19$  nm) compared with a neutral pH ( $K_D = 628$  nm).<sup>29</sup>

Thus, a putative PCSK9/LDLR inhibitor must be stable at acidic pH, i.e. when the affinity between PCSK9 and its protein partner is higher. Since *tert*-butyl ester is an acid-labile group, compound **44f** will be probably inactive or poorly active in cell based assays as it can easily generate the inactive acid **44i** in acidic endosomal environment. However, this issue could be easily addressed from a synthetic point of view, generating acid stable analogues of **44f**. On the other hand, compound **45h**, which showed a  $K_D$  value comparable to that of **44f**, has an unfavorable pharmacokinetic profile, with a predicted apparent Caco-2 cell permeability value (QPPCaco) of 2.247 nm/sec. (Table 5.4). On the contrary, its *tert*-butyl ester **45g** (not tested yet) has a more favorable QPPCaco value of 967.142 nm/sec. Thus, if Elisa assay will confirm the inhibitory activity of **45h**, compound **45g** can be referred as a precursor of active **45h**. Then,

regardless of whether its binding affinity evaluated by SPR and Elisa assays, compound **45g** should be in all cases evaluated in cell based assay to better assess its inhibitory activity.

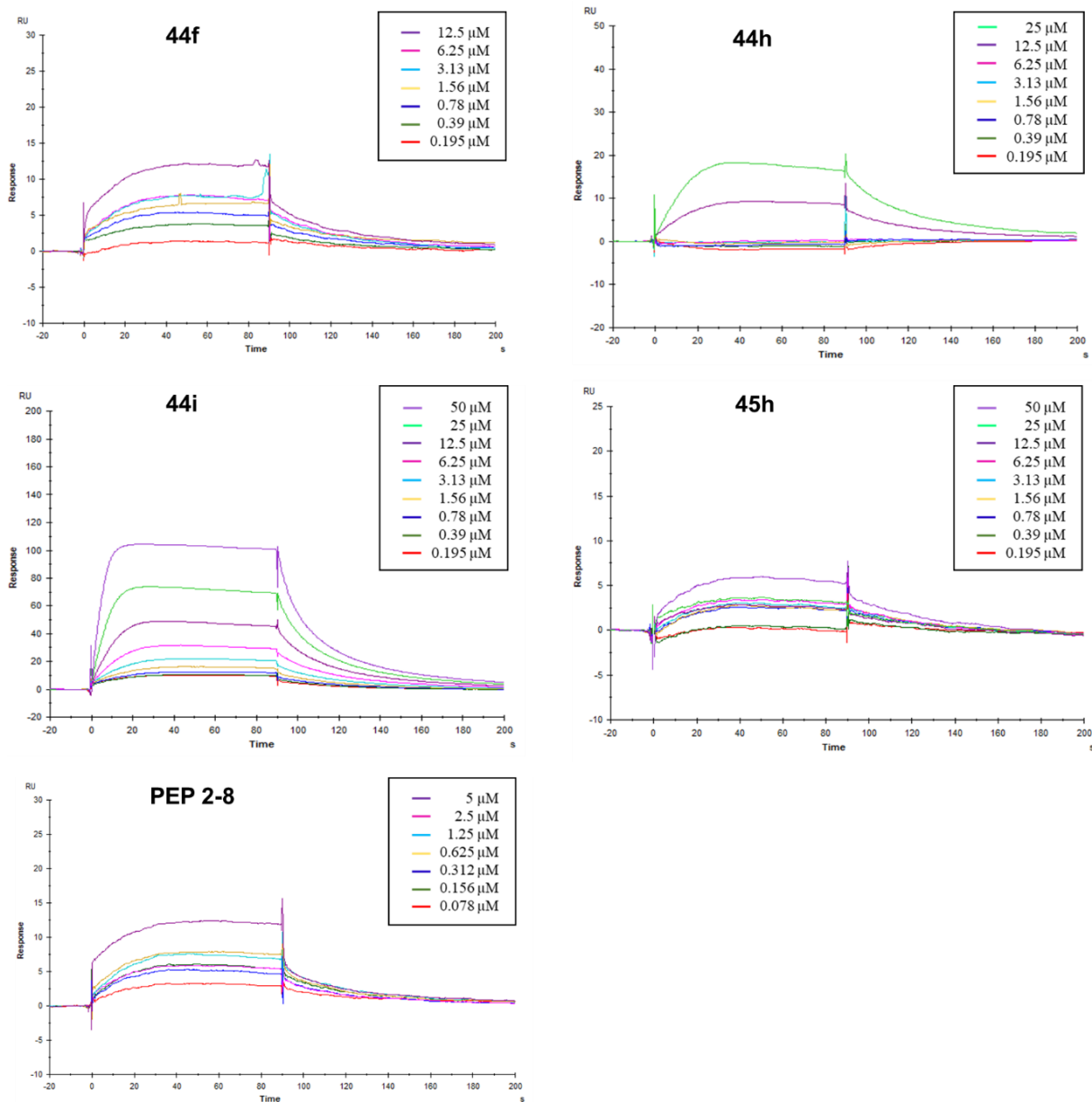
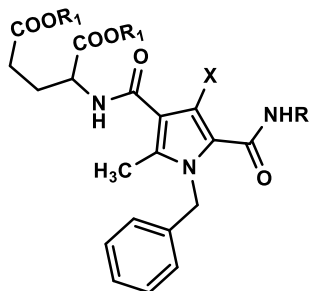


**Figure 5.7** SPR sensorgrams for compounds **44f,h,i**, **45h** and **Pep2-8**. The equilibrium dissociation constants ( $K_D$ ) were obtained from two independent SPR tests from the ratio between kinetic dissociation ( $k_{off}$ ) and association ( $k_{on}$ ) constant.

Table 5.4



Cpd	R	R <sub>1</sub>	X	K <sub>D</sub> (μM)	QPlogP o/w <sup>a</sup>	QPlogS <sup>b</sup>	QPPCaco <sup>c</sup>
44e		t-Bu	CH <sub>3</sub>	NA	8.147	-10.214	706.450
44f		t-Bu	CH <sub>3</sub>	0.459 ±0.039	7.088	-8.541	631.053
44h		H	CH <sub>3</sub>	121.400 ±1.384	4.945	-6.490	2.799
44i		H	CH <sub>3</sub>	98.720 ±0.883	1.307	-3.873	254
44j		H	CH <sub>3</sub>	NA	3.486	-5.454	433
44k		H	CH <sub>3</sub>	NA	4.898	-6.157	2.862
44l		H	CH <sub>3</sub>	NA	3.957	-4.697	2.107
45g		t-Bu	H	ND	7.568	-9.249	967.142
45h		H	H	0.633 ±0.058	4.589	-6.129	2.247
Pep2-8	-	-	-	3.993 ±0.016	ND	ND	ND

a) *QPlogPo/w* = Predicted octanol / water partition coefficient; recommended values -2.0–6.5; b) *QPlogS* = Predicted aqueous solubility, log *S*; recommended values -6.5–0.5; c) *QPPCaco* = Predicted apparent Caco-2 cell permeability in nm/sec; recommended values <25 poor, >500 great. NA= not active; ND= not determined.

## 5.5 Molecular docking studies

Docking studies were performed using the Schrödinger Glide algorithm (Glide, Schrödinger, LLC, New York, NY, 2021) at the SP (Standard Precision) accuracy, and the GlideScore function was used to rank the compounds.

Compound **44f**, displaying the most favorable  $K_D$  value in SPR assays, binds within a cleft comprised between a negatively charged area, shaped by the side chain of D367, and a hydrophobic pocket shaped by I369 and F379 (Figure 5.8, A). These areas are of great interest for structure-based design of PCSK9 inhibitors, as previously reported in literature.<sup>22</sup>

Compound **44f** was anchored by two strong H bonds between the ligand's carbonyl groups and the NH backbone of S153 (Figure 5.8, A). Moreover, the carbonyl group of the *N*-(2-(benzo[d][1,3]dioxol-5-yl)ethyl)carbamoyl branch formed another H-bond with the NH backbone of W156 whose side chain, in turn, engaged in hydrophobic interactions with the ligand benzylic group.

Several hydrophobic interactions between the *tert*-butyl group and I369, F379, P155 additionally stabilized the complex. In particular, F379 has been reported to be critical for EGF-A binding.<sup>8</sup> It is worth noting that **44f** explores an area that overlaps to a certain degree with the EGF-A domain of the LDLR (Figure 5.8, D), and thus possibly interfering with the binding of PCSK9.

Notably, the corresponding acid derivative of **44f**, **44i**, turned out to be unable to bind PCSK9 in SPR assays. The overlay of **44f** and **44i** docked poses revealed that the presence of the two ester functions, protecting the terminal glutamate residue in **44f**, greatly influenced the ligand binding mode (Figure 5.8, B). In fact, only the *N*-(2-(benzo[d][1,3]dioxol-5-yl)ethyl)carbamoyl branch in **44i** maintained an orientation similar to **44f**, whereas the side chain of the free glutamate residue was mostly solvent-exposed, thereby losing the favorable hydrophobic interactions with the key residue F379. Moreover, the benzylic moiety assumed a flipped

## Chapter 5

conformation with respect to **44f**. Thus, the presence of the two *tert*-butyl moieties likely contributes to the increased potency due to entropic factors, by locking the molecule into a highly favorable conformation for interaction with the binding site.

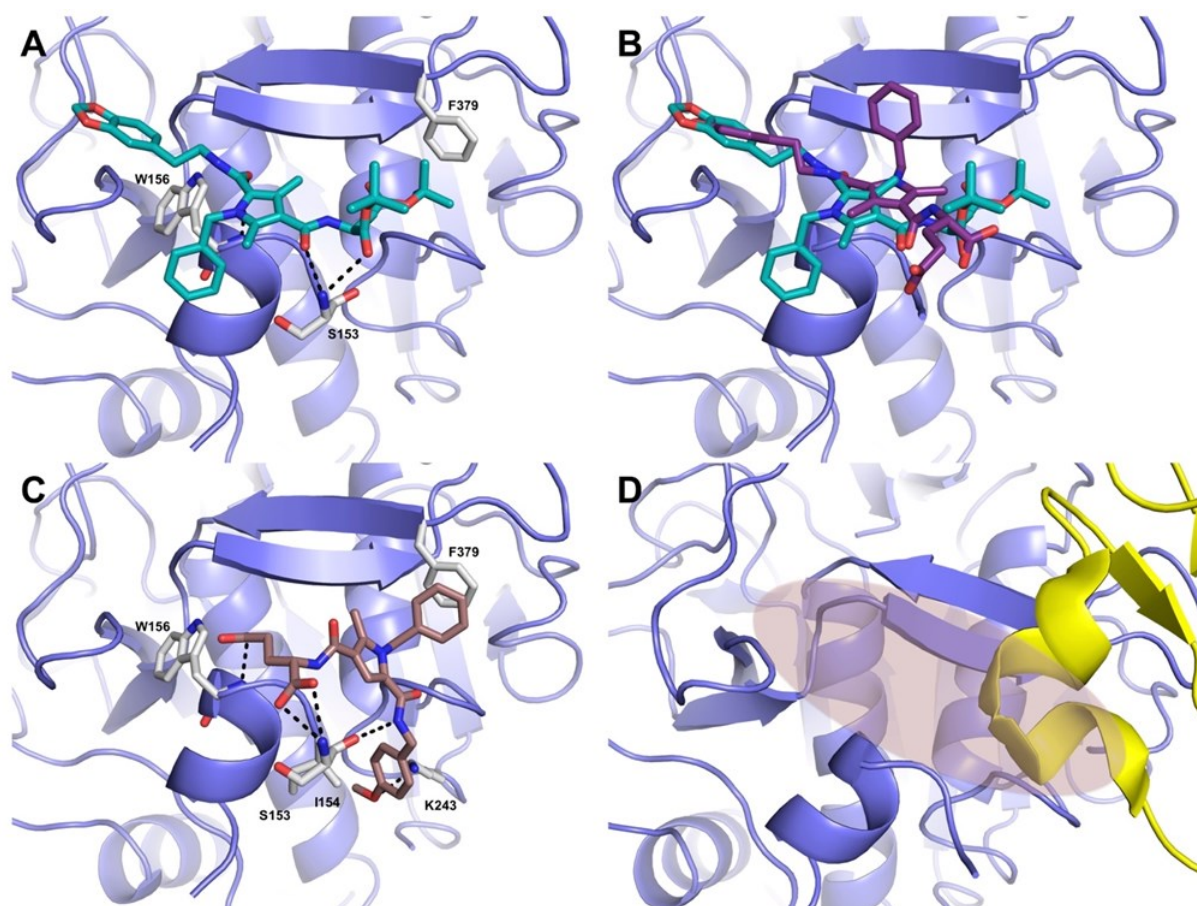


**Figure 5.8** A) Theoretical binding mode of compound **44f** into PCSK9 (PDB: 4NMX). The ligand is represented as teal sticks, while the protein is represented as slate ribbon model. Interacting residues are displayed as white sticks and labeled. H-bonds are depicted as dashed black lines. B) Overlay of **44f** and **44l** (purple sticks) docked poses. C) Theoretical binding mode of compound **45h** (dark salmon sticks). D) The area occupied by the docked poses of our derivatives partially overlaps with the EGF-A domain of LDLR (represented as yellow cartoon, PDB: 3GCX).

On the contrary, **45h**, bearing the free glutamate acid moieties, displayed a low micromolar  $K_D$  toward PCSK9. The predicted binding mode of **45h** showed that the shorter 4-methoxybenzylcarbamoyl group could be lodged in a small channel between I154 and K243, with this latter interacting with the 4-methoxy group (Figure 5.8, C). The benzyl moiety formed a strong  $\pi$ -stacking interaction with the side chain of F379, whereas S153 formed multiple interactions with the NH group of the 4-methoxybenzylcarbamoyl moiety as well as the

glutamate carboxylate group (Figure 5.8, C). In addition, the glutamate acidic side chain formed an H-bond with the NH backbone of W156. Therefore, a shorter and less bulky substituent on the carbamoyl branch and the absence of the methyl group at position 4 of the pyrrole core might induce a ligand conformation more favorably interacting with the binding site.

A different trend could instead be observed for the less potent inhibitors **44h** and **44i**. Both compounds displayed higher  $K_D$  values towards PCSK9 in SPR experiments (121 and 98  $\mu\text{M}$ , respectively), suggesting that they might interact with PCSK9 in a similar fashion. Docking simulations revealed that **44i** was able to engage D367 through its flexible Lys substituent, whereas the two carboxylic moieties were inserted into the pocket lined by K243, with this latter strongly interacting with the glutamate carboxylate group (Figure 5.9, A). As regards **44h**, the dimethoxybenzyl substituent formed an H-bond with the NH backbone of W156; again, the glutamate carboxylate group interacted with K243 side chain. For both ligands, the pyrrole core was positioned favorably to form  $\pi$ -stacking interactions with the side chain of F379 through the benzyl substituent (Figure 5.9, B).

These findings confirm that the enhancement in potency, observed in particular for **44f**, is largely entropically driven in nature, because additional polar direct interactions with the protein, as observed for **44h** and **44i**, apparently do not improve overall binding, indicating the direction for further structural optimization. A similar conclusion has been drawn also in a recent work reporting potent bi- and tricyclic PCSK9 inhibitor peptides.<sup>30</sup> The X-ray structures of PCSK9 in complex with some representative inhibitors revealed no significant direct interaction with the protein.<sup>30</sup> Another recent paper found out that some of the H-bonds initially observed between the inhibitor and the protein were not much stable during molecular dynamics simulations, instead W156 and F379 made great contributions to the binding.<sup>11</sup>

Further computationally demanding studies to rationalize the binding mode of this series of compounds are underway, and results will be reported in due course.

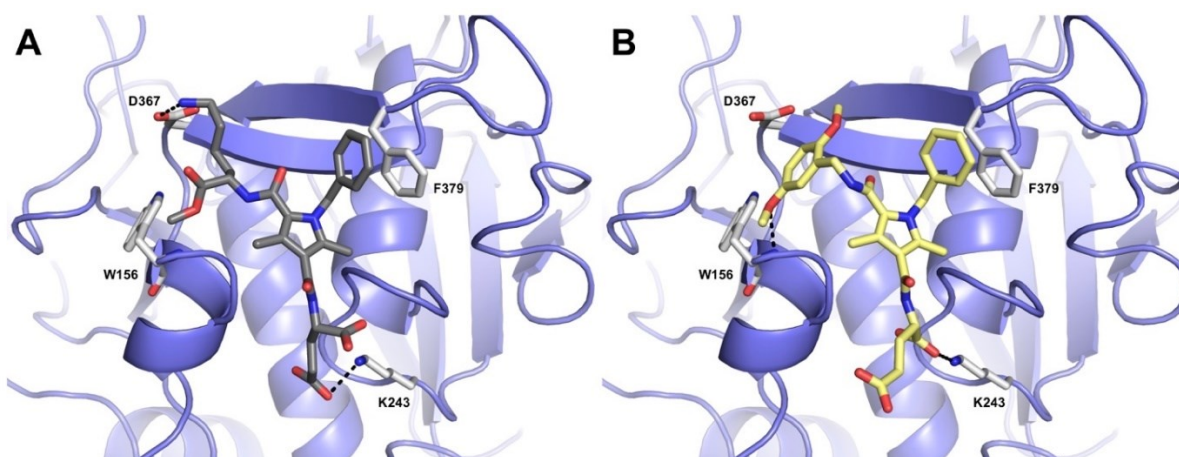


**Figure 5.9** Theoretical binding mode of compound **44i** (A, grey sticks) and **44h** (B, light yellow sticks) into PCSK9 (PDB: 4NMX), represented as slate ribbon model. Interacting residues are displayed as white sticks and labeled. H-bonds are depicted as dashed black lines.

## 5.6 Experimental section

### 5.6.1 General

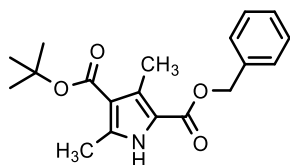
Starting materials and solvents were purchased from commercial suppliers and used without further purification. Reaction progress was monitored by TLC using silica gel 60 F254 (0.040–0.063 mm) with detection by UV. Silica gel 60 (0.040–0.063 mm) was used for column chromatography.  $^1\text{H}$  and  $^{13}\text{C}$  NMR spectra were recorded at 400 and 101 MHz, respectively, using a Bruker Avance 400 MHz spectrometer. Splitting patterns are described as singlet (s), doublet (d), triplet (t), quartet (q), quintuplet (qt), and broad (br). Mass spectra were obtained by electrospray ionization (ESIMS) using a Thermo Finnigan LCQ Deca XP Max ion-trap mass spectrometer equipped with Xcalibur software and an LTQ Orbitrap XL mass spectrometer (Thermo Fisher Scientific, San Jose, CA, USA) operating either in positive or negative ionization mode. The sample was dissolved in a mixture of water and methanol (50/50) and injected directly into the electrospray source, using a syringe pump, at constant flow (15  $\mu\text{L}/\text{min}$ ). The temperature of the capillary was set at 220  $^\circ\text{C}$ . The Orbitrap mass analyzer was calibrated according to the manufacturer's directions using a mixture of caffeine, methionine-arginine-phenylalanine-alanine-acetate (MRFA), and Ultramark 1621 in a solution of

acetonitrile, methanol, and acetic acid. Chromatographic separations were performed on silica gel (Kieselgel 40, 0.040–0.063 mm, Merck). Reactions and product mixtures were routinely monitored by thin-layer chromatography (TLC) on Merck 0.2 mm precoated silica (60 F254) aluminum sheets, with visualization by irradiation with a UV lamp.

Reversed-phase high-performance liquid chromatography (RP-HPLC) was performed on a preparative C18-bonded silica column (Phenomenex Kinetex AXIA 100 Å, 100 × 21.2 mm, 5 µm) using a Shimadzu SPD 20 A UV/VIS detector, with detection at 220 and 254 nm. The column was perfused at a flow rate of 15 mL/min with solvent A (5%, v/v, water in 0.1% aqueous TFA) and a linear gradient from 5 to 90% of solvent B (85%, v/v, acetonitrile in 0.1% aqueous TFA) over 20 min was adopted for compound elution. Analytical purity and retention time (rt) of each compound were determined using HPLC conditions in the above solvent system (solvents A and B) at a flow rate of 1.5 mL/min using a linear gradient from 5 to 90% B over 11 min, fitted with a C18-bonded silica column (Phenomenex Kinetex 100 Å, 50 × 4.6 mm, 2.6 µm). LC gradient was the following: 0,01–7 min, 5–90% B, 7.01–8 min, 90–5% B, 8–11 min isocratic for 3 min. All analogues showed >97% purity when monitored at 220 nm. Homogeneous fractions, as established using analytical HPLC, were pooled and lyophilized. Yields refer to purified products and are not optimized.

### 5.6.2 Synthesis of 49-53

#### 2-Benzyl 4-(tert-butyl) 3,5-dimethyl-1H-pyrrole-2,4-dicarboxylate **49**

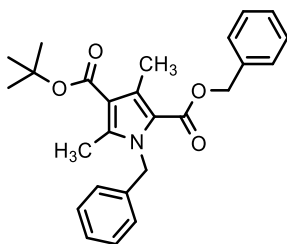


Benzyl acetoacetate **47** (1.00 g, 5.20 mmol) was diluted with glacial acetic acid (1.30 mL), and sodium nitrite (0.395 g, 5.72 mmol) was slowly added with stirring at 10°C. After 12h, the resulting white viscous mixture was slowly added to a well-stirred solution of *tert*-butyl

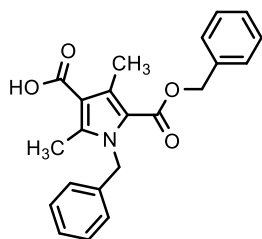
## Chapter 5

acetoacetate **48** (0.823 g, 5.20 mmol), ammonium acetate (0.802 g, 10.40 mmol), and zinc dust (0.986 g, 15.09 mmol) in acetic acid (2.60 mL) at 70°C. Upon complete addition, the red mixture was stirred vigorously at 95°C for 4h and then carefully poured over iced water (15 mL) and extracted with EtOAc (30 mL). The organic phase was washed with brine (2x15 mL), dried over anhydrous Na<sub>2</sub>SO<sub>4</sub>, filtered and solvent was removed under reduced pressure. The residue was purified by flash chromatography (SiO<sub>2</sub>, EtOAc/*n*-hexane 1:1 as eluent) and recrystallized from the minimum volume of methanol to give **49** as a white solid. Yield: 50%. <sup>1</sup>HNMR (CDCl<sub>3</sub>) δ: 1.56 (s, 9H), 2.47 (s, 3H), 2.56 (s, 3H), 5.31 (s, 2H), 7.31-7.42 (m, 5H), 9.12 (brs, 1H). HRMS (ESI) *m/z* [M+Na]<sup>+</sup> calcd for [C<sub>19</sub>H<sub>23</sub>NO<sub>4</sub>Na]<sup>+</sup> 352.1524, found 352.1519.

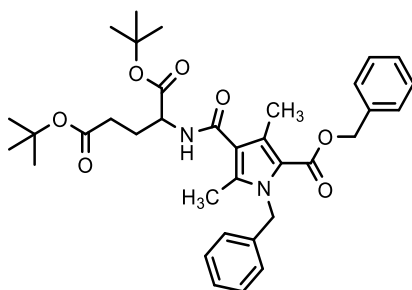
### *2-Benzyl 4-(tert-butyl)1-benzyl-3,5-dimethyl-1H-pyrrole-2,4-dicarboxylate* **50**



To a solution of **49** (0.525 g, 1.59 mmol) in dichloromethane (15 mL), NaOH (50% w/v in H<sub>2</sub>O, 3.18 mL), and a catalytic amount of tetrabutylammonium hydroxide (TBAH) (0.200 mL) were added. After 15 min, benzyl bromide (0.409 g, 2.39 mmol) was added, and the resulting mixture was stirred at room temperature for 12h. The mixture was washed with H<sub>2</sub>O (2x15 mL), and brine (2x15 mL), dried over anhydrous Na<sub>2</sub>SO<sub>4</sub>, filtered and solvent was removed under reduced pressure. The resulting residue was purified by flash column chromatography (SiO<sub>2</sub>, *n*-hexane/EtOAc, 7:3 v/v as eluent) to afford **50** as a white solid. Yield: 90%. <sup>1</sup>HNMR (CDCl<sub>3</sub>) δ: 1.54 (s, 9H), 2.41 (s, 3H), 2.54 (s, 3H), 5.20 (s, 2H), 5.55 (s, 2H), 6.86 (d, 2H, *J*=6.7 Hz), 7.19-7.32 (m, 8H). <sup>13</sup>CDEPTQ NMR (CDCl<sub>3</sub>) δ: 11.9, 13.1, 28.5, 48.5, 65.8, 80.2, 114.8, 119.6, 125.7, 127.0, 128.0 (2C overlapped), 128.5, 128.6, 131.8, 136.1, 137.6, 141.3, 161.7, 164.9. HRMS (ESI) *m/z* [M+H]<sup>+</sup> calcd for [C<sub>26</sub>H<sub>30</sub>NO<sub>4</sub>]<sup>+</sup> 420.2169, found 420.2176.

*1-Benzyl-5-((benzyloxy)carbonyl)-2,4-dimethyl-1H-pyrrole-3-carboxylic acid 51*

To a solution of **50** (0.567 g, 1.35 mmol) in dichloromethane (20 mL), trifluoroacetic acid (15.41 g, 0.135 mmol) was added, and the reaction mixture was stirred for 30 min at room temperature. Then, the solvent was removed under reduced pressure, and the residue was purified by flash chromatography (SiO<sub>2</sub>, *n*-hexane/EtOAc 7:3 as eluent) to give **51** as a white solid. Yield: 80%. <sup>1</sup>HNMR (CDCl<sub>3</sub>) δ: 2.50 (s, 3H), 2.63 (s, 3H), 5.23 (s, 2H), 5.60 (s, 2H), 6.88 (d, 2H, *J* = 6.6 Hz), 7.20-7.34 (m, 8H). <sup>13</sup>CDEPTQ NMR (CDCl<sub>3</sub>) δ: 12.1, 13.0, 48.6, 65.9, 112.1, 120.3, 125.7, 127.1, 128.1 (2C overlapped), 128.5, 128.7, 133.1, 136.0, 137.3, 143.2, 161.5, 170.3. HRMS (ESI) *m/z* [M-H]<sup>-</sup> calcd for [C<sub>22</sub>H<sub>20</sub>NO<sub>4</sub>]<sup>-</sup> 362.1398, found 362.1385.

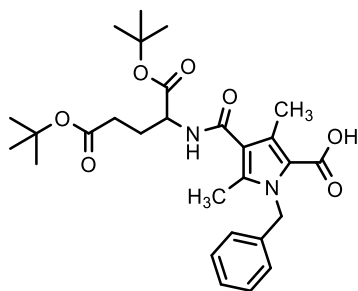
*(S)-di-tert-Butyl (1-benzyl-5-((benzyloxy)carbonyl)-2,4-dimethyl-1H-pyrrole-3-carboxyl) glutamate 52*

1-(3-Dimethylaminopropyl)-3-ethyl-carbodiimide (EDAC) (0.132 g, 0.688 mmol) was dissolved in DMF (2 mL), and the resulting solution was stirred at room temperature for 20 min at 0°C. Then the acid **51** (0.250 g, 0.688 mmol), and OxymaPure<sup>®</sup> (0.098 g, 0.688 mmol) were added. Two minutes after the addition of the reactants, L-glutamic acid di-*tert*-butyl ester (0.203 g, 0.688 mmol) was added to the mixture, followed by addition of DIPEA (0.089 g, 0.688 mmol) and the flask was flushed with nitrogen. The resulting mixture was stirred at 0°C for 1h and then allowed to warm to room temperature. After 15 hours, the solvent was removed under vacuo, and the residue was taken up in EtOAc, and washed successively with 1 M HCl,

## Chapter 5

saturated solution of Na<sub>2</sub>CO<sub>3</sub>, and brine. The organic phase was dried (Na<sub>2</sub>SO<sub>4</sub>), filtered, and concentrated under reduced pressure. The residue was purified by column chromatography (SiO<sub>2</sub>, *n*-hexane/EtOAc, 7:3 v/v, as eluent) to give **52** as a white solid. Yield: 81%. <sup>1</sup>HNMR (CDCl<sub>3</sub>) δ: 1.39 (s, 9H), 1.46 (s, 9H), 1.99 (m, 2H), 2.16-2.22 (m, 1H), 2.25-2.40 (m, 4H), 2.50 (s, 3H), 4.63-4.68 (m, 1H), 5.19 (s, 2H), 5.54 (s, 2H), 6.31 (d, 1H, *J* = 7.7 Hz), 6.87 (d, 2H, *J* = 6.9 Hz), 7.19-7.29 (m, 8H). <sup>13</sup>CDEPTQ NMR (CDCl<sub>3</sub>) δ: 11.2, 12.8, 27.8, 27.9 (2C overlapped), 31.5, 48.5, 52.4, 65.7, 80.6, 82.2, 118.5, 119.2, 125.7, 127.0 (2C overlapped), 128.0, 128.1, 128.4, 128.6, 136.1, 137.6, 137.7, 161.4, 165.5, 171.0, 172.2. HRMS (ESI) *m/z* [M+H]<sup>+</sup> calcd for [C<sub>35</sub>H<sub>45</sub>N<sub>2</sub>O<sub>7</sub>]<sup>+</sup> 605.3221, found 605.3191.

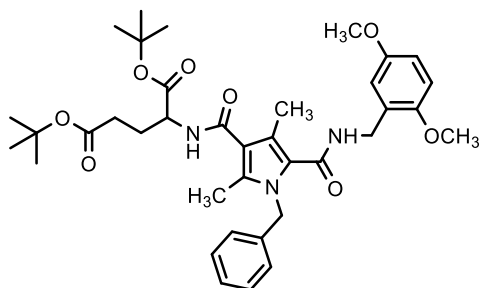
*(S)*-1-Benzyl-4-((1,5-di-*tert*-butoxy-1,5-dioxopentan-2-yl)carbamoyl)-3,5-dimethyl-1H-pyrrole-2-carboxylic acid **53**



A mixture of **52** (0.337 g, 0.557 mmol), ammonium formate (0.703 g, 11.14 mmol) and palladium on carbon 10% (0.033 g, 0.557 mmol) in dry methanol was heated for 2h at reflux. After cooling to room temperature, the reaction mixture was diluted with MeOH and filtered on a celite pad. The solvent was removed under reduced pressure, then the residue was acidified with 1 M HCl, and extracted with EtOAc. The organic phase was dried (Na<sub>2</sub>SO<sub>4</sub>), filtered, and the solvent was removed under vacuum. The resulting residue was purified by flash chromatography (SiO<sub>2</sub>, EtOAc/*n*-hexane 7:3 as eluent) to give **53** as a white solid in quantitative yield. <sup>1</sup>HNMR (CDCl<sub>3</sub>) δ: 1.44 (s, 9H), 1.51 (s, 9H), 1.98-2.09 (m, 1H), 2.19-2.49 (m, 6H), 2.57 (s, 3H), 4.67-4.72 (m, 1H), 5.60 (s, 2H), 6.38 (d, 1H, *J* = 7.8 Hz), 6.95 (d, 2H, *J* = 6.9 Hz), 7.22-7.32 (m, 3H).

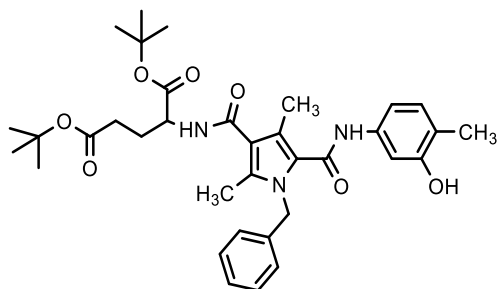
## 5.6.3 Synthesis of 44a-g

(*S*)-di-*tert*-Butyl(1-benzyl-5-((2,5-dimethoxybenzyl)carbamoyl)-2,4-dimethyl-1*H*-pyrrole-3-carbonyl)glutamate **44a**



The title compound was synthesized starting from **53** (0.236 g, 0.459 mmol) and following the same procedure reported for **52**. After purification by flash chromatography (SiO<sub>2</sub>, *n*-hexane/EtOAc, 1:1 v/v, as eluent) **44a** was obtained as a white solid. Yield: 87%. <sup>1</sup>HNMR (CDCl<sub>3</sub>) δ: 1.41 (s, 9H), 1.48 (s, 9H), 1.93-2.02 (m, 1H), 2.15-2.25 (m, 1H), 2.27-2.42 (m, 8H), 3.72 (s, 3H), 3.76 (s, 3H), 4.49 (d, 2H, *J* = 5.9 Hz), 4.64-4.69 (m, 1H), 5.43 (m, 2H), 6.21 (m, 2H), 6.78 (m, 2H, *J* = 1.7 Hz), 6.84 (brs, 1H), 6.94 (d, 2H, *J* = 6.5 Hz), 7.15-7.24 (m, 3H). HRMS (ESI) *m/z* [M+H]<sup>+</sup> calcd for [C<sub>37</sub>H<sub>50</sub>N<sub>3</sub>O<sub>8</sub>]<sup>+</sup> 664.3592, found 664.3599.

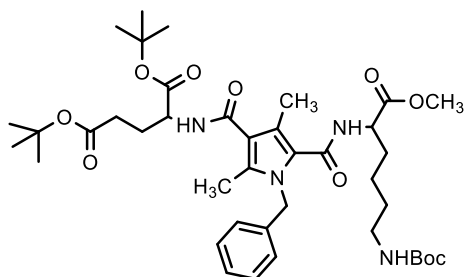
(*S*)-di-*tert*-Butyl(1-benzyl-5-((3-hydroxy-4-methylphenyl)carbamoyl)-2,4-dimethyl-1*H*-pyrrole-3-carbonyl)glutamate **44b**



The title compound was synthesized starting from **53** (0.178 g, 0.346 mmol) and following the same procedure reported for **52**. After purification by flash chromatography (SiO<sub>2</sub>, *n*-hexane/EtOAc, 1:1 v/v, as eluent) **44b** was obtained as a white solid. Yield: 73%. <sup>1</sup>HNMR (CDCl<sub>3</sub>) δ: 1.42 (s, 9H), 1.48 (s, 9H), 1.97-2.09 (m, 1H), 2.1-2.26 (m, 4H), 2.29-2.47 (m, 8H), 4.67 (m, 1H), 5.37 (d, 2H, *J* = 8.1 Hz), 6.37-6.49 (m, 1H), 6.65 (m, 1H), 6.91-7.01 (m, 2H), 7.17-7.28 (m, 5H), 7.39 (m, 1H). HRMS (ESI) *m/z* [M+H]<sup>+</sup> calcd for [C<sub>35</sub>H<sub>46</sub>N<sub>3</sub>O<sub>7</sub>]<sup>+</sup> 620.3330, found 620.3356.

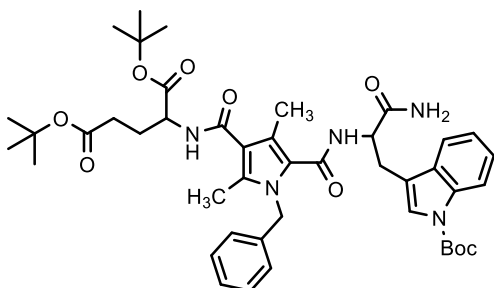
## Chapter 5

*(S)*-di-*tert*-Butyl (1-benzyl-5-((6-((*tert*-butoxycarbonyl)amino)-1-methoxy-1-oxohexan-2-yl)carbamoyl)-2,4-dimethyl-1*H*-pyrrole-3-carbonyl)glutamate **44c**



The title compound was synthesized starting from **53** (0.325 g, 0.631 mmol) and following the same procedure reported for **52**. After purification by flash chromatography (SiO<sub>2</sub>, *n*-hexane/EtOAc, 1:1 v/v, as eluent) **44c** was obtained as a white solid. Yield: 63%. <sup>1</sup>HNMR (CDCl<sub>3</sub>) δ: 1.19-1.31 (m, 2H), 1.40-1.45 (m, 20H), 1.51 (s, 9H), 1.60-1.71 (m, 3H), 1.79-1.88 (m, 1H), 1.97-2.07 (m, 1H), 2.20-2.47 (m, 6H), 2.88 (s, 3H), 3.73 (s, 3H), 4.66-4.73 (m, 2H), 5.48 (m, 2H), 6.16 (d, 1H, *J* = 8.0 Hz), 6.29 (d, 1H, *J* = 7.6 Hz), 6.96 (d, 2H, *J* = 7.6 Hz), 7.21-7.31 (m, 3H). HRMS (ESI) *m/z* [M+H]<sup>+</sup> calcd for [C<sub>40</sub>H<sub>61</sub>N<sub>4</sub>O<sub>10</sub>]<sup>+</sup> 757.4382, found 757.2435.

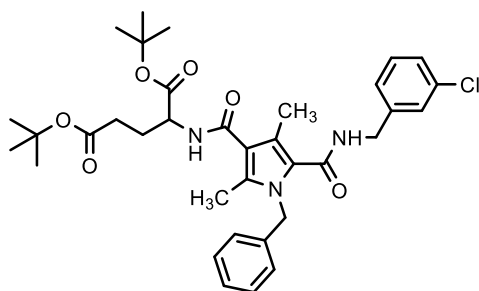
*(S)*-di-*tert*-Butyl(5-((1-amino-3-(1-(*tert*-butoxycarbonyl)-1*H*-indol-3-yl)-1-oxopropan-2-yl)carbamoyl)-1-benzyl-2,4-dimethyl-1*H*-pyrrole-3-carbonyl)glutamate **44d**



The title compound was synthesized starting from **53** (0.224 g, 0.435 mmol) and following the same procedure reported for **52**. After purification by flash chromatography (*n*-hexane/EtOAc, 7:3 v/v as eluent) **44d** was obtained as a white solid. Yield: 52%. <sup>1</sup>HNMR (CDCl<sub>3</sub>) δ: 1.43 (s, 9H), 1.50 (s, 9H), 1.67 (s, 9H), 1.95-2.07 (m, 1H), 2.17-2.25 (m, 1H), 2.29-2.34 (m, 4H), 2.35-2.45 (m, 4H), 3.10-3.21 (m, 2H), 4.64-4.70 (m, 1H), 4.86 (m, 1H), 5.23 (brs, 2H), 5.35 (d, 1H, *J* = 16.4 Hz), 5.48 (d, 1H, *J* = 16.4 Hz), 5.68 (brs, 1H), 6.29 (d, 1H, *J* = 7.6 Hz), 6.36 (d, 1H, *J* = 7.6 Hz), 6.92 (d, 2H, *J* = 7.1 Hz), 7.18-7.35 (m, 4H), 7.47 (s, 1H), 7.65 (d, 1H, *J* = 7.8 Hz), 8.13 (d, 1H, *J* = 8.3 Hz). <sup>13</sup>CDEPTQ NMR (CDCl<sub>3</sub>) δ: 11.2, 12.0, 27.9 (2C), 28.0,

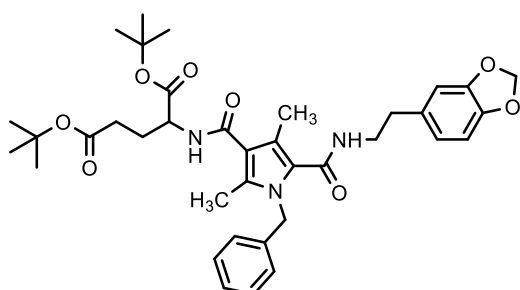
28.1, 28.2, 31.7, 47.9, 52.4, 52.8, 80.7, 82.3, 83.8, 115.3, 115.5, 117.4, 119.2, 120.8, 122.8, 123.8, 124.3, 124.8, 126.1, 127.2, 128.7, 130.0, 135.5, 137.8, 149.5, 162.1, 165.6, 171.4, 172.2, 172.9. HRMS (ESI)  $m/z$   $[M+H]^+$  calcd for  $[C_{44}H_{58}N_5O_9]^+$  800.4229, found 800.4227.

*(S)*-di-*tert*-Butyl(1-benzyl-5-((3-chlorobenzyl)carbamoyl)-2,4-dimethyl-1*H*-pyrrole-3-carbonyl)glutamate **44e**



The title compound was synthesized starting from **53** (0.163 g, 0.317 mmol) and following the same procedure reported for **52**. After purification by flash chromatography (*n*-hexane/EtOAc, 7:3 v/v as eluent) **44e** was obtained as a white solid. Yield: 69%.  $^1\text{H}$ NMR ( $\text{CDCl}_3$ )  $\delta$ : 1.43 (s, 9H), 1.50 (s, 9H), 1.97-2.06 (m, 1H), 2.18-2.27 (m, 1H), 2.29-2.43 (m, 8H), 4.51 (d, 2H,  $J$  = 5.9 Hz), 4.66-4.72 (m, 1H), 5.43-5.53 (m, 2H), 5.89 (brt, 1H,  $J$  = 6.0 Hz), 6.29 (d, 1H,  $J$  = 7.7 Hz), 6.94-7.00 (m, 3H), 7.17-7.31 (m, 6H).  $^{13}\text{C}$ DEPTQ NMR ( $\text{CDCl}_3$ )  $\delta$ : 11.3, 12.3, 27.9, 28.0, 28.1, 31.7, 42.9, 47.8, 52.4, 80.7, 82.3, 117.2, 119.9, 124.4, 125.6, 126.1, 127.3, 127.6, 127.7, 128.7, 130.0, 134.5, 135.2, 137.4, 140.2, 162.3, 165.7, 171.5, 172.4. HRMS (ESI)  $m/z$   $[M+H]^+$  calcd for  $[C_{35}H_{45}ClN_3O_6]^+$  638.2991, found 638.2980.

*(S)*-di-*tert*-Butyl(5-((2-(benzo[d][1,3]dioxol-5-yl)ethyl)carbamoyl)-1-benzyl-2,4-dimethyl-1*H*-pyrrole-3-carbonyl)glutamate **44f**

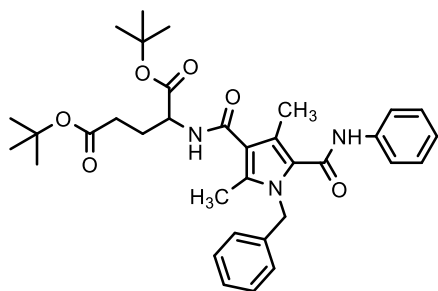


The title compound was synthesized starting from **53** (0.228 g, 0.443 mmol) and following the same procedure reported for **52**. After purification by flash chromatography (*n*-hexane/EtOAc, 3:7 v/v as eluent) **44f** was obtained as a white solid. Yield: 55%.  $^1\text{H}$ NMR

## Chapter 5

(CDCl<sub>3</sub>)  $\delta$ : 1.43 (s, 9H), 1.50 (s, 9H), 1.96-2.05 (m, 1H), 2.17-2.26 (m, 1H), 2.28 (s, 3H), 2.30-2.45 (m, 5H), 2.71 (t, 2H,  $J=6.7$  Hz), 3.57 (q, 2H,  $J=6.5$  Hz), 4.65-4.71 (m, 1H), 5.39-5.49 (m, 2H), 5.55 (brt, 1H,  $J=5.9$  Hz), 5.94 (s, 2H), 6.25 (d, 1H,  $J=7.6$  Hz), 6.51 (dd, 1H,  $J=1.7$  Hz), 6.60 (m, 1H), 6.71 (d, 1H,  $J=7.9$  Hz), 6.96 (d, 2H,  $J=6.8$  Hz), 7.22-7.32 (m, 3H). <sup>13</sup>CDEPTQ NMR (CDCl<sub>3</sub>)  $\delta$ : 11.3, 12.0, 27.9, 28.0, 28.1, 31.7, 35.3, 40.7, 47.8, 52.4, 80.7, 82.3, 109.0, 108.4, 108.9, 117.0, 119.5, 121.6, 125.0, 126.2, 127.2, 128.7, 132.4, 134.8, 137.9, 146.3, 147.9, 162.3, 165.7, 171.5, 172.4. HRMS (ESI)  $m/z$  [M+H]<sup>+</sup> calcd for [C<sub>37</sub>H<sub>48</sub>N<sub>3</sub>O<sub>8</sub>]<sup>+</sup> 662.3436, found 662.3475.

(*S*)-di-*tert*-Butyl(1-benzyl-2,4-dimethyl-5-(phenylcarbamoyl)-1*H*-pyrrole-3-carbonyl)glutamate **44g**



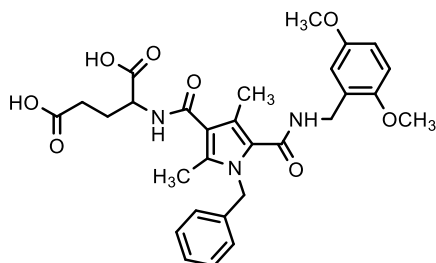
The title compound was synthesized starting from **53** (0.243 g, 0.472 mmol) and following the same procedure reported for **52**. After purification by flash chromatography (*n*-hexane/EtOAc, 7:3 v/v as eluent) **44g** was obtained as a white solid. Yield: 56%. <sup>1</sup>HNMR (CDCl<sub>3</sub>)  $\delta$ : 1.45 (s, 9H), 1.52 (s, 9H), 1.99-2.08 (m, 1H), 2.20-2.32 (m, 1H), 2.35-2.48 (m, 5H), 2.55 (s, 3H), 4.69-4.75 (m, 1H), 5.50 (m, 2H), 6.36 (d, 1H,  $J=7.7$  Hz), 7.03 (d, 2H,  $J=7.09$  Hz), 7.13 (m, 1H), 7.23-7.37 (m, 6H), 7.48 (m, 2H). HRMS (ESI)  $m/z$  [M+H]<sup>+</sup> calcd for [C<sub>34</sub>H<sub>44</sub>N<sub>2</sub>O<sub>6</sub>]<sup>+</sup> 590.3225 found 590.3207.

### 5.6.4 General procedure for the synthesis of 44h-l

To a solution of pyrrole derivatives **44a**, **c-f** (1 eq) in DCM (20 mL), trifluoroacetic acid (100 eq) was added and the mixture was stirred at room temperature until no starting material

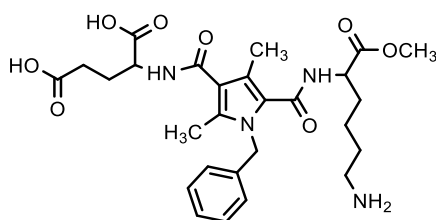
was detected by TLC (~ 1h). Then the resulting mixture was concentrated under reduced pressure and the residue was purified by HPLC.

*(S)*-(1-Benzyl-5-((2,5-dimethoxybenzyl)carbamoyl)-2,4-dimethyl-1H-pyrrole-3-carbonyl)glutamic acid **44h**



Starting from **44a** (0.177 g, 0.267 mmol) and following the general procedure, the title compound was obtained as a white solid, after purification by HPLC (rt= 3.18 min). Yield: 44%. <sup>1</sup>HNMR (MeOD) δ: 1.99-2.09 (m, 1H), 2.24 (m, 1H, overlapped), 2.28 (s, 3H), 2.33 (s, 3H), 2.47-2.53 (m, 2H), 3.66 (s, 3H), 3.78 (s, 3H), 4.45 (s, 2H), 4.60-4.63 (m, 1H), 5.40 (m, 2H), 6.78-6.84 (m, 2H), , 6.88 (d, 1H, *J*= 8.8 Hz), 6.98 (m, 2H), 7.19-7.28 (m, 2H). <sup>13</sup>CDEPTQ NMR (MeOD) δ: 9.8, 10.0, 26.4, 30.0, 38.6, 47.2, 52.0, 54.7, 54.8, 111.0, 112.6, 114.9, 117.4, 120.3, 125.1, 126.0, 126.8, 127.0, 128.3, 133.9, 138.0, 151.5, 153.6, 163.5, 168.0, 173.6, 175.0. HRMS (ESI) *m/z* [M+H]<sup>+</sup> calcd for [C<sub>29</sub>H<sub>34</sub>N<sub>3</sub>O<sub>8</sub>]<sup>+</sup> 552.2340, found 552,2321.

*(S)*-(5-((6-Amino-1-methoxy-1-oxopentan-2-yl)carbamoyl)-1-benzyl-2,4-dimethyl-1H-pyrrole-3-carbonyl)glutamic acid **44i**

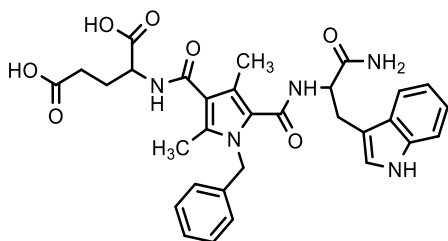


Starting from **44c** (0.115 g, 0.152 mmol) and following the general procedure, the title compound was obtained as a white solid, after purification by HPLC (rt= 5.33 min). Yield: 37%. <sup>1</sup>HNMR (MeOD) δ: 1.31-1.39 (m, 2H), 1.55-1.78 (m, 3H), 1.87-1.96 (m, 1H), 2.01-2.10 (m, 1H), 2.25-2.33 (m, 4H), 2.37 (s, 3H), 2.50 (m, 2H), 2.76-2.87 (m, 2H), 3.66 (s, 3H), 4.53 (dd, 1H, *J*= 9.5, 5.0 Hz), 4.62 (dd, 1H, *J*= 9.1, 5.0 Hz), 5.42 (m, 2H), 7.00 (d, 2H, *J*= 7.2 Hz), 7.21-7.32 (m, 3H). <sup>13</sup>CDEPTQ NMR (MeOD) δ: 9.8, 10.1, 22.4, 26.4, 26.5, 30.1, 30.4, 39.0,

## Chapter 5

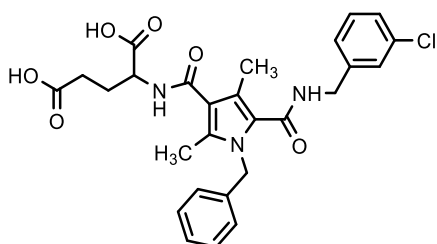
54.3, 52.0, 52.1, 117.4, 121.0, 124.5, 126.0, 126.8, 128.3, 134.2, 138.1, 163.7, 167.9, 172.4, 173.8, 175.1. HRMS (ESI)  $m/z$   $[M+H]^+$  calcd for  $[C_{27}H_{37}N_4O_8]^+$  545.2606, found 545.2579.

*(S)*-5-((1-Amino-3-(1*H*-indol-3-yl)-1-oxopropan-2-yl)carbamoyl)-1-benzyl-2,4-dimethyl-1*H*-pyrrole-3-carbonyl)glutamic acid **44j**



Starting from **44d** (0.204 g, 0.255 mmol) and following the general procedure, the title compound was obtained as a white solid, after purification by HPLC (rt= 4.56 min). Yield: 39%.  $^1\text{H}$ NMR (DMSO- $d_6$ )  $\delta$ : 1.76-1.88 (m, 1H), 1.97-2.05 (m, 4H), 2.18 (s, 3H), 2.30 (m, 2H), 3.03-3.09 (m, 1H), 3.16-3.21 (m, 1H), 4.27-4.33 (m, 1H), 4.60-4.66 (m, 1H), 5.20-5.35 (m, 2H), 6.94-7.10 (m, 5H), 7.18-7.27 (m, 3H), 7.32 (d, 1H,  $J$ = 8.1 Hz), 7.41 (s, 1H), 7.56 (d, 1H,  $J$ = 7.8 Hz), 7.62 (d, 1H,  $J$ = 7.9 Hz), 7.68 (d, 1H,  $J$ = 7.7 Hz), 10.8 (s, 1H).  $^{13}\text{C}$ DEPTQ NMR (DMSO- $d_6$ )  $\delta$ : 11.4, 11.6, 26.7, 28.1, 30.9, 47.5, 52.1, 54.1, 110.5, 111.7, 118.2, 118.6, 119.0, 119.8, 121.3, 124.2, 124.8, 127.2, 127.4, 127.8, 128.8, 133.0, 136.6, 138.7, 162.1, 165.9, 174.0, 174.2, 174.4. HRMS (ESI)  $m/z$   $[M+H]^+$  calcd for  $[C_{31}H_{34}N_5O_7]^+$  588.2453, found 588.2443.

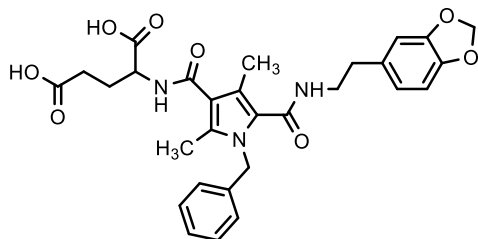
*(S)*-(1-Benzyl-5-((3-chlorobenzyl)carbamoyl)-2,4-dimethyl-1*H*-pyrrole-3-carbonyl)glutamic acid **44k**



Starting from **44e** (0.226 g, 0.354 mmol) and following the general procedure, the title compound was obtained as a white solid, after purification by HPLC (rt= 4.18 min). Yield: 27%.  $^1\text{H}$ NMR (MeOD)  $\delta$ : 2.00-2.10 (m, 2H), 2.25-2.39 (m, 8H), 2.48-2.52 (m, 2H), 4.45 (s, 2H), 4.61-4.64 (dd, 1H,  $J$ = 9.1, 4.9 Hz), 5.37-5.46 (m, 2H), 6.95 (d, 2H,  $J$ = 6.4 Hz), 7.05 (d,

1H,  $J = 6.7$  Hz), 7.18-7.29 (m, 6H). HRMS (ESI)  $m/z$   $[M+H]^+$  calcd for  $[C_{27}H_{29}ClN_3O_6]^+$  526.1739, found 526.1722.

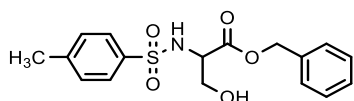
(*S*)-(5-((2-(Benzo[*d*][1,3]dioxol-5-yl)ethyl)carbamoyl)-1-benzyl-2,4-dimethyl-1*H*-pyrrole-3-carbonyl)glutamic acid **44i**



Starting from **44f** (0.194 g, 0.293 mmol) and following the general procedure, the title compound was obtained as a white solid, after purification by HPLC ( $rt = 3.90$  min). Yield: 37%.  $^1H$ NMR (MeOD)  $\delta$ : 1.99-2.09 (m, 1H), 2.18 (s, 3H), 2.24-2.39 (m, 4H), 2.49 (t, 2H,  $J = 8.1$  Hz), 2.73 (t, 2H,  $J = 7.2$  Hz), 3.48 (t, 2H,  $J = 7.2$  Hz), 4.61 (m, 1H), 5.34 (m, 2H), 5.88 (s, 2H), 6.61-6.67 (m, 2H), 6.71 (s, 1H), 6.97 (d, 2H,  $J = 7.3$  Hz), 7.21-7.30 (m, 3H).  $^{13}C$ DEPTQ NMR (MeOD)  $\delta$ : 9.8, 10.0, 26.4, 30.0, 34.7, 40.8, 47.3, 52.0, 100.7, 107.7, 108.7, 117.2, 120.1, 121.4, 125.2, 126.0, 126.8, 128.2, 132.8, 133.9, 138.1, 146.1, 147.7, 163.6, 168.0, 173.7, 175.1. HRMS (ESI)  $m/z$   $[M+H]^+$  calcd for  $[C_{29}H_{31}N_3O_8]^+$  550.2184, found 550.2173.

### 5.6.5 Synthesis of 55-60

#### Benzyl tosylserinate **55**

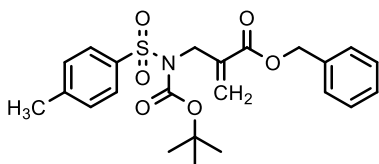


To a solution of ( $\pm$ ) serine benzyl ester hydrochloride **54** (3.09 g, 13.35 mmol) in dichloromethane (60 mL), triethylamine (2.72 g, 26.69 mmol) was added. The mixture was cooled to 0°C, and a solution of *p*-toluenesulfonyl chloride (2.544 g, 13.35 mmol) in dichloromethane (45 mL) was slowly added. The resulting mixture was allowed to warm to room temperature, and stirred in these conditions overnight, then was washed with 1N HCl (2x20 mL), and a saturated solution of  $NaHCO_3$  (2x20 mL). The organic phase was dried over

## Chapter 5

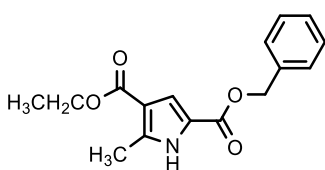
anhydrous  $\text{Na}_2\text{SO}_4$ , filtered, and concentrated under reduced pressure. The residue was purified by flash chromatography ( $\text{SiO}_2$ , EtOAc/*n*-hexane 7:3 as eluent) to give **55** as a white solid. Yield: 90%.  $^1\text{H NMR}$  ( $\text{CDCl}_3$ )  $\delta$ : 2.43 (s, 3H), 3.93(d, 2H,  $J=3.8$  Hz), 4.03-4.07 (m, 1H), 5.06 (s, 2H), 5.65 (d, 1H,  $J=7.7$  Hz), 7.23-7.26 (m, 4H), 7.37 (m, 3H), 7.74 (d, 2H,  $J=8.3$  Hz).

### Benzyl 2-((*N*-(*tert*-butoxycarbonyl)-4-methylphenyl)sulfonamido)acrylate **56**



To a solution of **55** (1.00g, 2.86 mmol) in acetonitrile (25 mL),  $(\text{Boc})_2\text{O}$  (1.56 g, 7.15 mmol) and DMAP (0.070 g, 0.572 mmol) were added, and the resulting mixture was stirred at room temperature for 3h. The organic solvent was removed under vacuo, and the residue was taken up in EtOAc (30 mL), and washed with 1M  $\text{KHSO}_4$  (2x15 mL), and brine (2x15 mL), dried over anhydrous  $\text{Na}_2\text{SO}_4$ , filtered and solvent was removed under reduced pressure. The residue was triturated with EtOAc/*n*-hexane (1:1) to afford **56** as a white solid. Yield: 55%.  $^1\text{H NMR}$  ( $\text{CDCl}_3$ )  $\delta$ : 1.23 (s, 9H), 2.41 (s, 3H), 5.21 (s, 2H), 6.08 (s, 1H), 6.65 (s, 1H), 7.21 (d, 2H  $J=8.3$  Hz), 7.29 (m, 2H), 7.32-7.35 (m, 3H), 7.90 (d, 2H,  $J=8.4$  Hz).

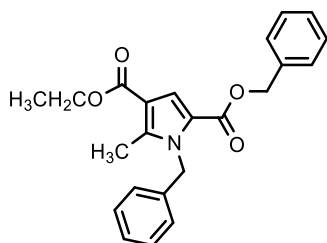
### 2-Benzyl 4-ethyl 5-methyl-1H-pyrrole-2,4-dicarboxylate **58**



To a stirred solution of benzyl 2-((*N*-(*tert*-butoxycarbonyl)-4-methylphenyl)sulfonamido)acrylate **56** (3.00 g, 6.95 mmol) in dry  $\text{CH}_3\text{CN}$  (30 mL), ethyl acetoacetate **57** (0.905 g, 6.95 mmol) and  $\text{Cs}_2\text{CO}_3$  (3.40 g, 10.5 mmol) were added, and the resulting mixture was stirred at room temperature overnight. The organic solvent was removed under vacuo and the residue was taken up in EtOAc and washed with brine (2x25 mL). The organic phase was dried over anhydrous  $\text{Na}_2\text{SO}_4$ , filtered and solvent was removed under reduced pressure. The crude was diluted with dichloromethane (20 mL), and TFA (5.32 mL, 69.5 mmol) was added. After 12h,

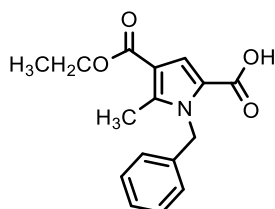
the mixture was washed with H<sub>2</sub>O (2x25 mL), saturated solution of NaHCO<sub>3</sub> (2x15 mL) and brine (2x15 mL). The organic phase was dried over anhydrous Na<sub>2</sub>SO<sub>4</sub>, filtered, and concentrated under reduced pressure. The residue was purified by flash chromatography (SiO<sub>2</sub>, *n*-hexane/EtOAc 7:3 as eluent) to give compound **58** as a white solid. Yield: 62%. <sup>1</sup>H NMR (CDCl<sub>3</sub>) δ: 1.34 (t, 3H, *J*= 7.1 Hz), 2.55 (s, 3H), 4.27 (q, 2H, *J*= 7.1 Hz), 5.31 (s, 2H), 7.30-7.43 (m, 6H), 9.39 (brs, 1H). <sup>13</sup>C NMR (CDCl<sub>3</sub>) δ: 13.4, 14.4, 59.8, 66.3, 114.3, 117.7, 120.3, 128.1, 128.3, 128.6, 135.8, 139.7, 160.8, 164.6.

*2-Benzyl 4-ethyl 1-benzyl-5-methyl-1H-pyrrole-2,4-dicarboxylate* **59**



The title compound was synthesized starting from **58** (1.00 g, 3.69 mmol) and following the same procedure reported for **50**. After purification by flash column chromatography (SiO<sub>2</sub>, *n*-hexane/EtOAc, 7:3 v/v, as eluent) **59** was obtained as a white solid. Yield: 80%. <sup>1</sup>H NMR (CDCl<sub>3</sub>) δ: 1.35 (t, 3H, *J*= 7.1 Hz), 2.51 (s, 3H), 4.28 (q, 2H, *J*= 7.1 Hz), 5.22 (s, 2H), 5.67 (s, 2H), 6.93 (d, 2H, *J*= 7.1 Hz), 7.21-7.37 (m, 8H), 7.50 (s, 1H). <sup>13</sup>CDEPTQ NMR (CDCl<sub>3</sub>) δ: 11.4, 14.4, 48.2, 59.8, 65.8, 113.2, 120.1, 121.3, 125.8, 127.3, 128.0, 128.1, 128.5, 128.7, 136.1, 137.0, 142.5, 160.5, 164.6.

*1-Benzyl-4(ethoxycarbonyl)-5-methyl-1H-pyrrole-2-carboxylic acid* **60**



A mixture of **59** (0.918 g, 2.43 mmol), ammonium formate (1.534 g, 24.33 mmol) and palladium on carbon 10% (0.146 g, 2.43 mmol) in dry ethanol was heated for 30 min at reflux. After cooling to room temperature, the reaction mixture was diluted with EtOH and filtered on

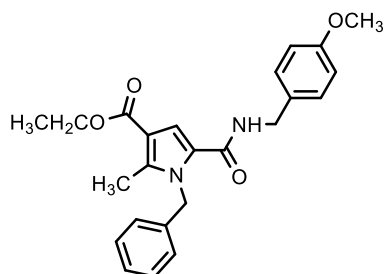
## Chapter 5

a celite pad. The solvent was removed under reduced pressure, then the residue was acidified with 2M HCl (pH ~ 3), and extracted with EtOAc. The organic phase was dried (Na<sub>2</sub>SO<sub>4</sub>), filtered, and the solvent was removed under vacuum. The resulting residue was recrystallized (methanol/ethyl ether) to afford **60** as a white solid, in quantitative yield. <sup>1</sup>HNMR (MeOD) δ: 1.37 (t, 3H, *J*= 7.1 Hz), 2.47 (s, 3H), 4.29 (q, 2H, *J*= 7.1 Hz), 5.74 (s, 2H), 6.97 (m, 2H), 7.22-7.26 (m, 1H), 7.29-7.33 (m, 2H), 7.41 (s, 1H). <sup>13</sup>CDEPTQ NMR (MeOD) δ: 12.3, 15.5, 61.7 (2C), 114.6, 121.6, 124.1, 127.7, 129.0, 130.5, 139.7, 144.5, 146.4, 167.1.

### 5.6.6 General procedure for the synthesis of 45a-c

To a solution of **60** (1 eq) in dry DCM (1 mL), thionyl chloride (6.0 eq) was added and the resulting mixture was stirred at reflux for 3h to obtain the corresponding acyl chloride. Then the solvent was removed in vacuo and the appropriate amine RNH<sub>2</sub> (1.5 eq) and dry triethylamine (1.5 eq) in dry DCM (2 mL) were added. The resulting mixture was refluxed for 3h. The solvent was removed under reduced pressure, and the resulting residue was taken up in EtOAc and washed successively with brine, 1M HCl and 1M NaHCO<sub>3</sub>. The organic phase was dried (Na<sub>2</sub>SO<sub>4</sub>), filtered, and concentrated under reduced pressure. The residue was purified by column chromatography (SiO<sub>2</sub>, *n*-hexane/EtOAc, 7:3 as eluent) and recrystallized from EtOAc/*n*-hexane to give the title compounds in good yields.

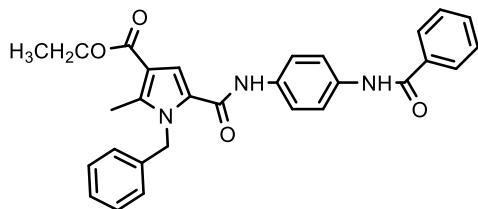
#### *Ethyl 1-benzyl-5-((4-methoxybenzyl)carbamoyl)-2-methyl-1H-pyrrole-3-carboxylate 45a*



White solid. Yield: 87%. <sup>1</sup>HNMR (CDCl<sub>3</sub>) δ: 1.33 (t, 3H, *J*= 7.1 Hz), 2.48 (s, 3H), 3.80 (s, 2H), 4.26 (q, 2H, *J*= 7.1 Hz), 4.43 (d, 2H, *J*= 5.7 Hz), 5.70 (s, 3H), 6.12 (brs, 1H), 6.83 (m, 2H), 6.95 (m, 2H), 7.00 (s, 1H), 7.15 (m, 2H), 7.21-7.30 (m, 3H). <sup>13</sup>CDEPTQ NMR (CDCl<sub>3</sub>) δ: 11.3,

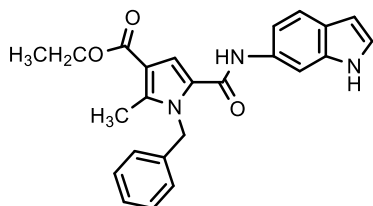
14.5, 42.9, 48.1, 55.3, 56.8, 112.3, 113.2, 114.1, 125.2, 126.1, 127.2, 128.7, 129.1, 130.3, 137.6, 140.9, 159.1, 161.3, 164.8.

*Ethyl 5-((4-benzamidophenyl)carbamoyl)-1-benzyl-2-methyl-1H-pyrrole-3-carboxylate 45b*



White solid. Yield: 62%. <sup>1</sup>HNMR (DMSO-*d*<sub>6</sub>) δ: 1.31 (t, 3H, *J* = 7.1 Hz), 2.44 (s, 3H), 4.24 (q, 2H, *J* = 7.1 Hz), 5.76 (s, 2H), 6.99 (m, 2H), 7.25 (m, 1H), 7.33 (m, 2H), 7.51-7.60 (m, 4H), 7.65-7.72 (m, 4H), 7.94-7.97 (m, 2H), 10.1 (s, 1H), 10.2 (s, 1H). HRMS (ESI) *m/z* [M+H]<sup>+</sup> calcd for [C<sub>29</sub>H<sub>28</sub>N<sub>3</sub>O<sub>4</sub>]<sup>+</sup> 482.2074, found 482.2080.

*Ethyl 5-((1H-indol-6-yl)carbamoyl)-1-benzyl-2-methyl-1H-pyrrole-3-carboxylate 45c*



White solid. Yield: 86%. <sup>1</sup>HNMR (CDCl<sub>3</sub>) δ: 1.38 (t, 3H, *J* = 7.1 Hz), 2.50 (s, 3H), 4.32 (q, 2H, *J* = 7.1 Hz), 5.72 (s, 2H), 6.48 (brs, 1H), 6.90 (dd, 1H, *J* = 8.4, 1.9 Hz), 7.00 (d, 2H, *J* = 7.1 Hz), 7.15 (m, 1H), 7.19-7.29 (m, 5H), 7.54 (d, 1H, *J* = 8.4 Hz), 7.78 (s, 1H), 8.21 (brs, 1H). <sup>13</sup>CDEPTQ NMR (CDCl<sub>3</sub>) δ: 11.4, 14.5, 48.2, 59.9, 102.5, 103.1, 112.5, 113.4, 113.6, 120.8, 124.5, 124.8, 125.7, 126.1, 127.2, 128.7, 132.6, 136.0, 137.4, 141.4, 159.4, 164.8. HRMS (ESI) *m/z* [M+H]<sup>+</sup> calcd for [C<sub>24</sub>H<sub>24</sub>N<sub>3</sub>O<sub>3</sub>]<sup>+</sup> 402.1812, found 402.1842.

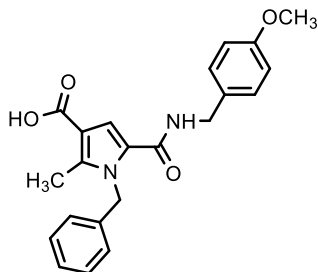
### 5.6.7 General procedure for the synthesis of 45d-f

To a solution of ester **45a-c** (1 eq) in ethanol (1 mL) was added NaOH (50% w/v in H<sub>2</sub>O, 3 mL), and the resulting mixture was refluxed until no starting material was detected by TLC (24-48h). The solvent was removed under reduced pressure, then the residue was acidified with 2M HCl (pH ~ 3), and extracted with EtOAc. The organic phase was dried (Na<sub>2</sub>SO<sub>4</sub>), filtered, and

## Chapter 5

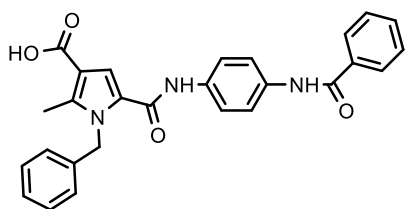
the solvent was removed under vacuum. The resulting residue was recrystallized from ethyl acetate/*n*-hexane, to give the title compounds in good yields.

### *1-Benzyl-5-((4-methoxybenzyl)carbamoyl)-2-methyl-1H-pyrrole-3-carboxylic acid 45d*



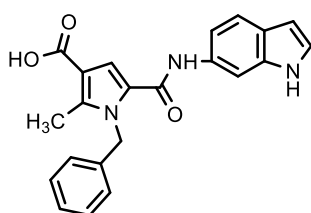
White solid. Yield: 92%  $^1\text{H}$ NMR ( $\text{CDCl}_3$ )  $\delta$ : 2.52 (s, 3H), 3.82 (s, 3H), 4.46 (d, 2H,  $J = 5.7$  Hz), 5.76 (s, 2H), 6.23 (brt, 1H,  $J = 5.7$  Hz), 6.86 (d, 2H,  $J = 8.6$  Hz), 7.00 (d, 2H,  $J = 6.9$  Hz), 7.05 (s, 1H), 7.17 (d, 2H,  $J = 8.6$  Hz), 7.24-7.34 (m, 3H). HRMS (ESI)  $m/z$   $[\text{M}+\text{H}]^+$  calcd for  $[\text{C}_{22}\text{H}_{23}\text{N}_2\text{O}_4]^+$  379.1652, found 379.1644.

### *5-((4-Benzamidophenyl)carbamoyl)-1-benzyl-2-methyl-1H-pyrrole-3-carboxylic acid 45e*



White solid. Yield: 76%.  $^1\text{H}$ NMR ( $\text{DMSO}_d_6$ )  $\delta$ : 2.43 (s, 3H), 5.75 (s, 2H), 6.99 (d, 2H,  $J = 7.2$  Hz), 7.25 (m, 1H), 7.31-7.35 (m, 2H), 7.56-7.61 (m, 4H), 7.65-7.71 (m, 4H), 7.94-7.97 (m, 2H), 10.02 (s, 1H), 10.20 (s, 1H).  $^{13}\text{C}$ DEPTQ NMR ( $\text{DMSO}_d_6$ )  $\delta$ : 11.4, 47.9, 112.6, 116.0, 120.7, 121.1, 125.3, 126.4, 127.4, 128.0, 128.8, 129.1, 135.1, 131.9, 135.4 (2C, overlapped), 138.5, 141.1, 159.8, 165.7, 166.1. HRMS (ESI)  $m/z$   $[\text{M}+\text{Na}]^+$  calcd for  $[\text{C}_{27}\text{H}_{23}\text{N}_3\text{O}_4\text{Na}]^+$  476.1586, found 476.1606.

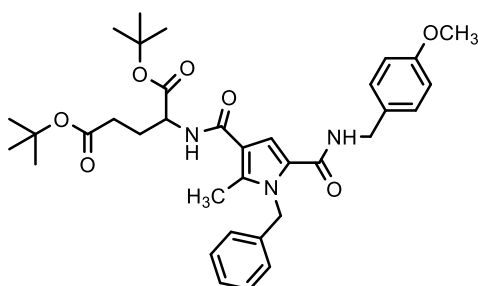
### *5-((1H-Indol-6-yl)carbamoyl)-1-benzyl-2-methyl-1H-pyrrole-3-carboxylic acid 45f*



White solid. Yield: 89%.  $^1\text{H NMR}$  ( $\text{DMSO-}d_6$ )  $\delta$ : 2.44 (s, 3H), 5.76 (s, 2H), 6.34 (brt, 1H,  $J=2.8$  Hz), 7.01 (d, 2H,  $J=7.1$  Hz), 7.20-7.26 (m, 3H), 7.32 (m, 2H), 7.42 (d, 1H,  $J=8.5$  Hz), 7.50 (s, 1H), 7.97 (s, 1H), 9.93 (s, 1H), 10.95 (s, 1H).

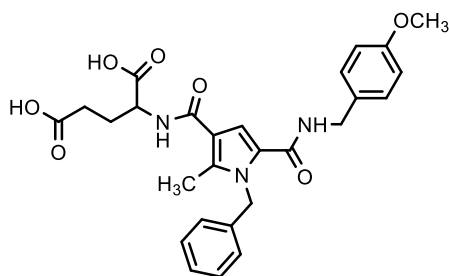
### 5.6.8 Synthesis of 45g,h

*(S)*-di-tert-Butyl(1-benzyl-5-((4-methoxybenzyl)carbamoyl)-2-methyl-1H-pyrrole-3-carbonyl) glutamate **45g**



Starting from **45d** (0.340 g, 0.90 mmol), and following the general procedure reported for the synthesis of **45a-c**, the title compound was obtained as a white solid after purification by column chromatography ( $\text{SiO}_2$ ,  $n$ -hexane/EtOAc, 7:3, as eluent) and recrystallization from EtOAc/ $n$ -hexane. Yield: 65%.  $^1\text{H NMR}$  ( $\text{CDCl}_3$ )  $\delta$ : 1.39 (s, 9H), 1.47 (s, 9H), 1.97 (m, 1H), 2.14-2.22 (m, 1H), 2.26-2.44 (m, 2H), 2.48 (s, 3H), 3.80 (s, 3H), 4.43 (d, 2H,  $J=5.6$  Hz), 4.59-4.64 (m, 1H), 5.67 (s, 2H), 6.11 (brs, 1H), 6.51 (d, 1H,  $J=7.6$  Hz), 6.78 (s, 1H), 6.84 (m, 2H), 6.95-6.97 (m, 2H), 7.15-7.29 (m, 5H). HRMS (ESI)  $m/z$   $[\text{M}+\text{H}]^+$  calcd for  $[\text{C}_{35}\text{H}_{46}\text{N}_3\text{O}_7]^+$  620.3330, found 620.3333.

*(S)*-(1-Benzyl-5-((4-methoxybenzyl)carbamoyl)-2-methyl-1H-pyrrole-3-carbonyl)glutamic acid **45h**



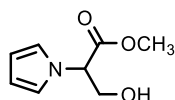
To a solution of **45g** (0.156 g, 0.25 mmol) in dichloromethane (4 mL), trifluoroacetic acid (2 mL) was added. After stirring for 2h at room temperature, the mixture was concentrated

## Chapter 5

under reduced pressure. After purification by HPLC (rt = 3.95 min), **45h** was obtained as a white solid. Yield: 36%.  $^1\text{H}$ NMR (MeOD)  $\delta$ : 2.03-2.12 (m, 1H), 2.24-2.33 (m, 1H), 2.42-2.67 (m, 5H), 3.77 (s, 3H), 4.39 (s, 2H), 4.60 (dd, 1H,  $J$ = 9.2, 4.9 Hz), 5.69 (s, 2H), 6.83 (d, 2H,  $J$ = 8.7 Hz), 6.98 (d, 2H,  $J$ = 6.6 Hz), 7.15-7.17 (m, 3H), 7.22-7.31 (m, 3H).  $^{13}\text{C}$ DEPTQ NMR (MeOD)  $\delta$ : 9.9, 26.4, 30.1, 41.9, 47.3, 51.7, 54.3, 111.5, 113.5, 114.7, 125.3, 125.8, 126.8, 128.3 (2C), 130.9, 138.0, 138.6, 158.9, 162.5, 166.6, 174.0, 175.3. HRMS (ESI)  $m/z$   $[\text{M}+\text{H}]^+$  calcd for  $[\text{C}_{27}\text{H}_{30}\text{N}_3\text{O}_7]^+$  508.2078, found 508.2051.

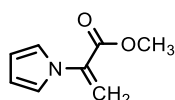
### 5.6.9 Synthesis of 62-71

#### Methyl 3-hydroxy-2-(1H-pyrrol-1-yl)propanoate **62**



A solution of 2,5-dimethoxytetrahydrofuran (2.04 g, 15.44 mmol) in water (20 mL), degassed and stirred under nitrogen, was refluxed for 2h. Then, the mixture was allowed to cool to room temperature, and a mixture of dichloromethane/ $\text{H}_2\text{O}$  (40 mL, 3:1), sodium acetate (3.04 g, 37.05 mmol), and ( $\pm$ )-serine methyl ester hydrochloride **61** (2.88 g, 18.52 mmol) was added. After 15h, the phases were separated, and the organic layer was dried ( $\text{Na}_2\text{SO}_4$ ), filtered, and concentrated under reduced pressure. The residue was purified by column chromatography ( $\text{SiO}_2$ , DCM as eluent) to give **62** as a colorless oil. Yield: 92%.  $^1\text{H}$ NMR ( $\text{CDCl}_3$ )  $\delta$ : 3.70 (s, 3H), 3.99 (m, 1H), 4.10 (m, 1H), 4.70 (t, 1H,  $J$ = 6.3 Hz), 5.23 (s, 1H), 6.15 (m, 2H), 6.70 (m, 2H).

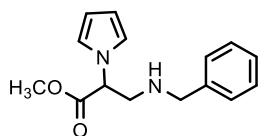
#### Methyl 2-(1H-pyrrol-1-yl)acrylate **63**



To a solution of pyrrole derivative **62** (2.88 g, 17.12 mmol) in dry acetonitrile (30 mL), DMAP (1.05 g, 8.9 mmol) was added followed by  $(\text{Boc})_2\text{O}$  (7.47 g, 34.24 mmol). The resulting mixture was vigorously stirring at room temperature for 6h. Then the solvent was removed

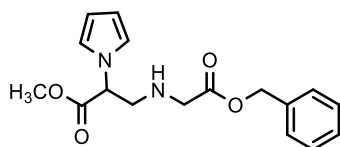
under vacuum, and the resulting residue was taken up in EtOAc, and washed with brine. After purification by column chromatography (SiO<sub>2</sub>, DCM/EtOAc 9:1 v/v as eluent) the title compound was obtained as a pale yellow oil. Yield: 80%. <sup>1</sup>HNMR (CDCl<sub>3</sub>) δ: 3.87 (s, 3H), 5.68 (s, 1H), 6.09 (s, 1H), 6.26 (t, 2H, *J* = 2.2 Hz), 6.91 (t, 2H, *J* = 2.2 Hz).

(±)-Methyl 3-(benzylamino)-2-(1*H*-pyrrol-1-yl)propanoate **66a**



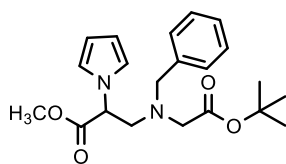
A mixture of compound **63** (1.32 g, 8.74 mmol) and benzylamine **64** (1.03 g, 9.61 mmol) was heated at 95°C in a sealed tube under solvent-free conditions. After 5h the resulting residue was taken up in EtOAc and washed with brine. The organic phase was dried (Na<sub>2</sub>SO<sub>4</sub>), filtered, and concentrated under reduced pressure. The residue was purified by column chromatography (SiO<sub>2</sub>, *n*-hexane/EtOAc, 1:1 v/v, as eluent) to give compounds **66a** as a yellow oil. Yield: 75% <sup>1</sup>HNMR (CDCl<sub>3</sub>) δ: 3.15-3.19 (m, 1H), 3.26-3.31 (m, 1H), 3.72 (s, 3H), 3.78 (m, 2H), 4.80 (t, 1H, *J* = 8.2 Hz), 6.20 (t, 2H, *J* = 2.1 Hz), 6.75 (t, 2H, *J* = 2.1 Hz), 7.31 (m, 5H). <sup>13</sup>CDEPTQ (CDCl<sub>3</sub>) δ: 50.6, 52.5, 53.3, 61.8, 109.0, 120.2, 127.1, 128.0, 128.4, 139.4, 170.2.

(±)-Methyl 3-((2-(benzyloxy)-2-oxoethyl)amino)-2-(1*H*-pyrrol-1-yl)propanoate **66b**



Starting from benzyl glycinate **65** (0.697 g, 4.22 mmol) and following the same procedure reported for **66a**, the title compound was obtained as a pale yellow oil. Yield: 45%. <sup>1</sup>HNMR (CDCl<sub>3</sub>) δ: 3.27-3.35 (m, 2H), 3.45 (m, 2H), 3.77 (s, 3H), 4.80 (dd, 1H, *J* = 8.1, 6.3 Hz), 5.19 (s, 2H), 6.24 (t, 2H, *J* = 2.2 Hz), 6.80 (t, 2H, *J* = 2.2 Hz), 7.40 (m, 5H).

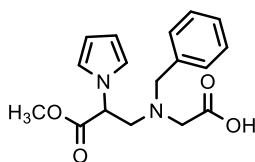
(±)-Methyl 3-(benzyl(2-(*tert*-butoxy)-2-oxoethyl)amino)-2-(1*H*-pyrrol-1-yl)propanoate **67**



## Chapter 5

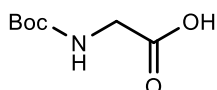
To a solution of derivative **66a** (0.200 g, 0.77 mmol) in dry acetonitrile (30 mL), *tert*-butyl bromoacetate (0.166 g, 0.85 mmol) and potassium carbonate (0.107 g, 0.77 mmol) were added. The resulting mixture was vigorously stirred at 60°C for 5h, and then was allowed to cool to room temperature. After 12h the solvent was removed under vacuum, and the resulting residue was taken up in EtOAc, and washed with brine. The residue was purified by column chromatography (SiO<sub>2</sub>, *n*-hexane/EtOAc, 7:3, as eluent) to give **67** as white needle-like crystals. Yield: 86%. <sup>1</sup>HNMR (CDCl<sub>3</sub>) δ: 1.44 (s, 9H), 3.10 (d, 1H, *J*= 17.4 Hz), 3.20 (d, 1H, *J*= 17.4 Hz), 3.31 (dd, 1H, *J*= 13.9, 7.1 Hz), 3.49 (dd, 1H, *J*= 13.9, 7.7 Hz); 3.71 (s, 3H), 3.84 (m, 2H), 4.66 (t, 1H, *J*= 7.4 Hz), 6.16 (t, 2H, *J*= 2.2 Hz), 6.72 (t, 2H, *J*= 2.2 Hz), 7.20-7.32 (m, 5H).

(±)-*N*-benzyl-*N*-(3-methoxy-3-oxo-2-(1*H*-pyrrol-1-yl)propyl)glycine **68**



To a solution of **67** (0.225 g, 0.60 mmol) in dichloromethane (10 mL), trifluoroacetic acid (6.89 g, 60.40 mmol) was added, and the reaction was stirred for 30 min at room temperature. Then, the solvent was removed under reduced pressure, and the residue was purified by flash chromatography (SiO<sub>2</sub>, EtOAc/*n*-hexane 7:3 as eluent) to give **68** as a white solid. Yield: 50%. <sup>1</sup>HNMR (CDCl<sub>3</sub>) δ: 3.27-3.37 (m, 3H), 3.47 (dd, 1H, *J*= 13.8, 6.7 Hz), 3.73 (s, 3H), 3.79 (d, 1H, *J*=13.2 Hz), 3.86 (d, 1H, *J*= 13.2 Hz), 4.890 (t, 1H, *J*= 13.2 Hz), 6.21 (t, 2H, *J*= 8.3 Hz), 6.69 (t, 2H, *J*= 2.2 Hz), 7.22 (m, 2H), 7.36 (m, 3H).

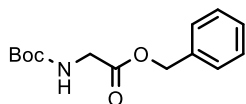
(*tert*-Butoxycarbonyl)glycine **70**



To a solution of glycine HCl **69** (2.58 g, 34.42 mmol) in H<sub>2</sub>O/dioxane (1:1, 88 mL) (Boc)<sub>2</sub>O (11.27 g, 51.62 mmol) and triethylamine (3.46 g, 34.42 mmol) were added, and the resulting mixture was stirred at room temperature for 16h. Then the solvent was removed under reduced pressure, and the residue was treated with a 2N HCl solution (~ pH 2) and the resulting aqueous

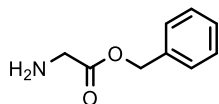
phase was extracted with EtOAc. The organic phase was dried over anhydrous  $\text{Na}_2\text{SO}_4$ , filtered and solvent was removed under reduced pressure. Compound **70** was obtained as a white solid and was used in the next step without further purification. Yield: 100%.  $^1\text{H NMR}$  ( $\text{CDCl}_3$ )  $\delta$ : 1.48 (s, 9H), 3.93 (brs, 1H), 3.99 (d, 2H,  $J=4.0$  Hz), 5.08 (brs, 1H).

*Benzyl (tert-butoxycarbonyl)glycinate 71*



To a solution of (*tert*-butoxycarbonyl)glycine **70** (2.58 g, 34.42 mmol) and  $\text{Cs}_2\text{CO}_3$  (16.82 g, 51.63 mmol) in  $\text{CH}_3\text{CN}$  (30 mL) a solution of benzyl bromide (5.89 g 34.42 mmol) in  $\text{CH}_3\text{CN}$  (15 mL) was slowly added, and the resulting mixture was stirred at room temperature for 16h. Then the solvent was removed under vacuum, and the resulting residue was taken up in EtOAc, and washed with brine. The residue was purified by column chromatography ( $\text{SiO}_2$ , *n*-hexane/EtOAc, 7:3 v/v, as eluent) to give compound **71** as a white solid. Yield: 100%.  $^1\text{H NMR}$  ( $\text{CDCl}_3$ )  $\delta$ : 1.43 (s, 9H), 3.98 (d, 2H,  $J= 4.0$  Hz), 5.20 (s, 2H), 7.32-7.41 (m, 5H).

*Benzyl glycinate 65*



To a solution of benzyl(*tert*-butoxycarbonyl)glycinate **71** (4.80 g, 18.1 mmol) in DCM (10 mL) trifluoroacetic acid (2.06 g, 18.1 mmol) was added and the resulting mixture was stirred at room temperature for 1h. The resulting residue was taken up in EtOAc, washed with a saturated solution of  $\text{Na}_2\text{CO}_3$ , and the organic extracts was dried ( $\text{Na}_2\text{SO}_4$ ), filtered, and concentrated under reduced pressure to obtain the compound **65** as a pale yellow oil. Yield: 64%.  $^1\text{H NMR}$  ( $\text{DMSO-d}_6$ ): 2.27 (s, 2H), 3.91 (s, 2H), 5.25 (s, 2H), 7.37 (m, 5H).

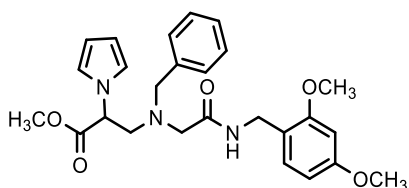
**5.6.10 General procedure for the synthesis of 46a-c**

To a solution of **68** (1 eq) in DMF (5 mL) HOBt (2 eq), HBTU (2 eq) and DIPEA (2.5 eq) were added, and the resulting mixture was stirred for 20 min at room temperature. Then the

## Chapter 5

appropriate amine (1.5 eq) was added, and the resulting mixture was stirred at room temperature overnight. The solvent was removed under reduced pressure, and the resulting residue was taken up in EtOAc and washed with brine. The organic phase was dried (Na<sub>2</sub>SO<sub>4</sub>), filtered, and concentrated under reduced pressure. The residue was purified by column chromatography (SiO<sub>2</sub>, EtOAc/*n*-hexane as eluent), and recrystallized from EtOAc/*n*-hexane to give the title compounds in good yields.

(±)-Methyl 3-(benzyl(2-((2,4-dimethoxybenzyl)amino)-2-oxoethyl)amino)-2-(1*H*-pyrrol-1-yl)propanoate **46a**



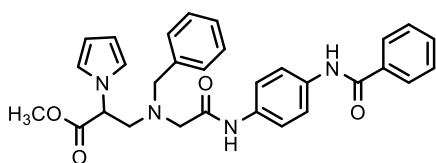
Colourless oil. Yield: 78%. <sup>1</sup>HNMR (CDCl<sub>3</sub>) δ: 3.09-3.23 (m, 4H), 3.50-3.68 (m, 5H), 3.83 (s, 6H), 4.26-4.38 (m, 2H), 4.60 (brt, 1H, *J* = 8.2 Hz), 6.12 (t, 2H, *J* = 2.2 Hz), 6.43-6.48 (m, 2H), 6.58 (t, 2H, *J* = 2.2 Hz), 6.97 (m, 1H), 7.10 (m, 3H), 7.27 (m, 3H). HRMS (ESI) *m/z* [M+H]<sup>+</sup> calcd for [C<sub>26</sub>H<sub>32</sub>N<sub>3</sub>O<sub>5</sub>]<sup>+</sup> 466.2336, found 466.2362.

(±)-Methyl 3-(benzyl(2-((4-methoxybenzyl)amino)-2-oxoethyl)amino)-2-(1*H*-pyrrol-1-yl)propanoate **46b**



Colourless oil. Yield: 89%. <sup>1</sup>HNMR (CDCl<sub>3</sub>) δ: 3.24 (m, 4H), 3.59-3.84 (m, 8H), 4.30-4.35 (m, 2H), 4.69 (m, 1H), 6.14 (m, 2H), 6.59 (m, 2H), 6.81-6.88 (m, 3H), 7.09-7.15 (m, 4H), 7.28 (m, 3H). HRMS (ESI) *m/z* [M+H]<sup>+</sup> calcd for [C<sub>25</sub>H<sub>30</sub>N<sub>3</sub>O<sub>4</sub>]<sup>+</sup> 436.2230, found 436.2231.

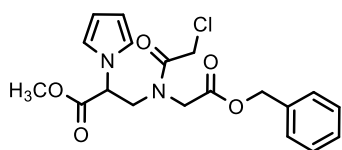
(±)-Methyl 3-((2-((4-benzamidophenyl)amino)-2-oxoethyl)(benzyl)amino)-2-(1*H*-pyrrol-1-yl)propanoate **46c**



White solid. Yield: 56%.  $^1\text{H NMR}$  ( $\text{CDCl}_3$ )  $\delta$ : 3.24-3.39 (m, 4H), 3.67-3.81 (m, 5H), 4.79 (brs, 1H), 6.23 (t, 2H,  $J=2.1$  Hz), 6.68 (t, 2H,  $J=2.2$  Hz), 7.23 (d, 2H,  $J=7.1$  Hz), 7.30-7.38 (m, 4H), 7.50-7.63 (m, 6H), 7.84 (brs, 1H), 7.89-7.91 (m, 2H), 8.54 (brs, 1H). HRMS (ESI)  $m/z$   $[\text{M}+\text{H}]^+$  calcd for  $[\text{C}_{30}\text{H}_{31}\text{N}_4\text{O}_4]^+$  511.2340, found 511.2332.

### 5.6.11 Synthesis of 46d,e

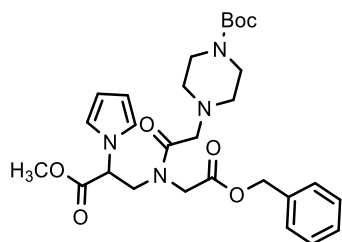
( $\pm$ )-Methyl-3-(*N*-(2-(benzyloxy)-2-oxoethyl)-2-chloroacetamido)-2-(1*H*-pyrrol-1-yl)propanoate **72**



To a solution of methyl 3-((2-(benzyloxy)-2-oxoethyl)amino)-2-(1*H*-pyrrol-1-yl)propanoate **66b** (0.588 g, 1.86 mmol) in dry DCM (10 mL), dry triethylamine (0.376 g, 3.72 mmol) and chloroacetyl chloride (0.315 g, 2.79 mmol) were added, and the resulting mixture was stirred at room temperature. After 1.5h, the residue was diluted in DCM and transferred to a separatory funnel. The resulting organic phase was extracted in  $\text{H}_2\text{O}$ , dried over anhydrous  $\text{Na}_2\text{SO}_4$ , filtered and the solvent was removed under reduced pressure. The resulting residue was purified by column chromatography ( $\text{SiO}_2$ , *n*-hexane/EtOAc 5:5 v/v as eluent) to give **72** as a yellow oil. Yield: 97%.  $^1\text{H NMR}$  ( $\text{CDCl}_3$ )  $\delta$ : (mix of two rotamers) 3.32 (d, 1H,  $J=18.8$  Hz), 3.47-3.60 (m, 2H), 3.71 (d, 1H,  $J=17.2$  Hz), 3.76 (s, 3H), 3.78 (s, 2H), 3.91-3.99 (m, 3H), 4.04 (s, 1H), 4.09 (m, 1H), 4.13 (m, 1H), 4.22 (d, 1H,  $J=17.2$  Hz), 4.29 (dd, 1H,  $J=14.1, 5.5$  Hz), 4.98 (dd, 1H,  $J=8.0, 4.2$  Hz), 5.07 (dd, 1H,  $J=9.0, 5.5$  Hz), 5.17 (s, 2H), 5.19 (s, 2H), 6.21 (t, 2H,  $J=2.2$  Hz), 6.24 (t, 2H,  $J=2.2$  Hz), 6.72 (t, 2H,  $J=2.2$  Hz), 6.82 (t, 2H,  $J=2.2$  Hz), 7.31-7.45 (m, 5H). HRMS (ESI)  $m/z$   $[\text{M}+\text{H}]^+$  calcd for  $[\text{C}_{19}\text{H}_{22}\text{ClN}_2\text{O}_5]^+$  393.1211, found 393,1207.

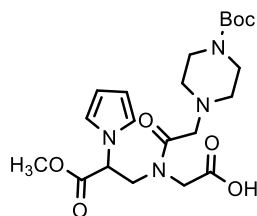
( $\pm$ )-*tert*-Butyl 4-(2-((2-(benzyloxy)-2-oxoethyl)(3-methoxy-3-oxo-2-(1*H*-pyrrol-1-yl)propyl)amino)-2-oxoethyl)piperazine-1-carboxylate **73**

## Chapter 5



To a solution of Boc-piperazine (0.151 g, 0.817 mmol) in acetonitrile (3 mL), triethylamine (0.207 g 2.04 mmol) was added and the resulting mixture was stirred at room temperature for 5 min. Then, methyl (±)-3-(*N*-(2-(benzyloxy)-2-oxoethyl)-2-chloroacetamido)-2-(1*H*-pyrrol-1-yl)propanoate **72** (0.268 g, 0.681 mmol) was added, and the resulting mixture was stirred at room temperature for 1.5h. The solvent was removed under reduced pressure, and the resulting residue was taken up in EtOAc and washed with brine. The organic phase was dried (Na<sub>2</sub>SO<sub>4</sub>), filtered, and concentrated under reduced pressure. The residue was purified by column chromatography (SiO<sub>2</sub>, EtOAc/*n*-hexane, 1:1 v/v, as eluent) to give **73** as a colorless oil. Yield: in 71%. <sup>1</sup>HNMR (CDCl<sub>3</sub>) δ: (mixture of two rotamers) 1.47 (s, 9H), 2.29 (t, 4H, *J*= 5.1 Hz), 2.44 (m, 2H), 2.87 (d, 1H, *J*= 13.7 Hz), 3.03 (m, 2H), 3.11 (d, 1H, *J*= 13.7 Hz), 3.24 (m, 4H), 3.31 (d, 1H, *J*= 18.5 Hz), 3.44 (m, 1H), 3.49-3.55 (m, 1H), 4.04 (m, 1H), 4.42-4.28 (m, 2H), 5.10-5.19 (m, 3H), 6.20 (t, 1H, *J*= 2.1 Hz), 6.21 (t, 1H, *J*= 2.1 Hz), 6.70 (t, 1H, *J*= 2.1 Hz), 6.73 (t, 1H, *J*= 2.2 Hz), 7.38 (m, 5H). HRMS (ESI) *m/z* [M+H]<sup>+</sup> calcd for [C<sub>28</sub>H<sub>39</sub>N<sub>4</sub>O<sub>7</sub>]<sup>+</sup> 543.2813, found 543.2792.

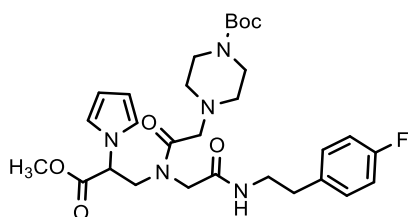
(±)-*N*-(2-(4-(*tert*-Butoxycarbonyl)piperazin-1-yl)acetyl)-*N*-(3-methoxy-3-oxo-2-(1*H*-pyrrol-1-yl)propyl)glycine **74**



A solution of (±)-*tert*-butyl 4-(2-((2-(benzyloxy)-2-oxoethyl)(3-methoxy-3-oxo-2-(1*H*-pyrrol-1-yl)propyl)amino)-2-oxoethyl)piperazine-1-carboxylate **73** (0.260 g, 0.480 mmol) palladium on carbon 10% (0.0288 g 0.480 mmol) and ammonium formate (0.303 g, 4.80 mmol)

in dry methanol (15 mL) was heated for 2.5h at reflux. After cooling to room temperature, the reaction mixture was diluted with MeOH and filtered on a celite pad to give **74** as a white solid in quantitative yield.  $^1\text{H-NMR}$  ( $\text{CDCl}_3$ )  $\delta$ : (mixture of two rotamers) 1.48 (s, 9H), 2.53 (m, 4H), 3.07-3.28 (m, 3H), 3.42-3.56 (m, 5H), 3.74 (s, 1H), 3.77 (s, 1H), 3.83 (m, 1H), 3.91-4.09 (m, 2H), 5.03-5.13 (m, 2H), 6.16 (t, 1H,  $J=2.1$  Hz), 6.20 (t, 1H,  $J=2.1$  Hz), 6.72 (t, 1H,  $J=2.1$  Hz), 6.79 (t, 1H,  $J=2.2$  Hz).

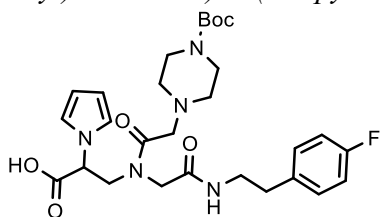
( $\pm$ )-*tert*-Butyl-4-(2-((2-((4-fluorophenethyl)amino)-2-oxoethyl)(3-methoxy-3-oxo-2-(1H-pyrrol-1-yl)propyl)amino)-2-oxoethyl)piperazine-1-carboxylate **46d**



To a solution of ( $\pm$ )-*N*-(2-(4-(*tert*-butoxycarbonyl)piperazin-1-yl)acetyl)-*N*-(3-methoxy-3-oxo-2-(1H-pyrrol-1-yl)propyl)glycine **74** (0.480 g, 0.217 mmol) in DMF (5 mL), HOBT (0.123 g, 0.960 mmol), HBTU (0.364 g, 0.960 mmol), 4-fluorophenethylamine (0.100 g, 0.720 mmol) and DIPEA (0.124 g, 0.960 mmol) were added, and the resulting mixture was stirred at room temperature overnight. The solvent was removed under reduced pressure, and the resulting residue was taken up in EtOAc and washed with brine. The organic phase was dried ( $\text{Na}_2\text{SO}_4$ ), filtered, and concentrated under reduced pressure. The residue was purified by column chromatography ( $\text{SiO}_2$ , EtOAc/MeOH, 9:1 v/v, as eluent) to give compound **46d** in 90% yield.  $^1\text{H-NMR}$  ( $\text{CDCl}_3$ )  $\delta$ : (mixture of two rotamers) 1.46 (s, 9H), 2.44 (m, 4H), 2.55 (d, 1H,  $J=14.8$  Hz), 2.75-2.82 (m, 3H), 3.08 (m, 1H), 3.15 (d, 1H,  $J=17.6$  Hz), 3.36-3.51 (m, 4H), 3.76-3.80 (m, 3H), 3.94-4.15 (m, 2H), 5.08 (m, 1H), 5.19 (m, 1H), 6.18 (m, 2H), 6.67 (m, 2H), 6.97 (m, 2H), 7.14 (m, 2H). HRMS (ESI)  $m/z$   $[\text{M}+\text{H}]^+$  calcd for  $[\text{C}_{29}\text{H}_{41}\text{FN}_5\text{O}_6]^+$  574.3035, found 574.3027.

## Chapter 5

(±)-3-(2-(4-(*tert*-Butoxycarbonyl)piperazin-1-yl)-*N*-(2-((4-fluorophenethyl)amino)-2-oxoethyl)acetamido)-2-(1*H*-pyrrol-1-yl)propanoic acid **46e**



To a solution of ester **46d** (0.480 g, 0.267 mmol) in methanol (5 mL), 4*N* NaOH (0.334 mL) was added, and the resulting mixture was stirred at room temperature for 1.5h. The solvent was removed under reduced pressure, then the residue was acidified with 2 M HCl (pH ~ 3), and extracted with EtOAc. The organic phase was dried (Na<sub>2</sub>SO<sub>4</sub>), filtered, and the solvent was removed under vacuum to give compound **46e** in quantitative yield. <sup>1</sup>HNMR (CDCl<sub>3</sub>) δ: (mixture of two rotamers) 2.10 (s, 9H), 2.81 (m, 4H), 3.21 (m, 2H), 3.44 (m, 4H), 3.50 (m, 2H), 3.94 (m, 4H), 4.15 (m, 2H), 5.15 (m, 1H), 6.79 (m, 1H), 6.91-6.99 (m, 3H), 7.14-7.19 (m, 2H). HRMS (ESI) *m/z* [M+H]<sup>+</sup> calcd for [C<sub>28</sub>H<sub>39</sub>FN<sub>5</sub>O<sub>6</sub>]<sup>+</sup> 560.2879, found 560.2853.

### 5.6.12 SPR binding assay

Human PCSK9 (residues 1-692) was acquired by Sino Biological (#29698-H08H). CM7 sensor chips, HBS-P+ buffer (0.01 M HEPES pH 7.4, 0.15 M NaCl, 0.05% v/v Surfactant P20), 1-ethyl-3-(3-diaminopropyl) carbodiimide hydrochloride (EDC), *N*-hydroxysuccinimide (NHS), ethanolamine (H<sub>2</sub>N(CH<sub>2</sub>)<sub>2</sub>OH), and regeneration solution were purchased from Cytiva.

The affinity of synthetic compounds for PCSK9 protein was determined at 25°C using Biacore T200 (Cytiva, Uppsala, Sweden) optical biosensor equipped with research-grade CM7 (Carboxy Methyl Dextran) sensor chip. Prior to the immobilization of the protein, a pH scouting was performed as follows. Solutions of 20 µg/mL of the ligand in 10 mM sodium acetate with pH values ranging from 4.47 to 6 were prepared and injected onto the surface. The PCSK9 protein (20 µg/mL in 10 mM sodium acetate, pH 4.59) was immobilized by using standard amine-coupling protocol obtaining densities of approximately 22000 RU. HBS-P+ buffer

supplemented with 2% DMSO was used as a running buffer and injected at a flow rate of 10  $\mu\text{L}/\text{min}$  over the chip to clean and equilibrate the immobilizes sensor surface, then a solvent correction was performed as indicated in Laboratory Guideline 29-0057-18 AA, GE Healthcare Life Sciences.

Each compound for binding affinity determination was initially dissolved in dimethyl sulfoxide to 10 mM as a stocking solution and serially diluted with a running buffer to certain concentrations (0.195-50  $\mu\text{M}$ ) when tested. Then, the test sample was injected at 25°C with a flow rate of 30  $\mu\text{L}/\text{min}$  for 90 s to contact with the protein immobilized on the chip, followed by dissociation from the chip for another 300 s. A regeneration step was not necessary.

The experiments were performed in duplicate. The SPR sensorgrams were solvent corrected, reference and buffer subtracted, and analyzed with BIA evaluation software (v2.02) provided with the Biacore T200 instrument (Cytiva) to determine  $K_D$  values. PEP 2-8 was tested as a positive control (0.078-5  $\mu\text{M}$ ).

## Chapter 5

### References

1. Xu, S.; Luo, S.; Zhu, Z.; Xu, J. Small molecules as inhibitors of PCSK9: current status and future challenges. *Eur. J. Med. Chem.* **2019**, *162*, 212–233. doi: 10.1016/j.ejmech.2018.11.011
2. Scott, D. E.; Bayly, A. R.; Abell, C.; Skidmore, J. Small molecules, big targets: drug discovery faces the protein-protein interaction challenge. *Nat. Rev. Drug Discov.* **2016**, *15*(8), 533–550. doi: 10.1038/nrd.2016.29
3. Loughlin, W. A.; Tyndall, J. D.; Glenn, M. P.; Hill, T. A.; Fairlie, D. P. Update 1 of: Beta-strand mimetics. *Chem. Rev.* **2010**, *110*(6), PR32–PR69. doi: 10.1021/cr900395y
4. Smith, M. C.; Gestwicki, J. E. Features of protein-protein interactions that translate into potent inhibitors: topology, surface area and affinity. *Expert Rev. Mol. Med.* **2012**, *14*, e16. doi: 10.1017/erm.2012.10
5. Buchwald, P. Small-molecule protein-protein interaction inhibitors: therapeutic potential in light of molecular size, chemical space, and ligand binding efficiency considerations. *IUBMB Life* **2010**, *62*(10), 724–731. doi: 10.1002/iub.383
6. Wells, J. A.; McClendon, C. L. Reaching for high-hanging fruit in drug discovery at protein-protein interfaces. *Nature* **2007**, *450*(7172), 1001–1009. doi: 10.1038/nature06526
7. Milroy, L. G.; Grossmann, T. N.; Hennig, S.; Brunsveld, L.; Ottmann, C. Modulators of protein-protein interactions. *Chem. Rev.* **2014**, *114*(9), 4695–4748. doi: 10.1021/cr400698c
8. Kwon, H. J.; Lagace, T. A.; McNutt, M. C.; Horton, J. D.; Deisenhofer, J. Molecular basis for LDL receptor recognition by PCSK9. *Proc. Natl. Acad. Sci. U. S. A.* **2008**, *105*(6), 1820–5. doi: 10.1073/pnas.0712064105
9. Bottomley, M. J.; Cirillo, A.; Orsatti, L.; Ruggeri, L.; Fisher, T. S.; Santoro, J. C.; Cummings, R. T.; Cubbon, R. M.; Lo Surdo, P.; Calzetta, A.; Noto, A.; Baysarowich, J.; Mattu, M.; Talamo, F.; De Francesco, R.; Sparrow, C. P.; Sitlani, A.; Carfi, A. Structural and biochemical characterization of the wild type PCSK9-EGF(AB) complex and natural familial hypercholesterolemia mutants. *J. Biol. Chem.* **2009**, *284*(2), 1313–1323. doi: 10.1074/jbc.M808363200
10. Lo Surdo, P.; Bottomley, M. J.; Calzetta, A.; Settembre, E. C.; Cirillo, A.; Pandit, S.; Ni, Y. G.; Hubbard, B.; Sitlani, A.; Carfi, A. Mechanistic implications for LDL receptor degradation from the PCSK9/LDLR structure at neutral pH. *EMBO Rep.* **2011**, *12*(12), 1300–1305. doi: 10.1038/embor.2011.205
11. Sun, H.; Wang, J.; Liu, S.; Zhou, X.; Dai, L.; Chen, C.; Xu, Q.; Wen, X.; Cheng, K.; Sun, H.; Yuan, H. Discovery of novel small molecule inhibitors disrupting the PCSK9-LDLR interaction. *J. Chem. Inf. Model.* **2021**, *61*(10), 5269–5279. doi: 10.1021/acs.jcim.1c00521
12. Zhang, Y.; Eigenbrot, C.; Zhou, L.; Shia, S.; Li, W.; Quan, C.; Tom, J.; Moran, P.; Di Lello, P.; Skelton, N. J.; Kong-Beltran, M.; Peterson, A.; Kirchhofer, D. Identification of a small peptide that inhibits PCSK9 protein binding to the low density lipoprotein receptor. *J. Biol. Chem.* **2014**, *289*(2), 942–955. doi: 10.1074/jbc.M113.514067

13. Lammi, C.; Zanoni, C.; Aiello, G.; Arnoldi, A.; Grazioso, G. Lupin peptides modulate the protein-protein interaction of PCSK9 with the low density lipoprotein receptor in HepG2 cells. *Sci. Rep.* **2016**, *6*, 29931. doi: 10.1038/srep29931
14. Stucchi, M.; Grazioso, G.; Lammi, C.; Manara, S.; Zanoni, C.; Arnoldi, A.; Lesma, G.; Silvani, A. Disrupting the PCSK9/LDLR protein-protein interaction by an imidazole-based minimalist peptidomimetic. *Org. Biomol. Chem.* **2016**, *14*(41), 9736–9740. doi: 10.1039/c6ob01642a
15. Zhang, Y.; Ultsch, M.; Skelton, N. J.; Burdick, D. J.; Beresini, M. H.; Li, W.; Kong-Beltran, M.; Peterson, A.; Quinn, J.; Chiu, C.; Wu, Y.; Shia, S.; Moran, P.; Di Lello, P.; Eigenbrot, C.; Kirchlofer, D. Discovery of a cryptic peptide-binding site on PCSK9 and design of antagonists. *Nat. Struct. Mol. Biol.* **2017**, *24*(10), 848–856. doi: 10.1038/nsmb.3453
16. Taechalertrpaisarn, J.; Zhao, B.; Liang, X.; Burgess, K. Small molecule inhibitors of the PCSK9-LDLR interaction. *J. Am. Chem. Soc.* **2018**, *140*(9), 3242–3249. doi: 10.1021/jacs.7b09360
17. Pettersen, D.; Fjellström, O. Small molecule modulators of PCSK9-A literature and patent overview. *Bioorg. Med. Chem. Lett.* **2018**, *28*(7), 1155–1160. doi: 10.1016/j.bmcl.2018.02.046
18. Abdel-Meguid, S. S.; Elshourbagy, N.; Meyers, H.; Mousa, S. A. Anti-protein convertase subtilisin kexin type 9 (anti-PCSK9) compounds and methods of using the same in the treatment and/or prevention of cardiovascular diseases. World Patent WO2014150326A1, September 25, **2014**.
19. Abou-Gharbia, M. PCSK9 inhibitors and methods of use thereof. World Patent WO2016040305A1, March 17, **2016**.
20. Barta, T. E.; Bourne, J.W.; Monroe, K. D.; Meuhlemann, M. M. Composition and methods of use of small molecules as binding ligands for the modulation of proprotein convertase subtilisin/kexin type 9 (PCSK9) protein activity. World Patent WO2016029037A1, February 25, **2016**.
21. Min, D. K.; Lee, H. S.; Lee, N.; Lee, C. J.; Song, H. J.; Yang, G. E.; Yoon, D.; Park, S. W. In silico screening of chemical libraries to develop inhibitors that hamper the interaction of PCSK9 with the LDL receptor. *Yonsei Med. J.* **2015**, *56*(5), 1251–1257.
22. Lammi, C.; Sgrignani, J.; Arnoldi, A.; Lesma, G.; Spatti, C.; Silvani, A.; Grazioso, G. Computationally driven structure optimization, synthesis, and biological evaluation of imidazole-based proprotein convertase subtilisin/kexin 9 (PCSK9) inhibitors. *J. Med. Chem.* **2019**, *62*(13), 6163–6174. doi: 10.1021/acs.jmedchem.9b00402
23. Evison, B. J.; Palmer, J. T.; Lambert, G.; Treutlein, H.; Zeng, J.; Nativel, B.; Chemello, K.; Zhu, Q.; Wang, J.; Teng, Y.; Tang, W.; Xu, Y.; Rathi, A. K.; Kumar, S.; Suchowerska, A. K.; Parmar, J.; Dixon, I.; Kelly, G. E.; Bonnar, J. A. Small molecule inhibitor of PCSK9 that antagonizes LDL receptor binding via interaction with a cryptic PCSK9 binding groove. *Bioorg. Med. Chem.* **2020**, *28*(6), 115344. doi: 10.1016/j.bmc.2020.115344
24. Zhang, D. W.; Garuti, R.; Tang, W. J.; Cohen, J. C.; Hobbs, H. H. Structural requirements for PCSK9-mediated degradation of the low-density lipoprotein receptor. *Proc. Natl. Acad. Sci. U. S. A.* **2008**, *105*(35), 13045–13050. doi: 10.1073/pnas.0806312105

## **Chapter 5**

25. Chorba, J. S.; Shokat, K. M. The proprotein convertase subtilisin/kexin type 9 (PCSK9) active site and cleavage sequence differentially regulate protein secretion from proteolysis. *J. Biol. Chem.* **2014**, *289*(42), 29030–29043. doi: 10.1074/jbc.M114.594861
26. Nyrada - Biotechnology Company. Cardiovascular. **2022** <https://www.nyrada.com/site/Science/Cardiovascular>
27. Smith, K. M.; Bisset, G. M. F. General Synthesis of Hydrocarbon-Soluble Porphyrins. *J. Org. Chem.* **1979**, *44*, 2077-2081.
28. Campbell, C. T.; Kim, G. SPR microscopy and its applications to high-throughput analyses of biomolecular binding events and their kinetics. *Biomaterials* **2007**, *28*(15), 2380–2392. doi: 10.1016/j.biomaterials.2007.01.047
29. Fisher, T. S.; Lo Surdo, P.; Pandit, S.; Mattu, M.; Santoro, J. C.; Wisniewski, D.; Cummings, R. T.; Calzetta, A.; Cubbon, R. M.; Fischer, P. A.; Tarachandani, A.; De Francesco, R.; Wright, S. D.; Sparrow, C. P.; Carfi, A.; Sitlani, A. Effects of pH and low density lipoprotein (LDL) on PCSK9-dependent LDL receptor regulation. *J. Biol. Chem.* **2007**, *282*(28), 20502–20512. doi: 10.1074/jbc.M701634200
30. Tucker, T. J.; Embrey, M. W.; Alleyne, C.; Amin, R. P.; Bass, A.; Bhatt, B.; Bianchi, E.; Branca, D.; Bueters, T.; Buist, N.; Ha, S. N.; Hafey, M.; He, H.; Higgins, J.; Johns, D. G.; Kerekes, A. D.; Koeplinger, K. A.; Kuethe, J. T.; Li, N.; Murphy, B.; Walji, A. A. Series of novel, highly potent, and orally bioavailable next-generation tricyclic peptide PCSK9 inhibitors. *J. Med. Chem.* **2021**, *64*(22), 16770–16800. doi: 10.1021/acs.jmedchem.1c01599

# Conclusions



In this PhD thesis the development of new lipid-lowering agents has been described. In this regard, two approaches have been investigated: a) targeting LDLR expression, and b) inhibition of PCSK9/LDLR interaction.

For the first approach a small library of LDLR modulators was designed and synthesized, employing berberine (BBR) as lead compound, with the aim to improve its bioavailability, and define the minimal structural requirements to enhance its hypolipidemic action.

The cytotoxicity of a small set of synthesized BBR analogues was evaluated by MTT assay on HepG2 and HaCaT cell lines, using BBR as reference compound. Compounds **25a**, **31** and **18l** showed a better safety profile compared to BBR, and thus were selected to interrogate their inhibitory activity against total cholesterol (TCHO) and triglycerides (TG) on HepG2 cell line. Our results indicated that dimers **31** and **25a** were endowed with higher lipid-lowering activity compared to benzoxazepine **18l**. Compounds **31** and **18l**, as representative derivatives of two different class of compounds, were further investigated by qRT-PCR assay to assess their effects on LDLR expression. Both tested compounds enhanced LDLR expression *vs* control.

Currently a qRT-PCR analysis is in progress to assess the ability of our tested compounds to modulate SREBP1 and SREBP2 levels, given that the expression of LDLR is predominantly regulated at the transcriptional level through a negative feedback mainly involving SREBP proteins.

Overall, our results encourage further lead optimization process. In particular, the synthetic approach employed for benzoxazepine **18l**, and for dimers **31** and **25a** enables to explore a wide chemical space, extend SAR analysis and identify novel hits. Thus, compared to the natural lead BBR, these compounds are not only less cytotoxic, but also possess better potential of structure optimization for enhancing their lipid-lowering properties. Moreover, this structural simplification is putatively associated with a more favorable pharmacokinetic profile and drug-like properties with respect to BBR and, finally, could be useful to clarify the key structural

## Conclusions

motifs to be retained for a selective hypolipidemic activity. However, a deep investigation is necessary to identify the molecular target of our leads for a rational design of new analogues.

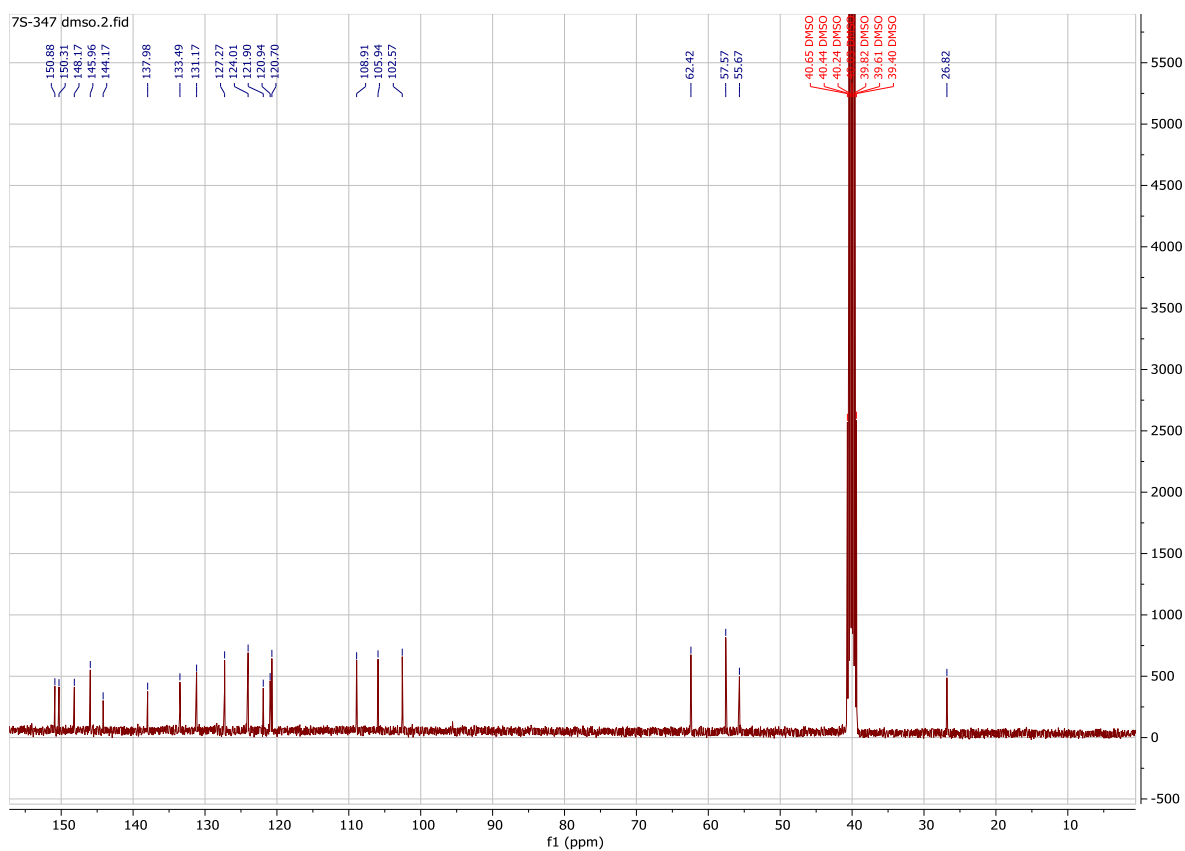
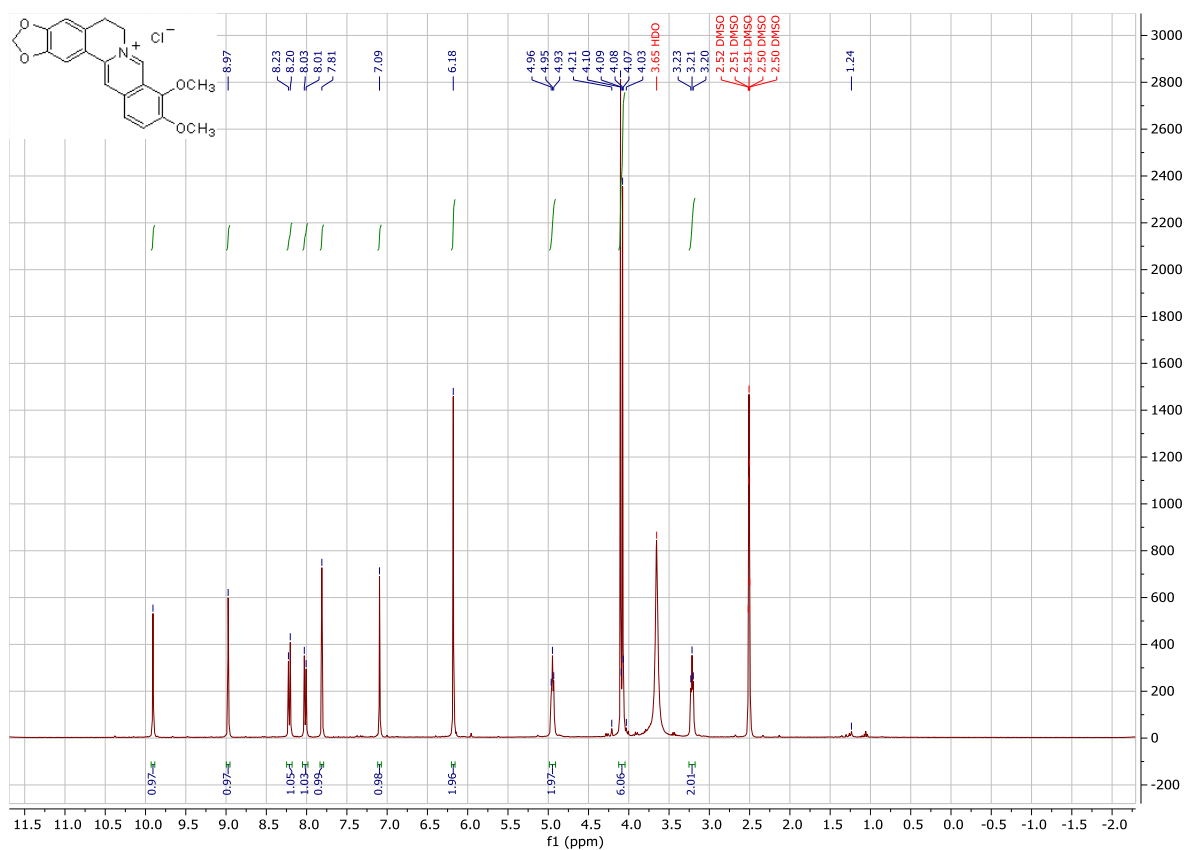
As a part of this research project, two sets of pyrrole derivatives were rationally designed in order to inhibit PCSK9/LDLR interaction. In general, targeting protein-protein interaction using small molecules has proven challenging given either the complexity of these highly dynamic systems or the wide, shallow, pocketless PPI interface itself. However, small molecules can disrupt PPI if they correctly mimic the topography and the nature of the side chains of so-called hot spot residues, i.e. functional residues which act as binding site anchors and stabilize the protein-protein complex. Although to date two PCSK9-blocking monoclonal antibodies (mAbs), alirocumab and evolocumab are in clinical use, the appeal of orally administrable small molecule inhibitors of PCSK9 over antibodies is rather clear, and not without reasons inhibitors with these features are regarded as the “Holy Grail” for many companies and institutions working in the field of hypolipidemic drugs.

Peptide Pep2-8, identified by Zhang and co-workers, is a good mimic of epidermal growth factor precursor homology domain A (EGF-A) of LDLR, and serves as a selective and potent PCSK9 inhibitor with an  $IC_{50}$  value of 0.8  $\mu$ M. For these reasons, the crystallographic structure of this peptide bound to PCSK9 (PDB code: 4NMX) has been chosen to carry out the structure-based drug design of our small set of pyrrole derivatives. Among them, compounds **44e**, **f**, **h-l** and **45h** were evaluated by SPR, and two pyrrole derivatives, **44f** and **45g**, reported  $K_D$  values of about 6 fold lower with respect to Pep2-8.

These preliminary results, although other *in vitro* assays are needed to appraise the overall potential of these compounds as PCSK9/LDLR inhibitors, provide important insights for the identification of new chemotypes with drug-like properties.

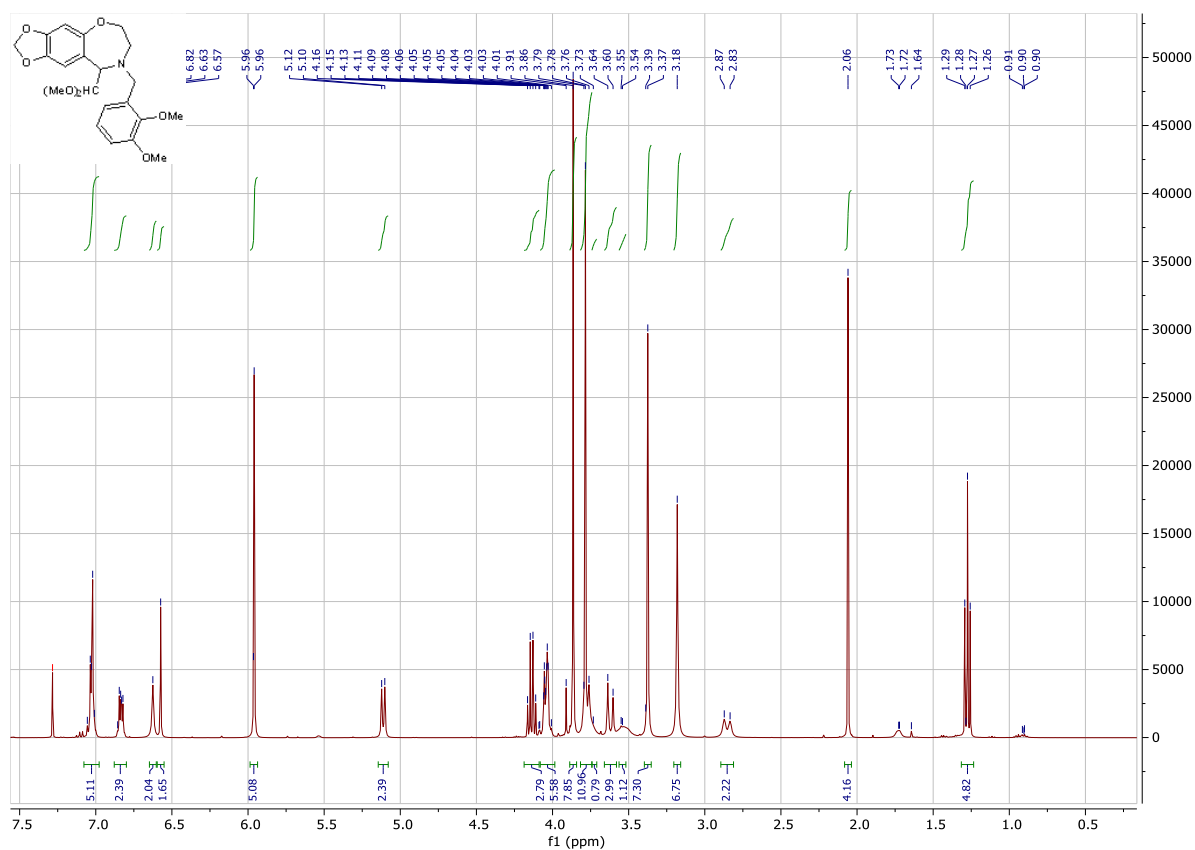
# Appendix



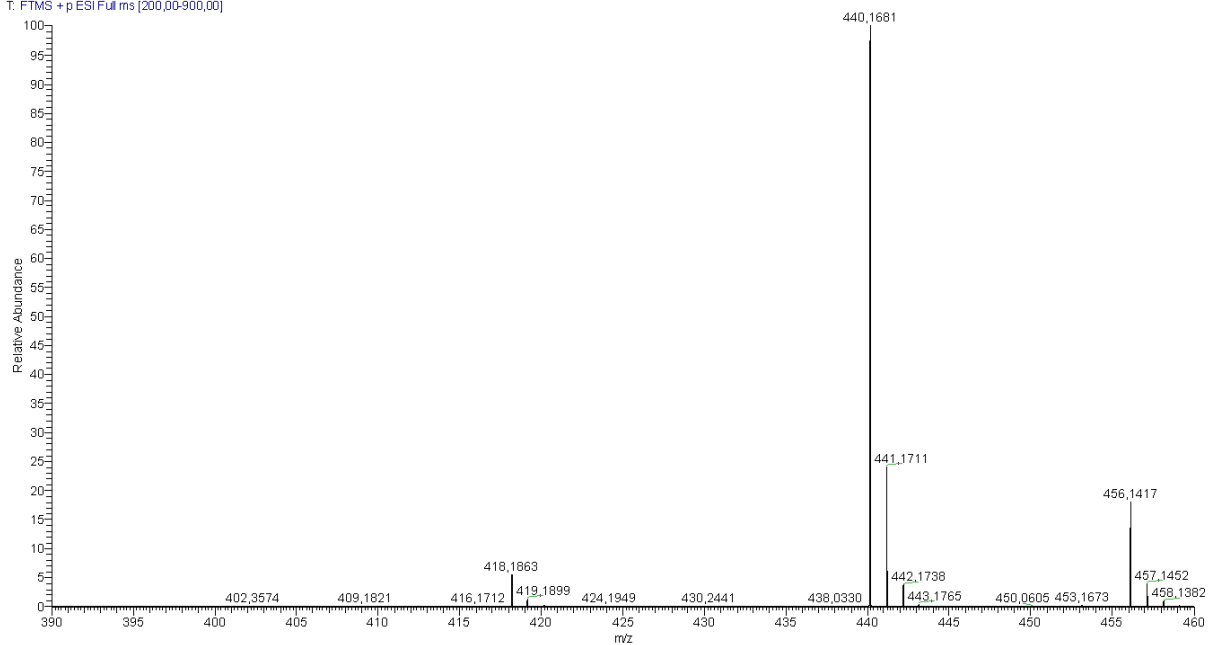


$^1\text{H}$ NMR (400 MHz,  $\text{DMSO-}d_6$ ) and  $^{13}\text{C}$  NMR (101 MHz,  $\text{DMSO-}d_6$ ) of **1** (BBR)

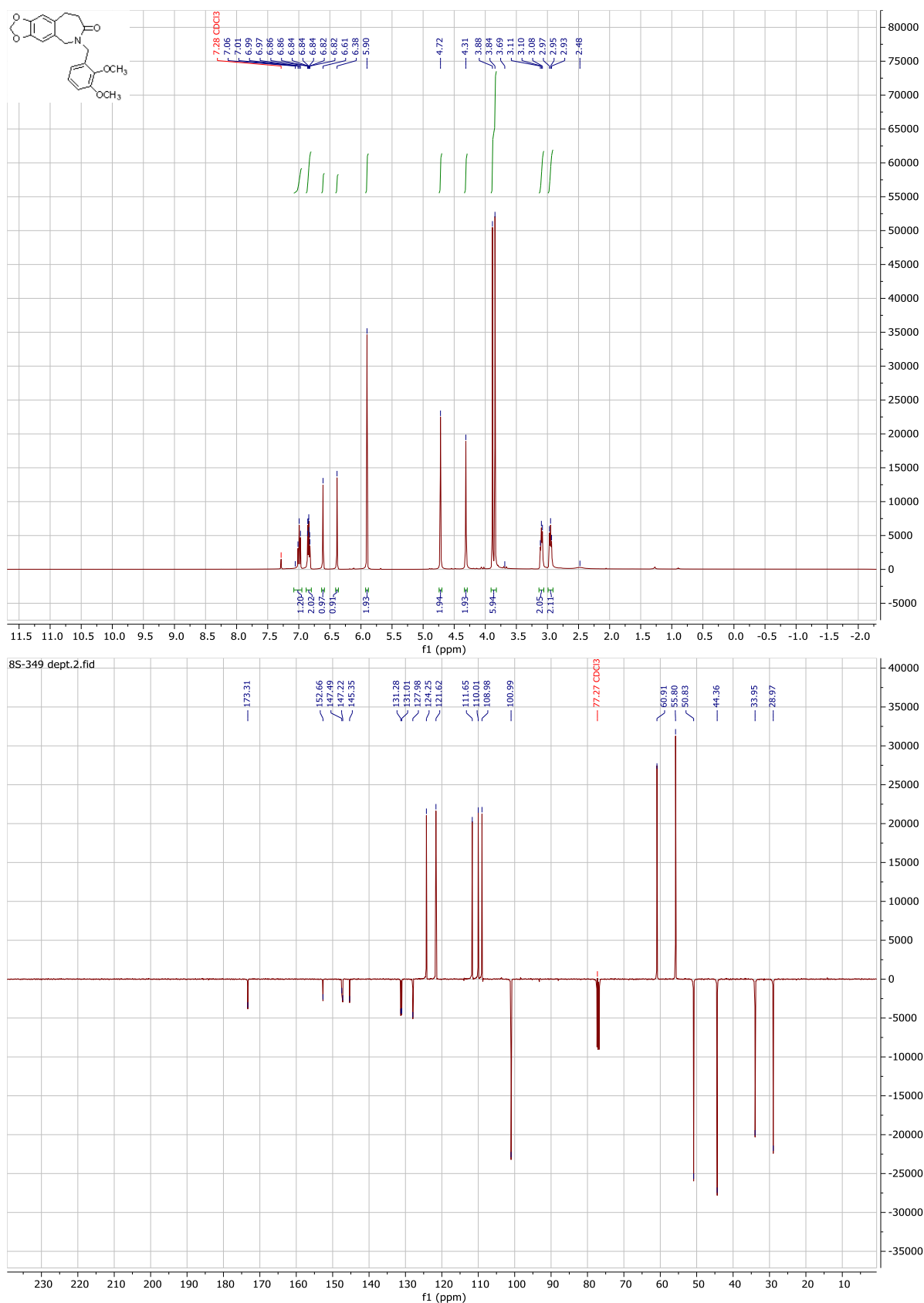
# Appendix



7S-480 #1 RT: 0.00 AV: 1 NL: 8,10E7  
T: FTMS + p ESI Full ms [200,00-900,00]

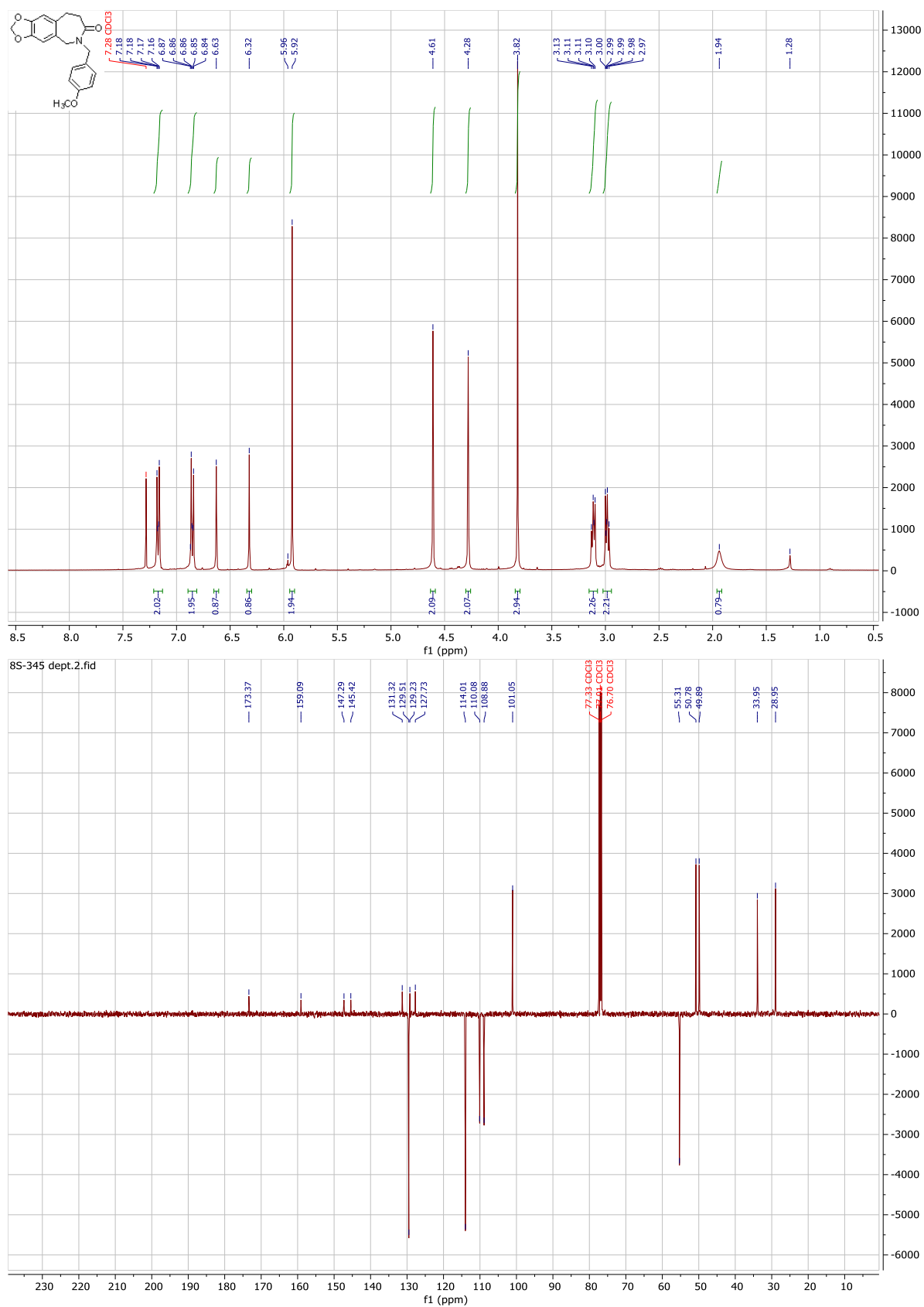


<sup>1</sup>H NMR (400 MHz, CDCl<sub>3</sub>) and HRMS (ESI) m/z of 17

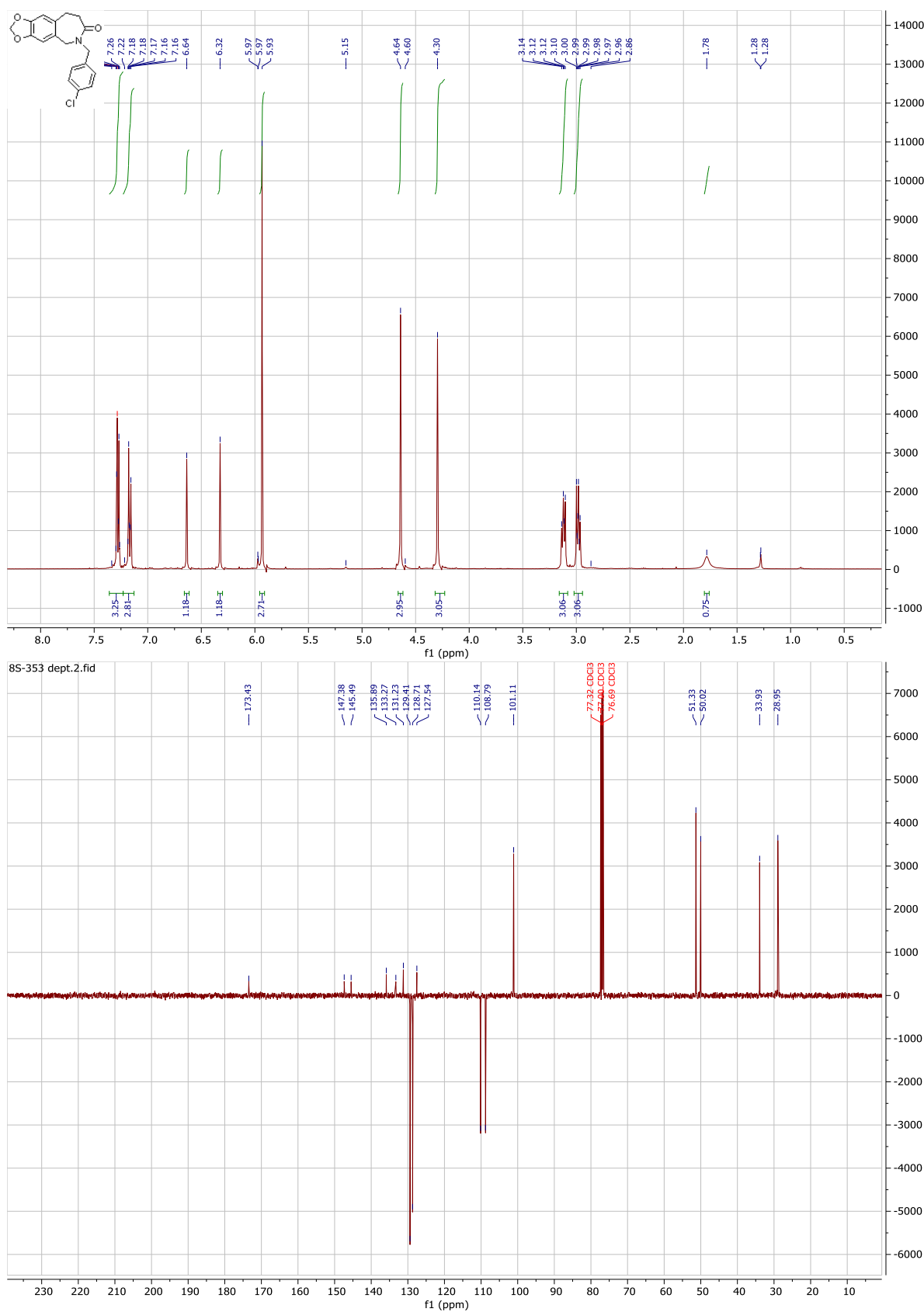


<sup>1</sup>H NMR (400 MHz, CDCl<sub>3</sub>) and <sup>13</sup>C DEPTQ NMR (101 MHz, CDCl<sub>3</sub>) of **18a**

# Appendix

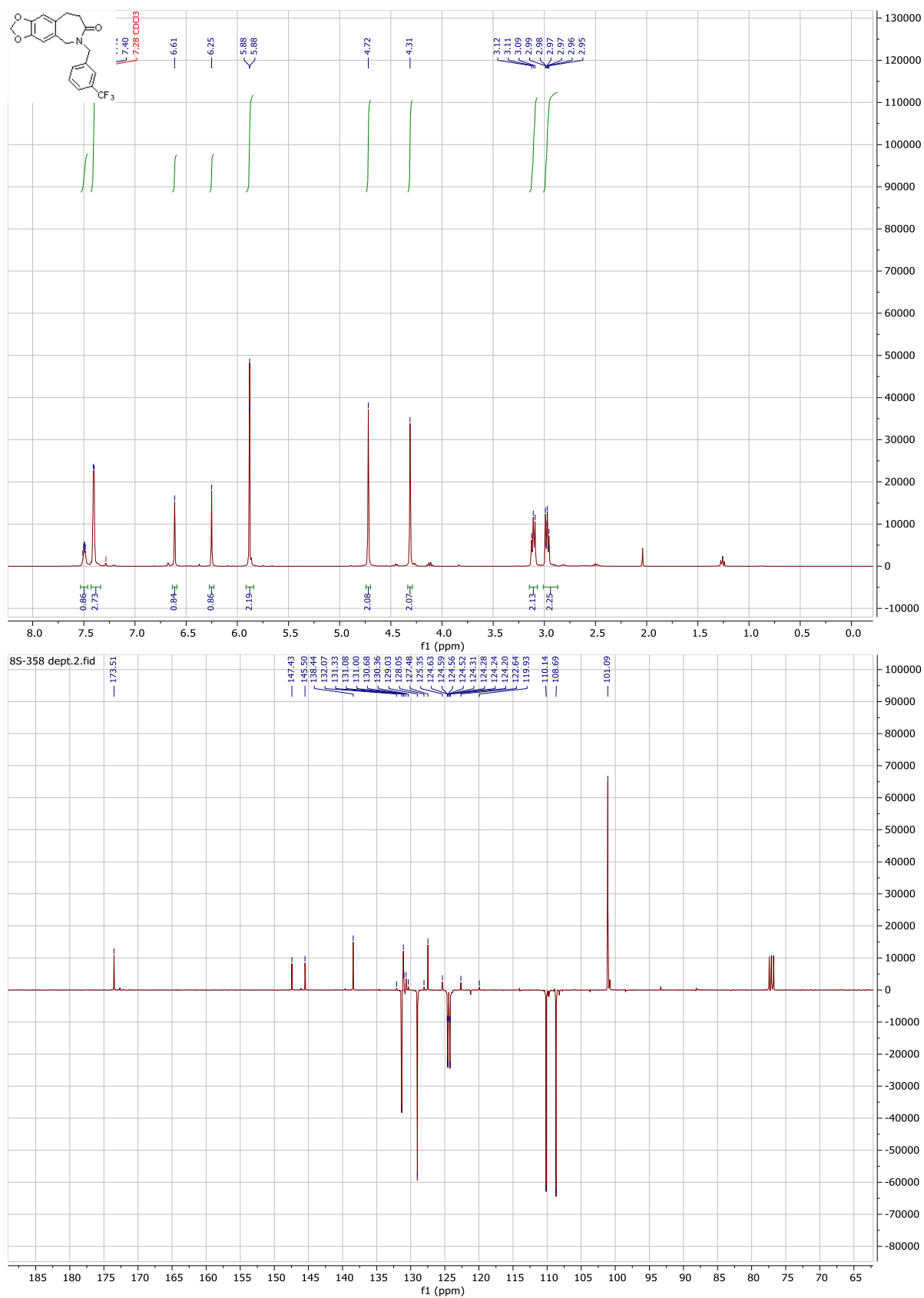


<sup>1</sup>H NMR (400 MHz, CDCl<sub>3</sub>) and <sup>13</sup>C DEPTQ NMR (101 MHz, CDCl<sub>3</sub>) of **18b**

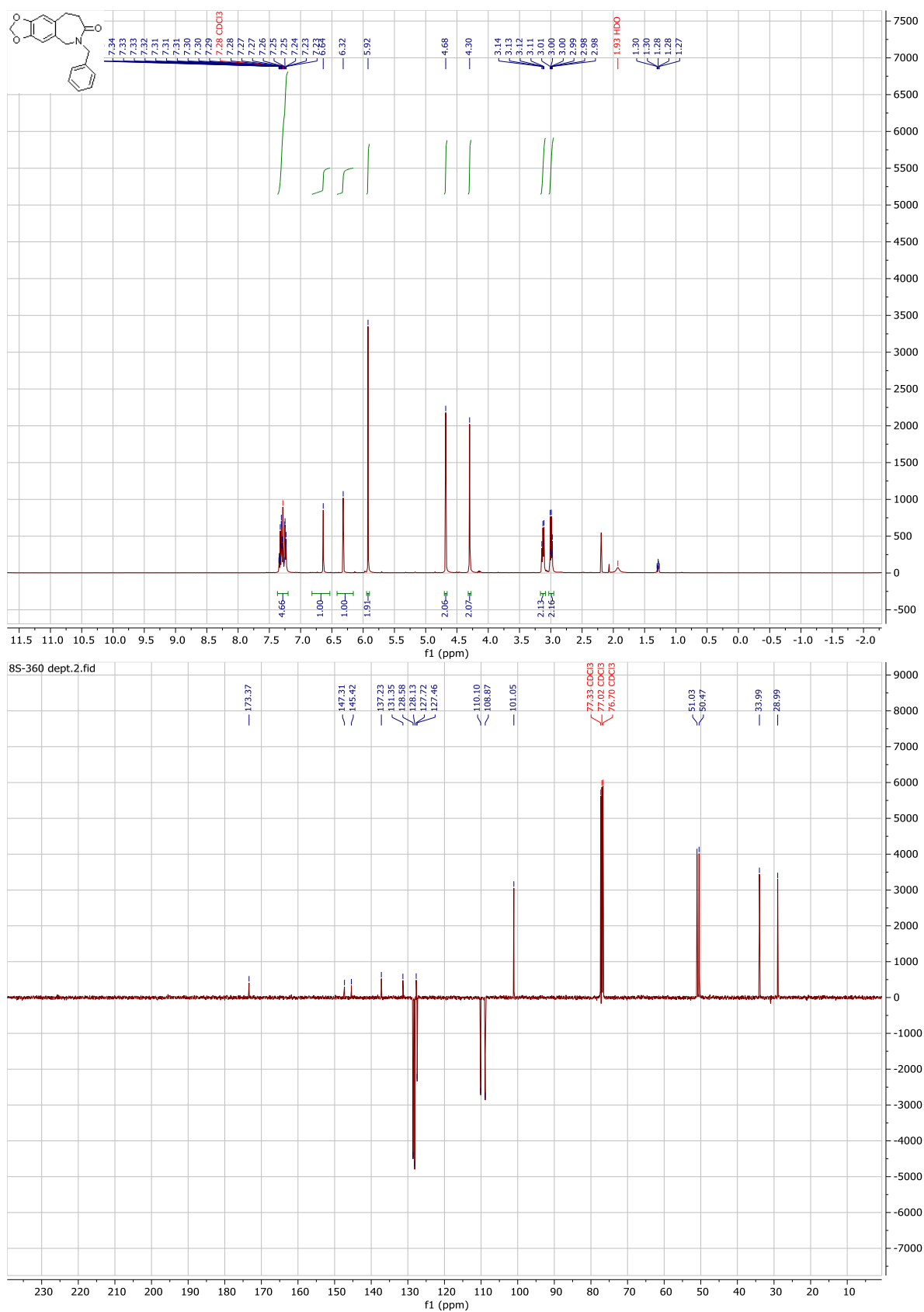


<sup>1</sup>H NMR (400 MHz, CDCl<sub>3</sub>) and <sup>13</sup>C DEPTQ NMR (101 MHz, CDCl<sub>3</sub>) of **18c**

# Appendix

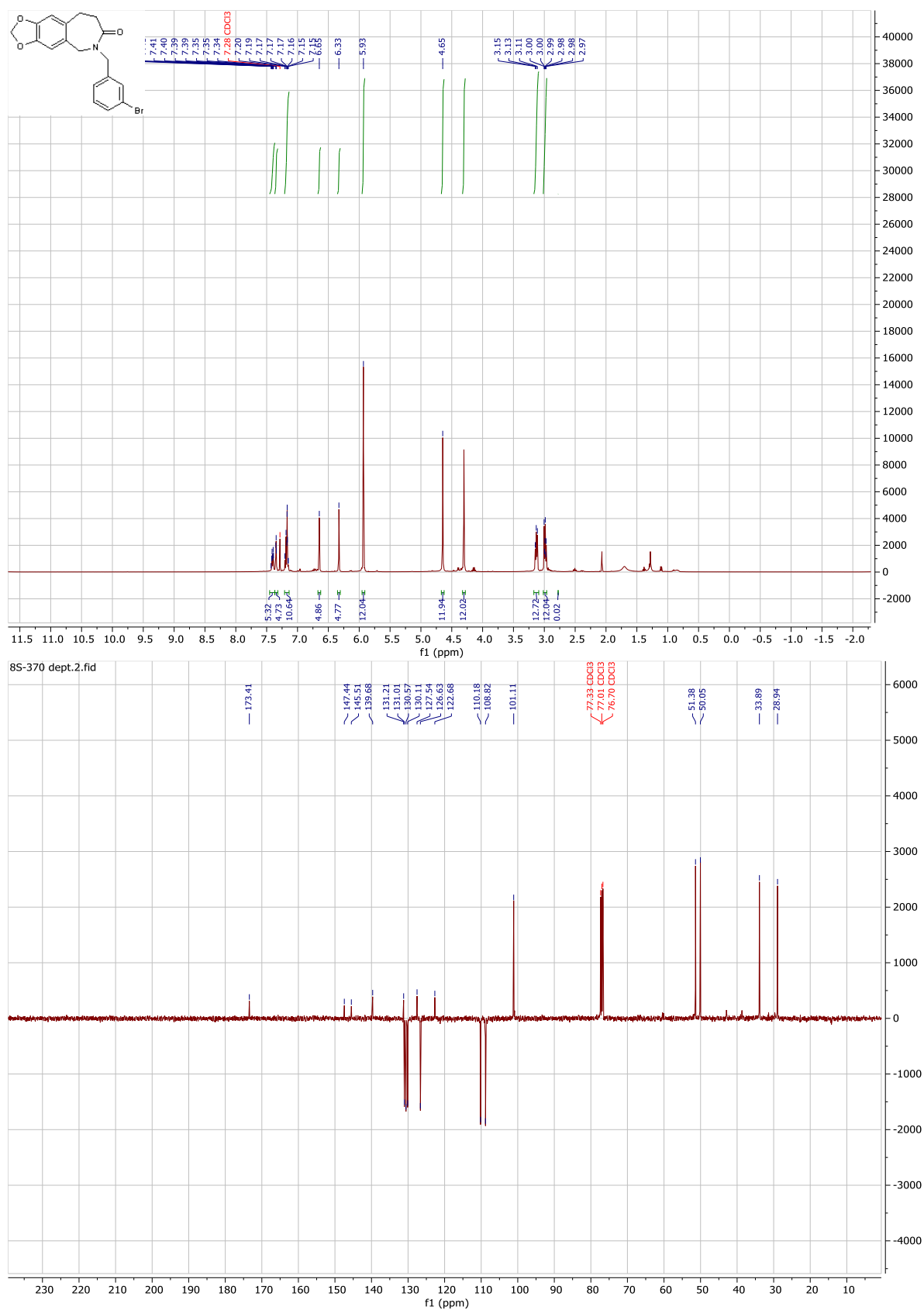


<sup>1</sup>H NMR (400 MHz, CDCl<sub>3</sub>) and <sup>13</sup>C DEPTQ NMR (101 MHz, CDCl<sub>3</sub>) of **18d**

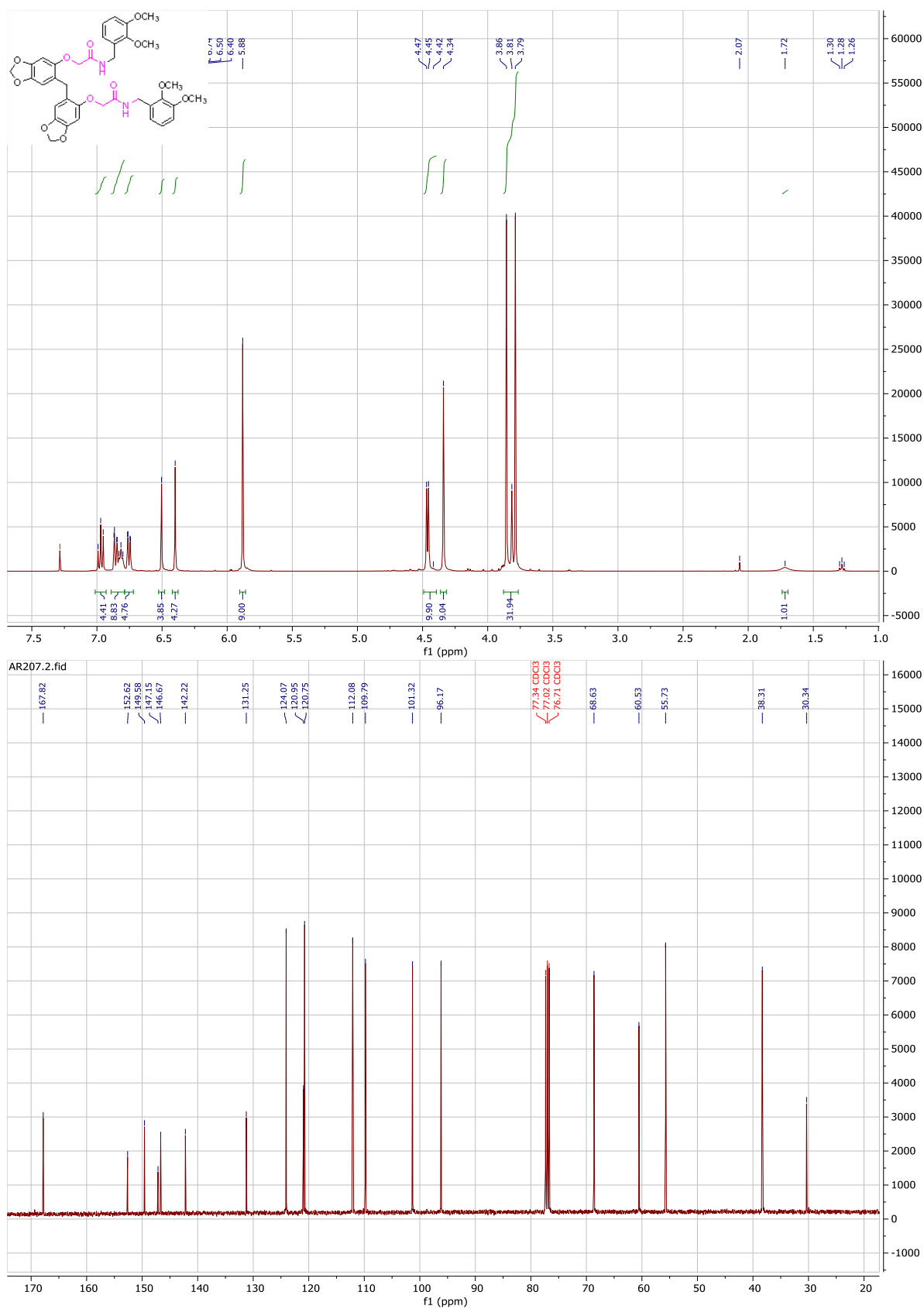


<sup>1</sup>H NMR (400 MHz, CDCl<sub>3</sub>) and <sup>13</sup>C DEPTQ NMR (101 MHz, CDCl<sub>3</sub>) of **18e**

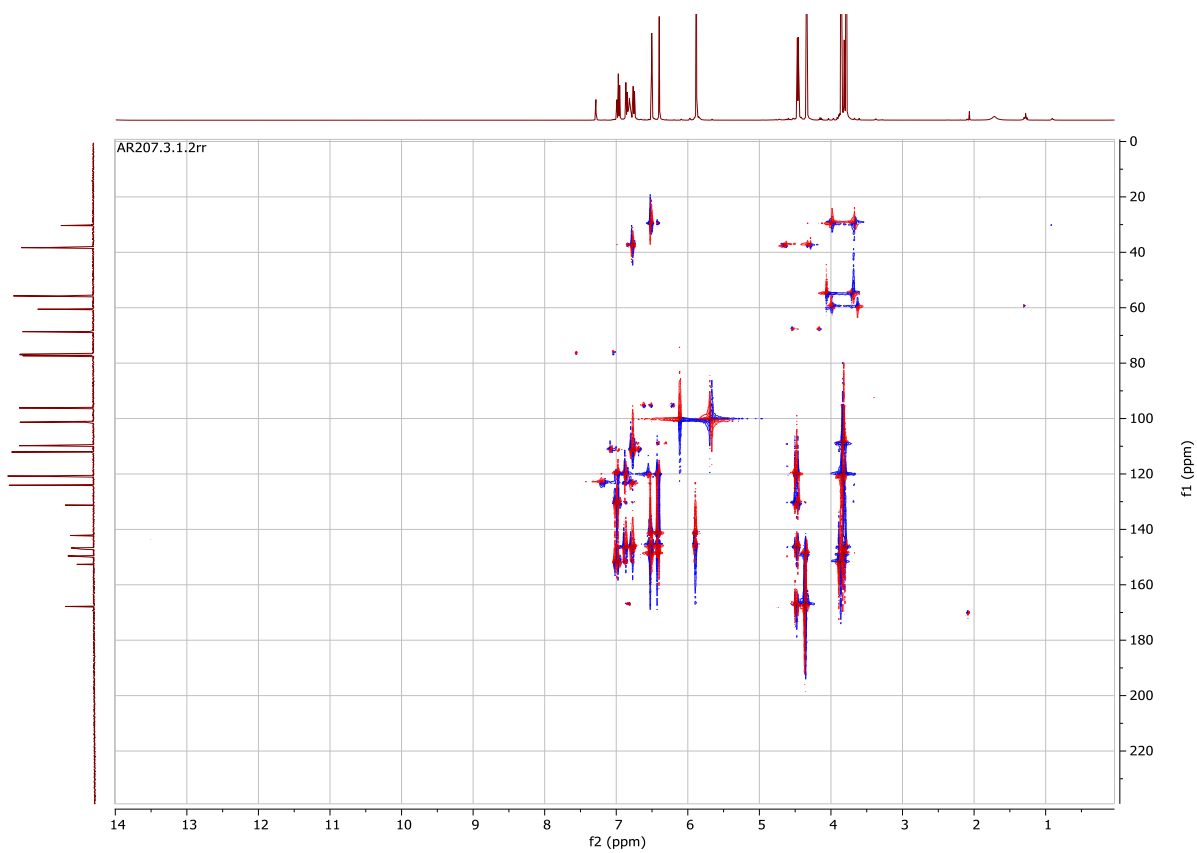
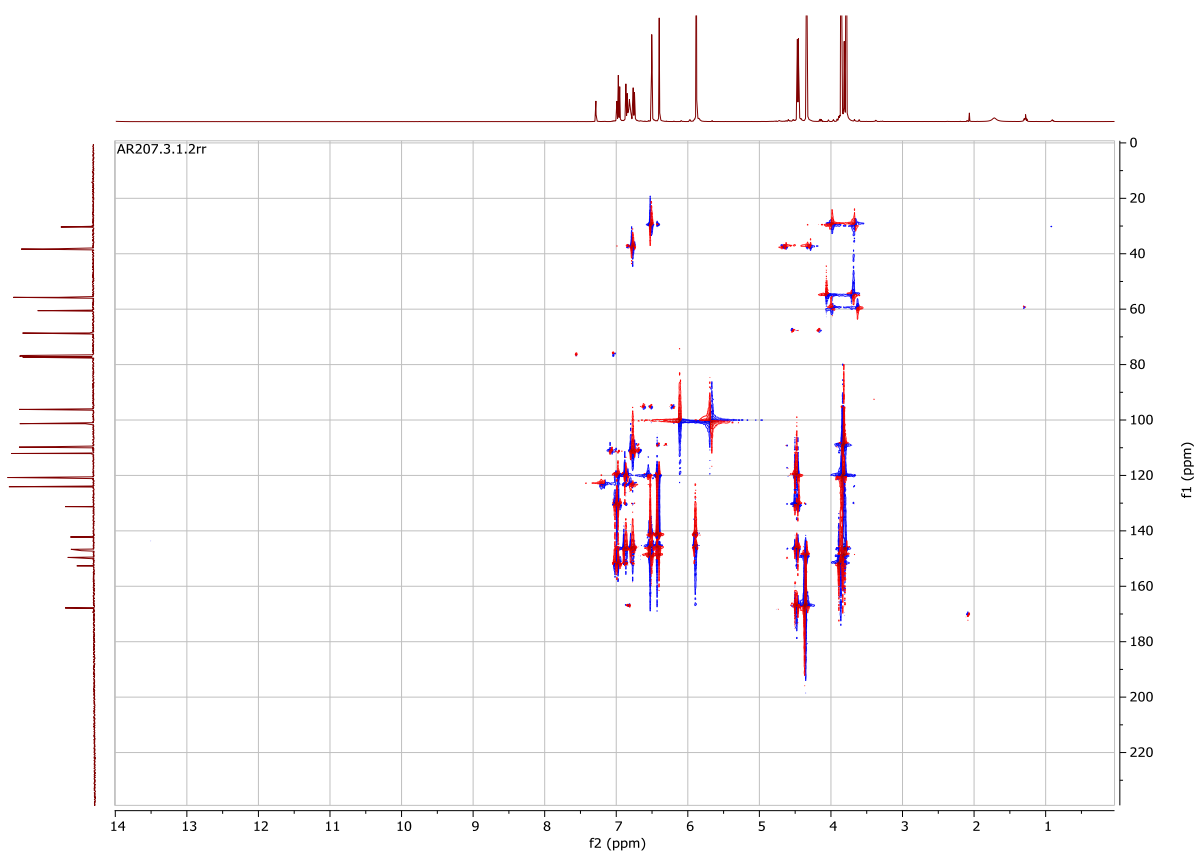
# Appendix



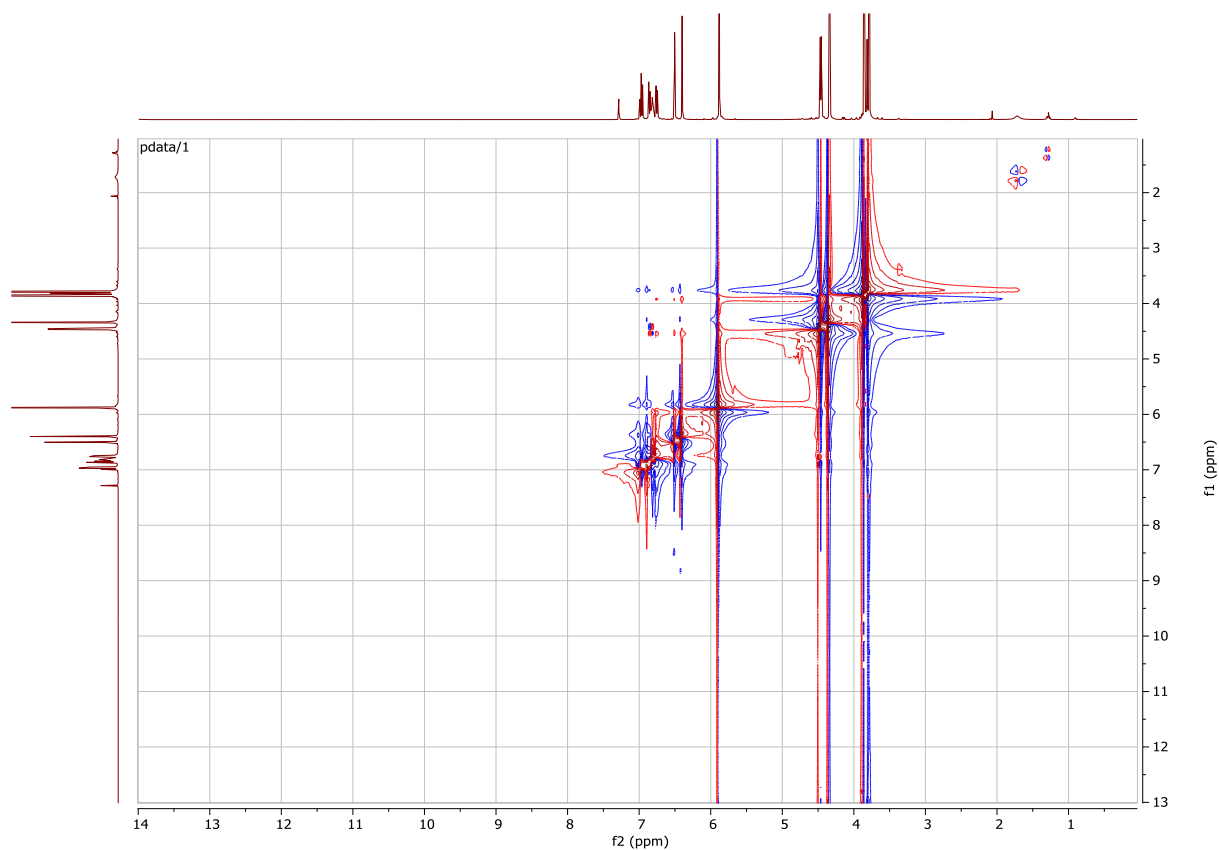
<sup>1</sup>H NMR (400 MHz, CDCl<sub>3</sub>) and <sup>13</sup>C DEPTQ NMR (101 MHz, CDCl<sub>3</sub>) of **18f**



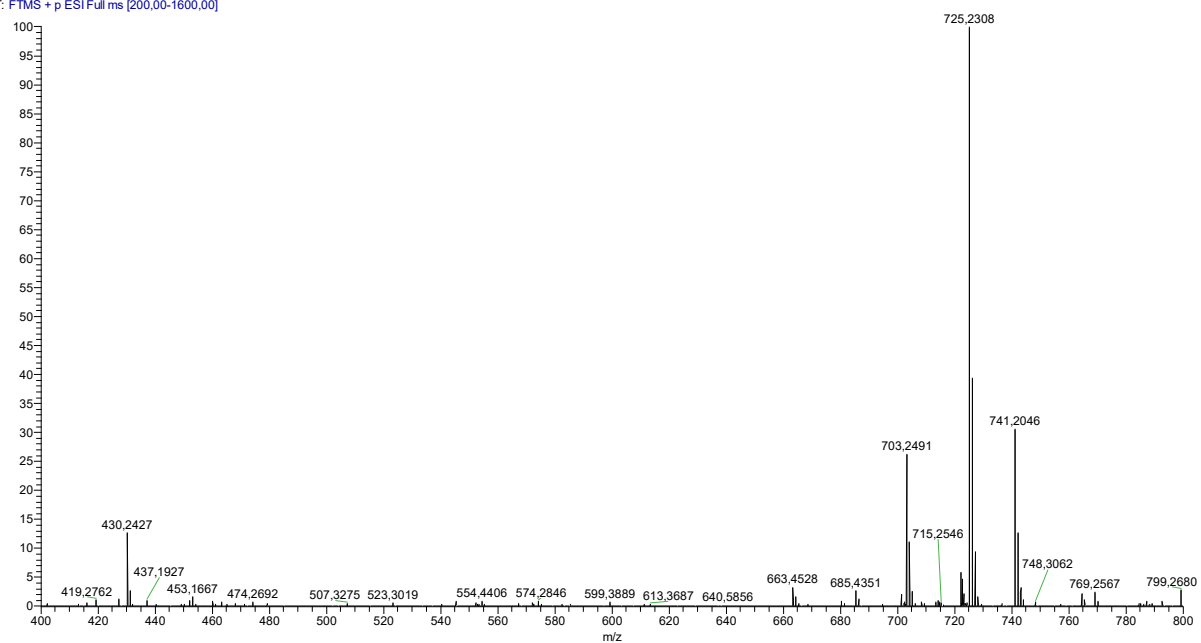
<sup>1</sup>H NMR (400 MHz, CDCl<sub>3</sub>) and <sup>13</sup>C DEPTQ NMR (101 MHz, CDCl<sub>3</sub>) of **25a**



HMBC and HSQC NMR ( $\text{CDCl}_3$ ) of **25a**

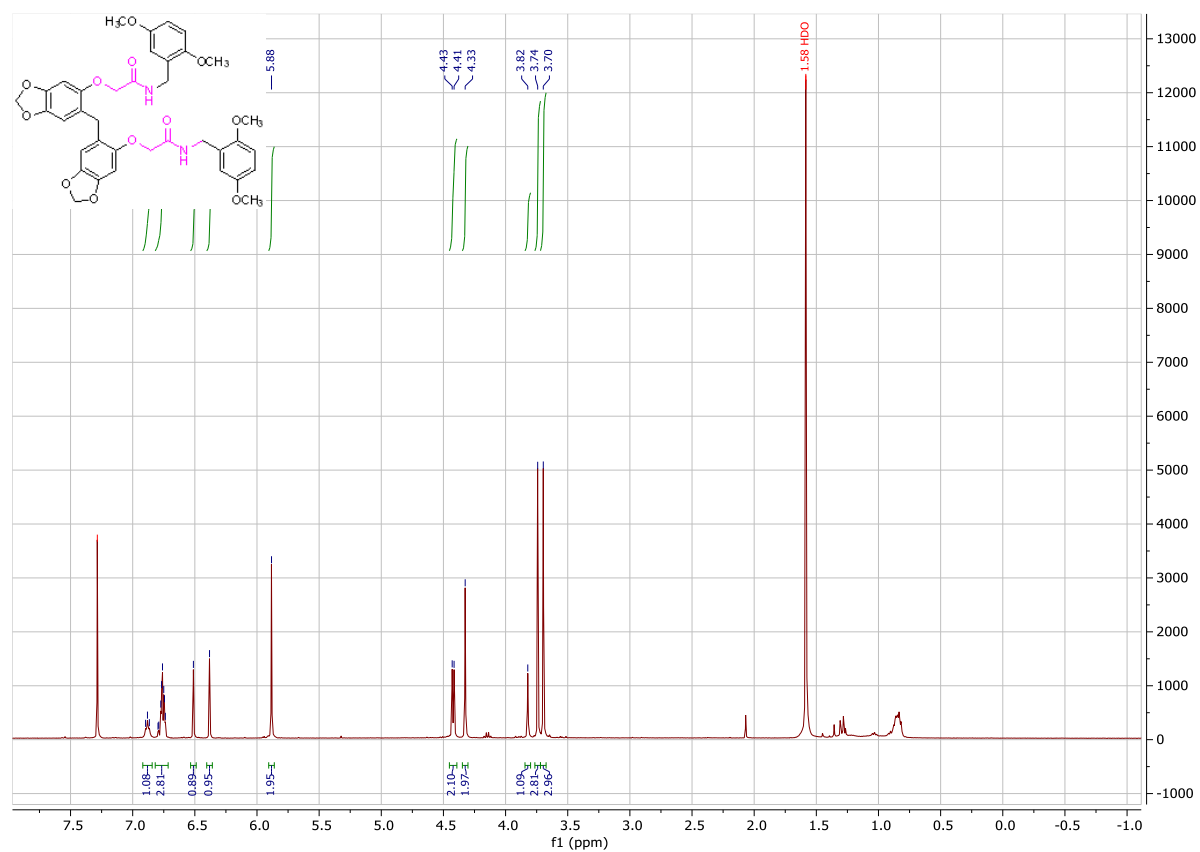


AR207\_Susy #1 RT: 0.00 AV: 1 NL: 2.82E7  
T: FTMS + p ESI Full ms [200.00-1600.00]

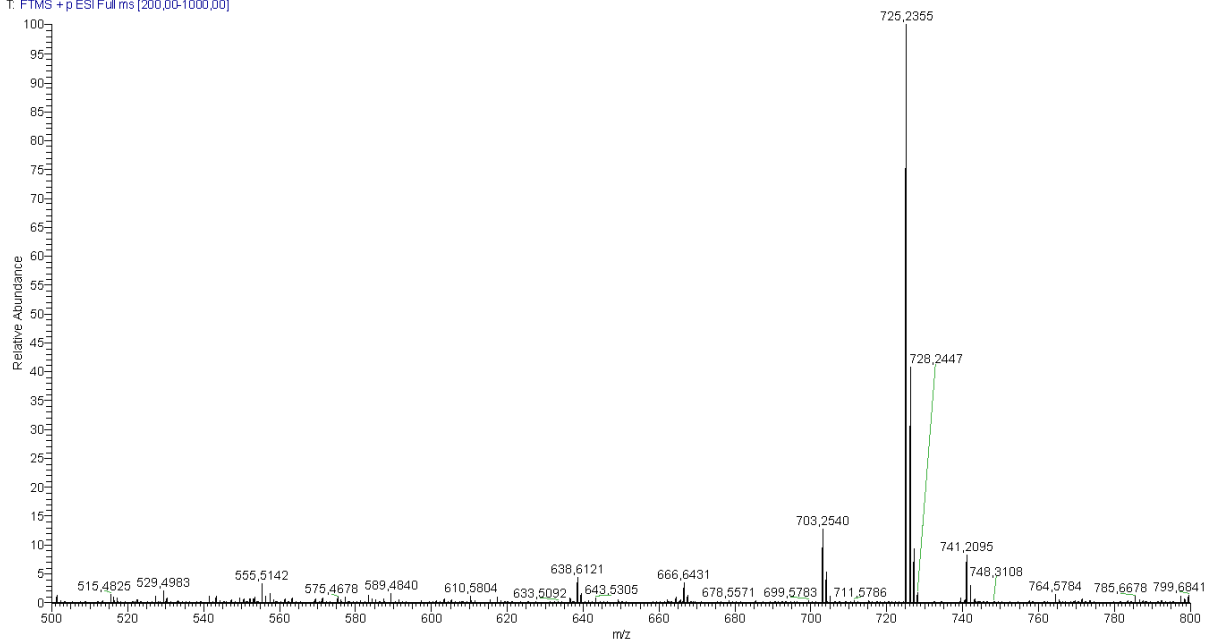


COSY NMR ( $\text{CDCl}_3$ ) and HRMS (ESI)  $m/z$  of **25a**

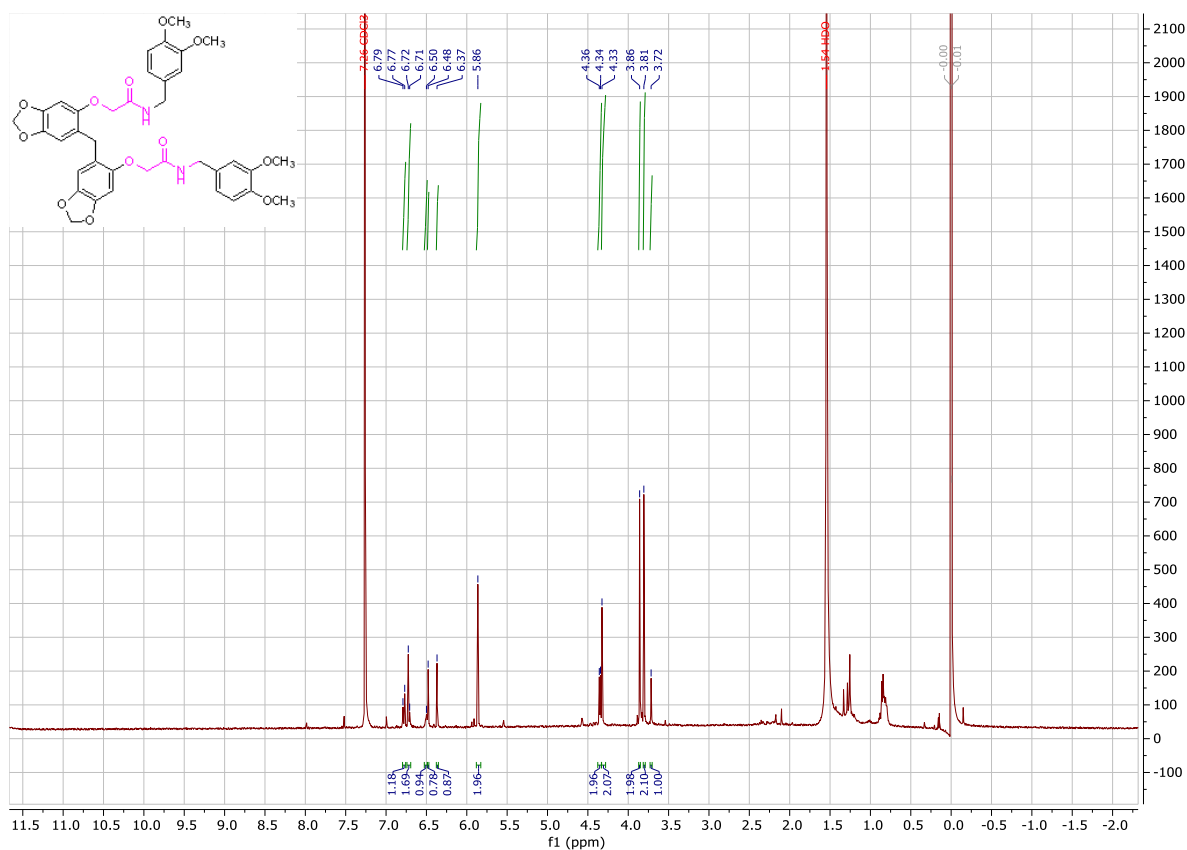
## Appendix



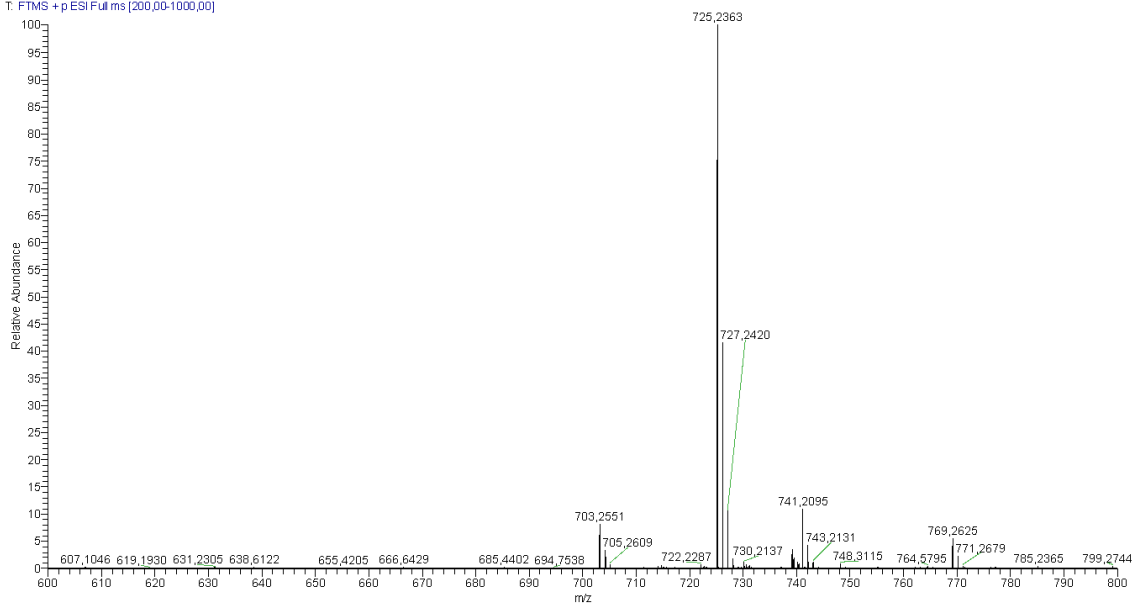
AR-224 #1 RT: 0.00 AV: 1 NL: 2.15E7  
T: FTMS + p ESI Full ms [200,00-1000,00]



<sup>1</sup>H NMR (400 MHz, CDCl<sub>3</sub>) and HRMS (ESI) m/z of **25b**

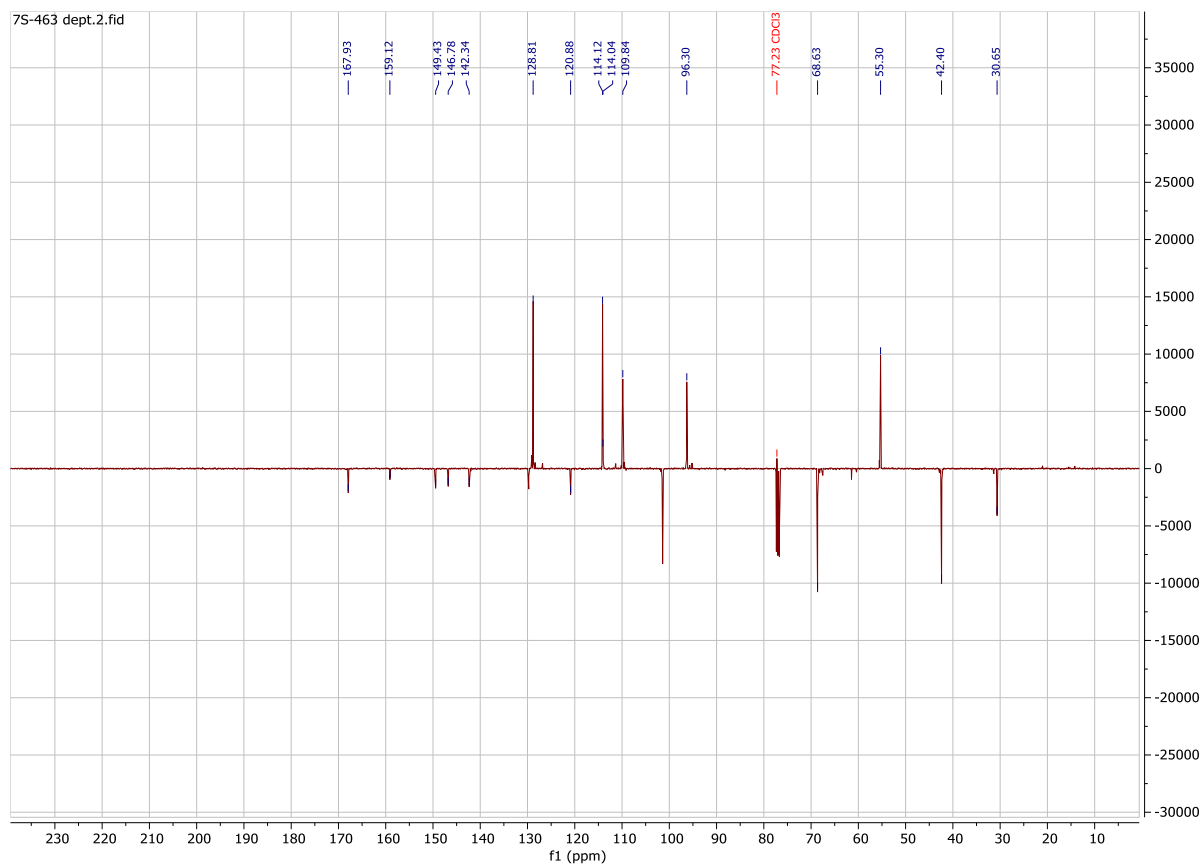
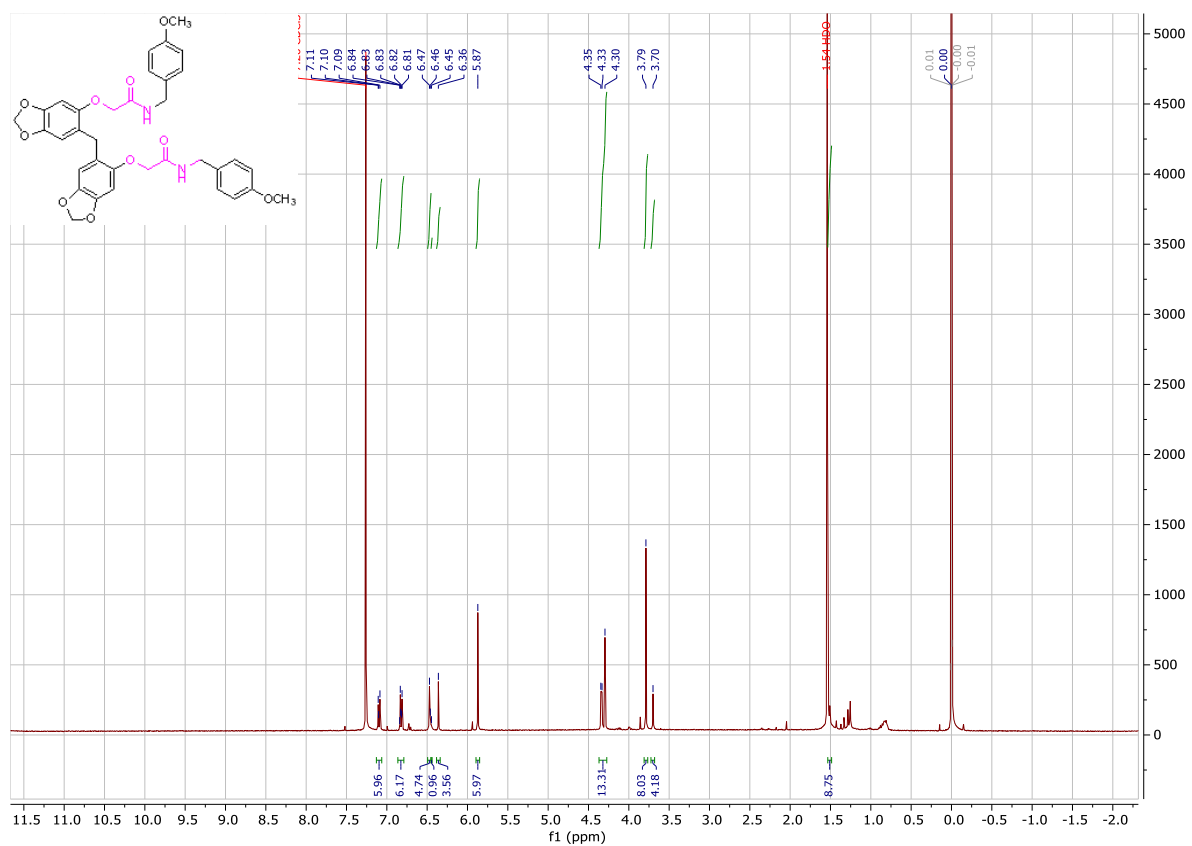


8S-256 BIS #1 RT: 0.00 AV: 1 NL: 7.63E7  
T: FTMS + p ESI Full ms [200.00-1000.00]

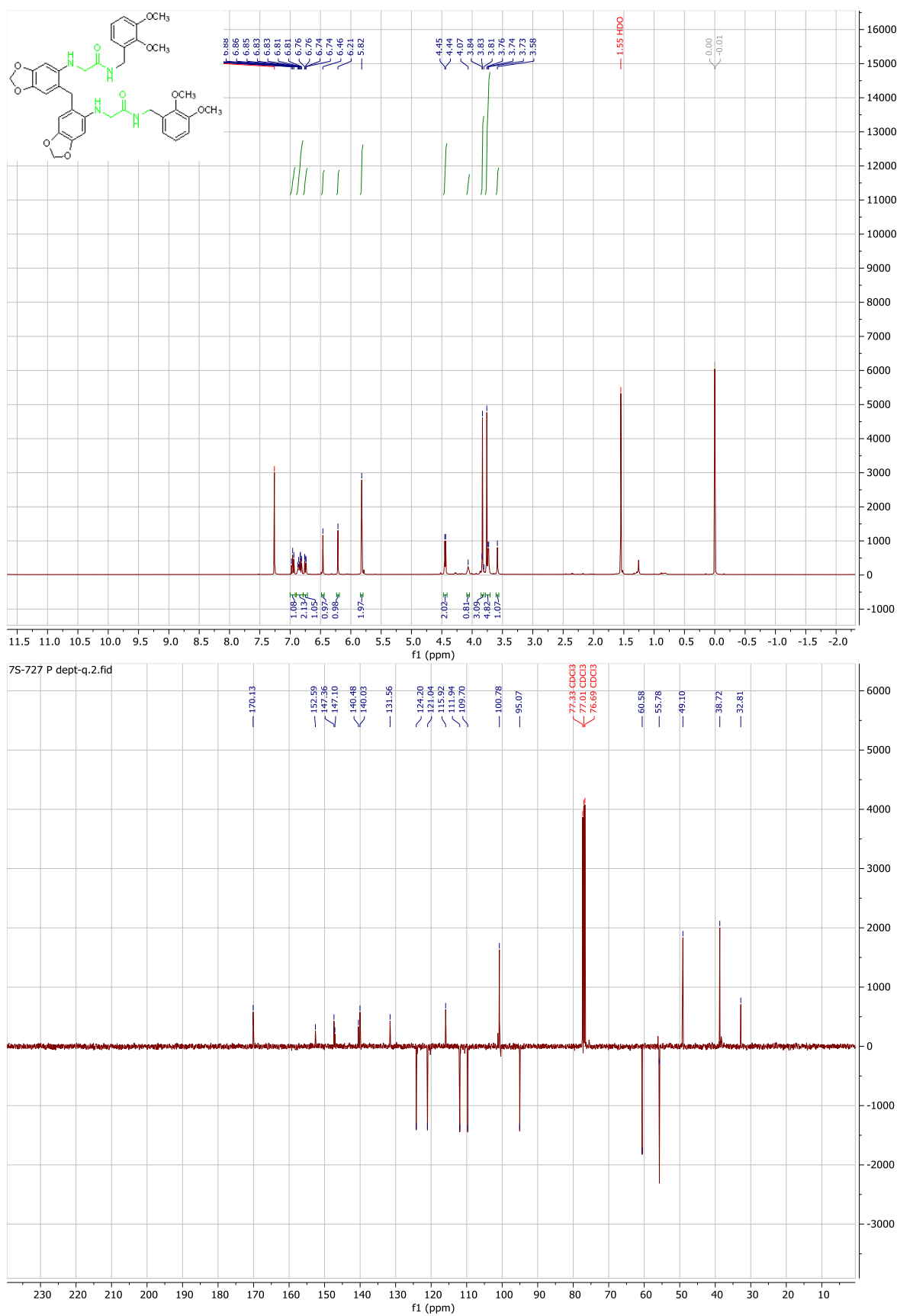


<sup>1</sup>H NMR (400 MHz, CDCl<sub>3</sub>) and HRMS (ESI) m/z of **25c**

# Appendix

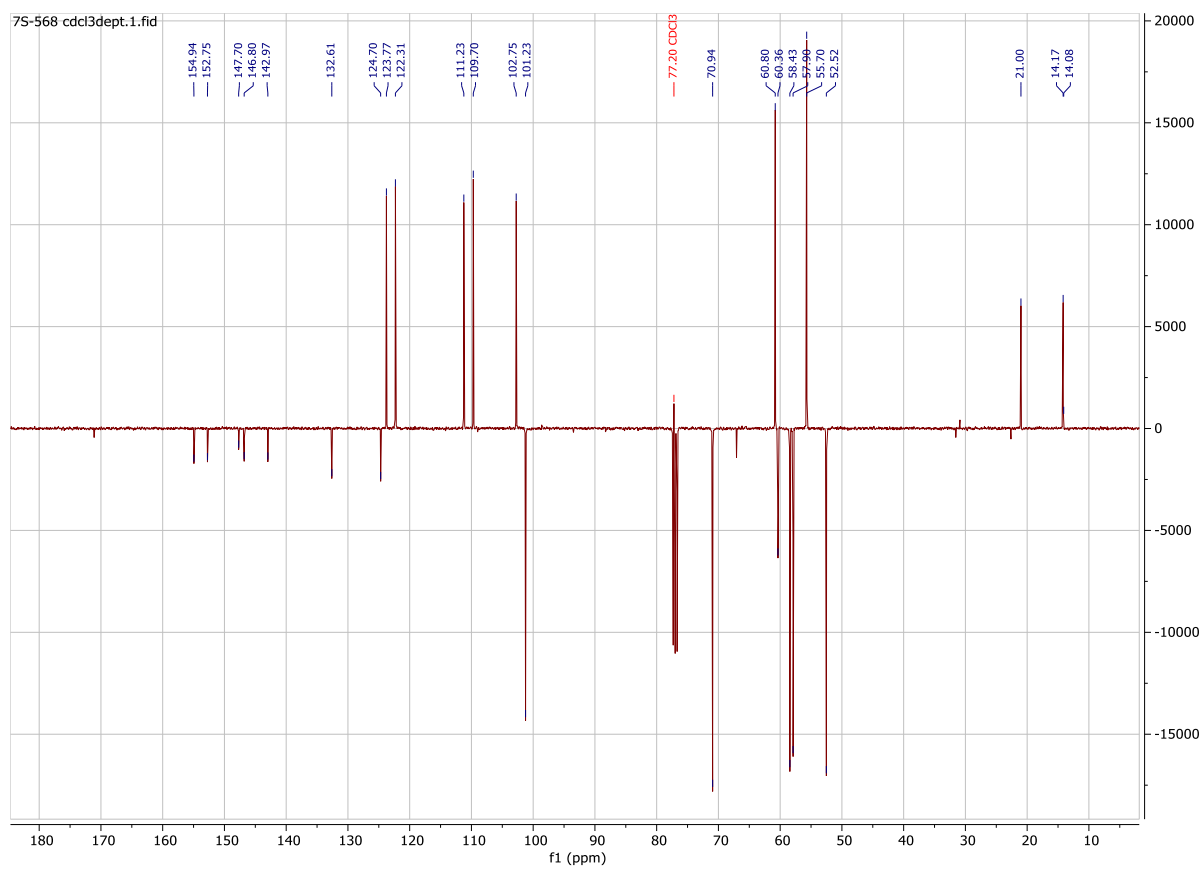
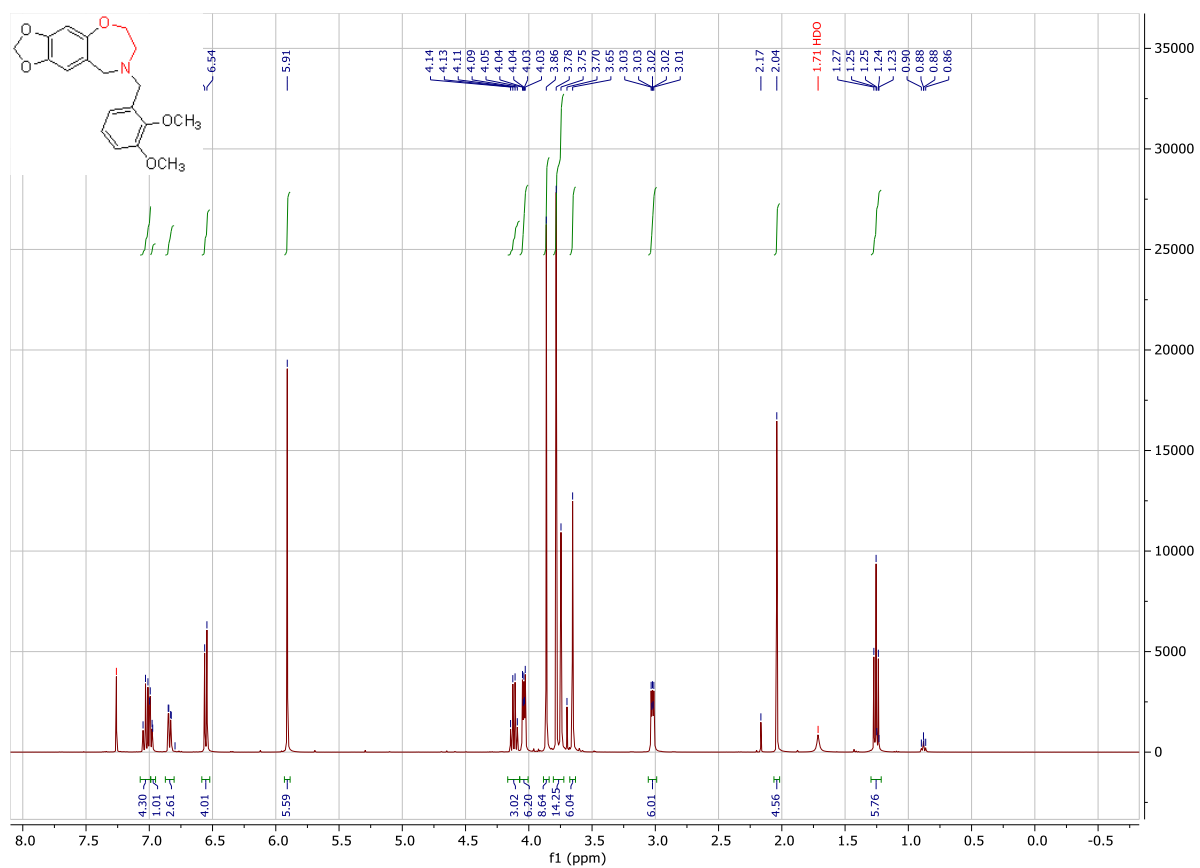


<sup>1</sup>H NMR (400 MHz, CDCl<sub>3</sub>) and <sup>13</sup>C DEPTQ NMR (101 MHz, CDCl<sub>3</sub>) of **25d**

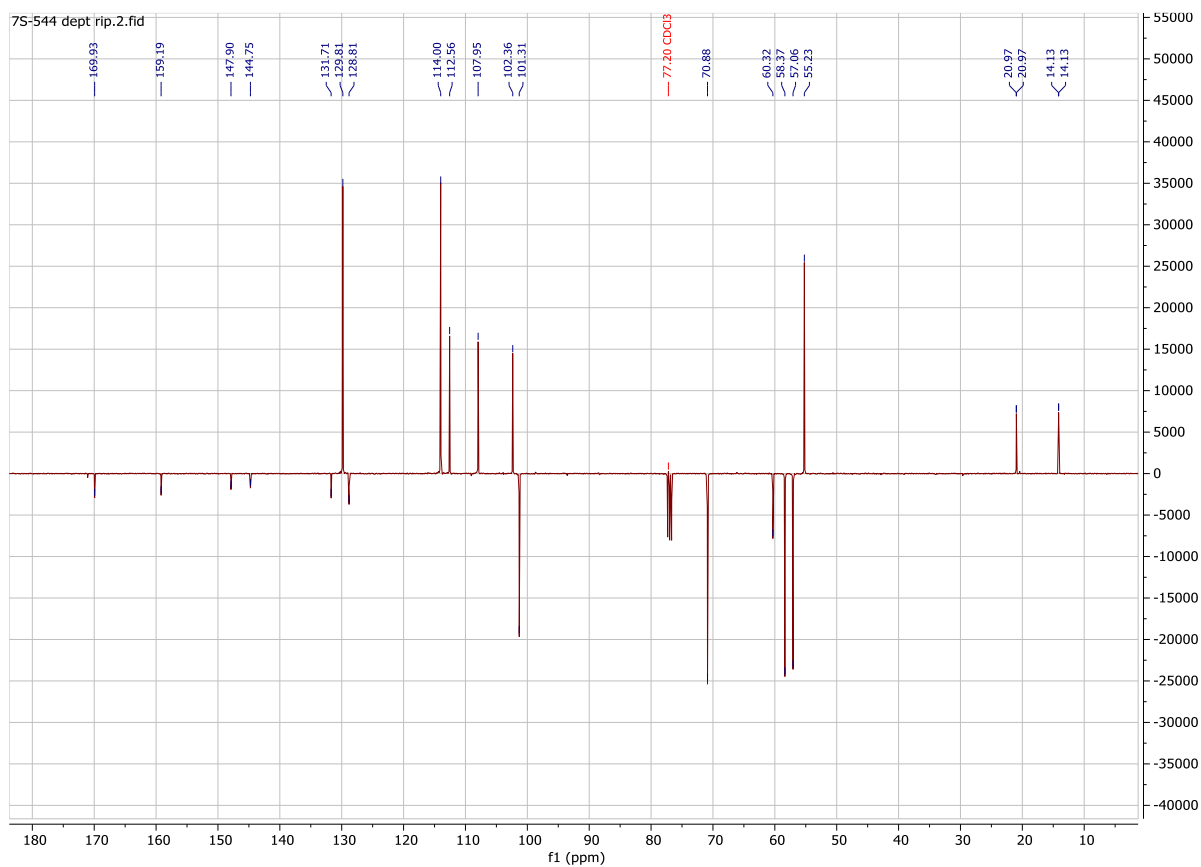
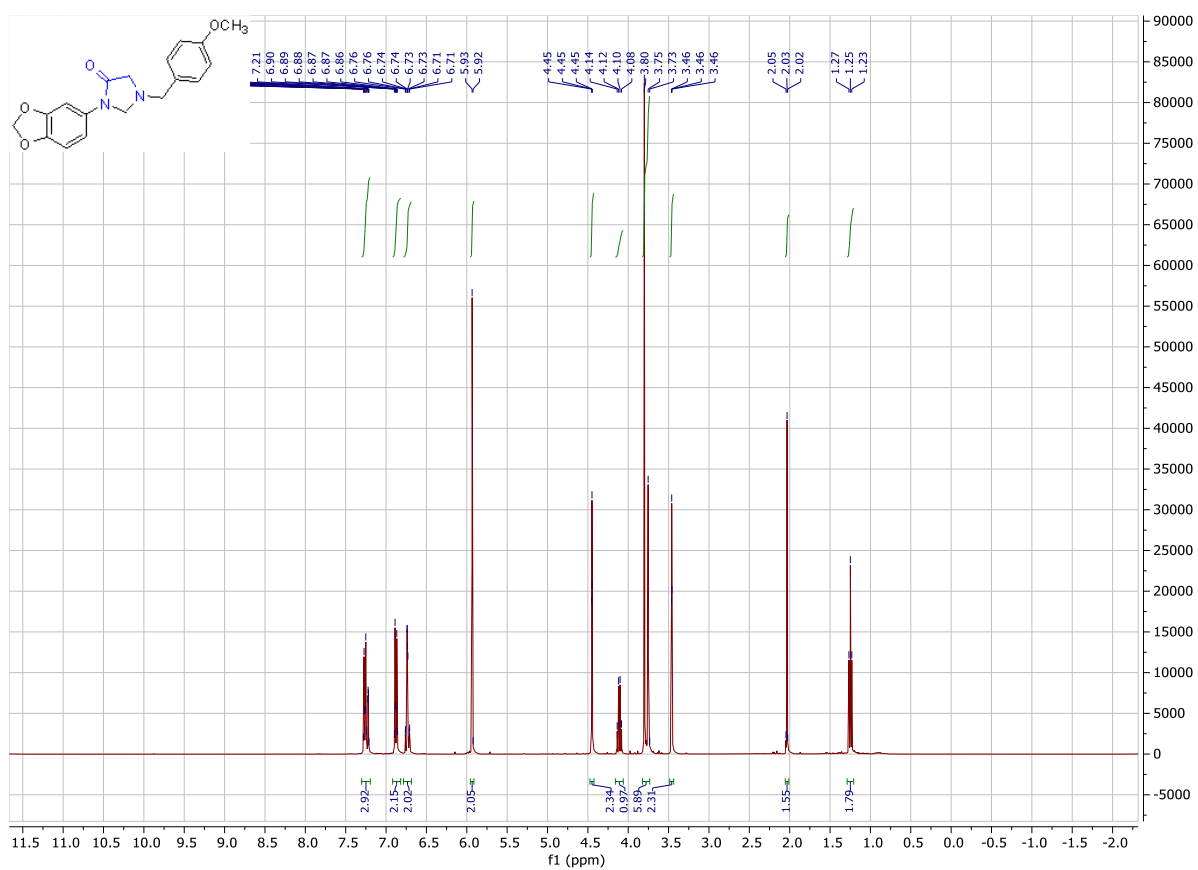


<sup>1</sup>H NMR (400 MHz, CDCl<sub>3</sub>) and <sup>13</sup>C DEPTQ NMR (101 MHz, CDCl<sub>3</sub>) of **31**

# Appendix

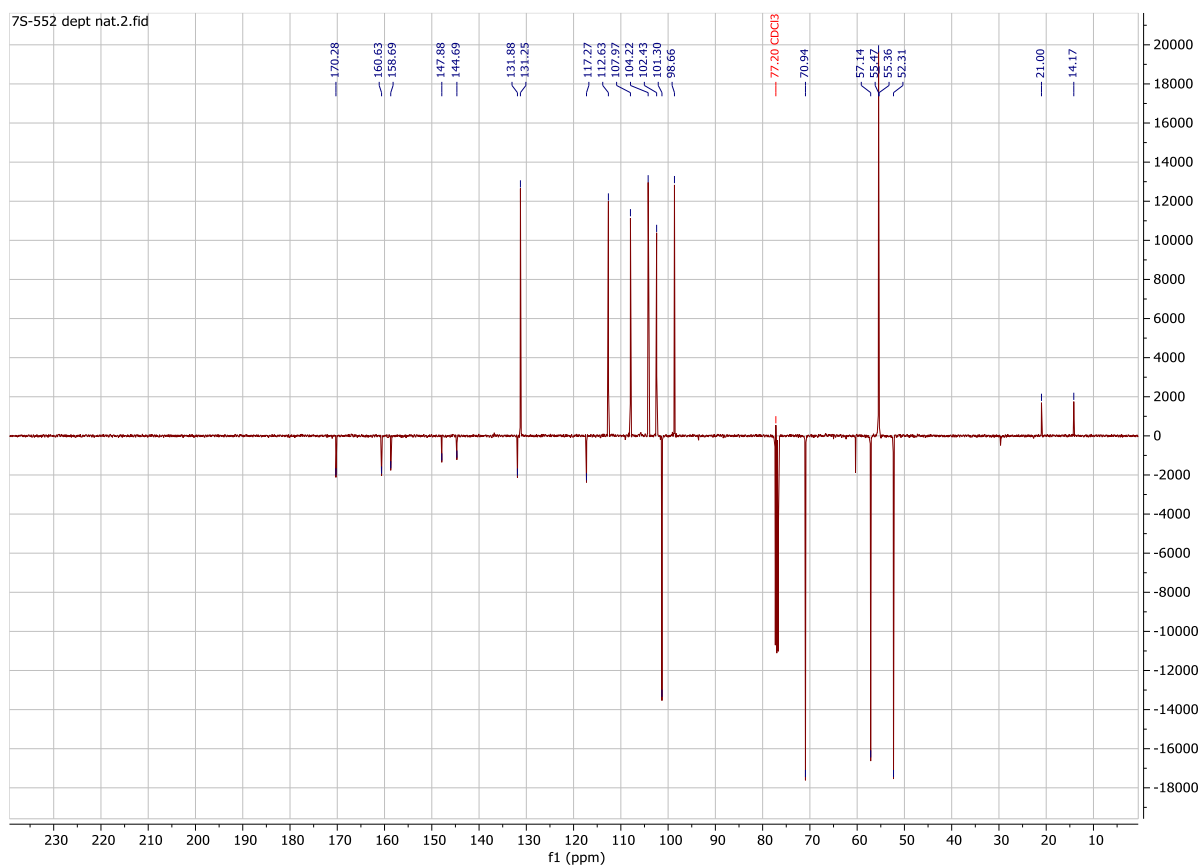
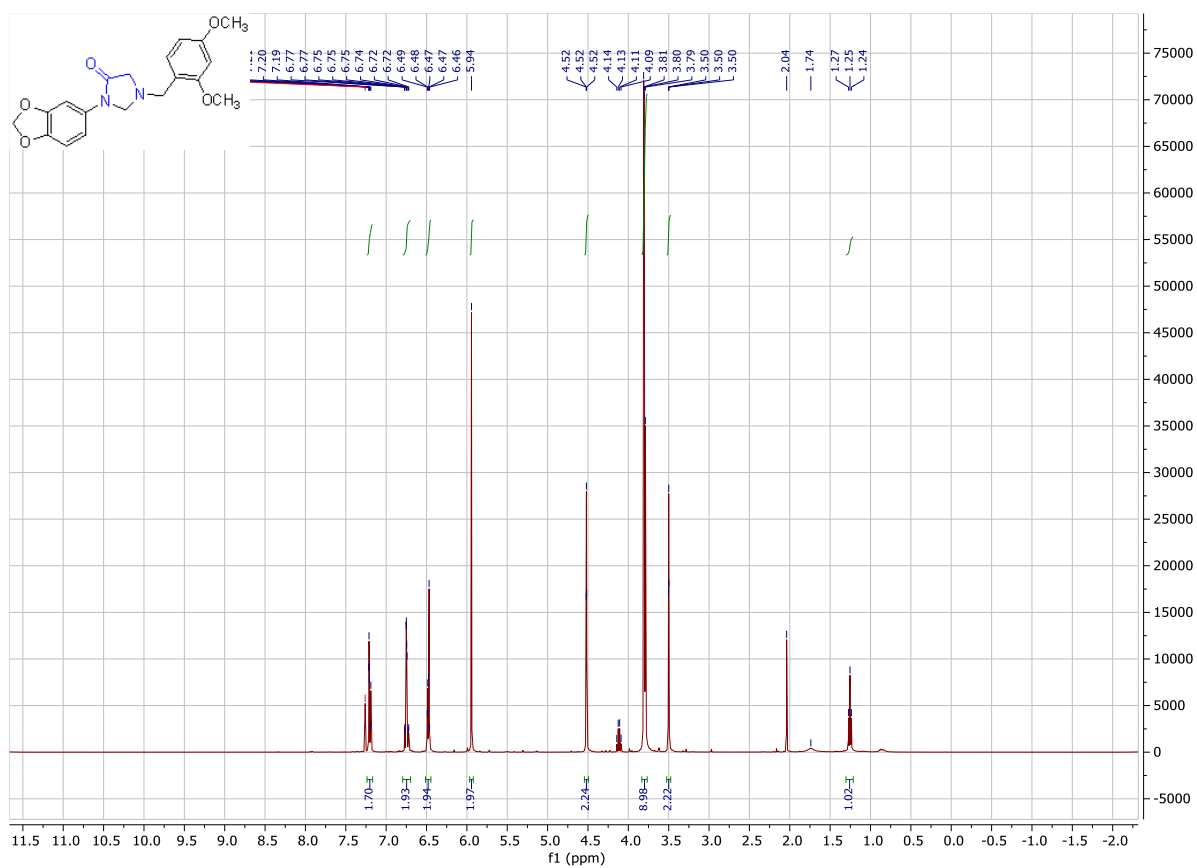


<sup>1</sup>H NMR (400 MHz, CDCl<sub>3</sub>) and <sup>13</sup>C DEPTQ NMR (101 MHz, CDCl<sub>3</sub>) of **181**

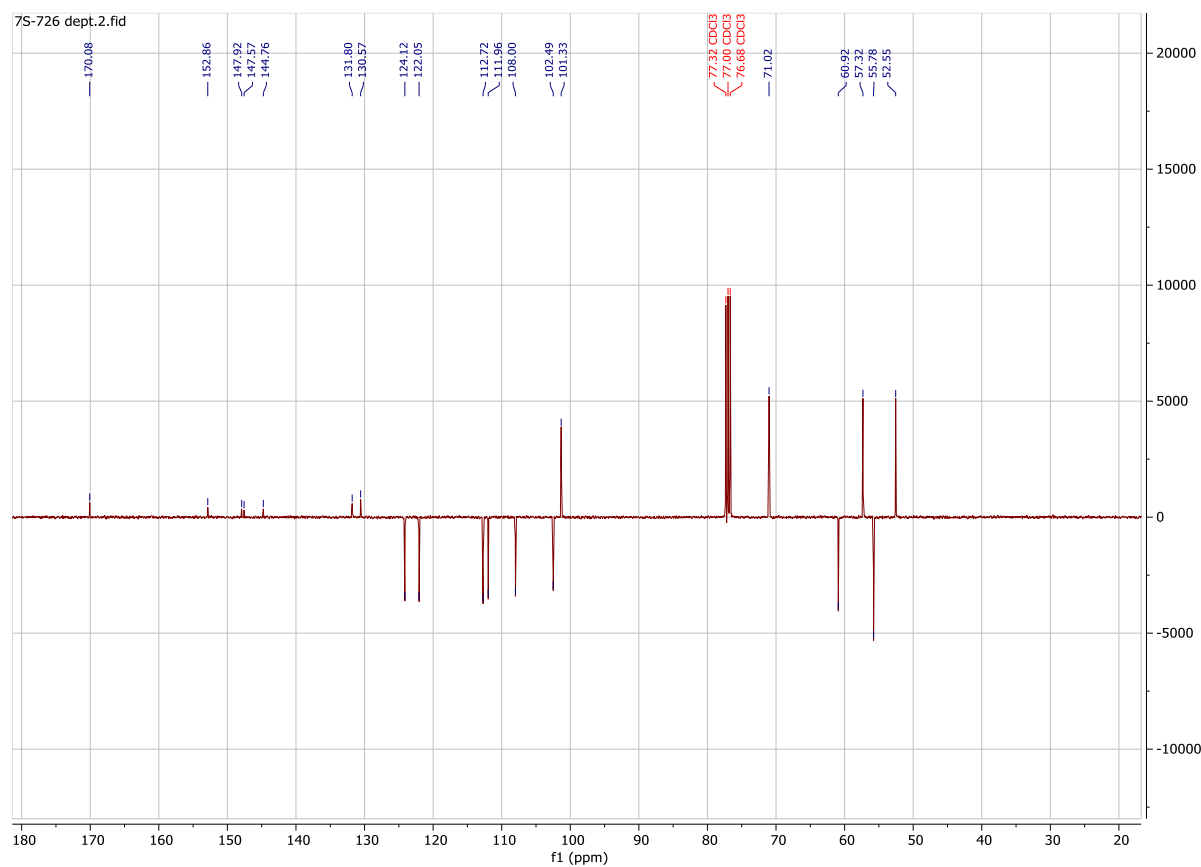
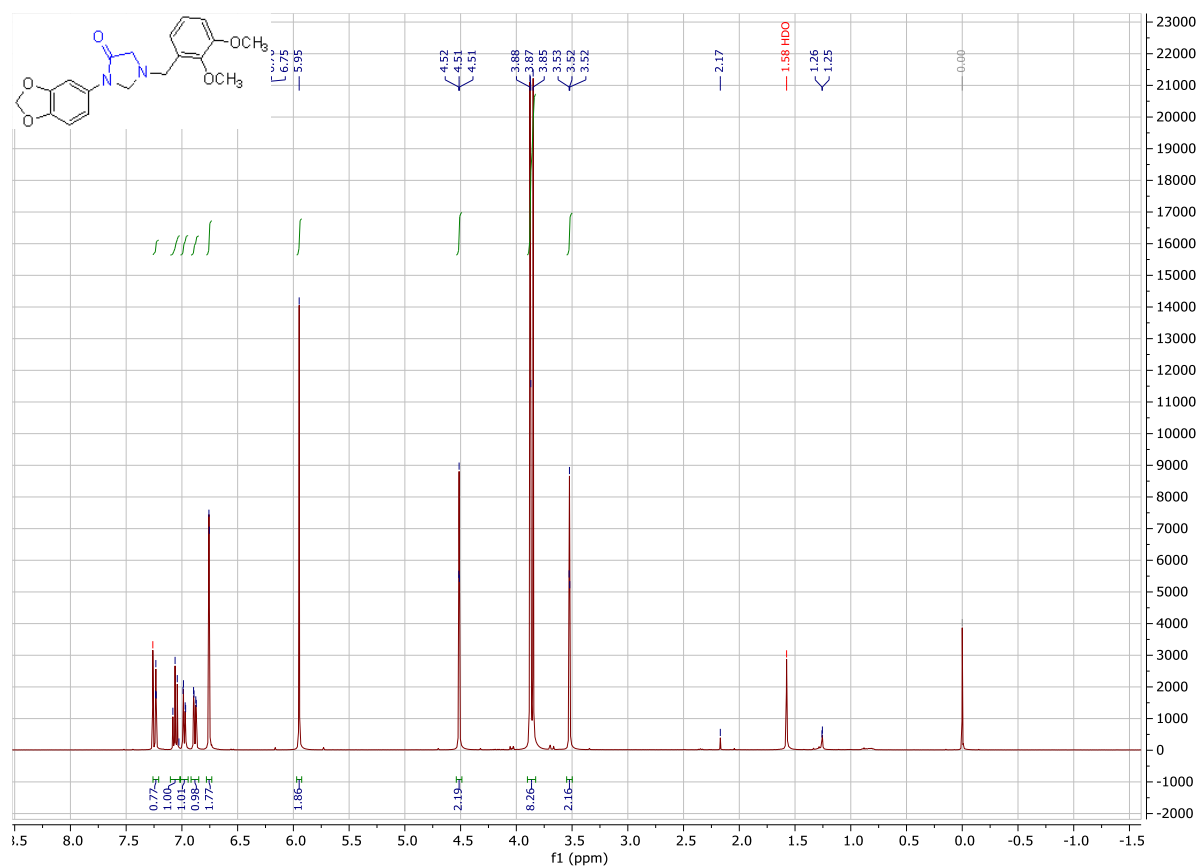


<sup>1</sup>H NMR (400 MHz, CDCl<sub>3</sub>) and <sup>13</sup>C DEPTQ NMR (101 MHz, CDCl<sub>3</sub>) of 19a

# Appendix

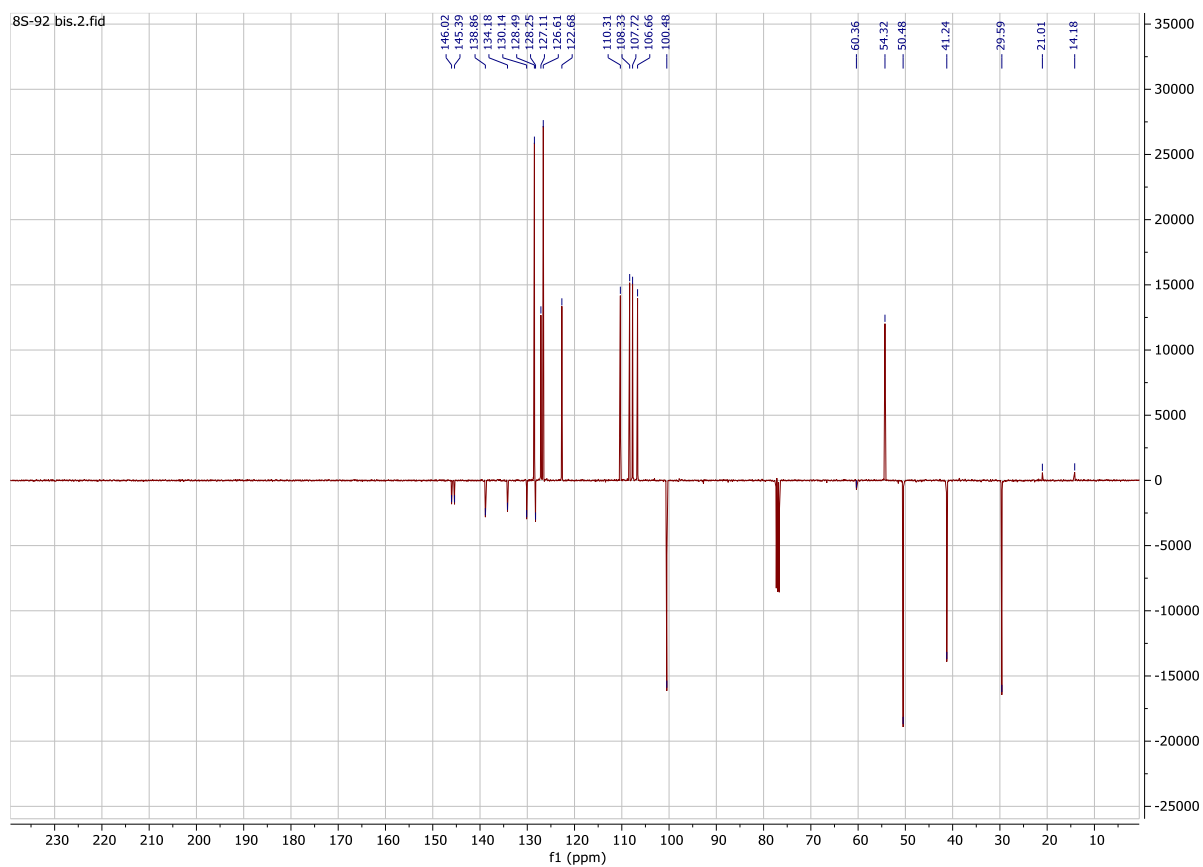
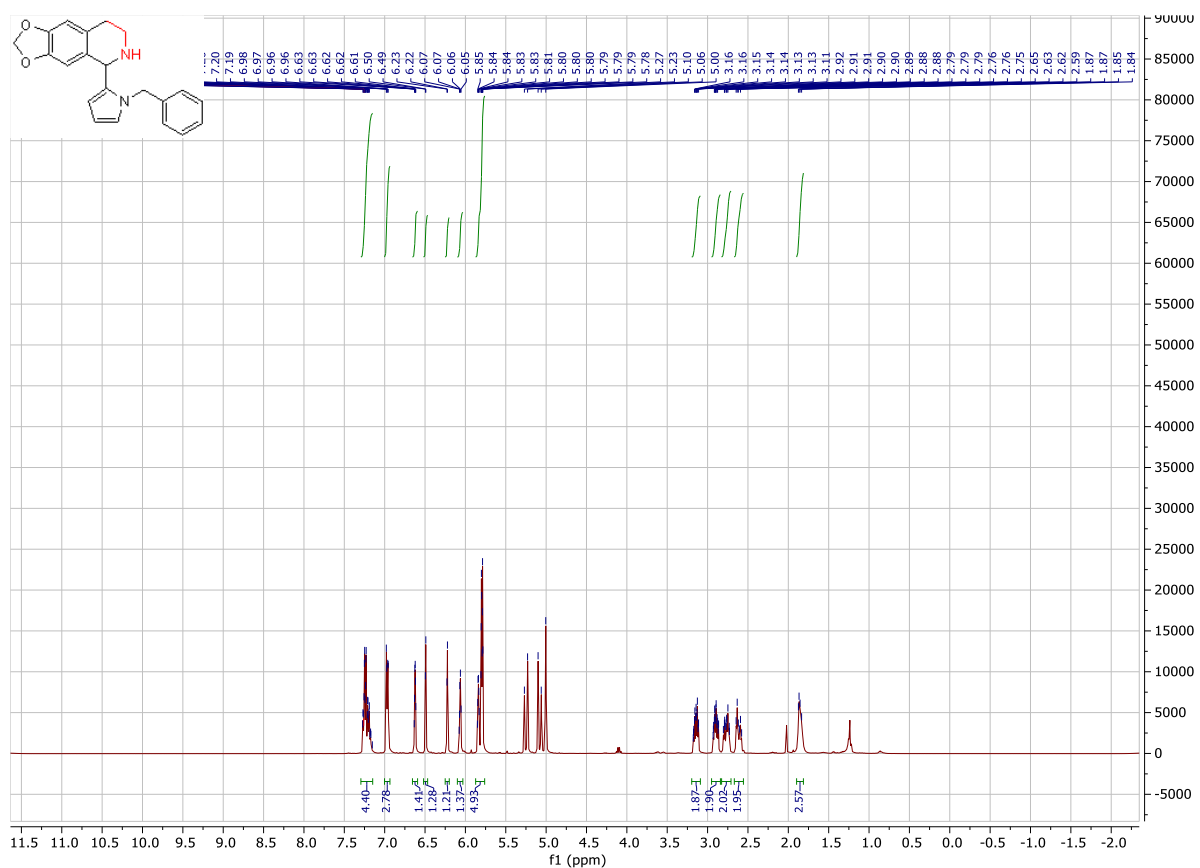


<sup>1</sup>H NMR (400 MHz, CDCl<sub>3</sub>) and <sup>13</sup>C DEPTQ NMR (101 MHz, CDCl<sub>3</sub>) of **19b**

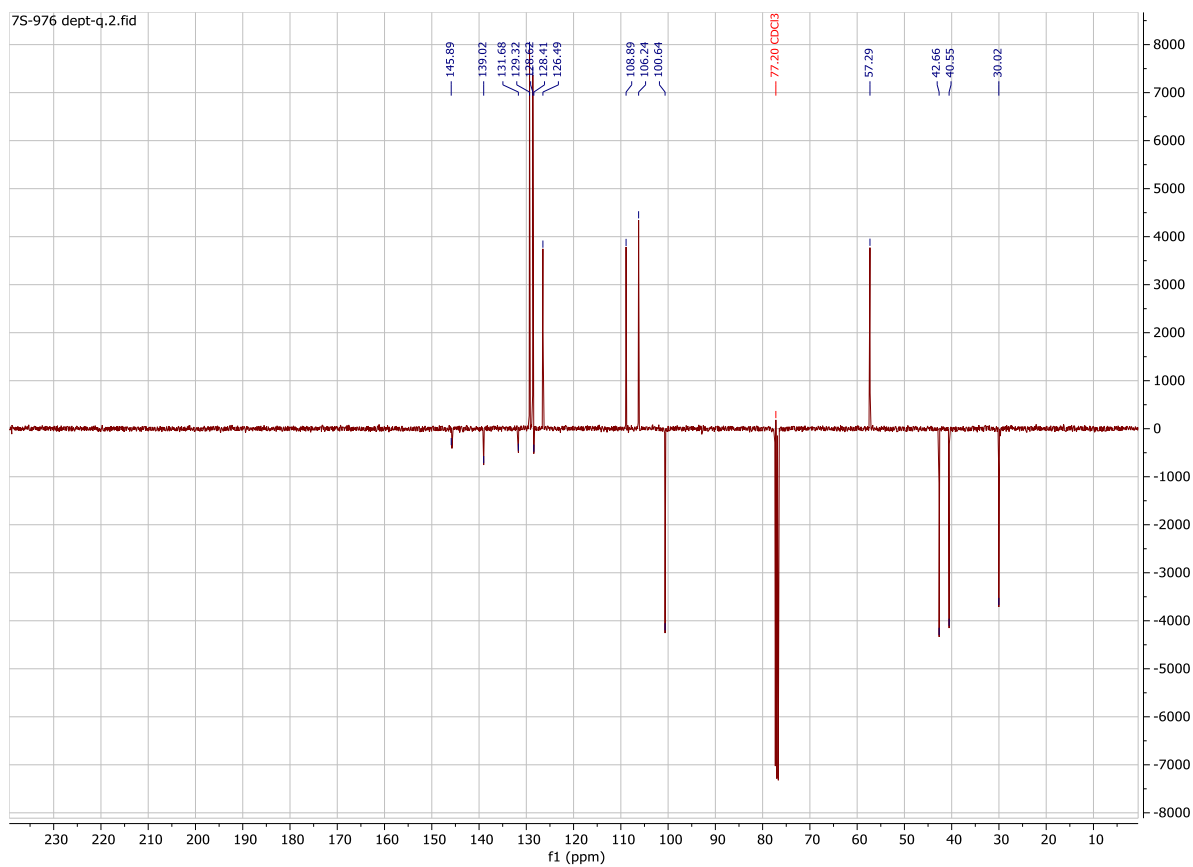
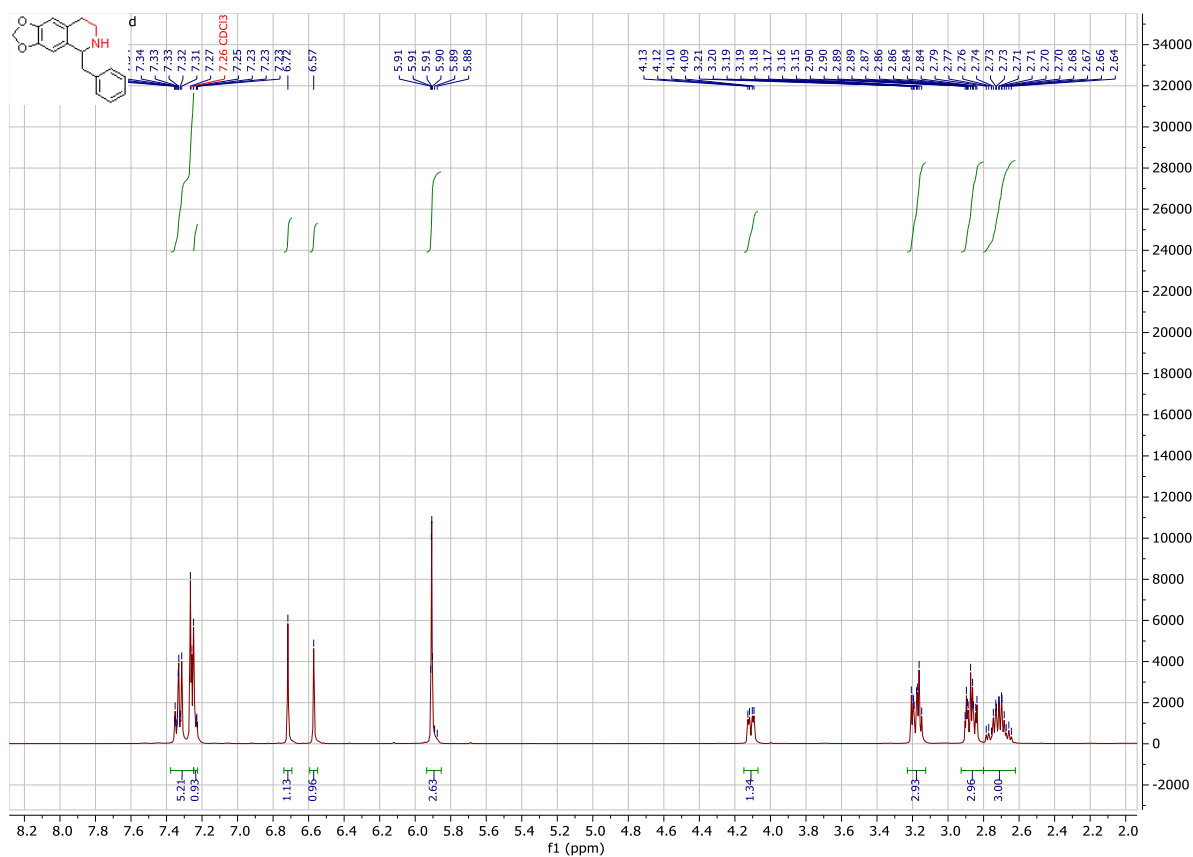


<sup>1</sup>H NMR (400 MHz, CDCl<sub>3</sub>) and <sup>13</sup>C DEPTQ NMR (101 MHz, CDCl<sub>3</sub>) of compound 19c

# Appendix

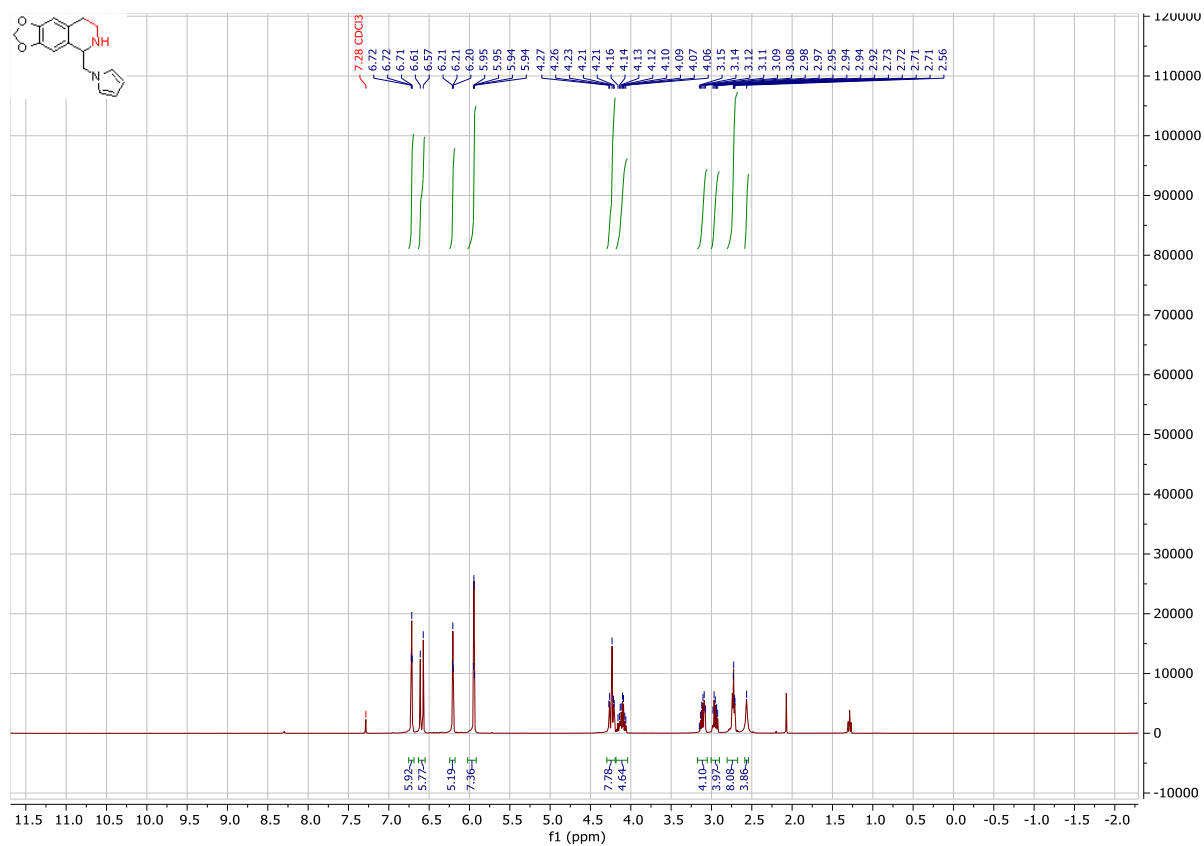


<sup>1</sup>H NMR (400 MHz, CDCl<sub>3</sub>) and <sup>13</sup>C DEPTQ (101 MHz, CDCl<sub>3</sub>) of compound **20a**

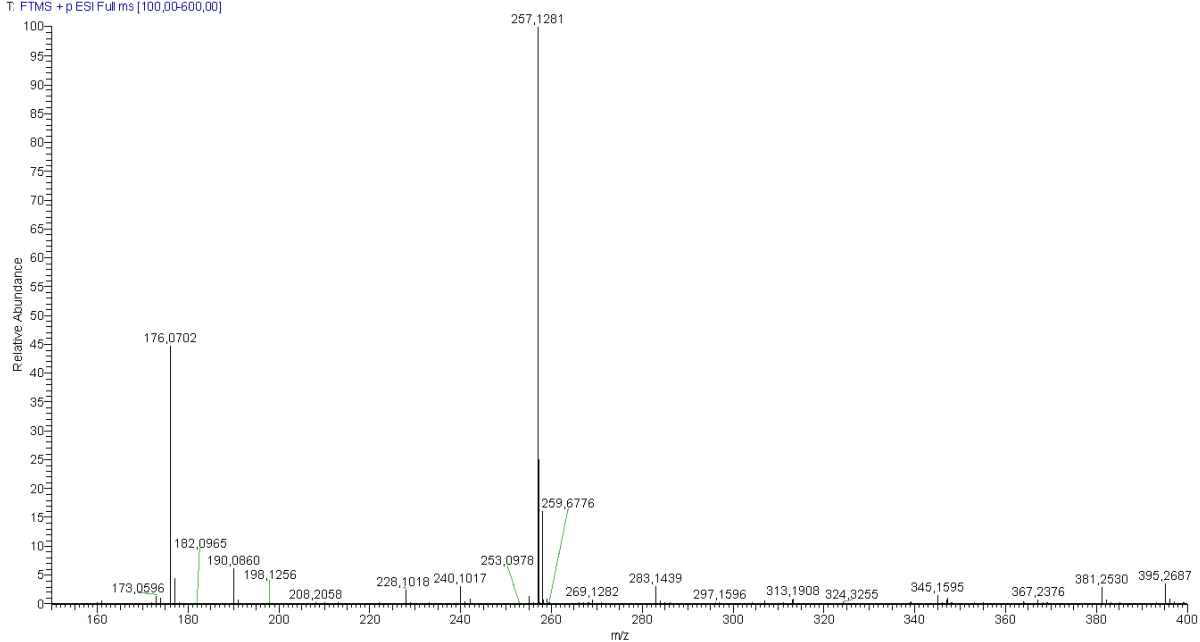


<sup>1</sup>H NMR (400 MHz, CDCl<sub>3</sub>) and <sup>13</sup>C DEPTQ NMR (101 MHz, CDCl<sub>3</sub>) of compound 20b

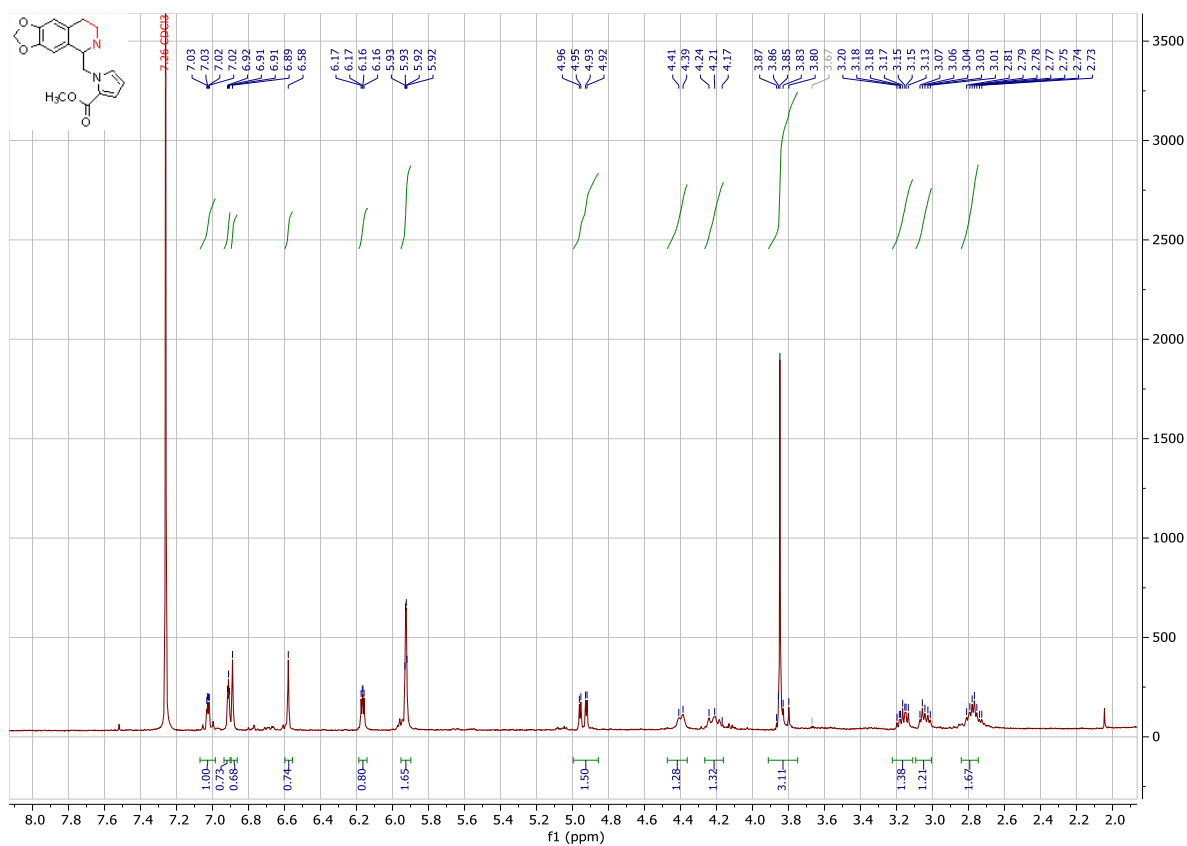
# Appendix



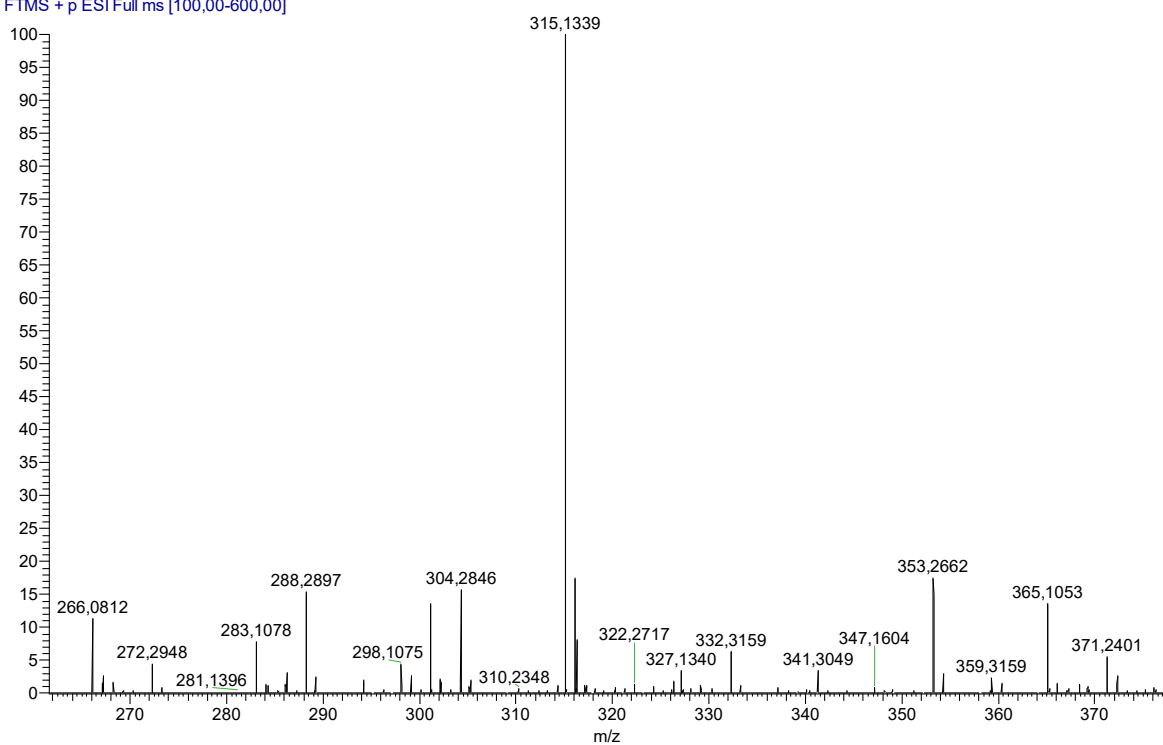
8S-77 #31 RT: 0.64 AV: 1 NL: 9.31E7  
T: FTMS + p ESI Full ms [100,00-600,00]



**<sup>1</sup>H NMR (400 MHz, CDCl<sub>3</sub>) and HRMS (ESI) m/z of 20c**

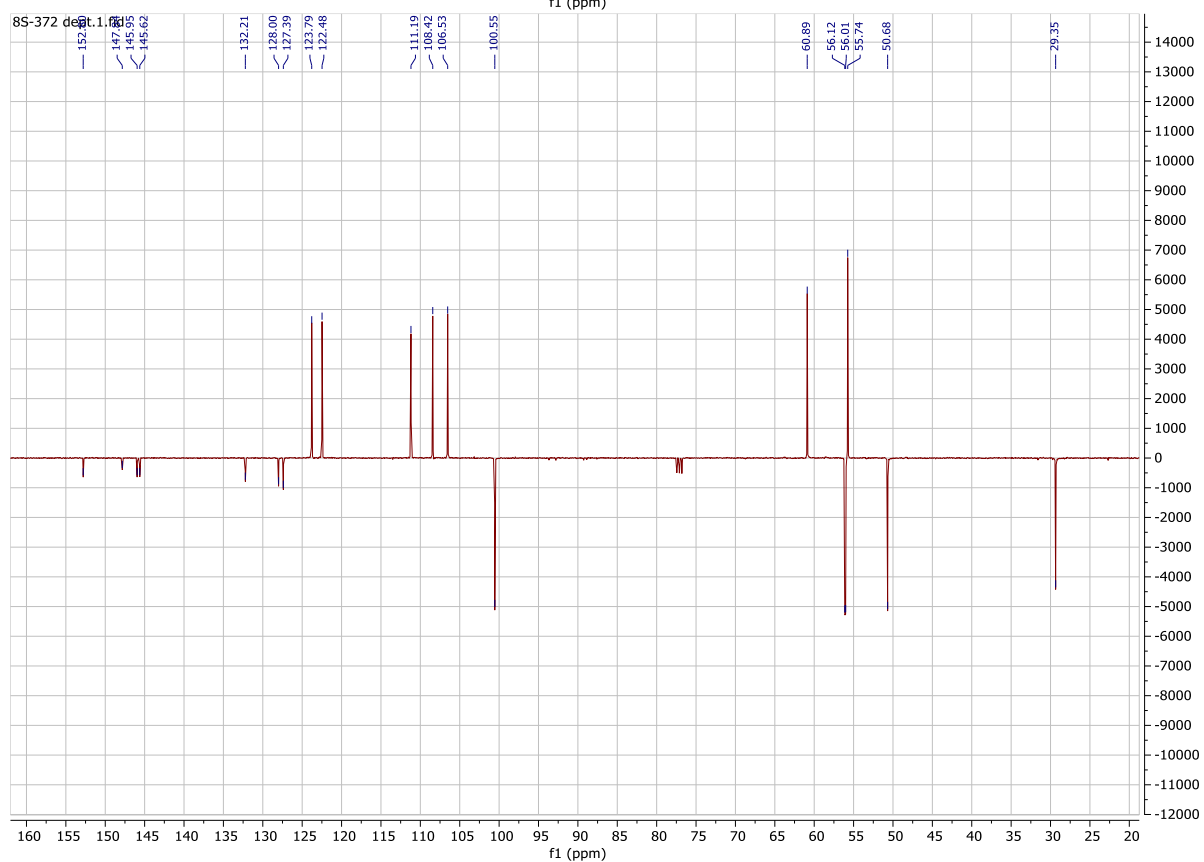
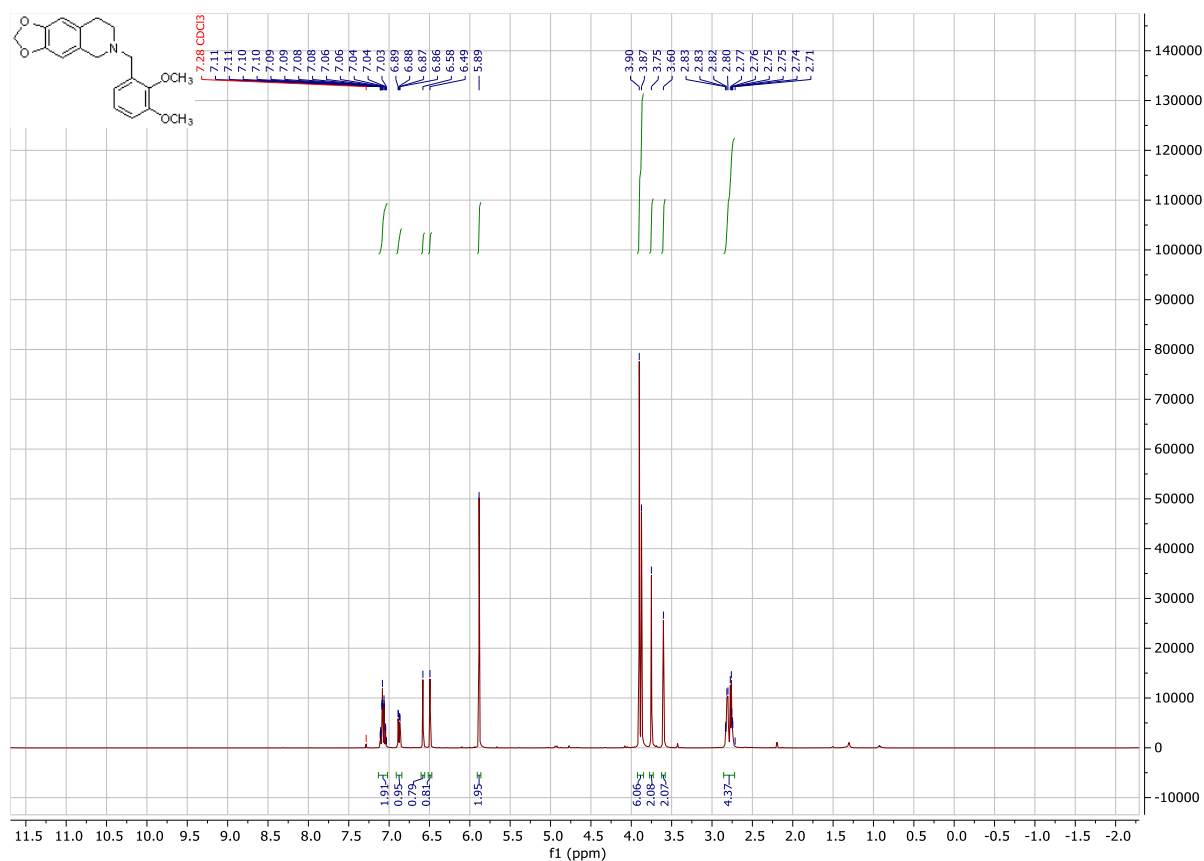


8S-405 puro pos #33 RT: 0,26 AV: 1 NL: 1,11E7  
T: FTMS + p ESI Full ms [100,00-600,00]

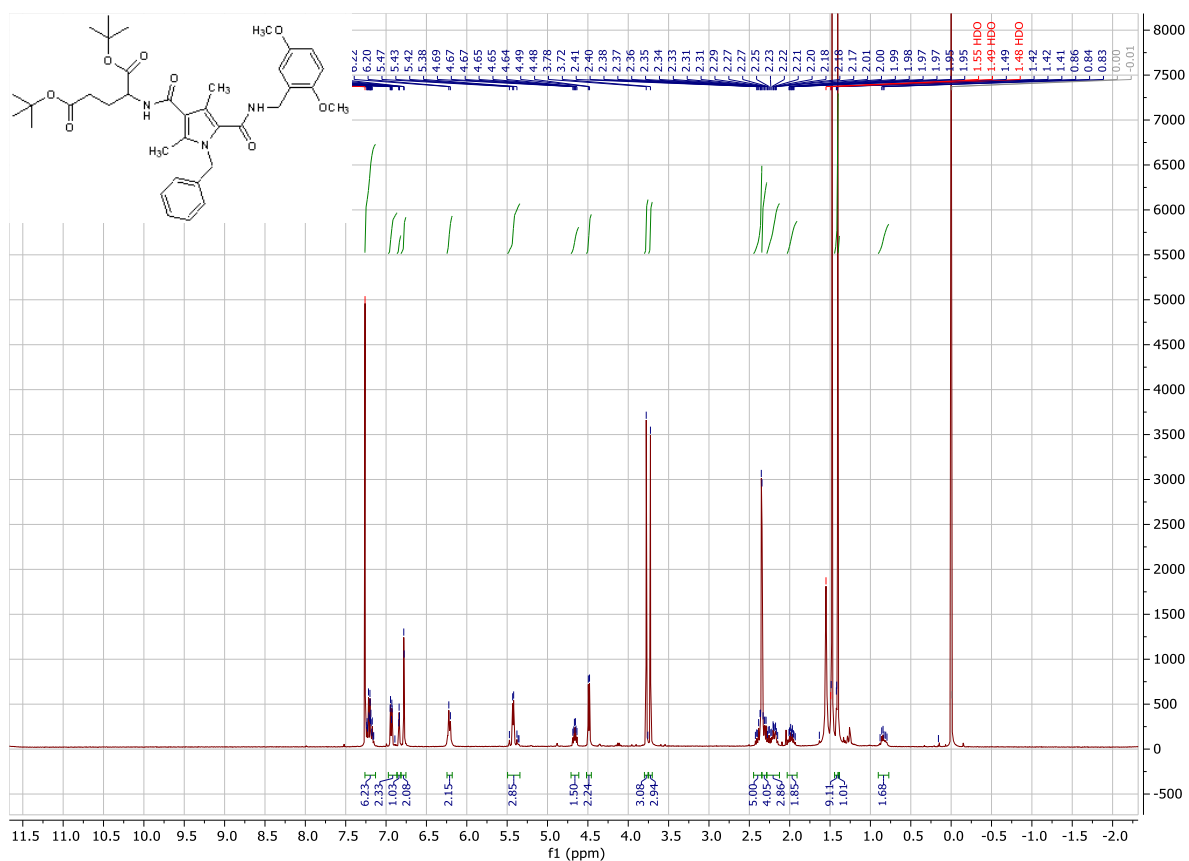


$^1\text{H}$ NMR (400 MHz,  $\text{CDCl}_3$ ) and HRMS (ESI) m/z of **20d**

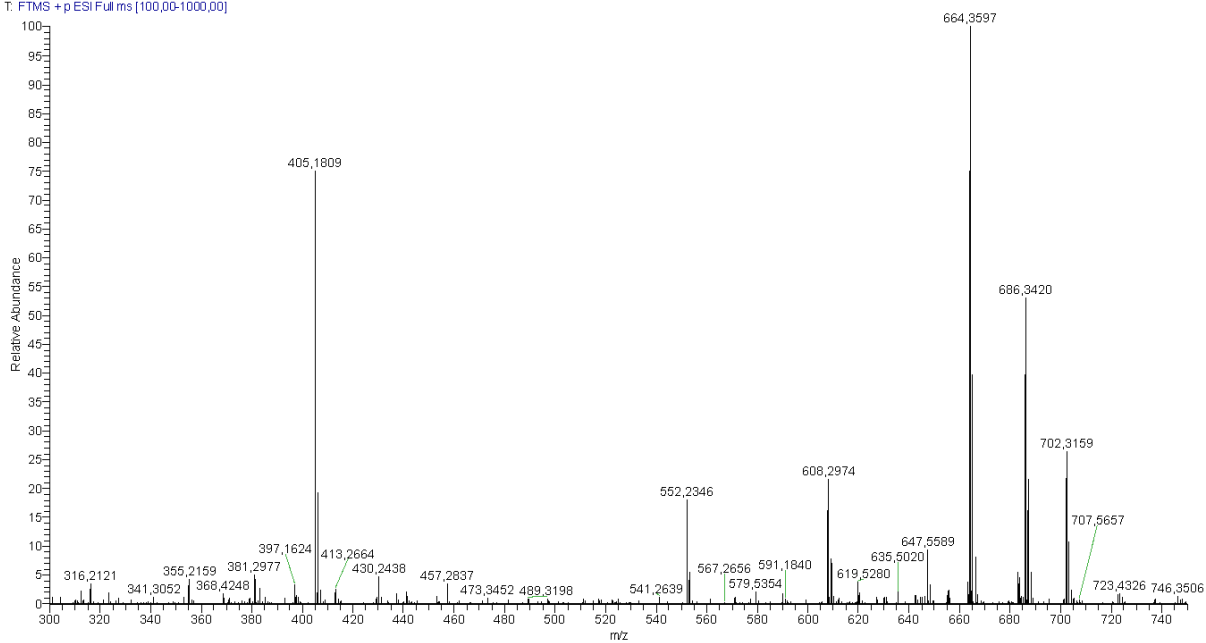
# Appendix



<sup>1</sup>H NMR (400 MHz, CDCl<sub>3</sub>) and <sup>13</sup>C DEPTQ NMR (101 MHz, CDCl<sub>3</sub>) of 20e

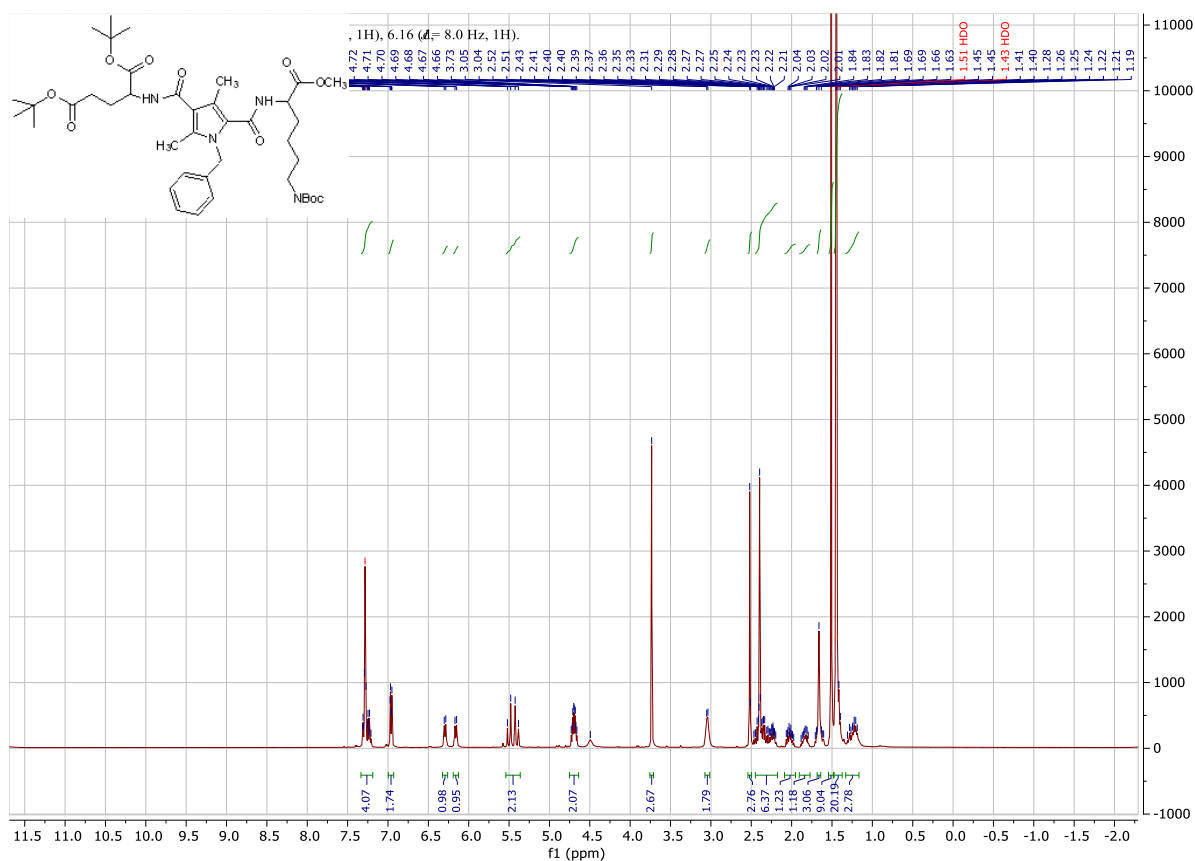


8S-181 #13 RT: 0.10 AV: 1 NL: 1.26E7  
T: FTMS + p ESI Full ms [100,00-1000,00]

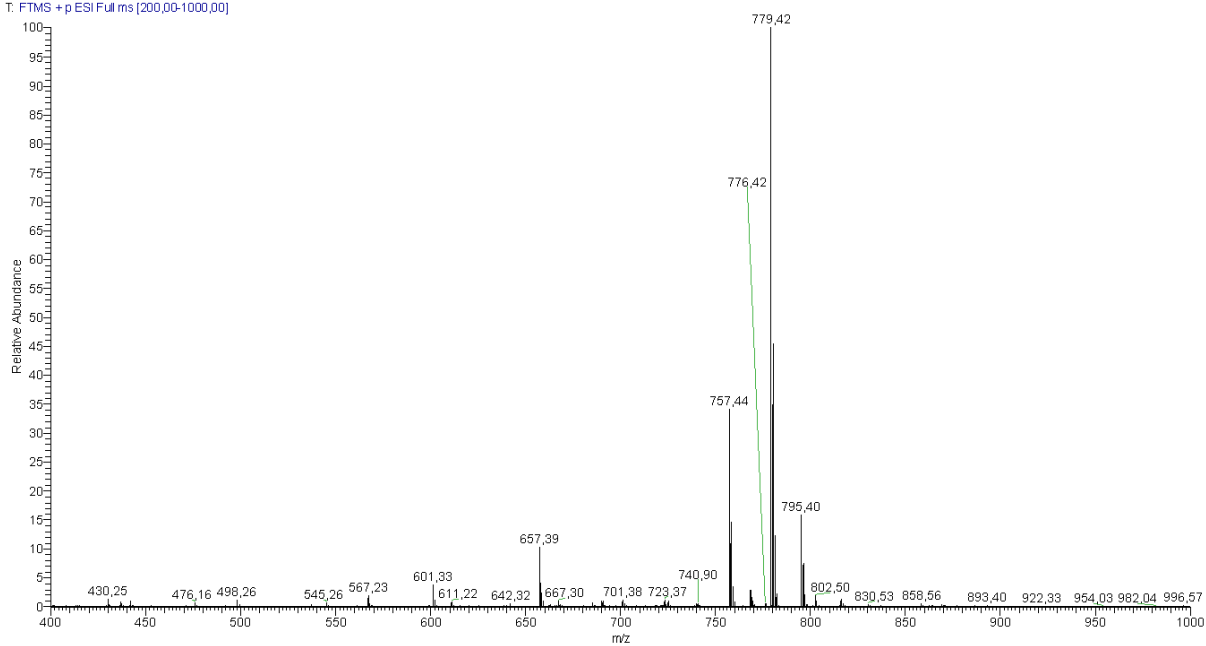


<sup>1</sup>H NMR (400 MHz, CDCl<sub>3</sub>) and HRMS (ESI) m/z of 44a



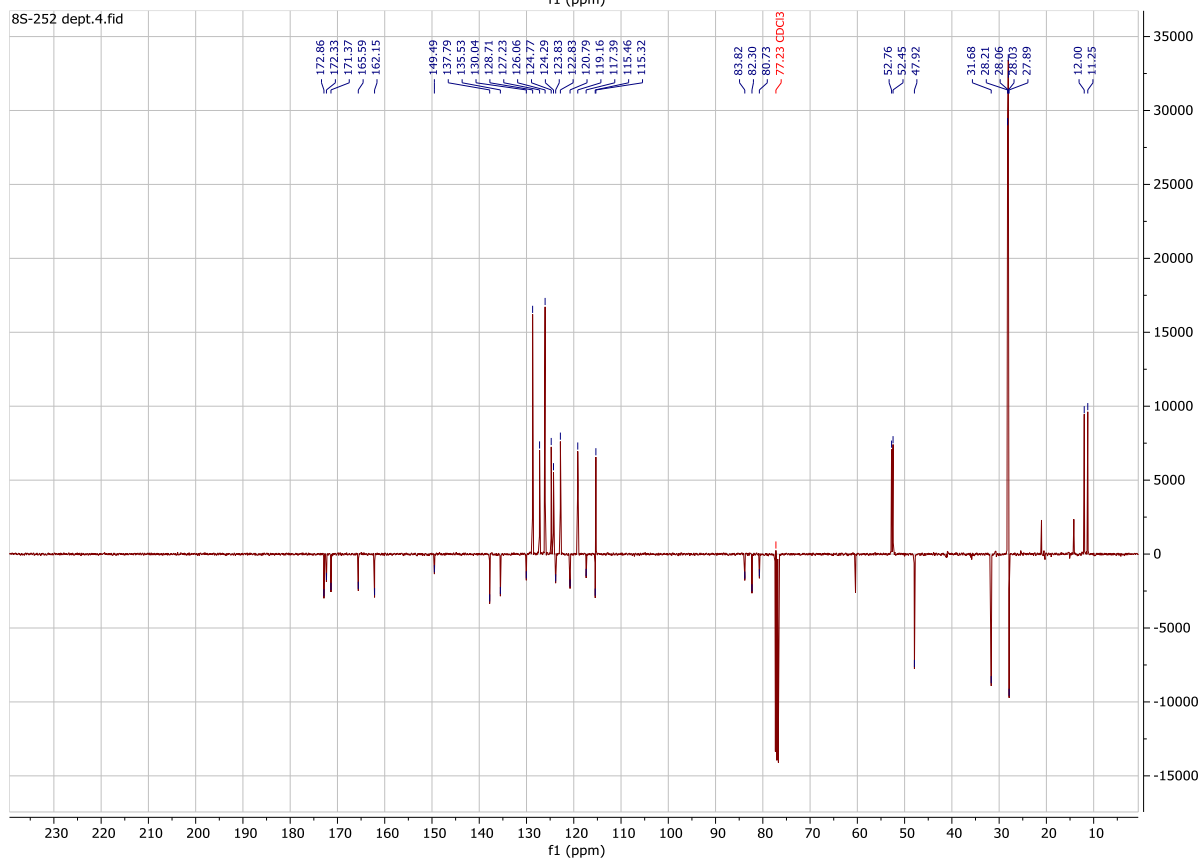
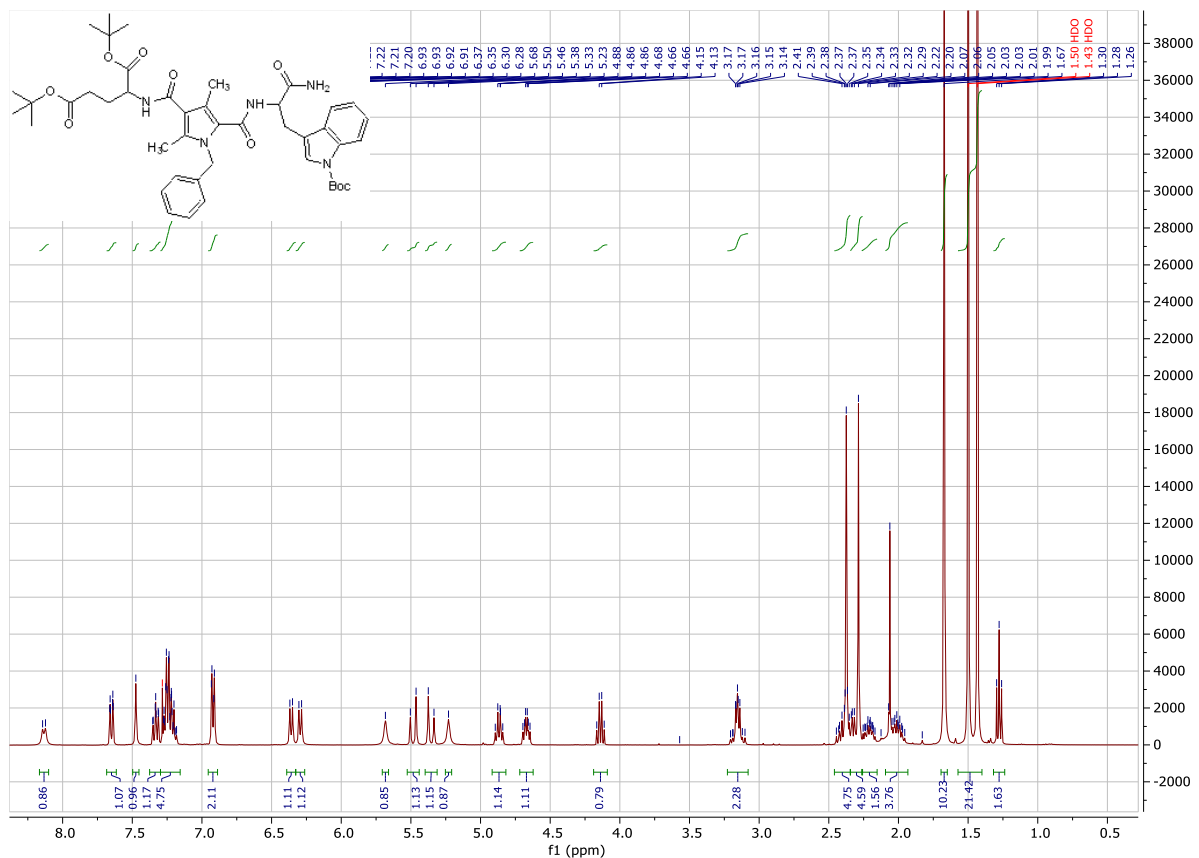


8S-225 #1 RT: 0.00 AV: 1 NL: 3.53E7  
T: FTMS + p ESI Full ms [200,00-1000,00]

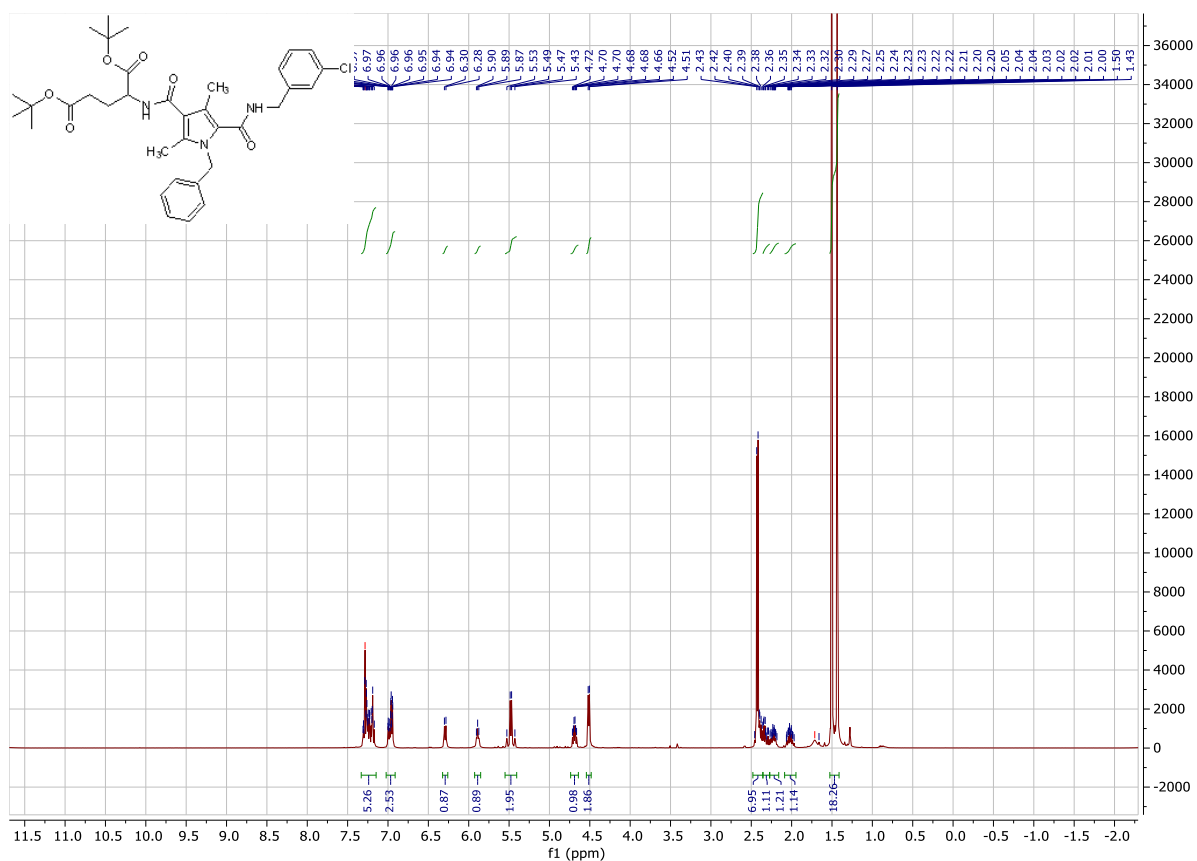


<sup>1</sup>H NMR (400 MHz, CDCl<sub>3</sub>) and HRMS (ESI) m/z of 44c

# Appendix



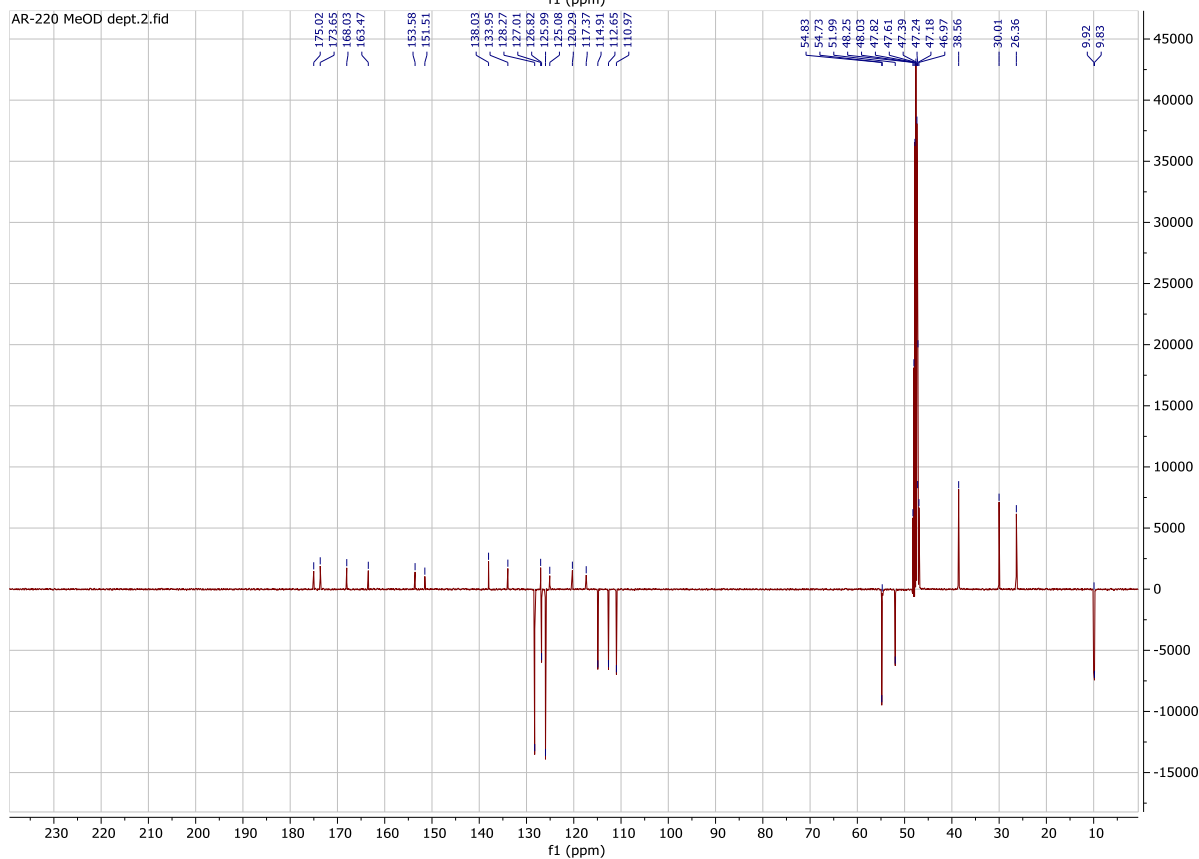
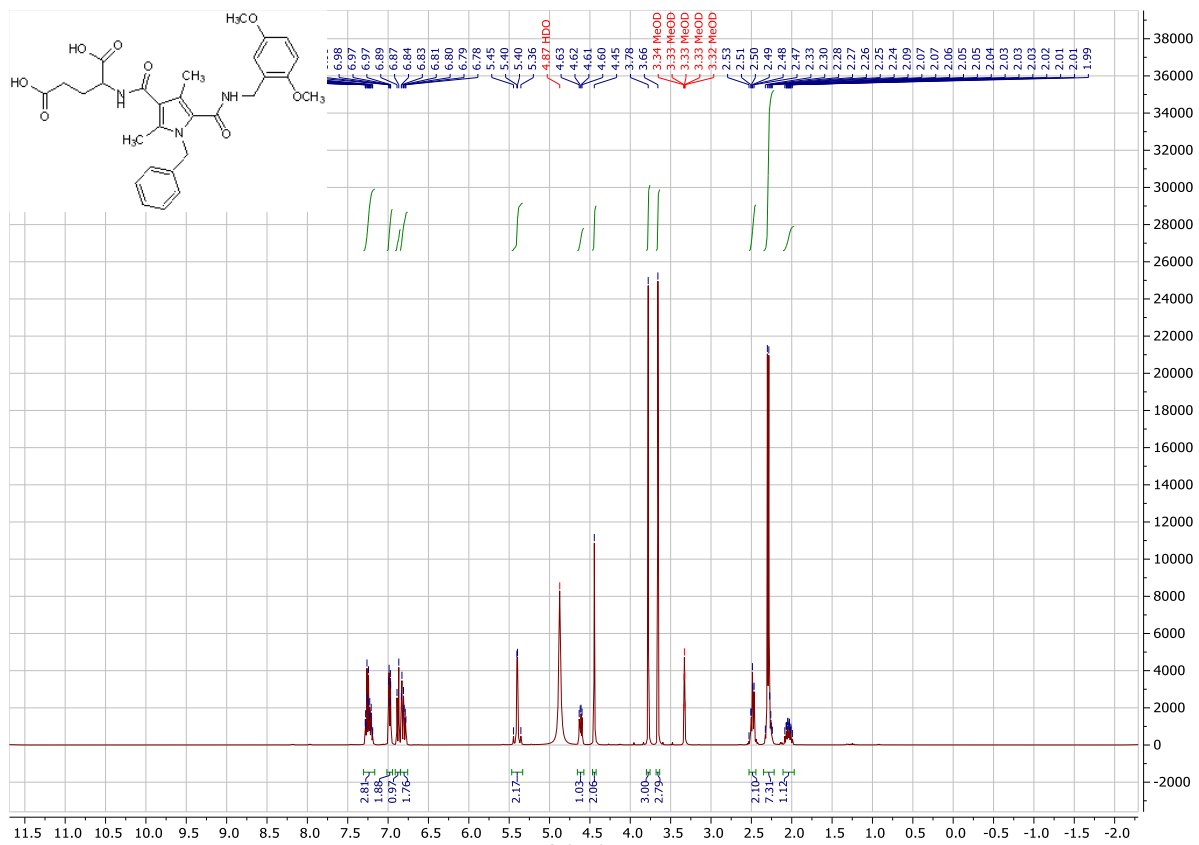
**<sup>1</sup>H NMR (400 MHz, CDCl<sub>3</sub>) and <sup>13</sup>C NMR (101 MHz, CDCl<sub>3</sub>) of 44d**



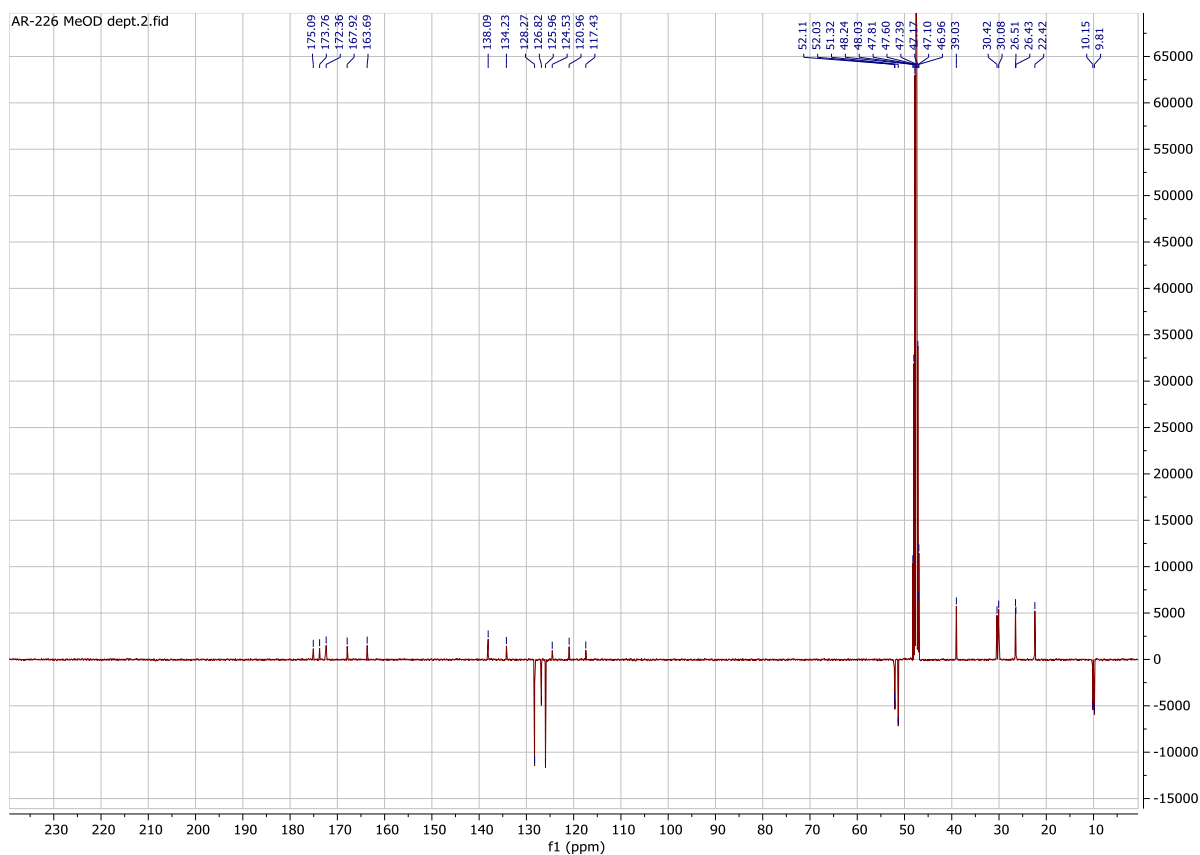
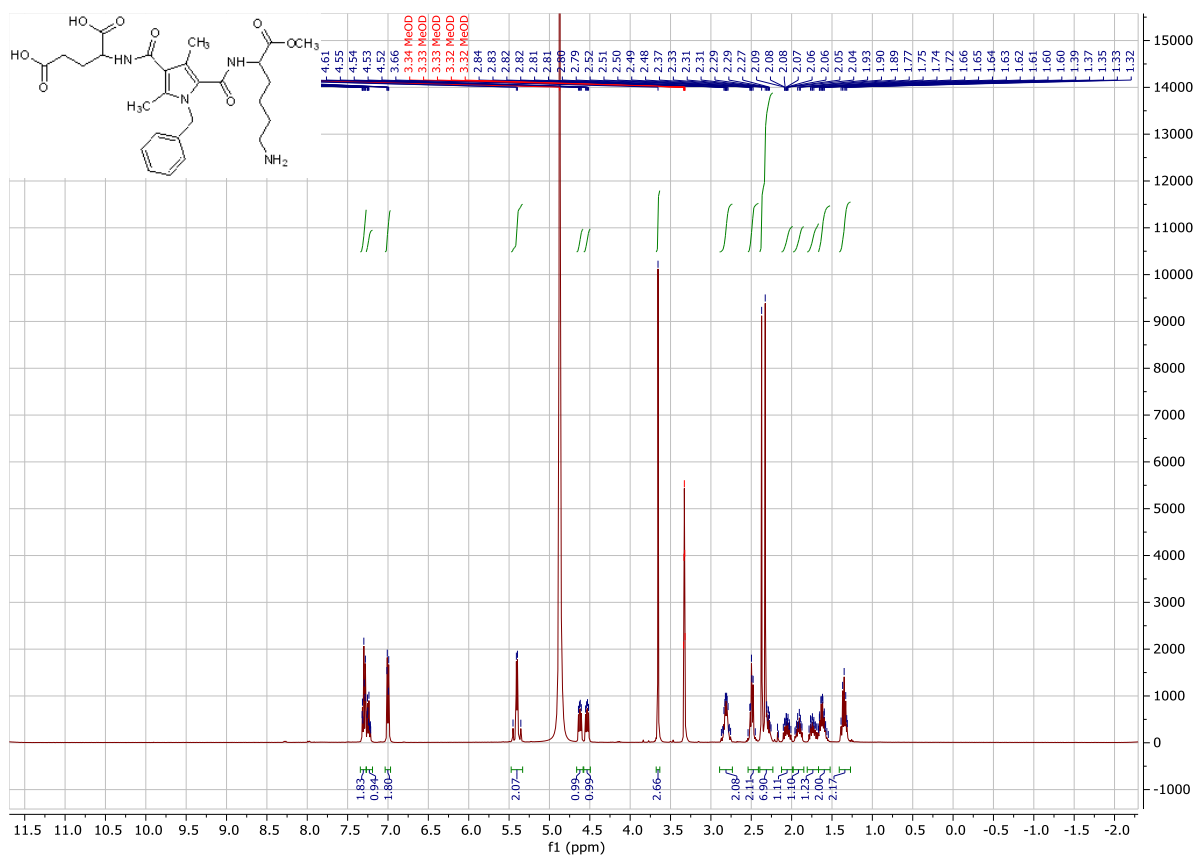




# Appendix

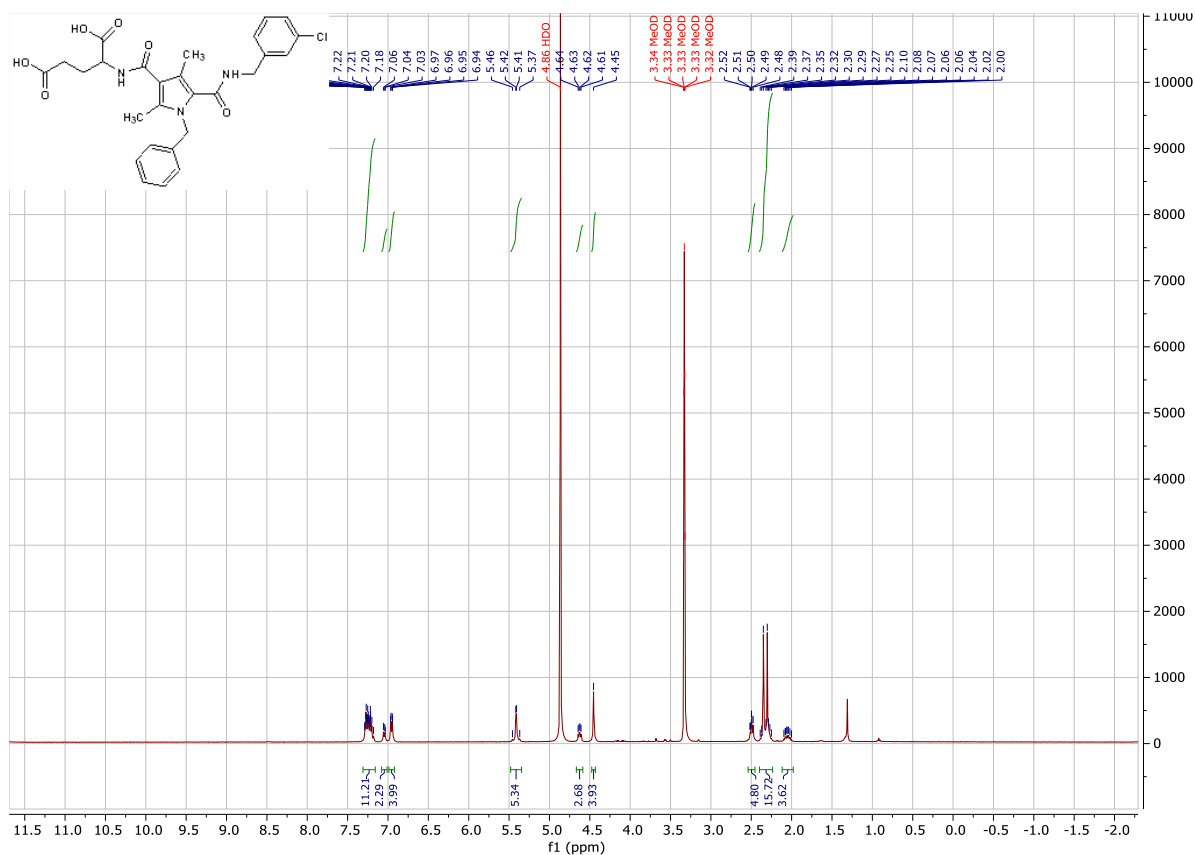


**<sup>1</sup>H NMR (400 MHz, MeOD) and <sup>13</sup>C DEPT NMR (101 MHz, MeOD) of 44h**

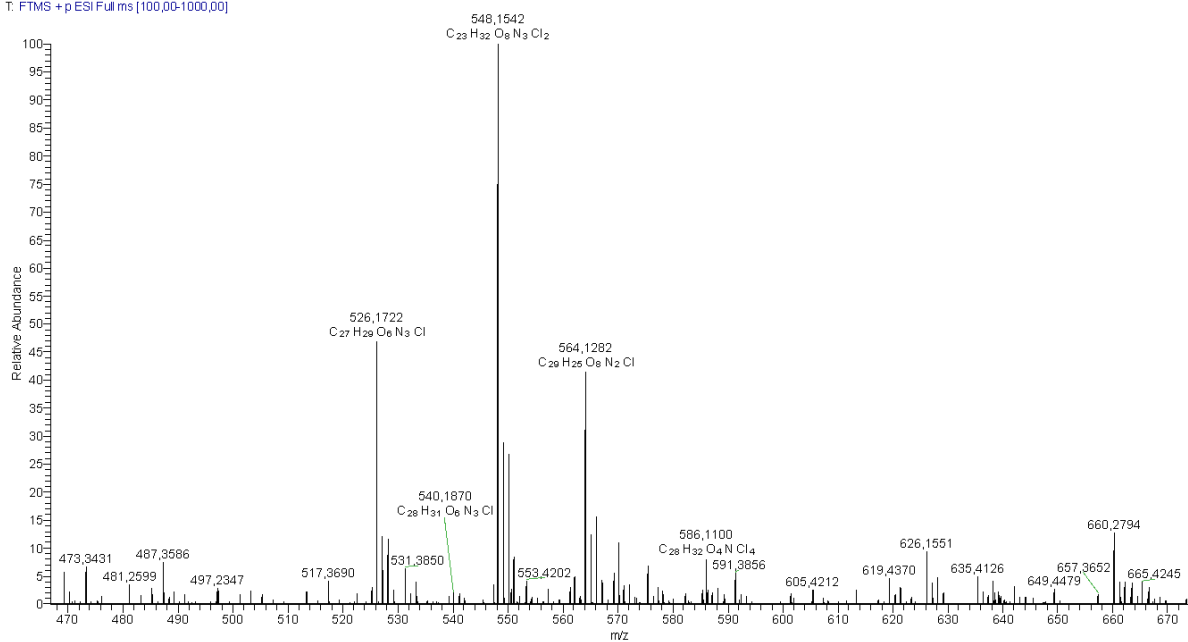


$^1\text{H NMR}$  (400 MHz, MeOD) and  $^{13}\text{C DEPTQ NMR}$  (101 MHz, MeOD) of 44i



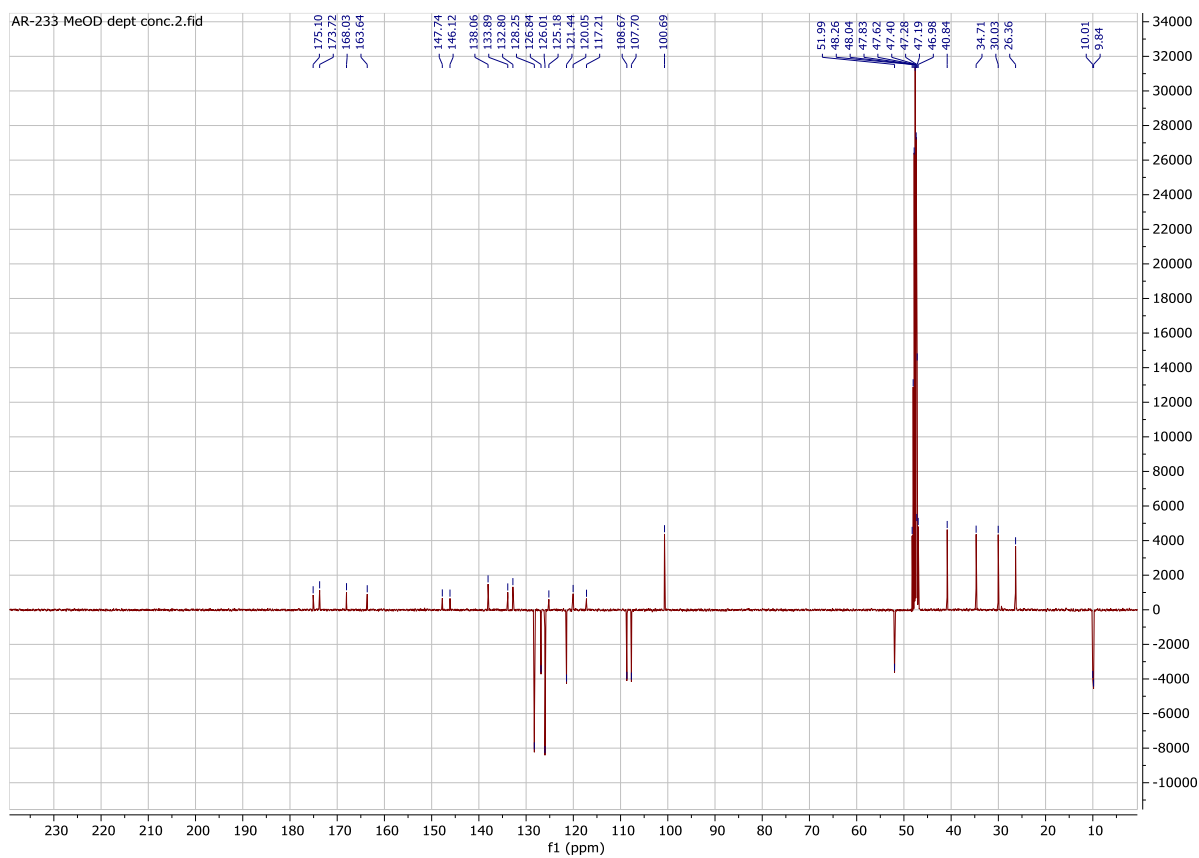
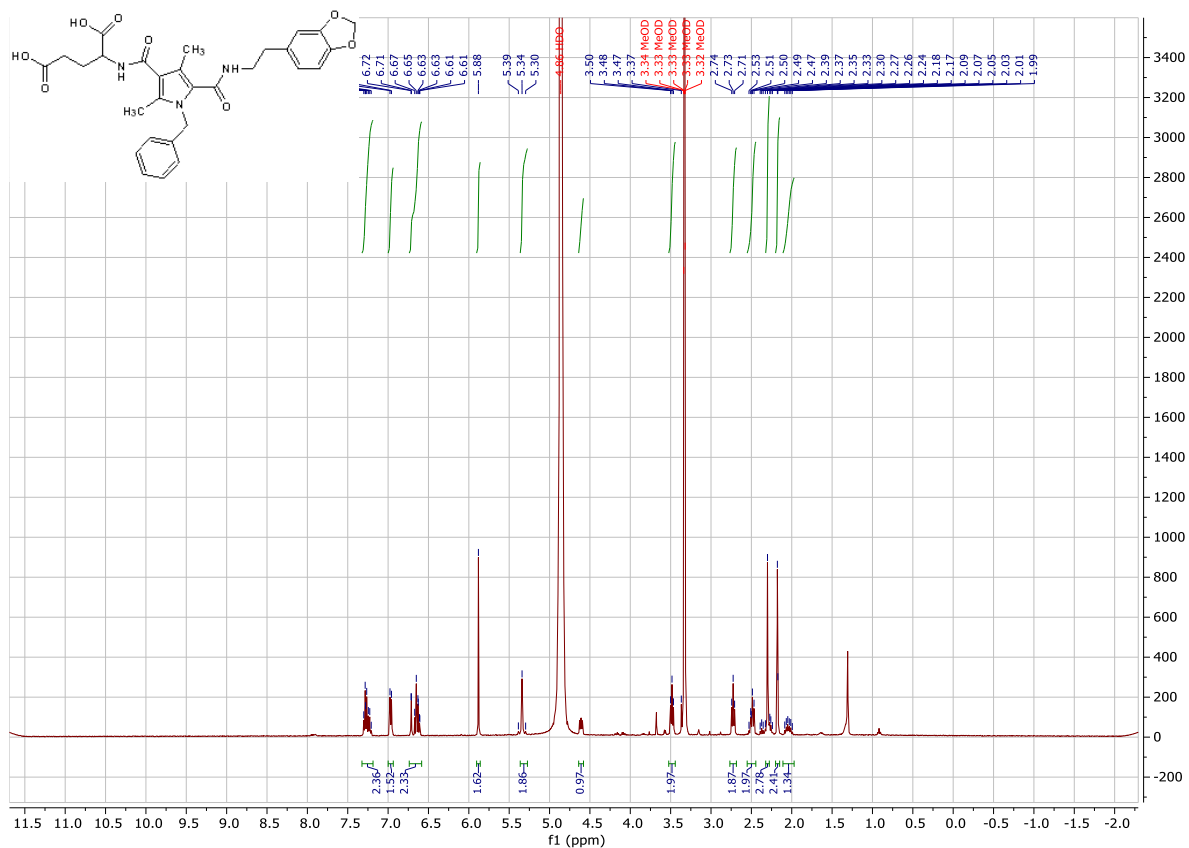


AR-232#28-29 RT: 0.22-0.23 AV: 2 NL: 2.65E6  
T: FTMS + pESI Full ms [100,00-1000,00]

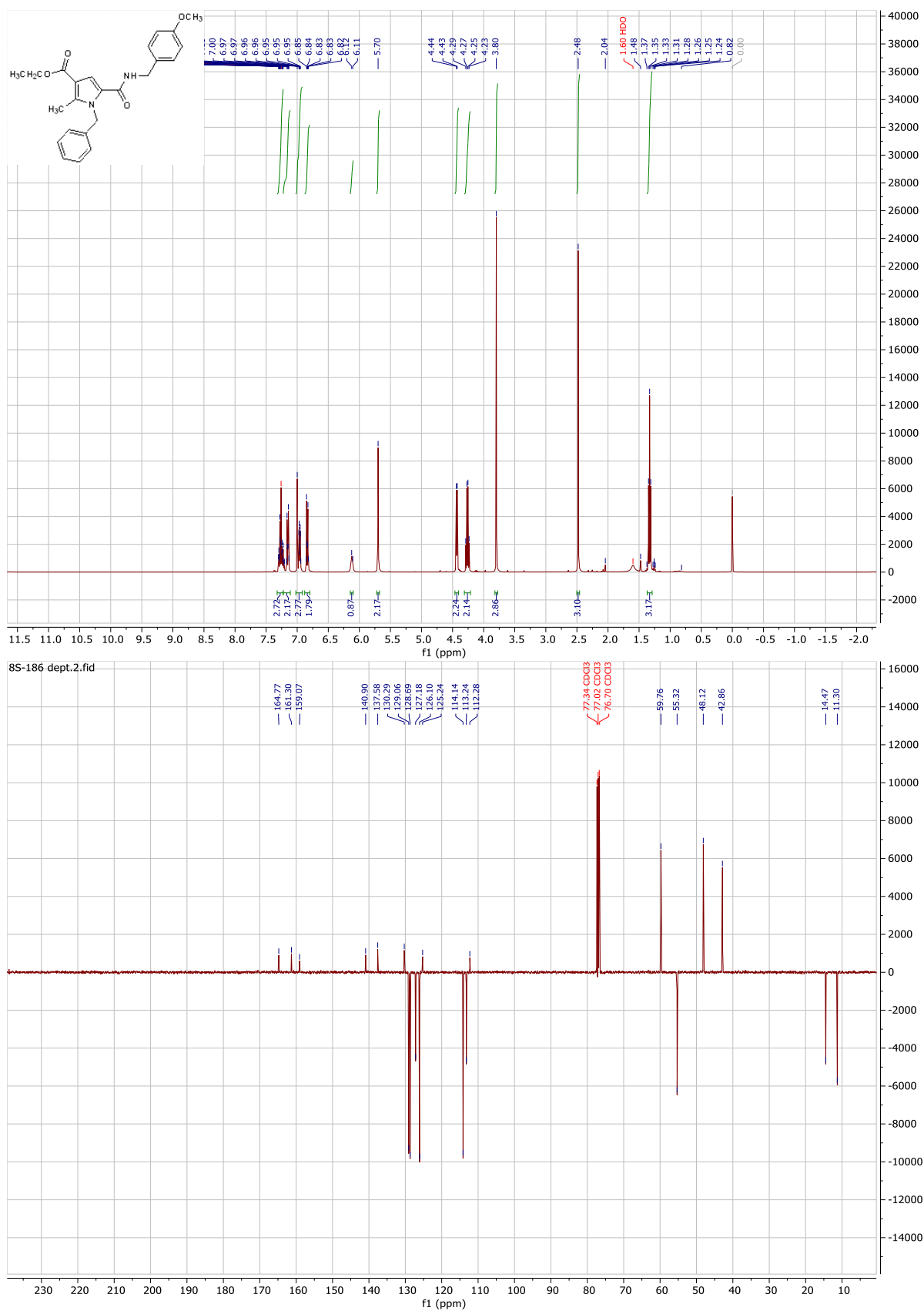


<sup>1</sup>H NMR (400 MHz, MeOD) and HRMS (ESI) m/z of 44k

# Appendix



<sup>1</sup>H NMR (400 MHz, MeOD) and <sup>13</sup>C DEPTQ NMR (101 MHz, MeOD) of 441

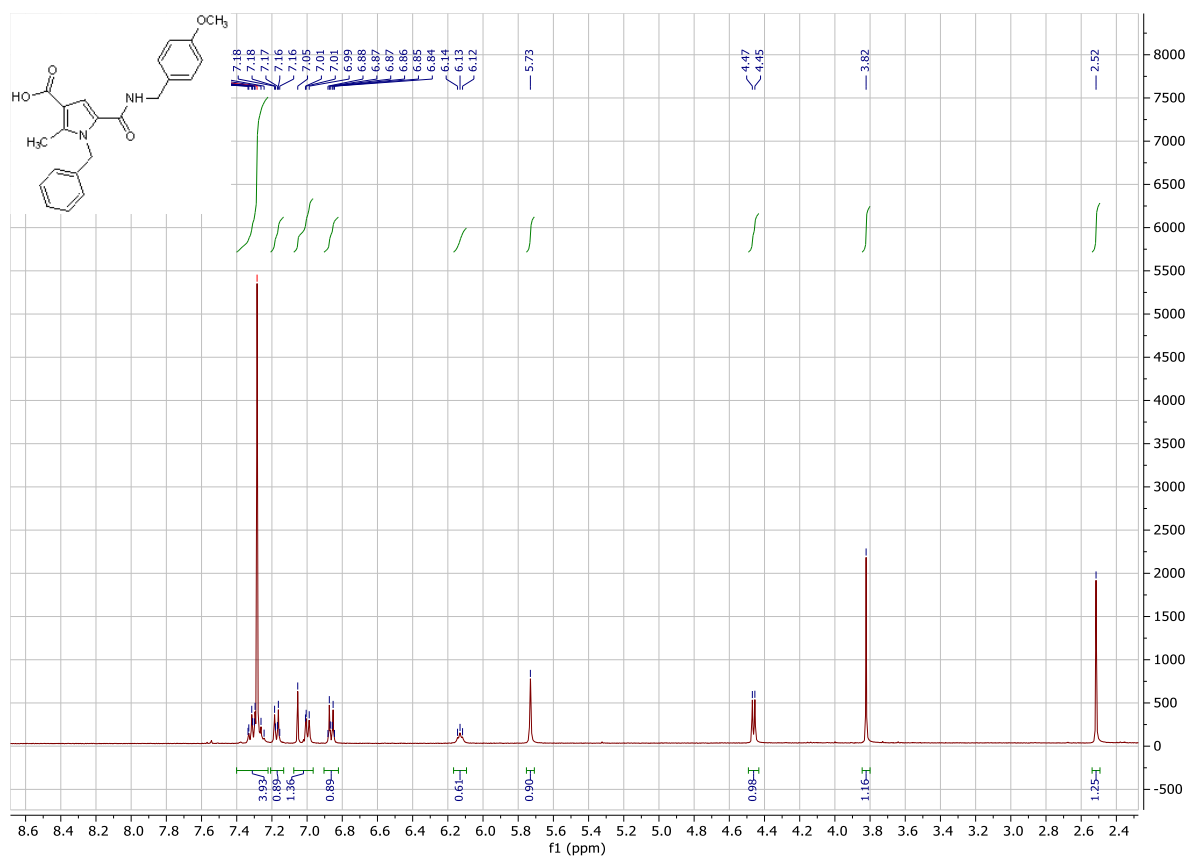


<sup>1</sup>H NMR (400 MHz, CDCl<sub>3</sub>) and <sup>13</sup>C DEPTQ NMR (101 MHz, CDCl<sub>3</sub>) of **45a**

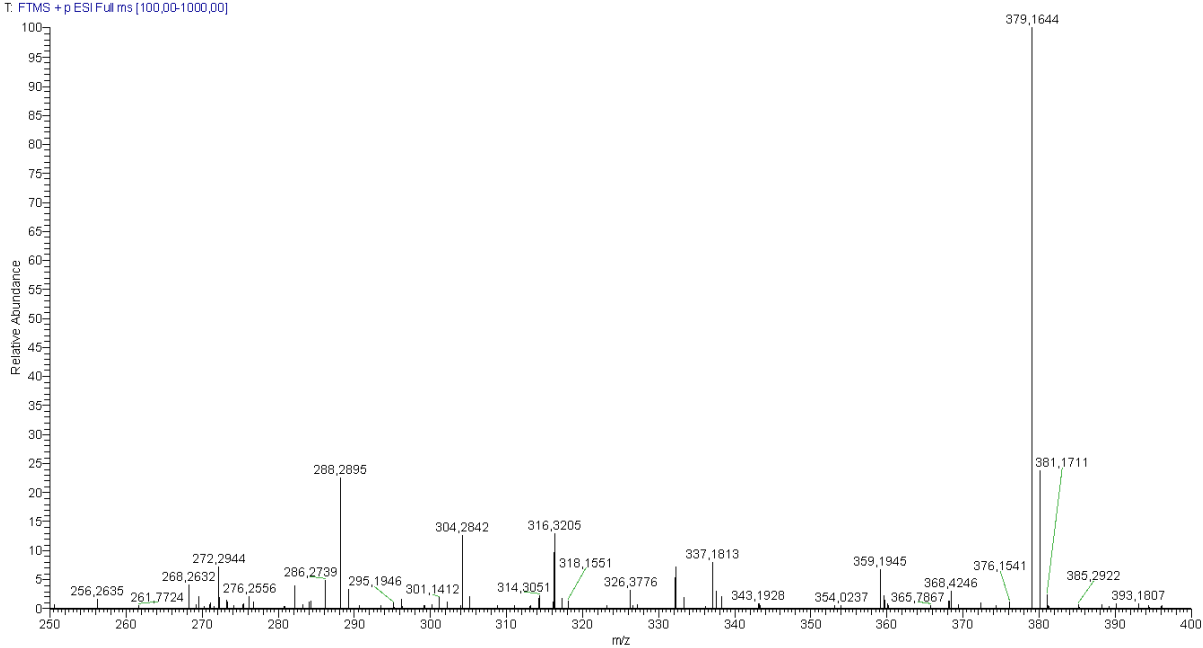




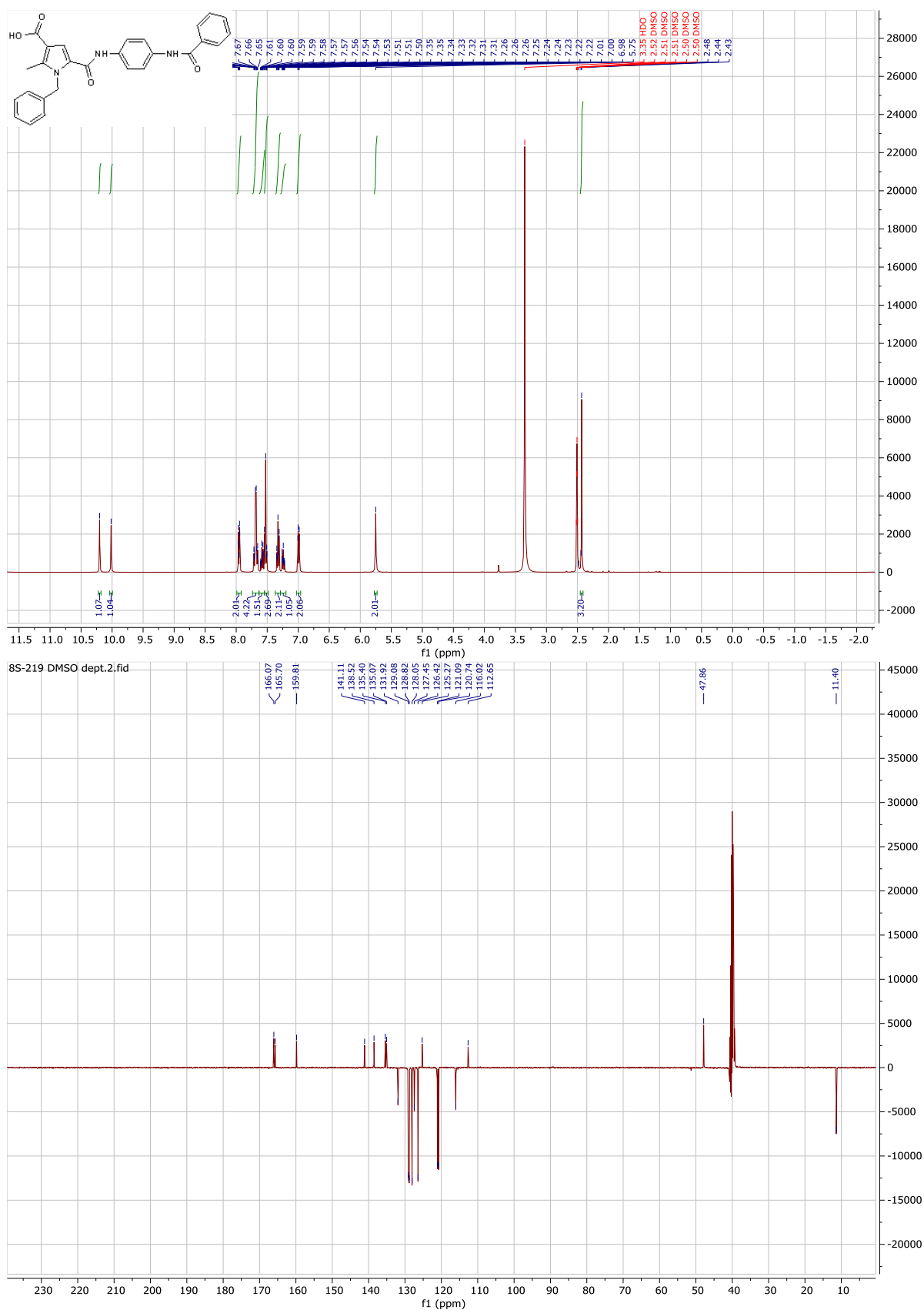
## Appendix



8S-193 #2 RT: 0.01 AV: 1 NL: 3.90E6  
T: FTMS + p ESI Full ms [100,00-1000,00]

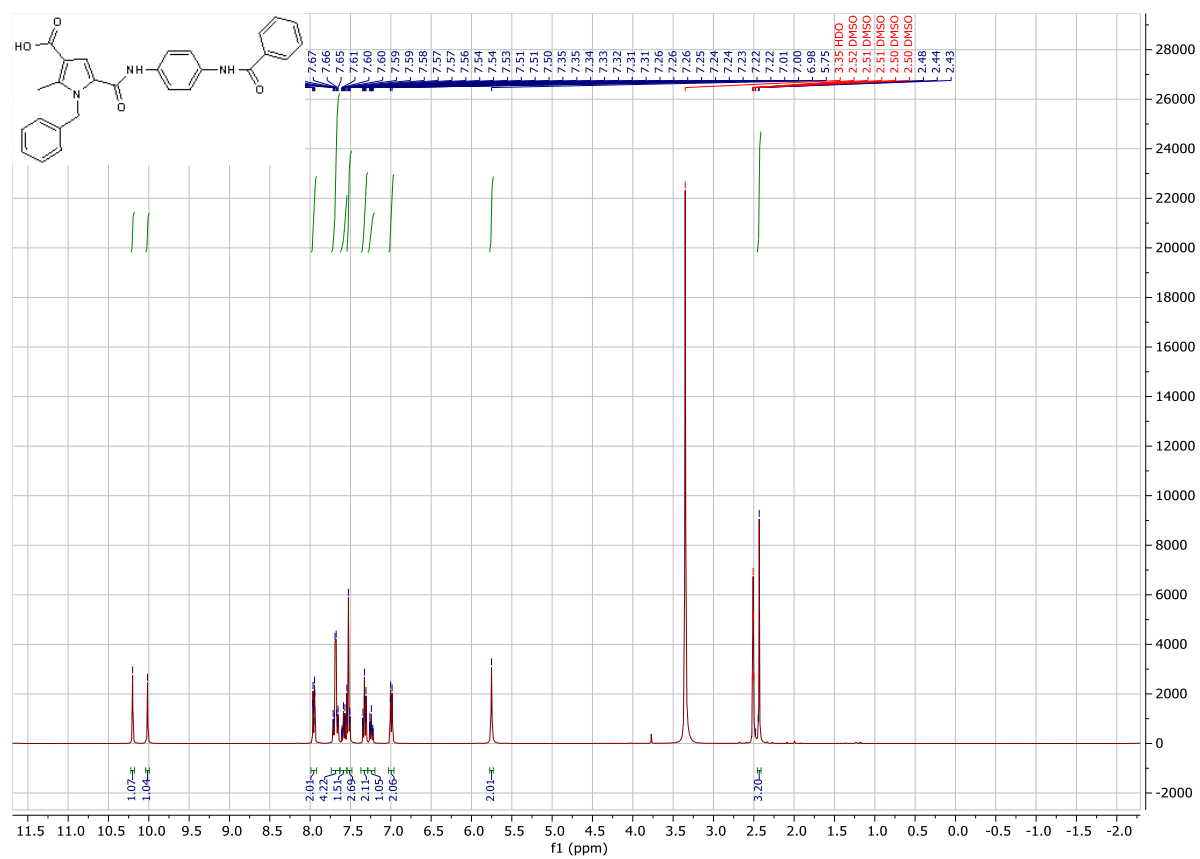


$^1\text{H NMR}$  (400 MHz,  $\text{CDCl}_3$ ) and HRMS (ESI)  $m/z$  of **45d**

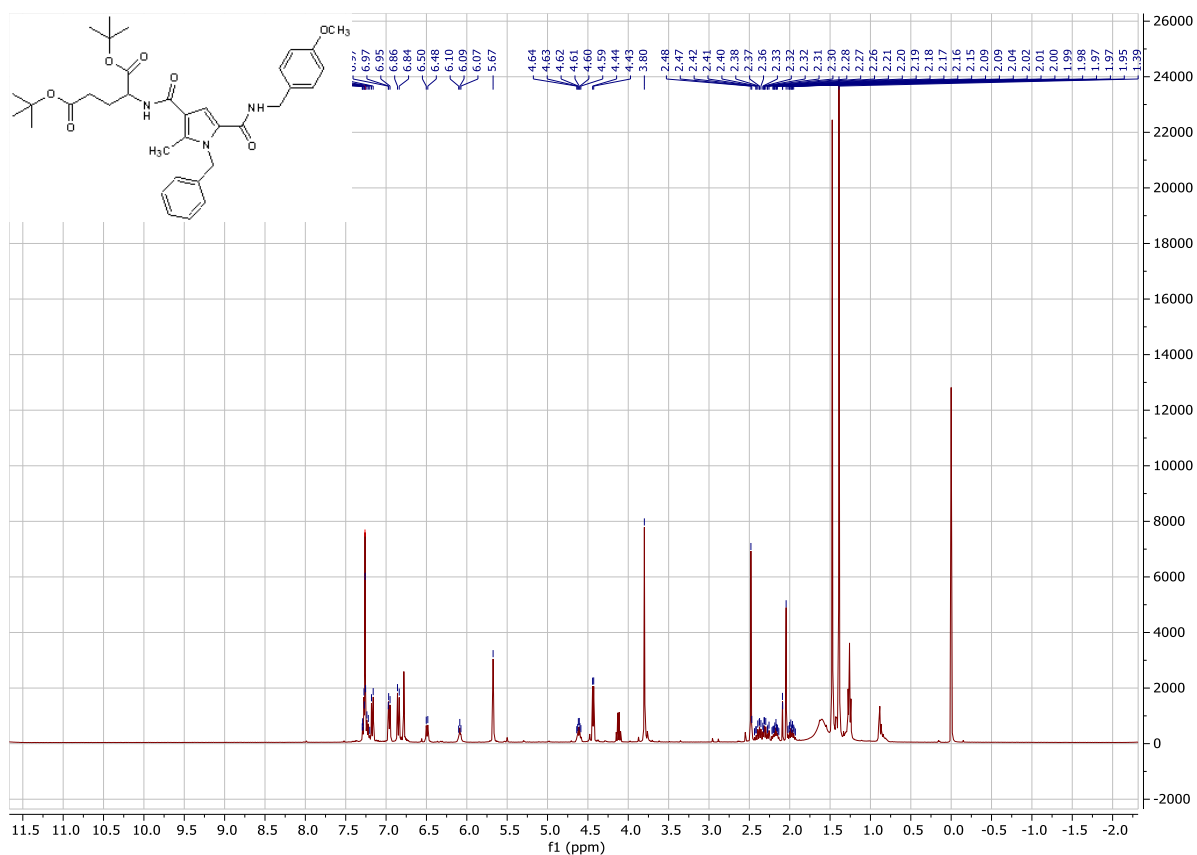


<sup>1</sup>H NMR (400 MHz, DMSO-d<sub>6</sub>) and <sup>13</sup>C DEPTQ NMR (101 MHz, DMSO-d<sub>6</sub>) of **45e**

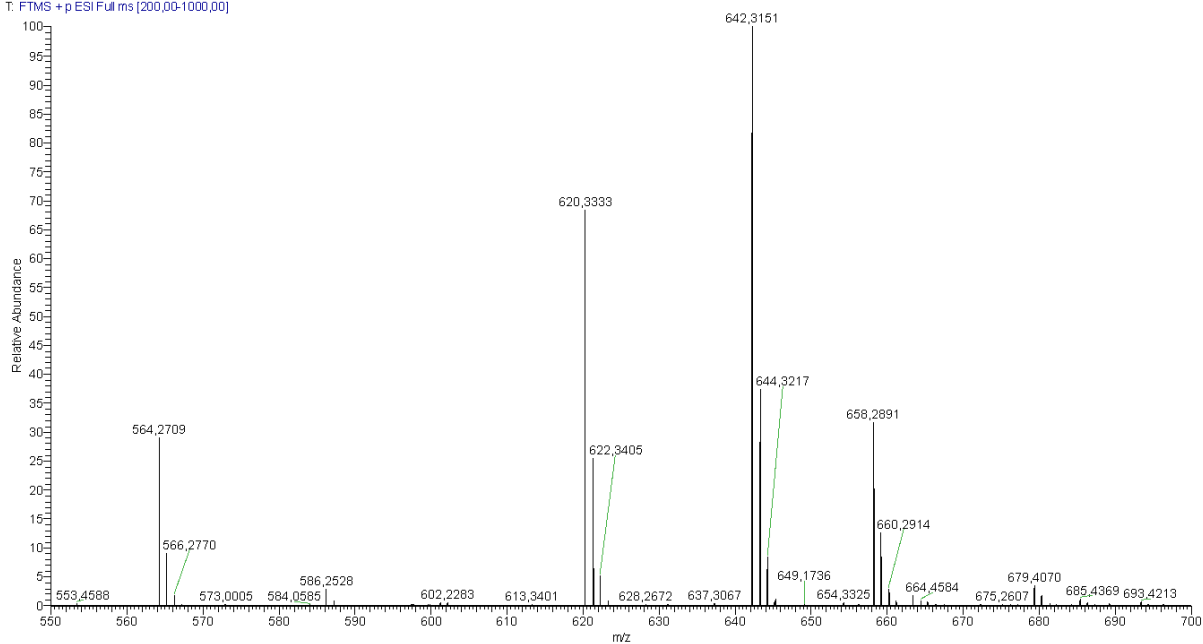
## Appendix



<sup>1</sup>H NMR (400 MHz, DMSO<sub>6</sub>) of **45f**

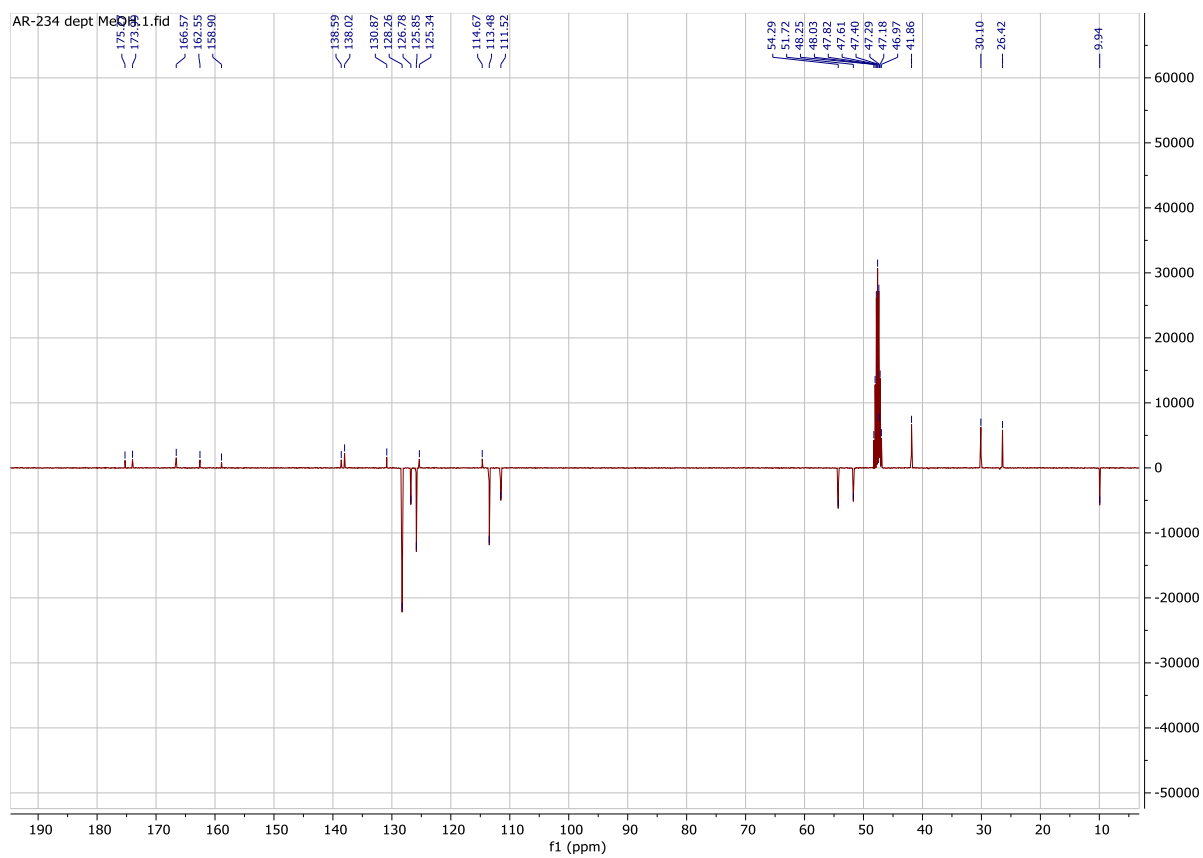
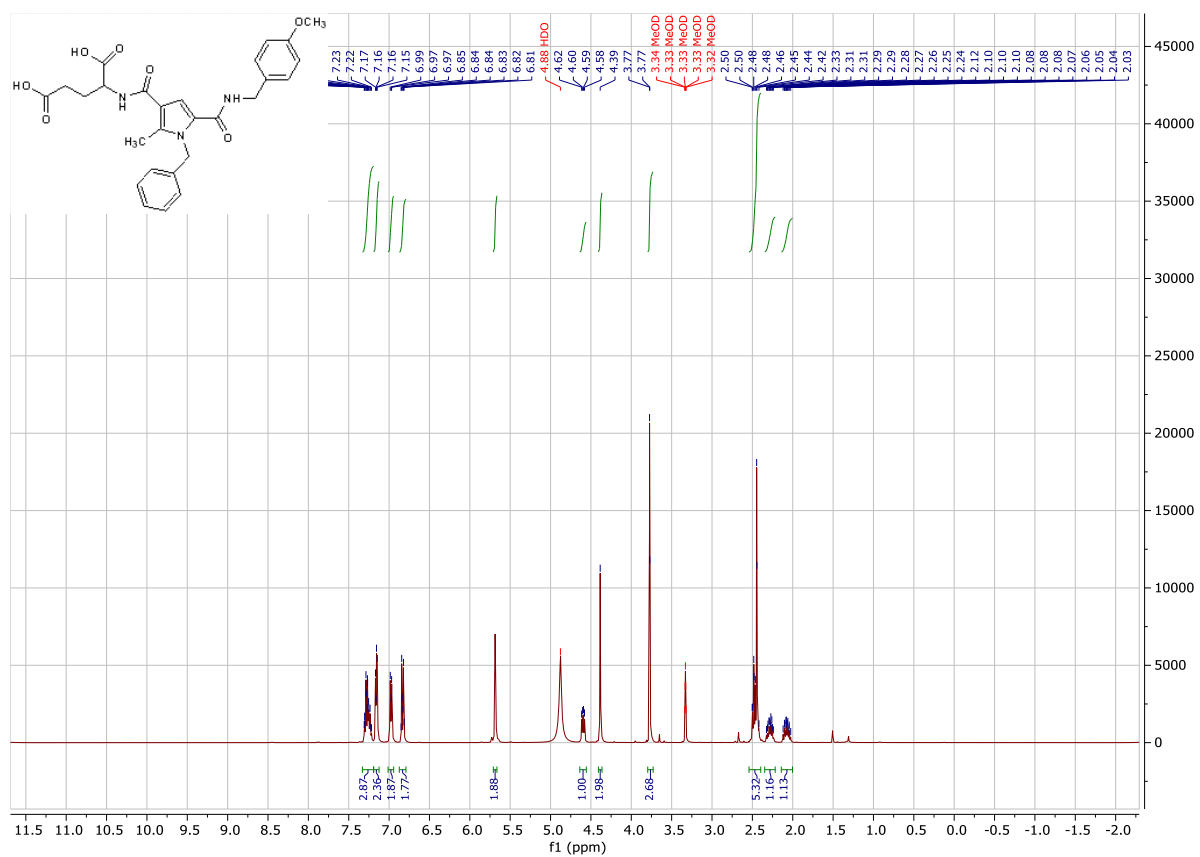


8S-198 #14 RT: 0.11 AV: 1 NL: 1.02E7  
T: FTMS + p ESI Full ms [200,00-1000,00]

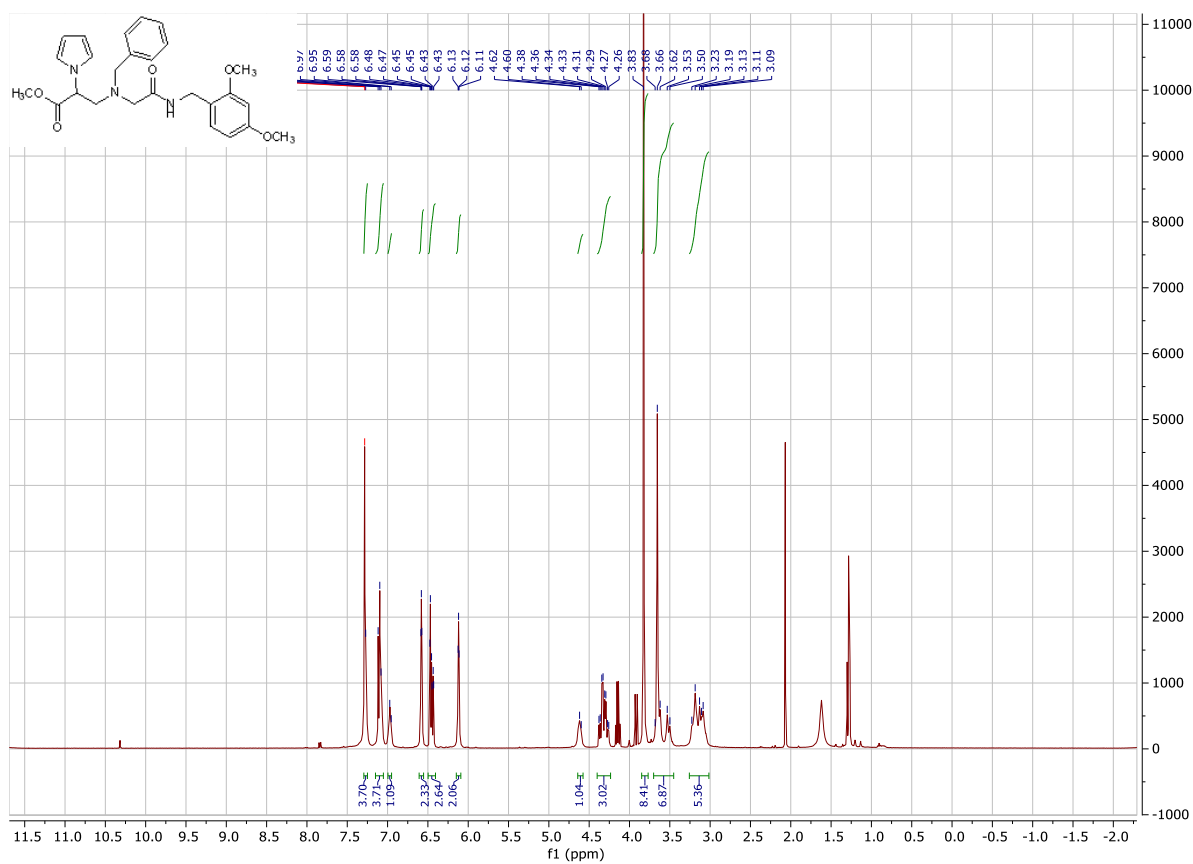


$^1\text{H}$ NMR (400 MHz,  $\text{CDCl}_3$ ) and HRMS (ESI) m/z of **45g**

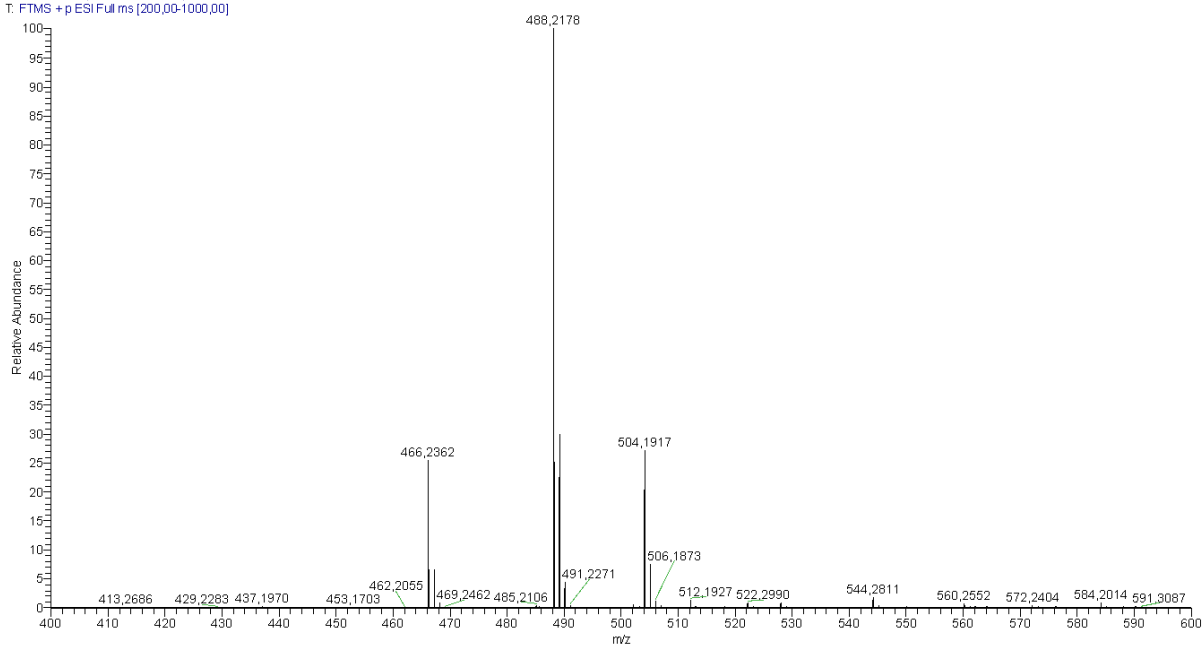
# Appendix



<sup>1</sup>H NMR (400 MHz, MeOD) and <sup>13</sup>C DEPTQ NMR (101 MHz, MeOD) of compound **45h**

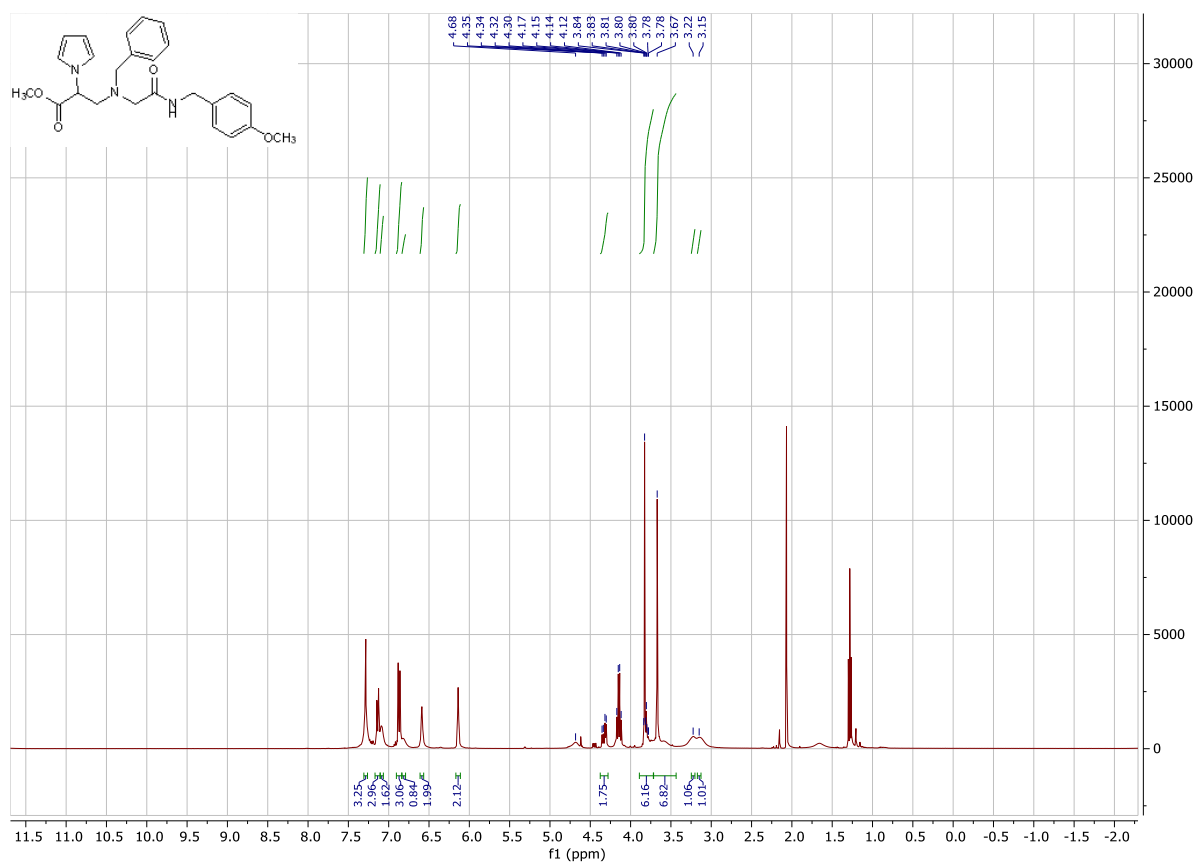


inc-1 #1 RT: 0.00 AV: 1 NL: 2,79E8  
T: FTMS + p ESI Full ms [200,00-1000,00]

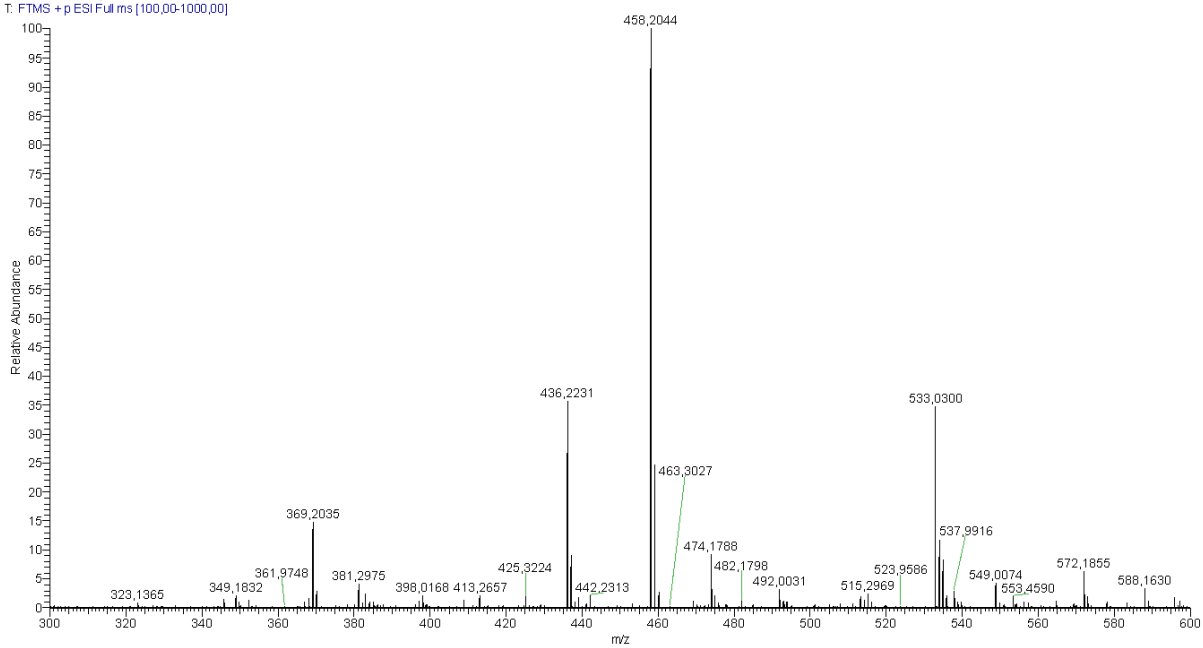


<sup>1</sup>H NMR (400 MHz, CDCl<sub>3</sub>) and HRMS (ESI) m/z of **46a**

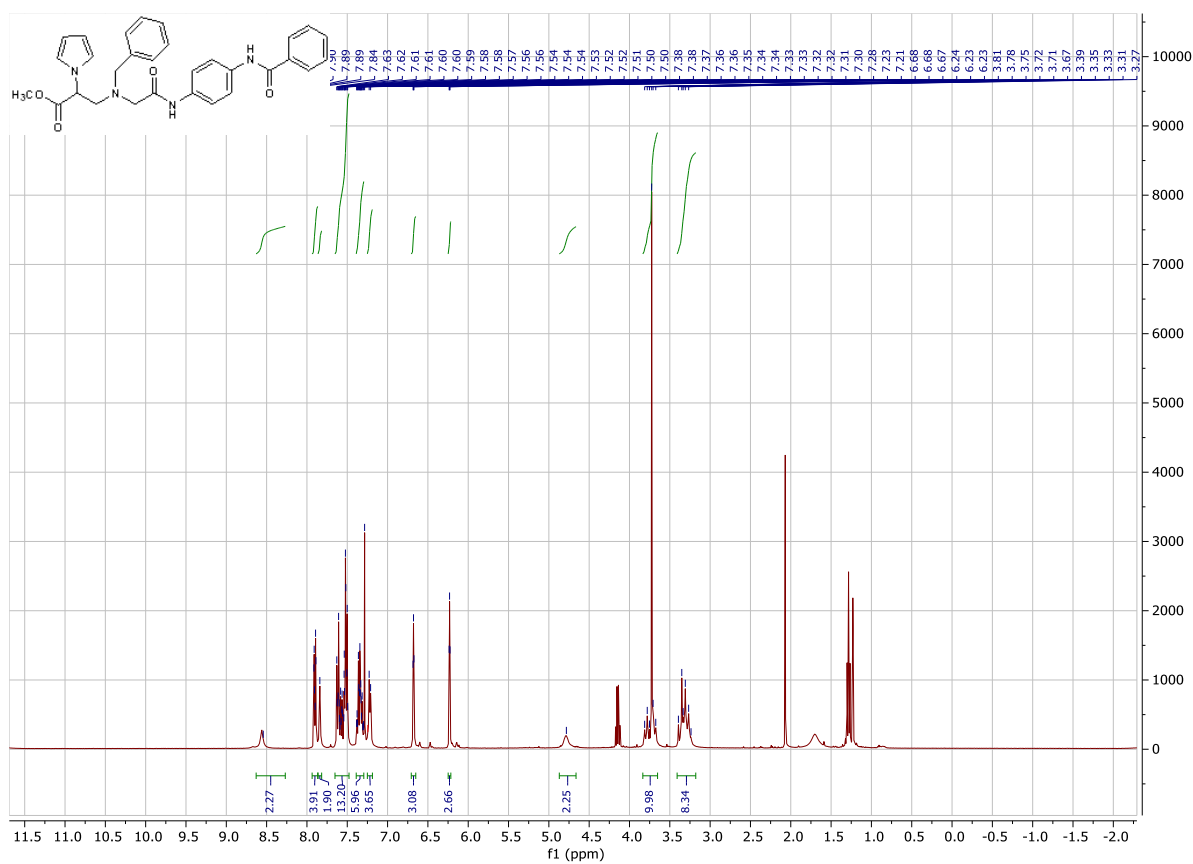
## Appendix



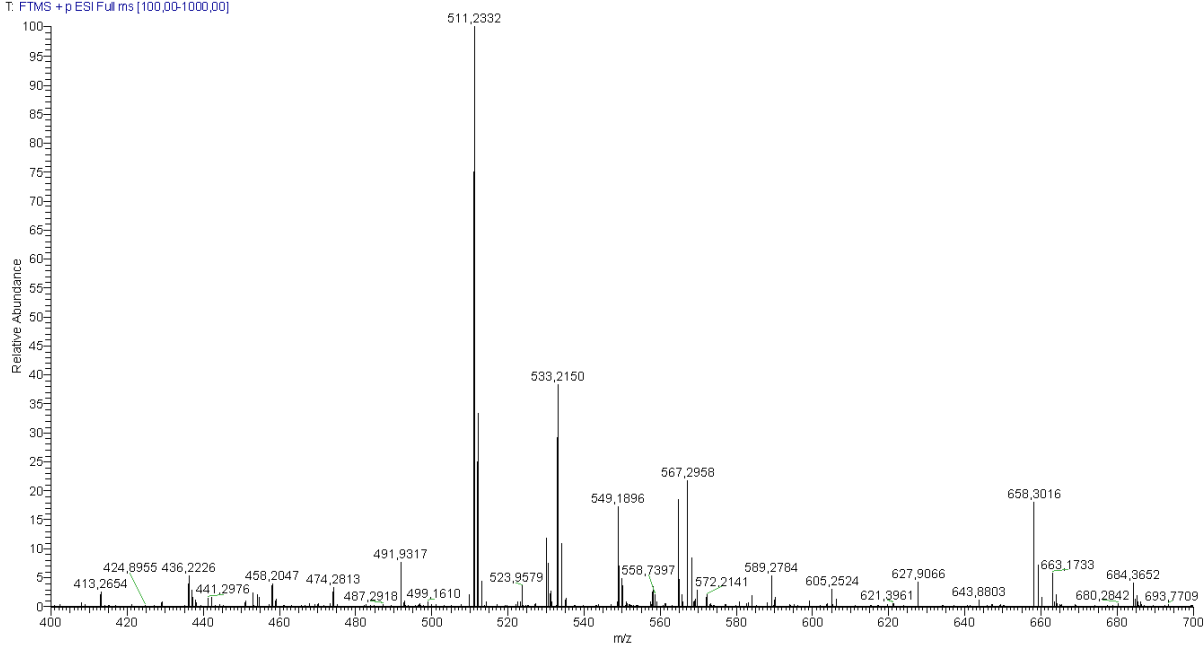
8S-365 #1 RT: 0.00 AV: 1 NL: 1.78E6  
T: FTMS + p ESI Full ms [100,00-1000,00]



$^1\text{H NMR}$  (400 MHz,  $\text{CDCl}_3$ ) and HRMS (ESI)  $m/z$  of **46b**



8S-338 ciommolon#43 RT: 0,35 AV: 1 NL: 2,25E6  
T: FTMS + p ESI Full ms [100,00-1000,00]



$^1\text{H NMR}$  (400 MHz,  $\text{CDCl}_3$ ) and HRMS (ESI)  $m/z$  of 46c



